

DEVELOPMENT AND CHARACTERISATION OF CARBON NANO FIBRE BASED MEMBRANE ELECTRODE ASSEMBLIES FOR PEM FUEL CELLS

Teză destinată obținerii
titlului științific de doctor inginer
la
Universitatea Politehnica Timișoara
în domeniul INGINERIA MATERIALELOR
de către

Eng. Ulrich Wilhelm Rost

Conducători științifici: prof. univ. dr. ing. Viorel-Aurel Șerban
prof. univ. dr. ing. Waltraut Brandl

Referenți științifici: prof. univ. dr. ing. Michael Brodmann
prof. univ. dr. ing. Petru Ilea
prof. univ. dr. ing. Nicolae Vaszilcsin

Ziua susținerii tezei: 13.10.2015

Seriile Teze de doctorat ale UPT sunt:

- | | |
|---|--|
| 1. Automatică | 9. Inginerie Mecanică |
| 2. Chimie | 10. Știința Calculatoarelor |
| 3. Energetică | 11. Știința și Ingineria Materialelor |
| 4. Ingineria Chimică | 12. Ingineria sistemelor |
| 5. Inginerie Civilă | 13. Inginerie energetică |
| 6. Inginerie Electrică | 14. Calculatoare și tehnologia informației |
| 7. Inginerie Electronică și Telecomunicații | 15. Ingineria materialelor |
| 8. Inginerie Industrială | 16. Inginerie și Management |

Universitatea Politehnica Timișoara a inițiat seriile de mai sus în scopul diseminării expertizei, cunoștințelor și rezultatelor cercetărilor întreprinse în cadrul Școlii doctorale a universității. Seriile conțin, potrivit H.B.Ex.S Nr. 14 / 14.07.2006, tezele de doctorat susținute în universitate începând cu 1 octombrie 2006.

Copyright © Editura Politehnica – Timișoara, 2015

Această publicație este supusă prevederilor legii dreptului de autor. Multiplicarea acestei publicații, în mod integral sau în parte, traducerea, tipărirea, reutilizarea ilustrațiilor, expunerea, radiodifuzarea, reproducerea pe microfilme sau în orice altă formă este permisă numai cu respectarea prevederilor Legii române a dreptului de autor în vigoare și permisiunea pentru utilizare obținută în scris din partea Universității Politehnica Timișoara. Toate încălcările acestor drepturi vor fi penalizate potrivit Legii române a drepturilor de autor.

România, 300159 Timișoara, Bd. Republicii 9,
Tel./fax 0256 403823
e-mail: editura@edipol.upt.ro

PREFACE

The presented work is the result of interdisciplinary research on efficient materials for energy conversion in the field of PEM fuel cells, conducted at the Westphalian University of Applied Sciences Gelsenkirchen (WHS). Regarding the development of fuel cell electrodes based on Pt/CNF electro catalysts, results have been obtained within the scope of past and ongoing research projects. For the confidence in my work, I would like to thank Prof. Dr. Brodmann who forwarded the research without obstacles. I appreciated the responsibility for the project "NanoFuelCells" which provided the necessary frame conditions for this Ph.D. thesis. I am looking forward to the prospective projects in this exciting field of hydrogen energy systems.

The strong cooperation between the working group of material science and the working group of hydrogen energy systems was essential for the mentioned research projects as well as this thesis. Furthermore, the scientific partnership between the Politehnica University Timisoara (UPT) and the Westphalian University, which was established in 2014, promoted the presented undertaking. It becomes obvious that without the close collaboration between all involved institutions – namely the department of Materials and Manufacturing Engineering (UPT), the Faculty of Industrial Chemistry and Environmental Engineering (UPT), as well as the Westphalian Energy Institute (WHS) – this thesis would not have been successfully finalised. Therefore, I would like to express my sincere thanks to my scientific supervisors Prof. Dr. Viorel-Serban, Prof. Dr. Nicolae Vaszilscin, Prof. Dr. Waltraut Brandl and Prof. Dr. Michael Brodmann for their advice, remarks, and inspiration for this thesis.

For their collegial discussions and warm-hearted collaboration during the experimental investigations carried out for my thesis, I would like to thank Dr. Gabriela Marginean, Dr. Veronica Pirvulescu, Dragos Pascal and Roxana Muntean from the working group of material science as well as Cristian Mutascu, Jeffrey Roth and Christoph Sagewka from the working group of hydrogen energy systems. Furthermore, I also want to thank the former students David Gasch and Pit Podleschny and all recent and former members of the working group for their helpful participation.

My deepest gratitude goes to my family, in particular to my wife Johanna and my son Florian, as well as to my friends for their indispensable moral support over the last years.

Dortmund, September 2015

Ulrich Wilhelm Rost

Rost, Ulrich Wilhelm

DEVELOPMENT AND CHARACTERISATION OF CARBON NANO FIBRE BASED MEMBRANE ELECTRODE ASSEMBLIES FOR PEM FUEL CELLS

ISSN:2285-1720

ISSN-L:2285-1720

ISBN: 978-606-35-0014-5

Teze de doctorat ale UPT, Seria 15, Nr. 20, Editura Politehnica, 2015, 150 pagini, 97 figuri, 20 tabele.

Keywords: PEM fuel cells, electrode preparation, carbon nano fibres, oxygen plasma activation, fuel cell test system, hydraulic compression

Abstract,

For this experimental work gas diffusion electrodes (GDE) with low platinum loading are prepared for the application as anodes in polymer electrolyte membrane fuel cells. As catalyst support material, carbon nano fibres (CNF) are investigated due to high specific surface area as well as high graphitisation degree. Optimisation is achieved by an economic and environmental friendly pre-treatment process in oxygen plasma. For electrode preparation an ink is used containing oxygen plasma activated CNFs as well as hydrophilic polymer. After spray coating of this CNF ink on a graphitic substrate, platinum is deposited by pulse plating method. Preliminary results established that the plasma activation improves considerably CNF dispersibility as well as the amount, respectively, the morphology of the deposited platinum. Morphology and microstructure are observed by electron microscopy. Platinum loading is determined by thermogravimetric analysis to be in the range of 0.010 to 0.016 mg cm⁻². Furthermore, MEAs are prepared from these GDEs and testing is performed in a novel modular test stack based on hydraulic compression. Technical information about the test stack design and functions are given in this work. In this test environment maximum specific power output of 182 mW cm⁻² has been obtained under robust operation conditions.

Rezumat,

Lucrarea de față își propune dezvoltarea și caracterizarea unor electrozi de difuzie a gazelor cu conținut scăzut de platină ce vor fi ulterior folosiți ca anodi în pilele de combustie cu electrolit polimeric (PEMFC). Materialul suport folosit pentru depunerea catalizatorului este constituit din fibre de carbon (CNF) datorită suprafeței lor specifice foarte ridicate cât și datorită gradului mărit de grafitizare. Funcționalizarea suprafeței fibrelor de carbon este realizată printr-un proces ecologic și totodată economic, utilizând plasma în atmosferă de oxigen. Pentru pregătirea electrozilor se folosește o dispersie obținută prin amestecarea fibrelor de carbon tratate anterior în plasmă cu izopropanol și un polimer hidrofilic. Amestecul este pulverizat pe un substrat grafitic, electrozul obținut este uscat și pe suprafața acestuia se depun particule de platină printr-un proces electrochimic. Rezultatele preliminare au stabilit că tratamentul fibrelor de carbon în plasmă de oxigen îmbunătățește considerabil atât dispersibilitatea acestora, cât și cantitatea respectiv morfologia depozitului de platină. Morfologia și structura electrozilor este analizată prin intermediul microscopiei electronice de baleiaj. Cantitatea de platină depusă pe fibrele de carbon este determinată prin analiză termogravimetrică, iar valorile obținute se încadrează în intervalul 0,010 – 0,016 mg cm⁻². Electrozii de difuzie a gazelor (GDE) sunt folosiți în cele din urmă pentru obținerea ansamblului membrană - electrod (MEA), iar testarea este realizată într-un stack modular inovator bazat pe compresie hidrolică. Informațiile tehnice despre designul și modul de funcționare al stackului sunt prezentate în această lucrare. În mediul de testare descris s-au obținut valori maxime de putere de până la 182 mW cm⁻², în condiții de operare severe.

CONTENT

PREFACE.....	3
CONTENT.....	5
LIST OF FIGURES.....	8
LIST OF TABLES	11
1. INTRODUCTION	12
1.1. Electricity Generation and Storage.....	14
2. STATE OF THE ART OF POLYMER ELECTROLYTE MEMBRANE FUEL CELLS.....	17
2.1. Thermodynamics and Kinetics	18
2.2. PEM Fuel Cell Design	22
2.2.1. Pole Plate.....	22
2.2.2. Gas Diffusion Layer	24
2.2.3. Polymer Electrolyte Membrane.....	25
2.2.4. Catalytic Layer.....	27
2.2.5. Catalyst Support Materials	29
2.2.6. PEM Fuel Cell Durability	31
2.2.7. PEM Fuel Cell Stacks.....	33
2.3. Motivation for this Work	36
3. METHODOLOGY AND EXPERIMENTAL EQUIPMENT	37
3.1. Methods for Material Characterisation.....	37
3.1.1. Electron Microscopy.....	37
3.1.2. X-ray Based Analyses	39
3.1.3. Thermogravimetry	41
3.1.4. Cyclic Voltammetry	42
3.1.5. Electrical Conductivity.....	44
3.2. Carbon Filament Coating and Decoration	47
3.2.1. Radio Frequency Induced Oxygen Plasma.....	47
3.2.2. Surface Energy	48
3.2.3. Ink Formulation	48
3.2.4. Preparation of Carbon Filament Layers.....	50
3.2.5. Catalyst Particle Deposition	51
3.3. Membrane Electrode Assembly Testing	55

6 Content

3.3.1. Membrane Electrode Assembly.....	55
3.3.2. Test Cell Design	56
3.3.3. PEMFC Test Stack in Pocket Design with Hydraulic Compression	57
3.3.4. PEMFC Test Bench.....	61
4. RESULTS AND DISCUSSION	67
4.1. Materials for MEA Manufacturing.....	67
4.1.1. Carbon Filaments	67
4.1.2. Gas Diffusion Layer	72
4.1.3. Cathode Material.....	76
4.1.4. Polymer Electrolyte Membrane.....	76
4.2. A Novel MEA Test Environment.....	78
4.2.1. Analysis of Pressure Distribution	78
4.2.2. Analysis of Current Density and Temperature Distribution	79
4.2.3. Effect of Compression Variation	81
4.2.4. Effect of Temperature Variation	82
4.2.5. Effect of Changing Air Stoichiometry.....	83
4.3. Standard Pt/C Electro Catalyst Based GDEs.....	84
4.3.1. Platinum Loading	85
4.3.2. Corrosion Resistance	85
4.3.3. Electrochemical Active Surface Area	87
4.3.4. Polarisation Behaviour	88
4.4. Carbon Filaments Based GDEs.....	89
4.4.1. Catalyst Preparation	91
4.4.2. Platinum Loading	99
4.4.3. Polarisation Behaviour	100
4.4.4. Long-Term Operation.....	103
4.4.5. Current Density Distribution	104
4.5. Optimisation of Pt/CNF Based Electrodes	106
4.5.1. Variation of Polymer Content	106
4.5.2. Utilisation of Heat Treated Carbon Nanofibres	108
4.5.3. Optimisation of the Catalyst Preparation	111
5. CONCLUSIONS	116
LIST OF PUBLICATIONS	118
REFERENCES	120
APPENDICES	132

CURRICULUM VITAE.....	150
Personal Details	150
Education and Work Experience	150

LIST OF FIGURES

Fig. 1: Schematic drawing of the first fuel cell system [28]	17
Fig. 2: Theoretical efficiencies of Carnot and fuel cell processes	19
Fig. 3: Typical polarisation curve of a H ₂ /air operated PEMFC	20
Fig. 4: Schematic drawing of a PEMFC's cross section	22
Fig. 5: Milled graphitic pole plate	23
Fig. 6: Metallic pole plates with noble metal coating	23
Fig. 7: Injection moulded graphitic pole plate (with friendly permission of the Zentrum für BrennstoffzellenTechnik [37])	23
Fig. 8: Schematic drawing of the interface between flow field and gas diffusion layer in cross section	24
Fig. 9: Microscopy of carbon cloth	25
Fig. 10: Microscopy of carbon fibre paper	25
Fig. 11: Schematic drawing of protons transport mechanism through PFSA	26
Fig. 12: Schematic drawing of the catalytic layers structure	28
Fig. 13: Micrograph of an unorganised bundle of MWCNTs	30
Fig. 14: Micrograph of helical-ribbon like CNFs [79]	30
Fig. 15: Vertically aligned CNTs [59]	31
Fig. 16: Schematic drawing of start/stop cycle induced carbon corrosion at the cathode compartment when air is introduced in the anode compartment after shutdown	32
Fig. 17: Schematic drawing of fuel cell stack in bipolar design with cooling plate in cross section	34
Fig. 18: Schematic drawing of the deformation of pressure plates due to application of clamping forces (exaggerated)	34
Fig. 19: Schematic drawing of a MEA test facility with mechanical actuator for adjusting test cell compression	36
Fig. 20: Schematic drawing of a scanning electron microscope [114]	38
Fig. 21: Schematic drawing of generation of continuous bremsstrahlung [114]	39
Fig. 22: Atom ionisation by a beam electron ejecting a K shell electron (1), L shell transition to K shell (2) and two possibilities how excess energy is released (3) [114]	40
Fig. 23: Typical X-ray spectrum achieved by an X-ray tube with copper anode target [114]	40
Fig. 24: Schematic drawing of the relation between wavelength λ , spacing between two atoms d and incident diffraction angle θ according to Bragg's law [114]	41
Fig. 25: Schematic drawing of an X-ray diffractometer [116]	41
Fig. 26: Thermogravimetric analysis of an electrode sample based on CNFs with platinum decoration	42
Fig. 27: Cyclic voltammogram of a PEMFC electrode with Pt/C electro catalyst [27]	44
Fig. 28: Photograph of a circuit board for resistivity measurement in xy-direction (in plane)	45
Fig. 29: Correction factor according to [117]	46
Fig. 30: Photograph of circuit boards for resistivity measurement in z-direction (through plane)	47
Fig. 31: CNT dispersion in H ₂ O (w/o previous plasma treatment)	49
Fig. 32: CNT dispersion in C ₂ H ₅ OH (w/o previous plasma treatment)	49

Fig. 33: Plasma treated CNT dispersed in H ₂ O	49
Fig. 34: Plasma treated CNT dispersed in H ₂ O after 60 minutes	49
Fig. 35: Plasma treated CNT dispersed in C ₂ H ₅ OH	49
Fig. 36: Plasma treated CNT dispersed in C ₂ H ₅ OH after 60 minutes	49
Fig. 37: Automated ink coating facility	50
Fig. 38: Travel path of the coating facility	51
Fig. 39: Schematic drawing of nickel plating.....	52
Fig. 40: SEM of a stainless steel pole plate with an anticorrosive gold coating (BSE mode)	53
Fig. 41: Typical waveforms for pulsed electro plating processes [124]	54
Fig. 42: Schematic drawing of an electro plating facility	55
Fig. 43: Schematic drawing of a PEMFC test cell (left: front view of a pole plate; right: explosion drawing of a test cell).....	56
Fig. 44: Schematic drawing of a PEMFC stack in pocket design with hydraulic compression (with four single fuel cells inserted)	58
Fig. 45: Photograph of the realised test stack for PEMFC MEAs (already integrated into the test bench).....	59
Fig. 46: Rear view of the novel MEA test stack with hydraulic compression	59
Fig. 47: Photograph of a PEMFC stack with mechanical compression over tie bolts	60
Fig. 48: Schematic drawing of a segmented pole plate	61
Fig. 49: Photograph of the novel test bench which is optimised for MEA testing (without front doors).....	62
Fig. 50: Main gas distribution within the test bench.....	62
Fig. 51: Process diagram of the humidifier with integrated gas heating	63
Fig. 52: Anodic gath path.....	64
Fig. 53: Cathodic gas path	64
Fig. 54: Human device interface for the novel fuel cell test bench (overview about settings for test cell 1 (feed gas and electronic load controls)	65
Fig. 55: XRD spectra of CNT and CNF raw material (powder).....	68
Fig. 56: TEM microscope image of CNFs with Pt decoration	69
Fig. 57: TEM microscopy of a CNF with adhered Pt cluster.....	69
Fig. 58: CV diagram of selected carbon fibres samples depending on the plasma treatment	71
Fig. 59: Polarisation curve of a MEA with platinum free anode	72
Fig. 60: Cross section of a GDL type Freundeberg H2315 I2C6 with friendly permission of Fredenberg FCCT [137].....	73
Fig. 61: Polarisation curve of MEA based on Gore® CCM depending on assembled GDL	75
Fig. 62: Polarisation characteristics of MEA depending on membrane material	77
Fig. 63: Analysis of pressure distribution over the active cell area by pressure sensitive film (a to c: mechanical compression; d to f: hydraulic compression; g: measuring scale)	79
Fig. 64: Current density distribution for 4, 8 and 16 A load current	80
Fig. 65: Deviation of measured current density from arithmetic average current density for 4, 8 and 16 A load current	80
Fig. 66: Temperature distribution for 4, 8 and 16 A load current	81
Fig. 67: Polarisation curves depending on stack pressure	82
Fig. 68: Polarisation curves depending on cell temperature	83
Fig. 69: Polarisation curves dependent on λ variation	84
Fig. 70: Corrosion test of selected PEMFC electrodes in 0.5 M H ₂ SO ₄	86
Fig. 71: CV diagrams of BC-H225-10F electrode sample (after 100 cycles).....	87

10 List of Figures

Fig. 72: polarisation curves of Pt/C based MEAs	88
Fig. 73: Schematic cross section of prepared MEAs	90
Fig. 74: Micrograph of platinum particles on GDL type Freudenberg H2315 I2C6 without (images A to C) and with previous plasma activation (images D – F)	92
Fig. 75: Micrograph of Pt particles on CNTs (5,000 magnitude).....	94
Fig. 76: Micrograph of Pt particles on CNTs (10,000 magnitude).....	94
Fig. 77: SEM study on the morphology doped CNTs decorated with Pt particles (10,000 magnitude): A) 10 mA cm ⁻² for 360 sec, B) 12 x 10 sec, C) 12 x 5 sec, D) 1 x 1 sec, E) 120 x 1 sec, and F) 12 x 1 sec.....	95
Fig. 78: Catalyst layer of an electrode sample based on platinum decorated CNFs (100 magnitude)	96
Fig. 79: Catalyst layer of an electrode sample based on platinum decorated CNFs (500 magnitude)	96
Fig. 80: Catalyst layer of an electrode sample based on platinum decorated CNFs (500 magnitude, BSE mode)	96
Fig. 81: EDX spectrum of an electrode sample based on Pt/CNF catalyst layer.....	97
Fig. 82: Micrograph of Pt particles on CNFs (10,000 magnitude)	97
Fig. 83: TEM image of Pt particles.....	98
Fig. 84: TEM image of Pt particles on CNFs	98
Fig. 85: Micrograph of Pt particles on CNFs - fracture of a sample.....	98
Fig. 86: Cross section of a Pt/CNF based electrode.....	99
Fig. 87: Polarisation curve of a Pt/CNF based MEA sample.....	101
Fig. 88: Tafel approximation for Pt/CNF based MEA.....	102
Fig. 89: Long-term test of a Pt/CNF based MEA	103
Fig. 90: Current density distribution of Pt/CNF based MEA	104
Fig. 91: Deviation of measured current density from arithmetic average current density for 2, 4 and 6 A load current	105
Fig. 92: Polarisation curves of MEAs containing Pt/CNF based anodes with varying Nafion® content.....	107
Fig. 93: Polarisation curves of selected MEA samples with and without Nafion® content within the catalyst layer	107
Fig. 94: Comparison of MEAs containing anodes based on CNFs depending on the graphitisation degree	110
Fig. 95: SEM study of Pt/CNF based electrode depending on current density for Pt particle electro deposition (AA 100 magnitude, i = 0.1 A cm ⁻² ; AB 1,000 magnitude, i = 0.1 A cm ⁻² ; AC 20,000 magnitude, i = 0.1 A cm ⁻² ; BA 100 magnitude, i = 0.2 A cm ⁻² ; BB 1,000 magnitude, i = 0.2 A cm ⁻² ; BC 20,000 magnitude, i = 0.2 A cm ⁻² ; CA 100 magnitude, i = 0.5 A cm ⁻² and CB 100 magnitude, i = 0.5 A cm ⁻² ; CC 20,000 magnitude, i = 0.5 A cm ⁻²).....	112
Fig. 96: CV diagram of selected electrode samples (after 100 cycles)	113
Fig. 97: Polarisation curve of an optimised MEA based on Pt/CNF electro catalyst	115

LIST OF TABLES

Tab. 1: Gas concentration of selected GHGs and their impact on anthropogenic induced global warming [2, 4]	13
Tab. 2: : Specific surface area of selected carbon support materials used in PEMFCs, data taken from [72 – 78]	29
Tab. 3: Properties of investigated carbon fibres	69
Tab. 4: Contact angle of oxygen plasma activated CNFs with plasma power of 150 W depending on treatment time	70
Tab. 5: Contact angle and surface energy of plasma activated CNFs depending on different plasma parameters	70
Tab. 6: Graphitisation degree of selected GDL samples.....	73
Tab. 7: In plane resistance of selected GDL samples	74
Tab. 8: Through plane resistance of selected GDL samples.....	74
Tab. 9: Results from TGA for Pt/C based electrodes	85
Tab. 10: Graphitisation degree of typical Pt on carbon blacks electro catalysts in comparison to CNFs	86
Tab. 11: Corrosion current of investigated PEMFC electrode samples.....	86
Tab. 12: Electrochemical active surface area for standard Pt/C based electrodes ..	88
Tab. 13: Platinum loading depending on pulses and CNT loading	94
Tab. 14: Results from XRF and TG analyses of selected electrode samples depending on CNF loading	100
Tab. 15: Results from Tafel approximation	103
Tab. 16: Graphitisation degree of investigated CNF raw material	109
Tab. 17: In-plane and through-plane resistivity of electrode samples depending on CNF coating	109
Tab. 18: Platinum loading for investigated electrode samples	109
Tab. 19: Results from XRF and TG analyses of selected samples depending on plasma treatment	112
Tab. 20: Electrochemical surface area of selected electrode samples depending on plasma treatment	114

1. INTRODUCTION

The natural greenhouse gas (GHG) effect causes mild climatic conditions on the earth's surface with a global mean temperature of about 15 °C. Without natural GHGs solar radiation would heat up the surface to just -18 °C. It is likely that development of human life would not have taken place under these harsh conditions [1 – 2]. The natural warming effect is explained by the atmosphere's permeability for short-wave radiation and the absorption of infrared radiation by gas molecules with at least three atoms. Infrared radiation emitted from the earth's surface is absorbed by these GHGs and reflected again. This effect stores thermal energy in the atmosphere. Gases belonging to the GHGs are amongst others carbon dioxide (CO₂), nitrous oxide (N₂O), methane (CH₄), ozone (O₃) and steam (H₂O) which are cycled naturally over various mechanisms [2–3].

For a time period of about 10,000 years the concentration of CO₂ was constant at a level of 100 ppm of the world's atmosphere. Since the beginning of the industrial revolution in the late 18th century CO₂ concentration has been raising rapidly due to the combustion of carbon based energy carriers and extensive agriculture. Furthermore, gases like chlorofluorocarbons (CFC), which had no share in the atmosphere before industrialisation, are emitted by industrial processes and have negative influence on the environment [3].

The use of CFCs, e.g. as cooling medium in refrigerators within the last century results in an increase of near-surface ozone (O₃). This increased concentration damages the environment, especially forests are affected. A similar effect is known due to sulphur dioxide (SO₂) pollutions. Harmed trees and other plants produce less biomass from photosynthesis of atmospheric CO₂. This leads to further CO₂ accumulation in the atmosphere. Furthermore, CFCs damage the ozonosphere which absorbs the energy-rich ultraviolet radiation. As a result the earth's surface is further heated. The use of CFCs has been forbidden in most countries since the 1990'. However, due to the very long residence time in the atmosphere, CFC concentration reduces slowly. Alternatives for CFC belong to the group of GHGs that absorb infrared radiation more effective than CO₂, CH₄ and N₂O. Concentration of selected GHGs is shown in Tab. 1. All these effects which lead to an increase of global mean temperature are known as anthropogenic induced global warming [3–4].

Tab. 1: Gas concentration of selected GHGs and their impact on anthropogenic induced global warming [2, 4]

Gas	Preindustrial concentration [ppm]	Concentration in 2005 [ppm]	Impact on the anthropogenic induced global warming [%]
CO ₂	280	379	50 – 60
CH ₄	0.71	1.74	19 – 20
N ₂ O	0.3	0.314	5 – 6
CF ₄	0.00004	0.000074	-
CFCs	-	about 0.00025	up to 10 (all CFCs together)

Although CO₂ does not have the highest potential for infrared absorption, the increase of the world's mean temperature is mainly due to the high CO₂ emissions by industrial as well as private combustion processes. Therefore, GHGs are normalised according to their equivalent global warming potential of CO₂. Conversion factors for the most important GHGs according to their CO₂ equivalent for a residence time of one hundred years according to the Intergovernmental Panel on Climate Change (IPCC) are: 1:1 (CO₂), 1:21 (CH₄), 1:296 (N₂O), 1:2,000 (near-surface O₃) and 1:5,700 (CF₄) [5].

Anthropogenic induced CO₂ emissions are identified to be responsible for the global increase of mean temperature which has been shown in scientific documents by the IPCC. Although, results of these IPCC studies are discussed controversially the climatic impact due to anthropogenic CO₂ emissions is widely accepted. Predictions for the future development of the global climate change and the consequences of further global warming are also discussed in detail by the IPCC. Examples are melting of the polar ice shields, increasing sea levels as well as more extreme weather phenomena all over the world. However, the complex topic of consequences by anthropogenic global warming is not part of this work and will not be discussed further. Additional information is given by the IPCC [6].

In order to minimise anthropogenic impact on global climate governments all over the world started regulation of GHG emissions. Annually the contract parties (conference of the parties – COP) negotiate within the United Nations Framework Convention on Climate Change (UNFCCC) how to result in global GHG regulations. In 1997 the first international climate treaty was adopted within this framework and it is ratified by high number of parties of the COP in 2005. This contract is known as the Kyoto Protocol with the binding target to reduce in mean 5.2% of the GHG emissions referred to the year 1990 of selected 38 participating countries till 2012. E.g. Germany as single contract partner committed to reduce its emissions by 21% and resulted in a reduction of about 24%. Scope of this contract was limited to the year 2012 but a serious problem of this contract is due to the fact that the main global polluter (USA, China and India) are no participating. No further treaty could yet be established. However, a general admitted document, known as the Copenhagen Accord, was prepared in 2009. In this Accord some parties of the COP stated that global warming should be limited to 2 °C referred to the preindustrial level and GHG concentration should not exceed 450 ppm CO₂ equivalent. The last climate conference (2014) was in Lima, Peru with the aim to prepare a global contract subsequent to the Kyoto Protocol [1, 7, 8].

1.1. Electricity Generation and Storage

The main energy carriers used for electricity generation in power stations are hard coal, lignite, methane (natural gas), oil and uranium. The combustion of carbon based energy carriers leads to CO₂ emissions. Fundamental stoichiometric reaction equations for the oxidation of carbon and methane are:



In 2008 two thirds of the world's electricity generation is based on combustion of carbons. 40 % of the global CO₂ emissions results directly from electrical power generation. The International Energy Association (IEA) predicts, that the global electricity generation will at least be doubled by 2050. In order to prevent further global warming due to CO₂ emissions it is common sense, that prospective solutions for electricity generation need to be CO₂ free and environmental friendly [9, 10].

In 2010 the German government published a strategy how to transform the carbon and uranium based German energy sector into a renewable one. With this step Germany wants to contribute to the Kyoto Protocol as well as to the Copenhagen Accord. Furthermore, it is obvious that this concept has been developed under the aspect of German dependency on energy imports. However, this so called „Energiewende“ is a long term concept with the aim to increase the share of electricity generation by renewable sources (mainly water, wind and solar power) as well as to reduce GHG emissions to prevent increasing of global concentrations above the 450 ppm CO₂ equivalent. It is pronounced that in 2020 GHG emissions will be reduced by 40% and in 2050 by 80% according to the reference emission level from 1990. Furthermore, in 2050 the share of electrical energy generated by renewables should be at least 80% [11].

The transformation of the German energy sector started earlier in the late 1990s. With subsidies, advantageous feed-in rules and decreasing capital costs for wind turbines and photovoltaic modules, installed peak power for electricity generation from volatile renewables increased rapidly. In 2013 the installed solar and wind power capacity exceeded 60 GW which is about 30% of the total installed peak power. But the share on the gross electrical energy generation is 8.2% for wind turbines and 4.9% for photovoltaic modules. However, wind turbines and photovoltaic modules, to some extend also water turbines, are highly dependent on the actual weather situation. This is indicated by the poor capacity factor of renewable power generation which gives information about the ratio of generated electricity to the potential amount generated in case of operation at rated power for 8,760 hours (100%) per year. For 2013 mean capacity factor of photovoltaics in Germany is about 10%. For wind turbines mean capacity factor is in the range of 18%. In comparison, the capacity factor of nuclear power stations in Germany is about 87% as operation of nuclear power stations is stopped just for few days a year for maintenance reasons. [2, 12–14].

Electrical energy is traded at the European Energy Exchange (EEX) in Leipzig [15]. Due to unfavourable conditions (e.g. imprecise prediction), prices for electricity turn negative. Different aspects need to be taken into account to explain this phenomenon. One explanation is that in times of higher energy generation by renewables than predicted, there is too little load connected to the electrical grid than needed to consume this additional energy. In such periods operators of electrical units pay a negative price to connect their consumer to the grid immediately. In contrast to

this, periods with very high prices for electricity occur in times when less power is supplied to the grid than predicted, e.g. due to an unexpected change in weather pattern (low wind or solar radiation) [16, 17]. In order to compensate volatile power generation, conventional power plants are controlled. However, to succeed in transforming the German energy sector by further increasing the share of renewable energies, a huge effort has to be made in improving such control strategies as well as in extending electrical energy storage.

Especially lignite and nuclear power stations cannot operate in partload mode and power output of hard coal and gas fired power stations can be reduced just to a certain extent. Therefore, large storage systems are integrated within the electrical grid to compensate fluctuating power supply. In Germany installed capacity for pumped hydro storage is about 7 GW. A demonstration unit for compressed air storage has a power output of 0.3 GW. However, the compressor of this power plant consumes just 60 MW so that negative power supply is negligible [18]. Unfortunately, there are few locations in Germany for further pumped hydro or compressed air storage. Therefore, extending the storage capacity by installing a large number of further units in Germany is unlikely.

In comparison to centralised energy storage with high power output, decentralised small scale storage systems can be a solution to compensate fluctuating feed-in by renewables. However, a large number of units distributed all over the grid is needed. Research and development concerning battery systems has been intensified within the last decade. Battery technology emerged to be appropriate for mobile as well as for stationary applications. This is indicated by an increasing number of electrical vehicles on the roads and demonstration projects for small and mid-size battery storage systems. However, problems occur due to poor storage capacity. State of the art battery systems which can be integrated into the electrical grid offer power output in the range of some megawatt but for only few hours. Therefore, batteries are meant to be suitable for short-term storage systems.

Hydrogen as environmental friendly energy carrier is thought to be a solution for long-term energy storage. Producing hydrogen (H_2) and oxygen (O_2) in water electrolyzers is a potential technology for using excess energy in periods of low demand or excess energy supply by renewables, respectively [19]. In some locations all over the world electrolyser systems with a power consumption in gigawatt range are in operation. Often alkaline electrolyzers are utilised which offer high efficiency above 75 %. However, these plants produce H_2 and O_2 continuously. In order to integrate electrolyzers into the electrical grid for discontinuous operation dependent on volatile energy generation by renewables, the focus of research and development is set on polymer electrolyte membrane (PEM) electrolyzers. Small scale as well as large scale applications have been investigated recently. Storing large amounts of hydrogen in caverns under ground and transportation of it in pipelines is shown at few locations worldwide [20]. Furthermore, storing H_2 in gas bottles (up to 700 bar), in cryo tanks (below 20 K) or in metal hydride containers (adsorption of hydrogen on metal surfaces) is well known for small amounts of H_2 .

By generation of electrical energy in times of high demand and low feed-in by renewables, stationary fuel cell systems can be powered with H_2 and O_2 or air (about 21% O_2). Due to high power density and dynamic part load operation PEM based fuel cell systems are appropriate for this purpose [21, 22]. Furthermore, unlike Carnot processes, efficiency of fuel cells is very high at ambient temperatures. For low temperature PEM fuel cells (operation below 80 °C) efficiency referred to electricity generation may be higher than for mature combined cycle gas turbines which is about

60%. However, waste heat of fuel cells may also be used in order to improve hydrogen utilisation.

Demonstration projects in Germany, which prove concepts with combined renewable energies, electrolyseurs and fuel cells like 'H2 Herten' or 'Falkenhagen', started operation within the year 2014 [23 – 24]. In 2011 the 'Nationale Organisation Wasserstoff' (national organisation for hydrogen in Germany - NOW) calculated the demand for hydrogen energy systems as positive (0.8 GW to 5.25 GW) and negative supply for varying power demand (0.68 to 4.3 GW) for the German energy economy in 2025 [25]. This indicates the potential of electrolyseur and fuel cel technology in Germany.

Research on polymer electrolyte membrane fuel cells (PEMFC) has been carried out since the 1960s. Today, results achieved show feasibility of PEMFC modules with power output in the range of up to 1 MW [21]. However, commercialisation of PEMFCs is poor and fuel cells still remain a matter of research. Main aspects are, amongst others, long term stability, catalyst utilisation, alternative non-noble catalysts, and upscaling of small devices in order to result in large scale units in the range of conventional power stations. This Ph.D. thesis contributes to the main research questions on PEMFCs.

2. STATE OF THE ART OF POLYMER ELECTROLYTE MEMBRANE FUEL CELLS

Fuel cells are devices which directly convert chemical energy of continuously supplied fuel and oxidant to electrical energy. In terms of operation with pure H_2 and O_2 /air the reaction product which evolves is water. Furthermore, fuel cells deliver heat due to internal losses. This makes fuel cells a possible solution for environmental friendly combined heat and power (CHP) systems.

In the middle of the 19th century the German scientist Christian Friedrich Schönbein discovered the effect that a voltage can be measured between two platinum wires held in an acid electrolyte where one wire is flown around by hydrogen (anode) and the other by oxygen (cathode). Together with the Welsh inventor Groves the first fuel cell design was developed. In Fig. 1 schematic drawing of this fuel cell apparatus is shown (A). The reverse operation, when sufficient voltage is applied to the same system, is shown schematically in Fig. 1 (B). However, history shows that for decades after inventing fuel cells more attention has been set on electricity generation by steam turbine driven dynamos, which still is the main source for electrical energy today [26 – 28].

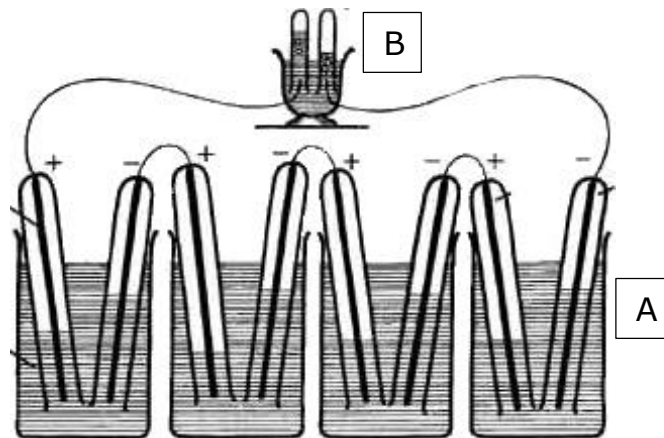


Fig. 1: Schematic drawing of the first fuel cell system [28]

One of the first commercial applications for fuel cells was the on-board power supply of space vehicles of the NASA's space programs. For the Gemini program in the 1960's the company General Electric (GE) developed fuel cells based on a proton exchange membrane (PEM). This membrane has the function of a solid electrolyte. However, while technical problems with GE's polymer electrolyte membrane fuel cell (PEMFC) encountered with the Gemini program, alkaline fuel cells (AFC) have been used at the Apollo program where astronauts have travelled to the moon [28].

2.1. Thermodynamics and Kinetics

The interest in fuel cell technology arises not only from carbon dioxide free exhausts but also from theoretical efficiency at ambient temperatures as well as from compact and modular design. The theoretical efficiency of hydrogen and oxygen operated fuel cells can be calculated from the enthalpy of reaction ΔH_R and the free reversible Gibbs enthalpy ΔG . The following equations 2-1 to 2-10 refer to the references [26 – 32]. Enthalpy of reaction is given by the chemical reaction equation



and according to the Hess law of constant heat summation the equation for ΔH_R

$$\Delta H_R = \Delta_B H_{RH_2O} - \Delta_B H_{RH_2} - \frac{1}{2} \Delta_B H_{RO_2} \quad (2-2)$$

where $\Delta_B H_{RH_2O}$ is the enthalpy of formation of water equal to -286 kJ mol^{-1} , $\Delta_B H_{RH_2}$ is the enthalpy of formation of hydrogen and $\Delta_B H_{RO_2}$ is the enthalpy of formation of oxygen. The enthalpy of formation of pure elements, which are stable at standard test conditions¹ (STC) like H_2 and O_2 , is equal to zero [32]. Therefore, ΔH_R is equal to -286 kJ mol^{-1} under STC and with the product water being in liquid phase. For negative values of ΔH_R chemical reaction is exothermic, which means energy can be consumed by the reaction of hydrogen with oxygen. This enthalpy of reaction is also known as higher heating value (HHV) of H_2 . In comparison to this, lower heating value (LHV) and respectively the enthalpy of the chemical reaction described by (2-1) with the product water being in gaseous phase is equal to -242 kJ mol^{-1} . As in general fuel cell exhausts are in gaseous phase the following calculations refer to the LHV of hydrogen.

ΔG is given by

$$\Delta G = \Delta H_R - \Delta S_R \cdot T \quad (2-3)$$

where ΔS_R is the entropy of reaction which is approximately $44 \text{ J mol}^{-1} \text{ K}^{-1}$ for (2-1) if the product water is in gaseous phase and T is the process temperature. Hence, ΔG_{LHV} is equal to -228 kJ mol^{-1} at STC. However, ΔG_{LHV} and ΔH_{RLHV} are dependent on operation temperature and pressure. Assuming the conversion of free reversible enthalpy completely into electrical energy the reversible fuel cell potential E_0 at STC can be calculated by

$$E_0 = \frac{\Delta G}{z \cdot F} \quad (2-4)$$

where z is the number electrons, passed through an external circuit per mole of hydrogen reacted within the fuel cell, equal to 2, and F is the Faraday constant, equal to $96,485 \text{ A sec mol}^{-1}$. Hence, E_0 is equal to 1.18 V. Referring to the enthalpy of reaction ΔH_{RLHV} the maximum possible efficiency $\eta_{\text{maxFuelCell}}$ can be calculated by:

¹ Standard test conditions are defined at $T = 25 \text{ }^\circ\text{C}$ and $p = 1.013 \text{ bar}$

$$\eta_{\max \text{FuelCell}} = \frac{\Delta G}{\Delta H_R} = \frac{-228 \text{ kJ mol}^{-1}}{-242 \text{ kJ mol}^{-1}} = 0.94 \quad (2-5)$$

With a maximum theoretical efficiency of around 94 % at room temperature fuel cell technology is one of the most efficient for energy conversion into electricity. Fig. 2 shows the differences in maximum theoretical efficiency of fuel cells in comparison to combustion processes according to the Carnot efficiency calculated by

$$\eta_{\text{Carnot}} = 1 - \frac{T_0}{T} \quad (2-6)$$

where T_0 is equal to 25 °C (ambient temperature) and T is the process temperature. It becomes obvious that theoretical efficiency of fuel cells drops with increasing process temperature due to increasing ΔS_R . Especially, for low temperatures theoretical maximum efficiency of fuel cell processes is superior over combustion processes.

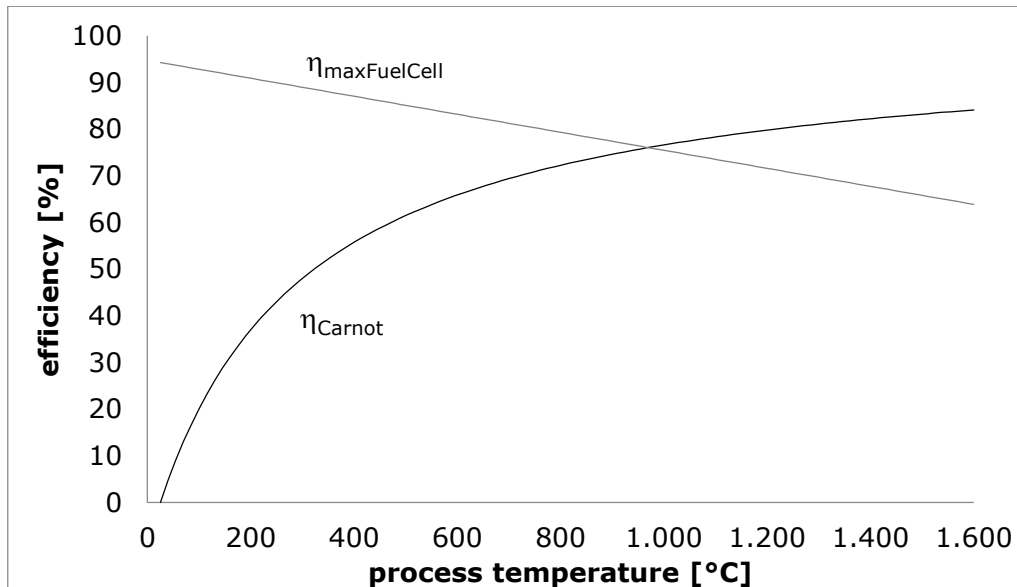


Fig. 2: Theoretical efficiencies of Carnot and fuel cell processes

The reversible fuel cell potential E_0 is the equilibrium potential at STC. However, like ΔG and ΔH_R the equilibrium potential is temperature and pressure dependent. The Nernst equation for H_2/O_2 reaction with product water evolving as steam takes account of these dependencies and is given by:

$$E = E_0 + \frac{R \cdot T}{z \cdot F} \cdot \ln \left(\frac{p_{\text{H}_2} \cdot p_{\text{O}_2}^{0.5}}{p_{\text{H}_2\text{O}}} \right) \quad (2-7)$$

where E is equal to the equilibrium potential at process environment, p_{H_2} is the partial pressure of hydrogen, p_{O_2} is equal to the partial pressure of oxygen and $p_{\text{H}_2\text{O}}$ is equal to the partial pressure of steam [30]. However, Nernst equation

describes the reversible fuel cell potential at open circuit conditions when power output is zero.

Losses which occur with the electrochemical reactions or due to the electrode design limit the potential when a fuel cell is under load. The PEMFC voltage U , which is measured between anode and cathode, follows a typical behaviour with increasing load current. Fig. 3 shows this typical polarisation curve of a H_2 /air operated PEMFC at STC.

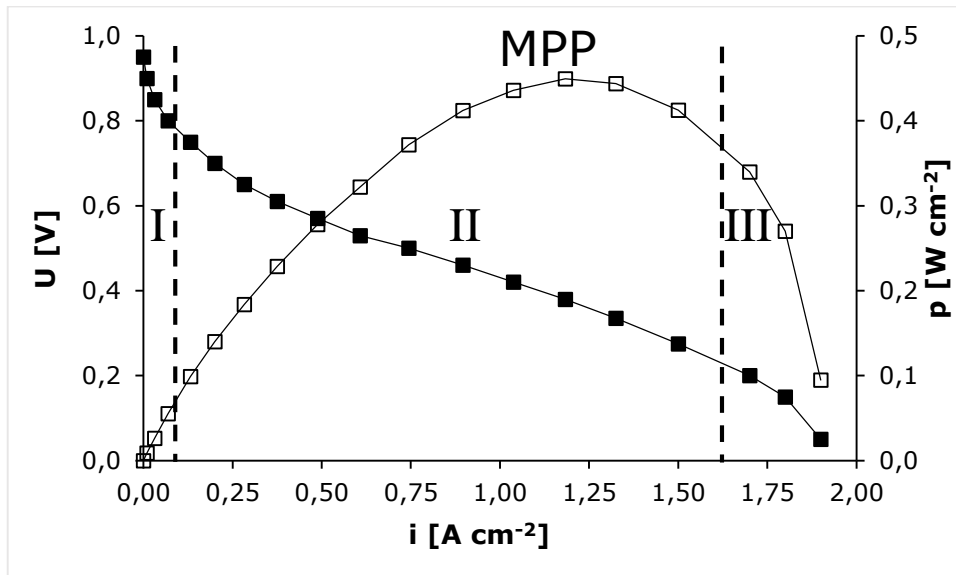


Fig. 3: Typical polarisation curve of a H_2 /air operated PEMFC

For a better comparison of different fuel cells current I is expressed relatively to the fuel cell's geometrical electrode area A as current density i [$A\ cm^{-2}$] given by:

$$i = \frac{I}{A} \quad (2-8)$$

From the diagram one can determine that U_{oc} is in the range of 1 V which results mainly from operation with air instead of pure oxygen and, furthermore, from the electrode's material composition (mixed potential). However, at fuel cell operation three different mechanisms decrease cell voltage with increasing current, known as overpotential. The diagram can be divided into three main areas (I, II and III) according to these overpotential mechanisms.

- I. For small load currents (below a few $mA\ cm^{-2}$) voltage drops rapidly. This voltage drop is mainly caused by activation polarisation U_{act} . Which means overpotential results from the reaction kinetics and the need to transfer electrons as well as break and form chemical bonds at the surface of catalyst particles within the electrodes.
- II. The voltage drop due to internal electrical resistance and electrolyte resistance (ohmic polarisation U_{ohm}) is nearly linear to the increase of load current.

- III. Voltage drop at high current densities (near to short circuit) occurs from mass transport or mass concentration limitations. The concentration polarisation U_{con} is due to a drop of concentration of oxygen and hydrogen as they are consumed by the reaction.

Other losses which can occur at fuel cell operation arise e.g. from gas leakage or internal electrical short circuits. However, design considerations especially to gasket can solve these problems. Furthermore, electron transfer and gas diffusion through the electrolyte is possible, but this effect is from minor importance for fuel cell performance. In sum, the measured fuel cell voltage at operation results from the subtraction of all overpotentials from the open circuit voltage U_{oc} .

$$U = U_{\text{oc}} - U_{\text{act}} - U_{\text{ohm}} - U_{\text{con}} \quad (2-9)$$

The fuel cell's efficiency η_{FuelCell} at certain load points can then be estimated by the following equation:

$$\eta_{\text{FuelCell}} = \frac{U \cdot z \cdot F}{\Delta H_{\text{R}}} \quad (2-10)$$

Although theoretical efficiency is very high for low temperatures, practically low temperature fuel cell systems run at rated power with an output voltage of about 0.6 V. According to (2-10) this voltage results in an efficiency of about 50 % (according to the thermodynamic maximum at STC). For the polarisation curve shown in Fig. 3 maximum power point (MPP) is determined for an output voltage of about 0.4 V, which corresponds to an efficiency of about 33 %. Commercially available fuel cell based CHP systems for households offer electrical efficiency of about 60 % [33] which means systems are operated in part load.

2.2. PEM Fuel Cell Design

The main component in PEMFCs is the membrane electrode assembly (MEA). MEAs for PEMFCs consist of an ions conducting but electrical insulating membrane, which is in touch with catalytic material from both sides and, furthermore, an electrical conducting gas diffusion layer (GDL) on the anode as well as on the cathode side. Such a MEA is placed between two pole plates with gas channels (flow field). Together these components form a single fuel cell (Fig. 4) [27].

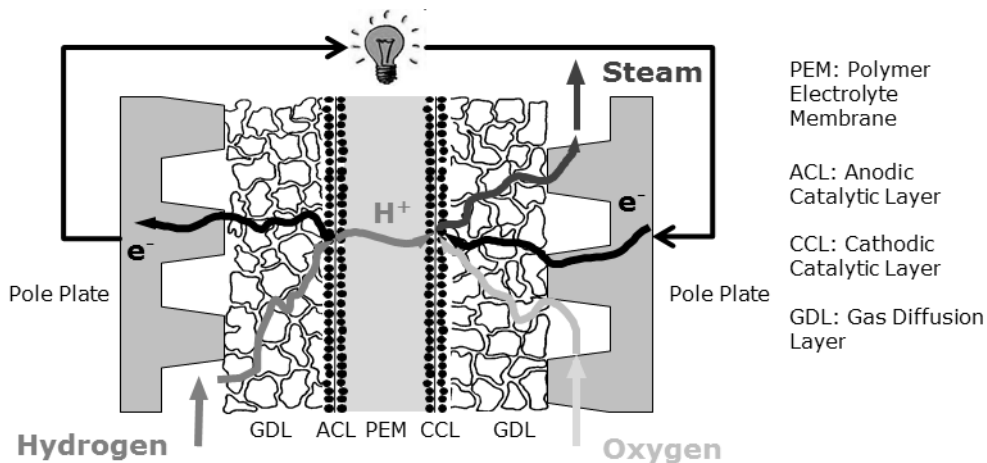


Fig. 4: Schematic drawing of a PEMFC's cross section

At operation H₂ and O₂ or air (about 21 % O₂) are supplied over the flow field and finely distributed to catalyst particles due to the high porosity of a GDL. In PEMFCs with proton conductive membrane H₂ is delivered to the anode and O₂ is delivered to the cathode, where product water evolves. PEMFCs belong to low temperature fuel cells with an optimal operating temperature of about 60 to 80 °C. However, start-up procedures at temperatures below freezing point of water has been shown as well as operation at temperatures above 100 °C [34].

2.2.1. Pole Plate

MEAs are cased between two electrical conductive pole plates. Typical materials for pole plates in PEMFCs are graphite composites or (stainless) steel. Usually, graphitic pole plates are manufactured by milling. This makes it an ideal material for prototyping or lab scale applications. For mass production hydroforming of metal sheets is more cost effective [35]. However, material stability is a serious issue with metallic pole plates as corrosion products can degrade the polymer membrane. Noble metal coatings e.g. achieved by electro plating are an efficient method to decrease electrical contact resistance as well as corrosion rate but costs for noble metal coatings are high. Corrosion of graphitic pole plates is negligible due to very slow reaction kinetic of carbon und PEMFC operation conditions² [36]. A promising alternative technique to produce graphitic pole plates is injection moulding of carbon composite material. Injection moulding leads to higher production rates in

² Compare to chapter 2.2.6. PEM Fuel Cell Durability

comparison to milling [29, 37]. Examples for pole plate are shown in Fig. 5, Fig. 6 and Fig. 7.

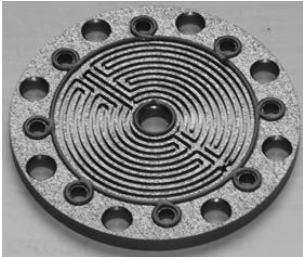


Fig. 5: Milled graphitic pole plate

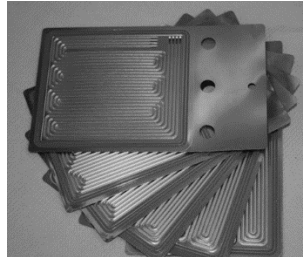


Fig. 6: Metallic pole plates with noble metal coating



Fig. 7: Injection moulded graphitic pole plate (with friendly permission of the Zentrum für BrennstoffzellenTechnik [37])

A MEA is embedded into this casing in a way that a gasket ensures safe operation. Gas leakage, especially of H_2 , can cause dangerous environment due to formation of explosive oxyhydrogen gas³. This is a safety issue outside the fuel cell but also problematic with gas crossover, where chemical reactions catalysed by platinum particles lead to local temperature increase. Those hot spots may puncture the membrane which results in rapid cell degradation, in most cases. Furthermore, leakage causes unwanted fuel losses which decreases fuel utilisation.

In order to provide necessary gases a flow field is shaped into the pole plate. The flow field is the main gas path. Often a serpentine channel design is used to distribute gas over the active cell area. However, various flow field designs are possible. Examples may be found from [38]. To optimise gas distribution to the catalyst particles as well as to minimise pressure drop, channel diameter is as large as possible. However, land dimensions need to be sufficient for optimal electrical connection between pole plate and GDL as in the channel areas GDL material is not sufficiently compressed (Fig. 8). Therefore, the ratio between land and channel needs to be optimised. Furthermore, a pocket can be formed into the pole plate for GDL positioning.

³ Explosion limits for H_2 in air: 4 Vol.% - 75 Vol.%

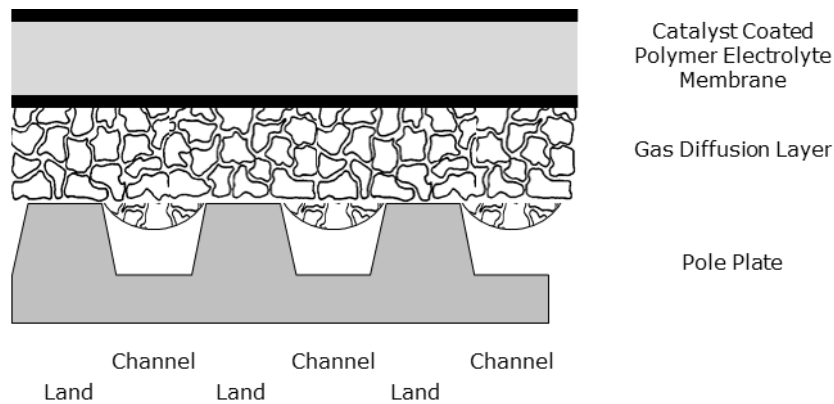


Fig. 8: Schematic drawing of the interface between flow field and gas diffusion layer in cross section

2.2.2. Gas Diffusion Layer

GDLs are gas permeable, electrical conductive and compressible due to their three functions:

- I. Media exchange
- II. Electron transfer
- III. Absorption of compression forces⁴

In order to provide H_2 and O_2 to the catalyst layer (CL) of an electrode, a GDL finely diffuses gas from the flow field to the electrochemical active catalyst particles. Due to the macro porosity of a GDL (pore size is about 20 to 50 μm) H_2 and O_2 can be distributed in plane to areas which are covered by the flow field's land. Gas diffusion is further improved by thin micro porous layers (MPL) with much smaller pore size in the range of 0.1 to 0.5 μm at the surface between GDL and CL. This ensures distribution to the whole active cell area. Porosity of commercially available GDLs is in the range of 70 to 80 % [27]. Furthermore, it is necessary to prevent GDLs from water flooding which would decrease porosity and hinder gas diffusion. Therefore, the solid phase of a GDL is treated with hydrophobic material like polytetrafluoroethylene (PTFE) to provide channels for water removal from the CL to the flow field. Usually the MPL is highly hydrophobic. Over the main gas path water droplets and steam are removed from the electrode.

In state of the art PEMFCs carbon fibre based GDL is used. Carbon fibres are heat treated at about 2,000 $^{\circ}C$ to increase graphitisation and, therefore, electrical and thermal conductivity of the material. High electrical conductivity reduces voltage drop due to electron transfer through the fuel cell's electrodes. As thickness of GDLs is in the range of 200 to 400 μm through plane conductivity contributes less to internal cell resistance. More importance is concerning contact resistance between GDL and flow field as well as between GDL and CL. Contact resistance is mainly dependent on flow field design and in-plane GDL conductivity. In order to reduce contact resistance compression forces are applied to the fuel cell. It is necessary that the GDL is soft and flexible to absorb these compression forces without losing to much of their porosity.

⁴ Compare to chapter 2.2.6.

Depending on the applied GDL type, while operation a GDL is compressed to about 75 % of its original thickness [39 – 41].

Literature distinguishes two main sorts of carbon based GDL – carbon fibre paper and woven carbon cloth (Fig. 9 and Fig. 10). Metallic GDLs are also known e.g. meshes or felts from corrosion resistant metals like titanium. However, these are often used in PEM electrolyzers instead of in PEMFC [42].

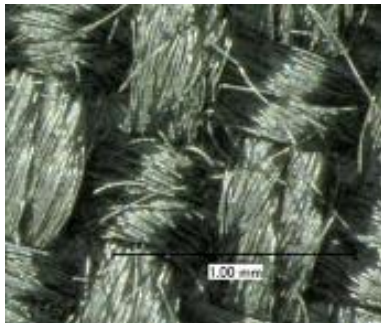


Fig. 9: Microscopy of carbon cloth

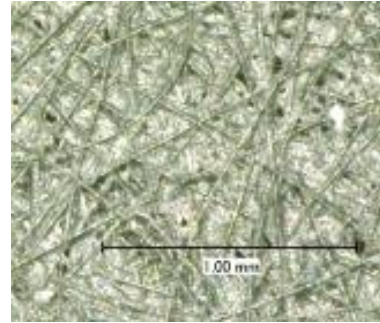


Fig. 10: Microscopy of carbon fibre paper

Carbon paper is stiff in comparison to carbon cloth. Compressive stress in the range of 25 bar results in compressive strain of about 25 % for carbon paper and of above 30 % for carbon cloth [27]. The high compression pressure maintains low electrical contact resistance which makes carbon paper superior in terms of internal cell resistance. Contrariwise, processing the carbon paper raw material is difficult as it is brittle. The carbon cloth is rather flexible and raw material can be processed from a coil.

2.2.3. Polymer Electrolyte Membrane

In order to fulfil the function of a solid electrolyte, membranes used for low temperature PEMFCs are required to be ions conducting but electrical insulating, stable to heat, oxidation and hydrolysis as well as impermeable for gases. The material studied most intensively is perfluorinated sulphonic acid (PFSA) which is commercially available e.g. from Asahi Glass Co., Japan, Asahi Chemical Co., Japan and DuPont, USA. The product name of membranes from DuPont is Nafion®. Nafion® is protons conductive and thermally stable up to 80°C. Gas permeation from anode to cathode and vice versa is negligible for fuel cell operation if gases are provided with low overpressure referred to atmospheric conditions [27].

There are few manufactures worldwide supplying membranes for fuel cell applications. Amongst others the company Gore® supplies PEMFC MEA components, where the membrane is a chemical variation of PFSA [43]. Furthermore, anion exchange membranes are known but have limited access to the commercial market due to stability issues [44]. In this chapter PFSA membranes are described in more detail.

The transport mechanism for hydrogen cations through a PFSA membrane is the Grotthuss effect which describes proton transfer via a vehicle mechanism (Fig. 11). Hydronium ions (H_3O^+) exchange their positive charge with adjacent water molecules in order to be transported from anode to cathode [30]. Furthermore, protons transport is affected by diffusion and convection of species within the membrane material [27]. Therefore, protons conductivity is highly dependent on water content

of the membrane material. PFSA membrane consists of a hydrophobic main chain with hydrophilic sulphonic acid groups which attract water molecules.

By means of providing conductivity a membrane's water uptake is assumed to be in the range of at least four to six water molecules per sulphonic acid group. However, at 100% relative humidity of the feed gases water uptake is about twenty water molecules per sulphonic acid group which results in about 15 wt.-% weight increase for Nafion® referred to a dry membrane. Protons conductivity is best for completely humidified membranes. For Nafion® membranes conductivity is in the range of 0.1 S cm^{-2} . However, for less humidified membranes conductivity is one to two magnitudes lower. Furthermore, protons conductivity is affected by temperature. Conductivity is increased at higher temperatures.

For cell design it has to be taken into account that water uptake results in considerable swelling of the membrane. This leads to changing compression conditions which may affect functionality and may need considerations concerning cell design [27, 43]. Protons conductivity is also dependent on membrane thickness. Typically, membranes used in PEMFC have a thickness of 20 to 200 μm . Thinner membranes with a thickness below 25 μm have higher conductivity, however, mechanical stability is decreased and gas cross over is increased. This effect needs also to be considered concerning cell design [45].

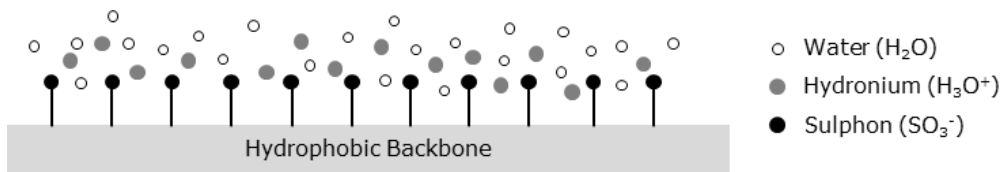


Fig. 11: Schematic drawing of protons transport mechanism through PFSA

There are mechanisms in PFSA membranes which result in water transport when a fuel cell is operated. The main contributor to water uptake is H_2O generation on the cathode side. According to Faraday's Law

$$\dot{n} = \frac{I}{z \cdot F} \quad (2-11)$$

where \dot{n} is the number of molecules generated in mol sec^{-1} , H_2O formation is linear to operation current [30]. However, each proton transported from anode to cathode drags water molecules in the same direction. This flux of water molecules is known as electroosmotic drag and it is dependent on water content in within the membrane. Both mechanisms result in large concentration gradient from anode to cathode. This gradient contrarily leads to water back diffusion from cathode to anode. Furthermore, pressure difference between anode and cathode may also result in water transport which is not caused by one of the previously explained mechanisms. Summarised, it becomes obvious that intelligent operating strategies concerning current control, humidification and gas pressure are needed, in order to result in optimal membrane performance [27].

2.2.4. Catalytic Layer

The main function of the catalytic layer (CL) is to provide active sites for the electrochemical reactions. According to this, catalytic material is needed in order to break the bonds of gas molecules fed to the fuel cell. Platinum and platinum group metals (PGM) are known to be feasible catalysts due to their ability to increasing the reaction kinetics and their corrosion stability in acid or alkaline environment.

Catalytic properties of a material result in the electrochemical part reactions which happen even at nearly ambient operating conditions. At the anode hydrogen is oxidised (hydrogen oxidation reaction – HOR) and at the cathode oxygen is reduced (oxygen reduction reaction – ORR) [46 – 47]. The entire process leads to the overall reaction equation (2-1).



As electrochemical reactions occur on the surface of catalyst particles, a large active surface within the CL is necessary in order to achieve high power density. Therefore, in current state of the art PEMFCs active surface is increased by the use of carbon supported catalyst nano-particles (< 5 nm) which are structured directly at the interface between the electrolyte membrane and the porous electrode material⁵ [48]. In [49] an up to six times increased electrochemical active surface area has been reported by the use of carbon supported platinum particles in comparison to unsupported platinum blacks.

Structure of a CL is porous as gas molecules are used to diffuse to the catalyst particles. However, for electron transfer catalyst particles need to be connected electrically and, furthermore, for proton exchange catalyst particles need to be in touch with the membrane. This reaction room is known as three phases reaction zone (Fig. 12) [48]. A further aspect refers to hydrophobic and hydrophilic material within the CL which influences water content during operation. Typically, a CL contains a small amount of the membrane material which works on the one hand as binder and on the other hand as proton conducting pathways to utilise catalyst particles within the CL. For proton conductivity reasons the hydrophilic content needs to be humidified. Therefore, in operation the CL must not dry out. However, hydrophobic content may be used by means of water removal, especially, at the cathode side. This is necessary in order to prevent the CL from water flooding which decreases gas flux [50 – 53].

Therefore, an optimum composition of catalytic, electrical conductive, hydrophilic and hydrophobic material is needed to meet the criterions for a high share active reaction sites. In state of the art PEMFCs one main problem is related to those catalyst particles which are situated in the depth of the CL. Deeper particles may remain inactive as they e.g. do not have connection to the membrane or may be covered with polymer which insulates them electrically or hinders gas flux. MEA catalyst loading in commercially available state of the art PEMFC is in the range of 0.5 mg_{Pt} cm⁻². CL architecture for air operated PEMFCs shows power density of 0.5 to 1 W cm⁻² depending on operation conditions. As an indicator for the degree of platinum utilisation, this results in specific power density of 1 to 2 W mg⁻¹_{Pt} [54].

⁵ More information on carbon supported catalysts is given in chapter 2.2.5.

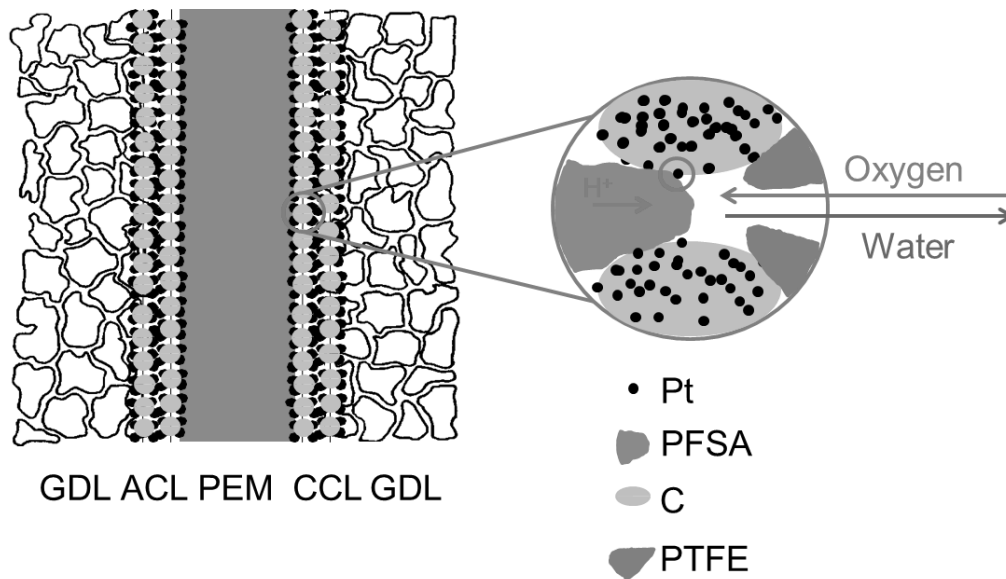


Fig. 12: Schematic drawing of the catalytic layers structure

In order to increase power output or, respectively, to decrease noble metal loading in PEMFCs, research is carried out on advanced CL architectures which improve catalyst utilisation. One followed route describes the synthesis of core-shell-particles which have a non-noble metal or a carbon core and a PGM shell. For an ideal particle only a monolayer of noble metal atoms enclose the core in a way that all noble metal atoms refer to surface atoms. The catalyst particle preparation is often extensive as different complex process steps in liquid chemicals are needed (electrolyte formulation, alloying, leaching, and cleaning). Therefore, core-shell-catalysts remain scientifically interesting [55].

Furthermore, different studies looked on alternative catalysts which may be more cost effective than PGMs like silver, nickel or cobalt [56]. However, these and other materials have been studied but reaction kinetics and/or material stability are poor in comparison to PGMs and high power density as well as long term stability are needed for commercial applications. Therefore, different attempts are discussed which aim on higher specific electrochemical activity referred to platinum (especially for the cathodic CL) e.g. the use of platinum alloys. Investigated platinum alloys involve amongst others, platinum-iridium, platinum-nickel [57], platinum-cobalt [58] or platinum-cobalt-manganese [59 – 60].

Laboratory scale MEAs with ultra-low loading have been reported e.g. in [59, 60]. Here an over $5 \text{ W mg}^{-1}_{\text{catalyst}}$ has been shown, but an experimental nano-structured thin film of platinum-cobalt-manganese alloy was used as catalyst material instead of pure platinum. However, long term stability seems to be an issue for that experimental electrode. Studies performed in H_2/O_2 operation show significantly higher power densities, but this may not be feasible for commercial applications, especially, for mobile applications.

2.2.5. Catalyst Support Materials

Support materials that offer itself a high specific surface area contribute to a large active catalyst surface within the CL. Furthermore, the support material needs to be stable at fuel cell operation and electrical conductive for low-loss electron transfer from (anode) and to (cathode) the catalyst particles. Graphitic nano-particles are favourable for the use as support material for PGM catalysts as these meet the necessary criterions. Graphite is one of the allotropes of the element carbon consisting of hexagonally arranged carbon atoms (honey comb structure) forming graphene layers which are stacked interplanarly to a 3-dimensional structure. In graphite form, carbon atoms are bonded covalently with sp^2 hybridisation. This means there is one free electron remaining which is not part of the hybridisation.

The graphene layers of graphite have interlayer spacing of 0.335 nm (3.35 Å). As a measure for graphene layer parallelism and orientation graphitic materials are categorised referred to their graphitisation degree. For determination of graphitisation degree highly oriented pyrolytic graphite (HOPG) with an angular spread of graphene layers below 1° is often used as reference.

In comparison to the strong inter-atomic bindings, forces between the graphene layers, which hold them together, are relative weak like van-der-Waals forces. As a result it is easy to split graphite along to its graphene layers which makes graphite powder favourable for the use in lubricant solvent. Graphite is thermal stable in atmosphere up to about 400 °C. Due to the 'free' electrons graphite is a good thermal and electrical conductor in the direction of its graphene layers. However, normal to those graphene planes graphite is almost an insulator.

Typically, a platinum on carbon blacks catalyst is reported for PEMFCs [61 – 63]. Here, carbon blacks (e.g. Vulcan XC72 from Cabot) with a particle size of about 40 nm and a specific surface area of about $75 \text{ m}^2 \text{ g}^{-1}_c$ is used as support for platinum crystallites with a particle size in the range of 2 up to 5 nm. Pt/C catalyst powders are commercially available with different Pt to C ratios (10 to 80 wt.-% Pt). In respect to electrochemical active surface area (ECSA) an optimum Pt on carbon blacks ratio has been found for 40 wt.-% Pt [27].

Furthermore, interest is on more graphitised (and less turbostratic) carbon supports like carbon nanotubes (CNT) [64 – 66] or carbon nanofibres (CNF) [67 – 68]. Also graphene sheets have been studied as support material [69 – 70]. However, layers from graphene sheets or graphene flakes may have disadvantageous properties concerning gas flux due to formation of a roof tile structure [69]. CNTs and CNFs show high specific surface area (Tab. 2) and are believed to be superior in comparison to turbostratic graphitic structures (like e.g. carbon blacks). As corrosion resistance against oxygen is higher this makes them favourable, especially, for the use at fuel cell cathodes [71]. More information about CNTs and CNFs is given in chapter 2.2.5.1. Carbon Nanotubes and Carbon Nanofibres.

Tab. 2: : Specific surface area of selected carbon support materials used in PEMFCs, data taken from [72 – 78]

Material	Specific Surface Area [$\text{m}^2 \text{ g}^{-1}$]
Carbon blacks	240 – 1,600
Carbon blacks graphitised	25 – 240
Carbon nanotubes (single wall)	400 – 900
Carbon nanotubes (multi wall)	200 – 400
Carbon nanofibres	130 – 450
Graphene	280 – 640

2.2.5.1 Carbon Nanotubes and Carbon Nanofibres

Carbon nano-filaments like CNTs or CNFs belong to the group of graphitic nano-materials. These have a diameter of up to 100 nm and a length in μm range (Fig. 13). This special aspect ratio results in some unique material properties like very high electrical resistivity ($6 \times 10^{-5} \Omega \text{ cm}$) and thermal conductivity ($30 \text{ W cm}^{-2} \text{ K}^{-1}$) in axial direction (after heat treatment in inert atmosphere at up to $3,000 \text{ }^\circ\text{C}$) [71]. CNTs and CNFs differ in the arrangement of graphene layers. CNTs are composed of one (single wall carbon nanotube – SWCNT) or up to several hundred (multi wall carbon nanotube – MWCNT) graphene layers which are rolled up to a cylindrical tube. These graphene planes are concentric to the filament's axis. Nano-filaments with graphene layers arranged in a different structure e.g. as stacked cups or like helical-ribbon (Fig. 14) belong to CNFs [79].

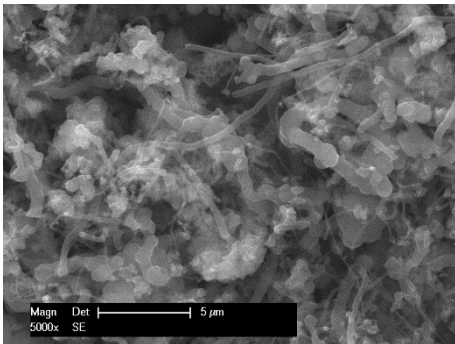


Fig. 13: Micrograph of an unorganised bundle of MWCNTs

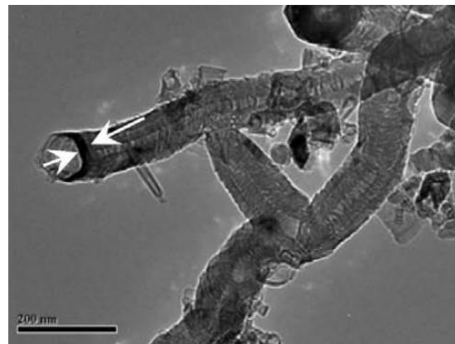


Fig. 14: Micrograph of helical-ribbon like CNFs [79]

Both types of filaments are produced from a catalytic chemical vapour deposition (c-CVD) in reducing atmosphere (hydrogen) at high temperatures up to $1,200 \text{ }^\circ\text{C}$. For this process hydro carbons like acetylene or methane get cracked in the presence of transition metal catalysts (iron, nickel or cobalt). The carbon fraction deposits on the catalyst surface. During the process a filament starts to grow from these catalyst particles. Depending on the process parameters (like feedstock, temperature, pressure or treatment time) a certain type of vapour grown carbon fibres (VGCF) can be produced. For large scale production an organometallic dispersion like e.g. ferrocene ($\text{Fe}(\text{C}_5\text{H}_5)_2$) together with the feedstock is sprayed into a heated fluidised bed reactor. Typically, the catalyst particle remains within the produced carbon filament [79, 80].

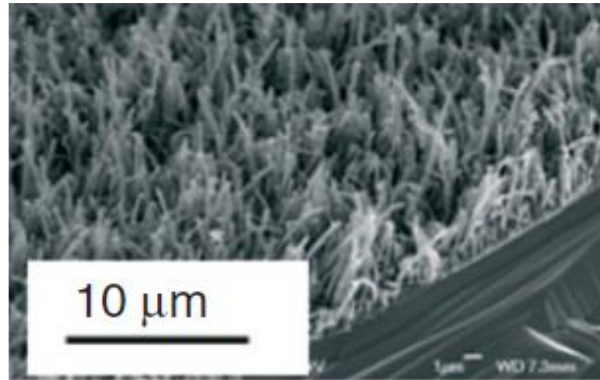


Fig. 15: Vertically aligned CNTs [59]

Different studies already looked on the potential of the use of Pt/CNT or Pt/CNF electro catalysts for the use in PEMFCs. Often, CNTs or CNFs have been nanostructured in order to achieve vertically aligned catalyst supports (Fig. 15) which contributes to a decreased internal resistance [59, 81]. Due to the extensive pre-treatment of GDLs (homogeneous deposition of transition metal nano-catalysts) as substrate for carbon nano-filament growth, only small scale production is possible [79]. However, this leads to the advantage of depositing catalyst particles subsequently to CNT/CNF layer preparation. The subsequent catalyst deposition results in an advanced CL architecture with catalyst particles being directly at the interface of membrane and electrode. The share of particles can be decreased which remain 'too deep' within the CL.

2.2.6. PEM Fuel Cell Durability

Material stability is primordial needed for long term operation, whereat degradation is related to all components in PEMFCs [34]. For GDL as well as graphitic pole plate material corrosion is of minor importance for impacts on cell performance [82 – 83]. Corrosion of metallic pole plates can cause fuel cell degradation by continuous dissolution of metal at high electrode potentials (0.5 to 0.7 V versus standard hydrogen electrode (SHE)). The predominant degradation mechanism results from metal cations reducing at sulphon side groups within the membrane. Those metal depositions affect the number of free charge carriers and decrease proton conductivity of the membrane. As corrosion resistant metals like titanium or aluminium have poor electrical properties and copper or nickel with high electrical conductivity are prone to corrosion, stainless steel is material of choice. Stainless steel e.g. type 1.4404 is a good compromise between electrical conductivity, corrosion resistance and costs. Nevertheless, surface treatment is necessary as the formation of an oxide layer in presence with O₂/air leads to undesired high contact resistance. Although, a gold coating offers optimal properties, depending on the application more cost effective coatings achieved by nitration are commonly used [84].

More critical concerning degradation is the CL where electrochemical reactions occur and material loss directly results in performance loss. As it can be taken from Fig. 3 fuel cell potential during dynamic operation is in the range between 0.4 V at MPP and 1 V in open circuit. This affects carbon corrosion at the cathode side, due to the standard potential of carbon of 0.2 V versus SHE at STC [85].



Carbon corrosion rate may be increased due to catalyst particles within the CL. However, kinetics for the formation of carbon dioxide is slow at PEMFC operation conditions ($T < 80\text{ }^\circ\text{C}$, $U < 1\text{ V}$). Experimental results from [72] predicted carbon loss of 7 wt.-% after 5,000 h operation at 0.9 V which is close to open circuit potential. Even in dynamic operation voltage level is typically below 0.7 V. More complicated for PEMFC durability is carbon corrosion happening on the cathode side during start/stop cycling. While a fuel cell is stopped the anode gets partially covered by oxygen due to leakage from the outside and minimal permeability of the membrane. Gas leakage is more likely when a fuel cell is stopped and pressure level in the anode sinks to ambient conditions. In the presence of oxygen HOR and ORR taking place on the anode side at the same time, where electrons generated by HOR are consumed by the local cathodic reaction. On the cathode side this phenomenon results in ORR and two concomitant anodic reactions, carbon dioxide formation and oxygen evolution reaction (OER). Electrons from the anodic reaction are consumed by the ORR.



Locally, potential difference exceeds 1.4 V which results in remarkable carbon corrosion and therefore in catalyst loss [72]. Carbon corrosion mechanism at start/stop cycles is presented in Fig. 16. Due to the minimal permeability of the membrane this phenomenon may also occur during normal operation. However, more effect concerning carbon corrosion is due to the oxygen diffusing from ambient environment.

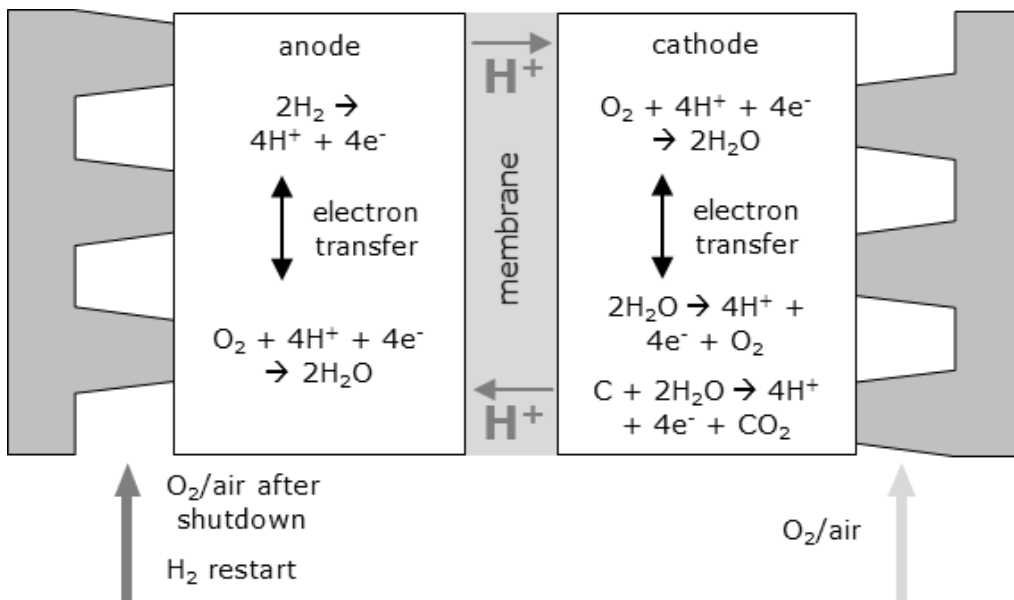


Fig. 16: Schematic drawing of start/stop cycle induced carbon corrosion at the cathode compartment when air is introduced in the anode compartment after shutdown

For these reasons corrosion resistance of the catalyst support material plays an important role for PEMFC durability, which directly affects the catalyst utilisation after some hundred operating hours or respectively after a high number of start/stop cycles [54, 86 – 88]. Graphitisation degree of a carbon material contributes to the corrosion stability. A high graphitisation degree indicates increased corrosion resistance in comparison to amorphous or turbostratic carbons [72]. Therefore, CNTs and CNFs are ideal catalyst support materials for PEMFCs.

2.2.7. PEM Fuel Cell Stacks

In order to develop a PEMFC stack all components of a single fuel cell (pole plate, MEA etc.) need to be integrated. Therefore, some macroscopic design considerations are described in the following chapters. State of the art fuel cell stacks consist of several single fuel cells connected electrically in series which increases stack voltage at constant current. For gas distribution all cells of a stack are connected by means of a parallel channel system. Inlet and outlet of a cell's flowfield are applied to main gas paths so that the length for all side paths (through the cell) is identical. To reduce electrical stack resistance pole plates are constructed in bipolar design, so that a flow field is arranged on each side of the plates. Monopolar plates are placed on the stacks extremities with a flow field only on one side [27].

To reduce reactance within a fuel cell (describing gas flow losses as well as electrical losses) without setting down porosity of the electrode's layers, an optimal compression over the whole cell surface is needed. Typically, for PEMFCs necessary compression forces are induced over two massive endplates which are pulled together by tie bolts which are arranged around the active cell area [89 – 96].

Since temperature conditions as well as temperature distribution within a fuel cell have impact on the operation characteristics, it has to be taken account of. Special cooling plates with channels for a cooling medium may be arranged between two cells [27, 30, 97]. Waste heat caused by internal losses can be removed from the stack in order to protect it from overheating. However, temperature gradients between cooling water inlet and outlet are likely. Fig. 17 shows a schematic drawing of typical PEMFC stack in cross section.

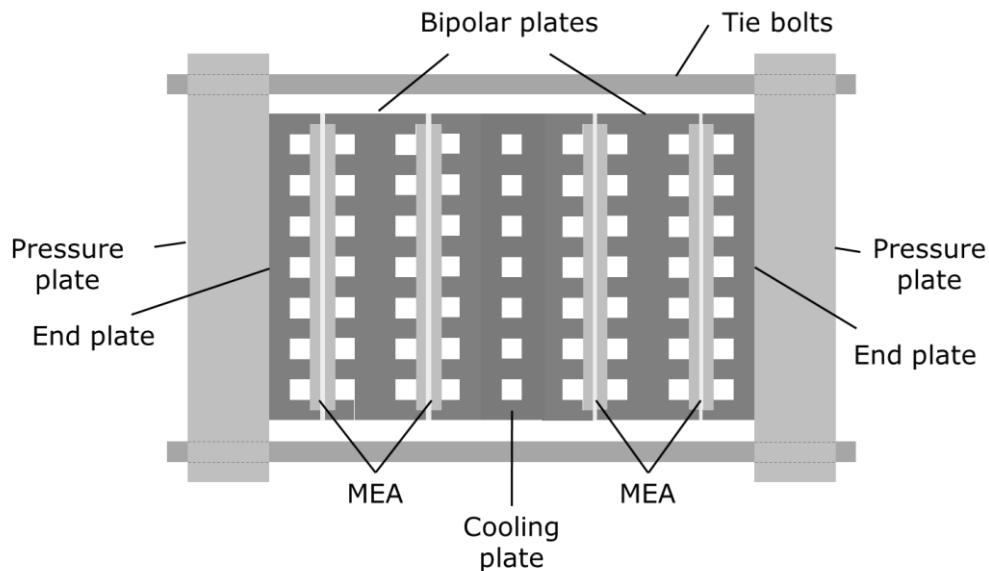


Fig. 17: Schematic drawing of fuel cell stack in bipolar design with cooling plate in cross section

Clamping pressure is a central requirement for fuel cell stacks by means of reducing contact resistance between the electrode's components. Furthermore, gaskets need to be compressed in order to prevent the active cell area from leakage. Due to distortion phenomena for all components of a stack an ideal compression via tie bolts is not possible (Fig. 18). As cell compression is directly related to the internal electrical resistance, homogeneous pressure distribution is necessary in order to optimise electrical current distribution as well as temperature distribution. As a result of in-homogeneous current distribution hot spots would occur which lead to local overheating and may result in increased cell degradation [97 – 99]. Therefore, special interest is on the pressure plate's design by means of optimising pressure distribution over the active cell area [100].

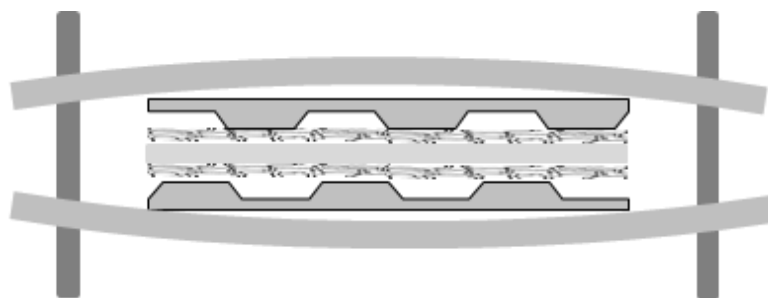


Fig. 18: Schematic drawing of the deformation of pressure plates due to application of clamping forces (exaggerated)

In order to contribute to optimal MEA compression a novel stack design for electrochemical cells based on hydraulic compression of single cells has been suggested [101]. With this stack design fuel cell systems can be constructed which contain a variable defined number of single cells which are connected in series over flexible copper ribbon cables. These are arranged in flexible pockets within a pressure tank filled up with fluid. In operation cells are fixed within the tank by increasing pressure level of this fluid. However, e.g. for maintenance reasons pressure can be released so that changing cells is possible [102].

During operation a hydraulic medium surrounds each cell of the novel stack in the way that surface pressure on each cell is identical. The hydraulic pressure within the stack is controlled by a pneumatic actuator. The system's pressure control keeps a constant pressure level. This is necessary e.g. at start-up procedure, when stack temperature rises from room temperature to operating temperature (about 60 °C to 80 °C). Furthermore, temperature of the whole stack can be controlled by cooling the hydraulic medium. This guarantees homogeneous temperature distribution for each cell as well as protection against overheating. Waste heat recuperation for a CHP system can easily be realised.

Hence, operation conditions with this type of stack are nearly ideal, if the parameters of the delivered process gases are constant. In order to deliver gases with identical physical characteristics to each fuel cell, these are connected in parallel to temperature controlled manifolds (for O₂/air as well as for H₂). Each cell has a clip which connects it to this manifold. However, connecting cells gas technically in series is also possible with another kind of manifold which joins a cell's outlet with the next cell's inlet. However, due to unfavourable pressure drop after each cell, delivering the gases in series is limited to only few cells.

For investigations carried out on MEAs, typically stacks with special design concerning temperature and compression control are used. Equipment is either operated with an adjustable mechanism for achieving a surface pressure over the cell area (Fig. 19) or with screws, for compression over tie bolts [27, 103]. This pressure is induced for contacting the membrane electrode assembly with a sample holder. Sample holders with temperature controls are often used. Test systems with one sample holder or short stacks with only few cells are utilised. Hence, for investigations on several MEAs at the same time for each MEA sample separate test equipment is necessary [104]. For setting constant operation parameters (like gas or stack temperature) a climate chamber is often required [105, 106]. However, measuring the process parameters especially of the delivered gases is a challenging task [27]. Details on design and construction of a MEA test environment based on hydraulic compression and with temperature controls is given in Chapter 3.

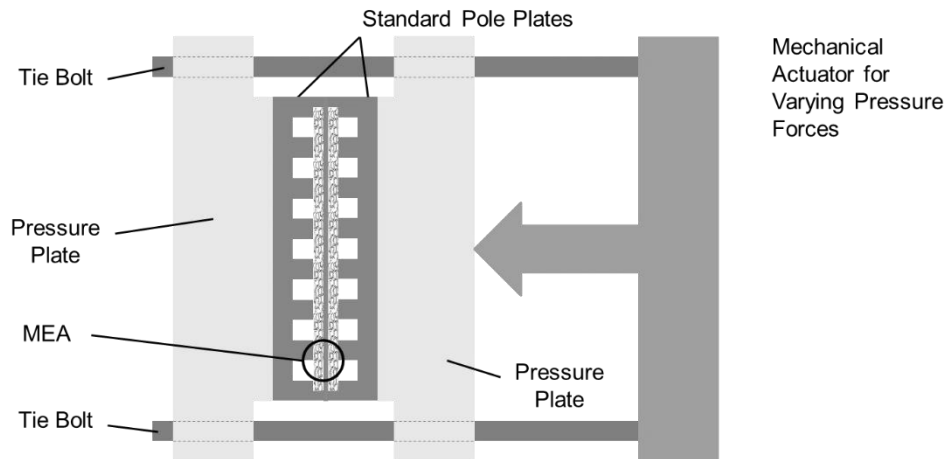


Fig. 19: Schematic drawing of a MEA test facility with mechanical actuator for adjusting test cell compression

2.3. Motivation for this Work

Due to their compact design as well as high efficiency PEMFCs are believed to play a key role for environmental friendly vehicles in the near future [107 – 111]. Furthermore, for stationary applications fuel cell technology can be a solution for carbon dioxide free combined heat and power generation in households as well as in large scale power units [112, 113]. However, fuel cells still belong to technical curiosities which is related to their short life time in dynamic operation and their high costs. Therefore, the development of durable as well as more cost effective fuel cells is necessary for prospective PEMFC applications. Especially, for stationary applications which are designed for a service life of a few decades, durability and investment costs are important issues.

One main aspect regarding costs refers to the reduction of rare and expensive platinum catalyst. However, increasing material stability for long term performance increases return of invest. This results in further reduction of overall costs. In order to contribute to these aspects carbon filaments (CNTs and CNFs) which are produced in industrial scale have been investigated as support material for platinum particles in PEMFC electrodes. Due to their high graphitisation degree, electrical as well as thermal conductivity is high. Higher corrosion resistance than for typically used carbon blacks is expected. Furthermore, their specific surface area of up to 200 m² is advantageous for this purpose. A low cost preparation approach has been developed, in order to result in electrodes with low platinum loading.

MEAs have been prepared by the use of carbon filament coated GDL with subsequent platinum deposition. Regarding electrochemical characteristics these have been tested in a novel test system based on the modular stack design with hydraulic compression. A prototype has been constructed with three slots for standardised sample holders. Therefore, operation of three samples at the same time is possible. This prototype is integrated into an automated fuel cell test bench which provides controlled gas delivery, cell compression as well as temperature controls and an electronic load for fuel cell operation. As operation conditions for each sample holder is nearly ideal, differences in electrochemical behaviour refer to differences in electrode composition.

3. METHODOLOGY AND EXPERIMENTAL EQUIPMENT

Aim of this experimental work is the development of carbon filament based electrodes with low Pt loading for application in (acid) PEMFCs. A preparation method for PEMFC electrodes has been investigated for this study in order to result in a 'simple' and low cost approach. Target of this attempt is the development of an industrial scale production process subsequently to this scientific work.

For this purpose CNTs and CNFs have been investigated as well as various graphitic substrate materials used for the preparation of gas diffusion electrodes (GDE). Suitable coating techniques have been identified. For catalyst particle deposition an electro plating process was studied. Optimisation has been achieved according to the carbon filament pre-treatment in a plasma reactor. Furthermore, a test environment for MEAs has been developed within the scope of this work. The key component of the test environment is a modular PEMFC stack with hydraulic compression. Such a stack has been extended and integrated into a test bench with gas conditioning, stack heating and hydraulic pressure controls.

Material research and test environment engineering have been performed in parallel. Therefore, chapter 3 is divided into three parts. The first part gives information about the methodology of material characterisation. The second part refers to sample preparation regarding the surface treatment and particle deposition. The last part of chapter 3 explains the test bench development for application and evaluation of prepared MEA samples.

3.1. Methods for Material Characterisation

In the frame of this experimental study raw material as well as prepared electrodes have been investigated in respect of morphology, microstructure as well as electrochemical properties. Furthermore, samples have been analysed according to their mechanical and electrical properties. Therefore, samples were characterised by means of scanning electron microscopy combined with energy dispersive X-ray analysis, transmission electron microscopy, thermogravimetry, X-ray diffraction as well as X-ray fluorescence analysis. In order to determine the catalyst particle's electrochemical active surface area cyclic voltammetry has been performed in sulphuric acid. Moreover, electrical resistivity of prepared GDEs have been determined.

3.1.1. Electron Microscopy

Scanning electron microscopy (SEM) is widely used to visualise structures of electrical conductive samples with a resolution up to nm (10^{-9} m) scale by analysis of the interaction of surface atoms excited by a focussed electron beam⁶. Therefore, this technique is helpful for the presented study on graphitic and metallic nano-particles in order to investigate morphology as well as microstructure of prepared samples.

⁶ Depending on the energy of the electron beam (up to 30 keV) also atoms near to the samples surface are excited.

Furthermore, with SEM three-dimensional structures can be imaged due to excellent depth of field.

The electron beam is generated by an electron gun (cathode, e.g. an electrically heated tungsten filament) at high voltage up to 30 kV, whereat the beam is focused on a sample (anode) by several electromagnetic lenses. This arrangement is situated in an evacuated chamber (vacuum down to 10^{-5} Pa) in order to avoid interaction of the beam with contained gases. The microscope controls the electron beam to scan the surface in a certain pattern (line wise). The image is then computer generated from sample information analysed point by point. A schematic drawing is shown in Fig. 20.

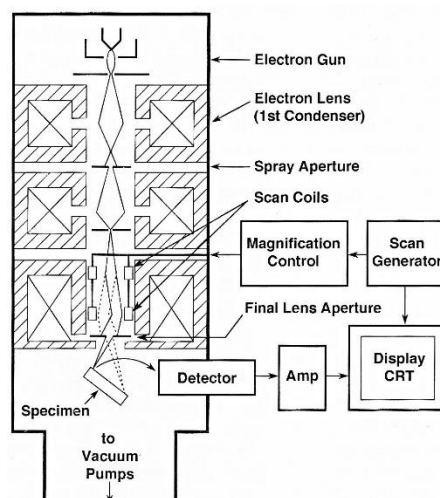


Fig. 20: Schematic drawing of a scanning electron microscope [114]

To get contrast to an image the differences in intensity obtained by a detector are visualised. By exciting surface atoms (or surface near atoms) information can be obtained such as concerning secondary electrons (SE), back scattered electrons (BSE) and energy dispersive X-ray (EDX). EDX analysis gives information about sample composition due to determination of material specific spectres [114]. More detailed information regarding EDX is given in chapter 3.1.1.2 X-ray Based Analyses.

For this work a SEM type ESEM XL 30 from Philips (The Netherlands) was used. Here an electron gun with a heated tungsten filament is utilised. The microscope has detectors for: SE, BSE as well as for EDX. Electrode samples have been investigated from on top. Furthermore, a cross section has been prepared by embedding a sample in resin and polishing the cut surface. The structure of electrode samples can be estimated. Additionally, a SEM type Hitachi S4500 with LaB_6 (lanthanum hexaboride) cathode has been used for investigations on fractured (at deep temperature) samples which have neither been embedded nor polished.

Transmission electron microscopy (TEM) works similar to a light microscope due to the effect that an electron beam has a certain wavelike character. Resolution of TEM is up to 10^{-10} m which is several magnitudes higher than for light microscopes and higher than for SEM. Therefore, it can be used to visualise metallic nanoparticles synthesised in the frame of this Ph.D. program or even the graphitic structure of the carbon nanoparticles.

A transmission electron microscope is equipped with a lenses system as in SEMs which focuses the beam on a sample. However, a high voltage of 60 to 300 kV electron beam is used in order to result in wavelength in the pm (10^{-12} m) range. Depending on the voltage this electron beam is able to penetrate a sample with a thickness up to some hundred μm . As transmission through a sample is limited, it is essential to prepare a sample regarding to meet these conditions. It is typical to embed a sample in resin and cut a thin section with a microtome [115].

For this work structure of the prepared electrode samples is brittle, so that preparation of a thin section was not possible. Therefore, a small fraction of a prepared CL has been scratched from its substrate in order to investigate particular CNFs with platinum decorations. A TEM type fei CM200 with LaB_6 cathode has been used.

3.1.2. X-ray Based Analyses

X-ray radiation is high energy electromagnetic radiation with a wavelength below ultra violet light. Technical X-rays are generated in a vacuum X-ray chamber by an electron beam accelerated on a metallic target by a high voltage electric field. By interaction of accelerated electrons with the metallic target a continuous and a target specific discrete X-ray spectrum is achieved. The continuous radiation occurs with deceleration of electrons. Due to their negative charge electrons are scattered by the positive cores of target atoms which results in a change of direction and velocity. As a decelerated electron must lose part of its kinetic energy, radiation is emitted. Coming from German language, this form of continuous radiation is called bremsstrahlung (Fig. 21).

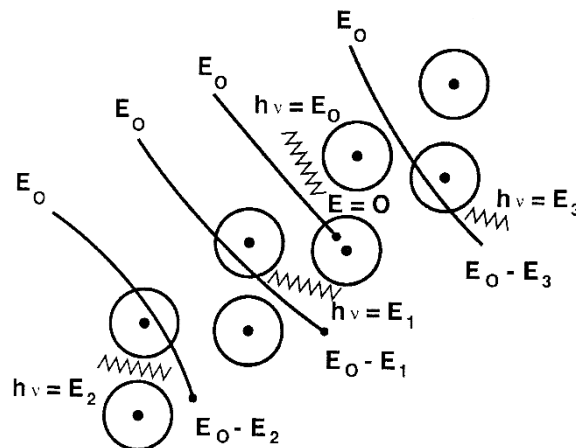


Fig. 21: Schematic drawing of generation of continuous bremsstrahlung [114]

Furthermore, one can obtain a discrete, target material specific spectrum which results from interaction of a beam electron with an electron of the atoms of the target material. By collision it is possible to eject an inner shell electron (e.g. from the affected atoms K shell). An excited, ionised atom remains which will relax to its ground state (lowest energy for the particular electron configuration). This means an electron of an outer shell (e.g. from the excited atoms L shell) will fill the inner shell gap. From this transition, the 'moving' electron loses energy with the specific value of

potential energy difference between the two shells. This excess energy can be released in two ways: a) The energy difference results in ejecting another shell electron by increasing its kinetic energy or b) generation of material characteristic X-ray radiation (Fig. 22). A typical X-ray spectrum of an X-ray tube with copper target can be seen in Fig. 23 [114, 116].

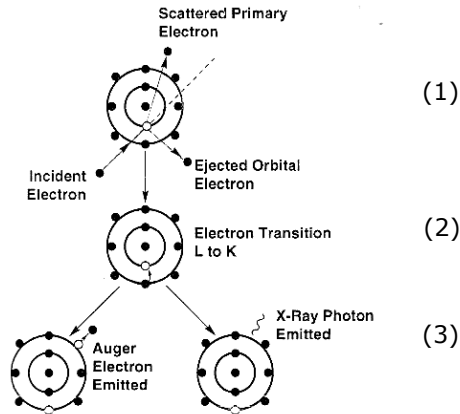


Fig. 22: Atom ionisation by a beam electron ejecting a K shell electron (1), L shell transition to K shell (2) and two possibilities how excess energy is released (3) [114]

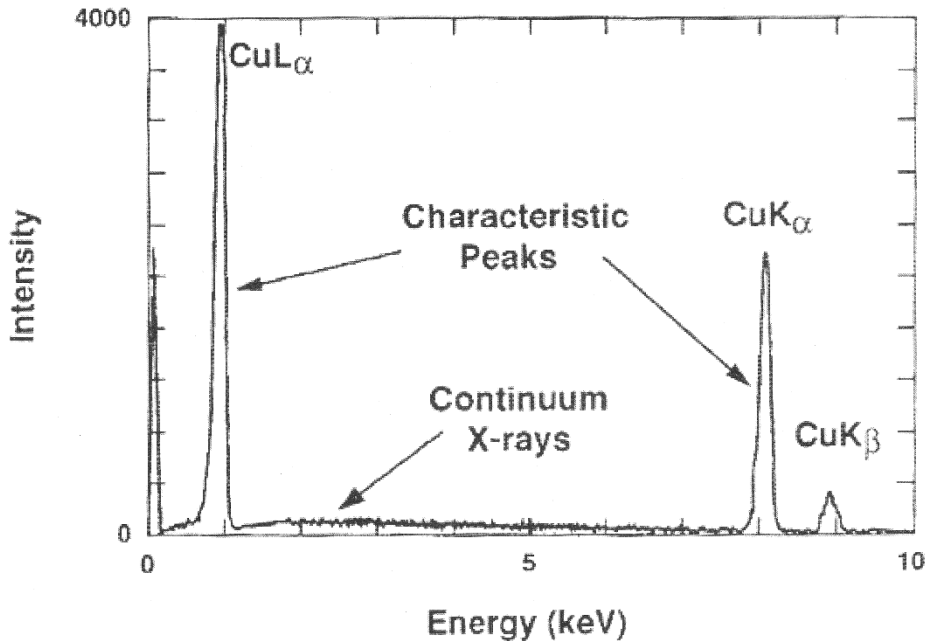


Fig. 23: Typical X-ray spectrum achieved by an X-ray tube with copper anode target [114]

Energy dispersive X-ray (EDX) spectroscopy is included to the ESEM XL 30 from Phillips. The principle is based on the generation of X-rays by the electron beam scanning a sample surface for SEM. An X-ray sensitive detector situated within the vacuum chamber of the SEM analyses the spectrum emitted by the sample. The

spectrum is visualised for qualitative determination of the sample composition. EDX has been used to identify the material composition of prepared samples [114].

X-ray diffraction (XRD) spectroscopy is a method to identify crystalline materials due to the diffraction pattern resulting from a monochromatic X-ray directed on a sample. For this work a XRD type Philips X'Pert was used. X-ray is generated from a copper target. According to Bragg's law

$$n \cdot \lambda = 2d \cdot \sin \theta \quad (3-1)$$

X-ray is diffracted at the lattice of a crystalline sample. For formula 3-1 n means number of the analysed maximum, λ means the wavelength of the X-ray, d is the space between the diffracting atoms and θ refers to the incident angle between sample and the detected maximum (Fig. 24). As λ is known for the monochromatic X-ray d can be calculated from the measured angle θ . Schematic drawing of an XRD spectroscope is shown in Fig. 25 [114, 116]. For graphitic materials, d_{002} is the value for the interlayer spacing between two graphene layers which has been determined by XRD for different graphitic materials as well as for CNT as well as for CNF based electrodes prepared for this work.

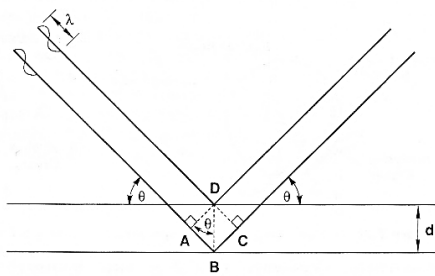


Fig. 24: Schematic drawing of the relation between wavelength λ , spacing between two atoms d and incident diffraction angle θ according to Bragg's law [114]

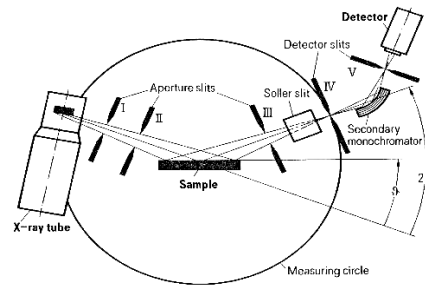


Fig. 25: Schematic drawing of an X-ray diffractometer [116]

X-ray fluorescence (XRF) spectroscopy is widely used to determine the material composition of a sample. The material's specific discrete X-ray spectrum generated by the interaction with a high energy X-ray beam is analysed. For this work a XRF spectrometer type SPECTRO MIDEX has been used in order to determine platinum loading of prepared electrodes as well as catalyst content of the CNT and CNF raw material.

3.1.3. Thermogravimetry

Thermogravimetric analysis (TGA) is used in order to determine the mass change of a sample as a function of temperature/time. For this purpose a sample holder with heating is situated in a furnace with controlled atmosphere (defined flux of gas e.g. oxygen). The sample holder is connected to a precise balance. A constant heating rate is set, resulting in linear temperature increase. Weight and temperature are determined over time. Typically, TGA is performed up to 1,200 °C.

In this work especially metallic residues have been determined by TGA type Netzsch STA 449F1 Jupiter. In order to measure metallic content of CNTs and

42 3. Methodology and Experimental Equipment

respectively CNFs which are related to their production process, powder fractions (raw material) have been analysed. For investigated electrodes, pieces with one square centimetre size were cut off from a large sample for TGA. Starting from nearly ambient conditions (30 °C) the samples were completely burnt off with a heating rate of 20 °C min⁻¹ up to 1,200 °C. Determined residues are related to non-flammable electrode components. A typical TGA plot is presented in Fig. 26.

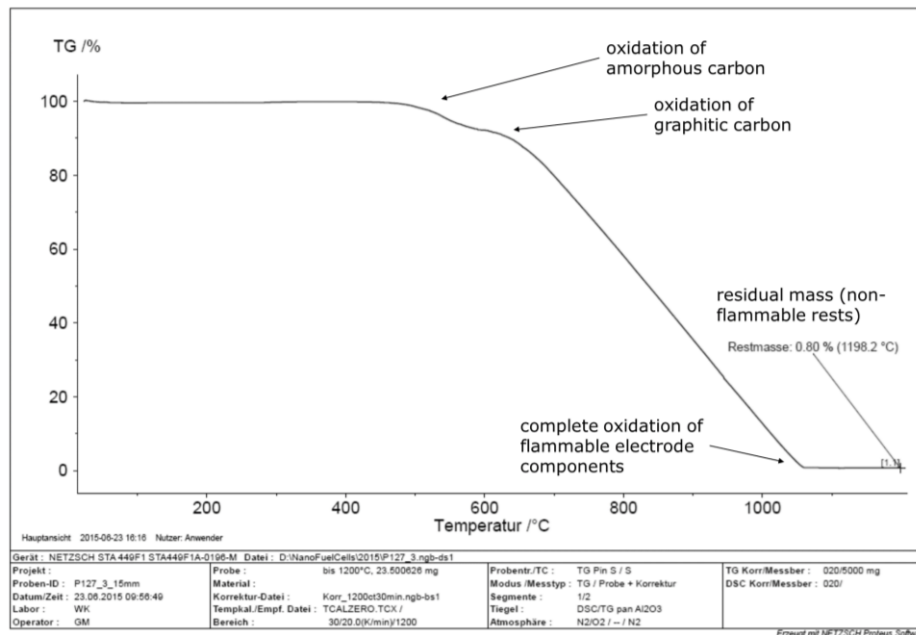


Fig. 26: Thermogravimetric analysis of an electrode sample based on CNFs with platinum decoration

3.1.4. Cyclic Voltammetry

Cyclic voltammetry (CV) describes an electrochemical method to analyse interaction of an electrode with a surrounding electrolyte according to an electrode's potential at quasi stationary conditions. The potential of the working electrode (WE), which is the investigated specimen, is increased linearly over time from a defined starting potential by a potentiostat. The scan rate is expressed in [mV sec⁻¹] or [mV min⁻¹]. A further electrode is necessary as counter electrode (CE) in order to complete the galvanic system. Often a platinum disk is used as CE.

If the target potential is reached (reverse potential), the potential is decreased with the same scan rate off to the starting potential and reverse again. Depending on the performed analysis a number of cycles is measured. Typically, the reverse potentials are set between the specific potentials where hydrogen evolution and oxygen evolution happen [30].

As overpotential occurs at the CE in most cases the potential between WE and CE is not interesting, but the specific potential at the WE. In this case potential difference is measured between WE and a reference electrode (RE) which can be applied to a potentiostat additionally. REs have a nearly stable potential over large temperature range. Due to high ohmic input resistance of a voltage meter (typically

in the range of $G\Omega$ ($10^9 \Omega$), measurement current through the RE is nearly zero. Therefore, overpotential at the RE is negligible. That means measured potential difference refers to the equilibrium potential of RE and WE potential. Examples for typical REs are silver/silver chloride or calomel (mercury/mercury chloride) electrodes. The potential of a saturated calomel electrode (SCE) is about 25 mV. Furthermore, a standard hydrogen electrode (SHE) can be used which is described as a pure platinum electrode blown with pure hydrogen. At STC and for an electrolyte with H^+ activity⁷ a (H^+) of 1 the potential of SHE is 0 V by convention. The potential of a saturated calomel electrode (SCE) at room temperature is about +240 mV vs. SHE.

Current corresponding to the applied voltage is measured and a cyclic voltammogram is plotted as a function of WE potential [30]. Cyclic voltammogram of a PEMFC electrode vs. SHE is shown in Fig. 27. The two current peaks which are pointed out at the left side of the plot refer to hydrogen oxidation reaction (desorption), respectively, to hydrogen reduction reaction (adsorption) on the surface of platinum catalyst particles. Peak currents for desorption and adsorption are almost proportional to the catalytic activity of the electrodes. Current increase at the right side of the plot refer to oxide formation, which in most cases is irreversible due to CO_2 formation. For this reason CV for electrodes with Pt/C electro catalysts are carried out not further than to 1 V vs. SHE [27].

The carbon content within this electrode sample contributes to an increase in double layer capacity. The double layer current and the corresponding charge (which is a result of scan rate multiplied with current for double layer) is also indicated in the figure. Concerning hydrogen desorption or hydrogen adsorption the corresponding charge can be determined by the area underneath the peaks of the voltammogram. Double layer charge needs to be subtracted [27, 30].

By comparison of either the charge of hydrogen desorption or of hydrogen adsorption with the corresponding charge of a plane platinum electrode, the active electrochemical surface area (ECSA) of a sample can be calculated. For a pure platinum electrode, adsorption charge of $210 \mu C cm^{-2}$ is reported. ECSA calculation follows the equation:

$$ECSA (cm^2 g_{Pt}^{-1}) = \frac{\text{Charge } (\mu C cm^{-2})}{210 (\mu C cm^{-2}) \cdot \text{Catalyst Loading } (g_{Pt} cm^{-2})} \quad (3-2)$$

Problems with this calculation occur due to signals measured from interaction of the carbon support. E.g. redox reactions of functional groups on the carbon surface can alter the measured current [27, 30].

⁷ The activity coefficient of chemical substances is a dimensionless value which is defined by concentration of a substance multiplied with its individual (concentration depending) activity coefficient. For low concentrations, such as below $0.001 mol l^{-1}$, activity coefficient is nearly 1. For gases, activity refers to partial pressure. Further information may be taken from [30].

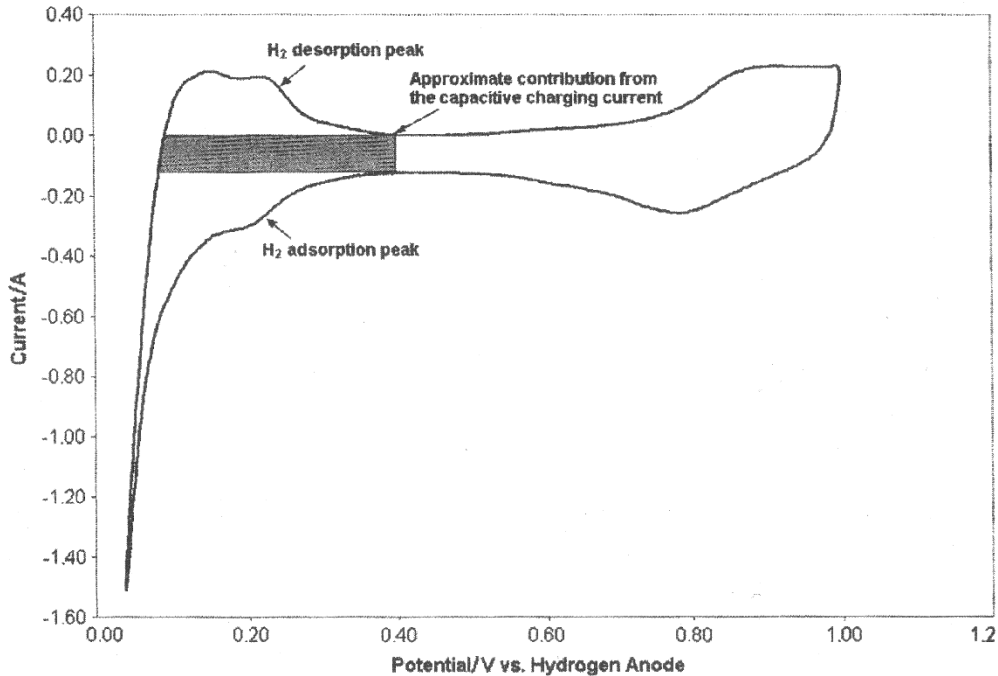


Fig. 27: Cyclic voltammogram of a PEMFC electrode with Pt/C electro catalyst [27]

In order to analyse prepared PEMFC electrodes, cyclic voltammetry has been performed in 0.5 M sulphuric acid at room temperature in a galvanic cell type Radiometer Analytical CEC/TH with a three electrodes configuration with a platinum CE and a saturated calomel RE. Two types of potentiostats have been used, for small scan rates (potentiostat type VoltaLab PGP201) and for high scan rates (potentiostat type Ivium Technologies Vertex). Cyclic voltammograms of prepared catalyst layers with and without platinum catalysts have been determined. Regarding the determined platinum loading, the catalyst particle's specific electrochemical active surface area (ECSA) of prepared CLs has been calculated.

3.1.5. Electrical Conductivity

Internal resistance has major effect on the power output of a fuel cell. The resistance is the sum of the electrical resistance of the fuel cell's components and the ionic resistance of the membrane. For this study electrical resistance in-plane of the prepared GDEs has been determined by means of van-der-Pauw-method which is well-known in electrical engineering. This four-point probe is used for direct determination of electrical in-plane (IP) conductivity (xy-direction) for thin layers, originally used in semiconductor engineering [117 - 119].

For this measurement a circuit board (Fig. 28) is constructed with electrical contacts situated in square with an edge length of 45 mm (according to the edge length of GDEs prepared for this Ph.D. program). Current is applied to two of the contacts and voltage is measured at the other. Current is supplied by a power unit type Voltcraft PS 303 Pro from 100 mA to 1 A (100 mA per step). The corresponding

voltage is measured by multimeter type Picoset M3510A. For low contact resistance the board is pressed on the tested sample with 150 N.

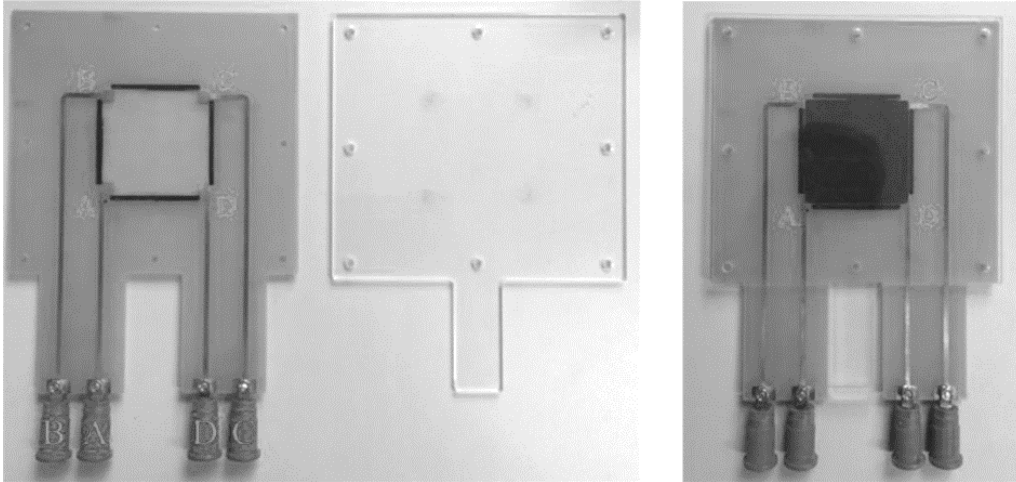


Fig. 28: Photograph of a circuit board for resistivity measurement in xy-direction (in plane)

For determination of the resistivity in xy-direction initially the current I_{AB} is applied to the contacts A and B. Voltage U_{CD} is measured at the contacts C and D. From Ohm's law

$$U = R \cdot I \quad (3-3)$$

the resistance $R_{AB,CD}$ can be calculated. For calculation mean value of all measurements has been taken. As a next step the resistance $R_{BC,DA}$ needs to be determined from I_{BC} and U_{DA} .

According to van-der-Paw's law specific resistance ρ is calculated by:

$$\rho \left[\frac{\Omega \cdot mm^2}{m} \right] = \rho [\Omega m \times 10^{-6}] = \frac{d \cdot \Pi}{\ln 2} \cdot \frac{R_{AB,CD} + R_{BC,DA}}{2} \cdot f \quad (3-4)$$

with d means thickness of the sample and f means correction factor according to the following diagram (Fig. 29).

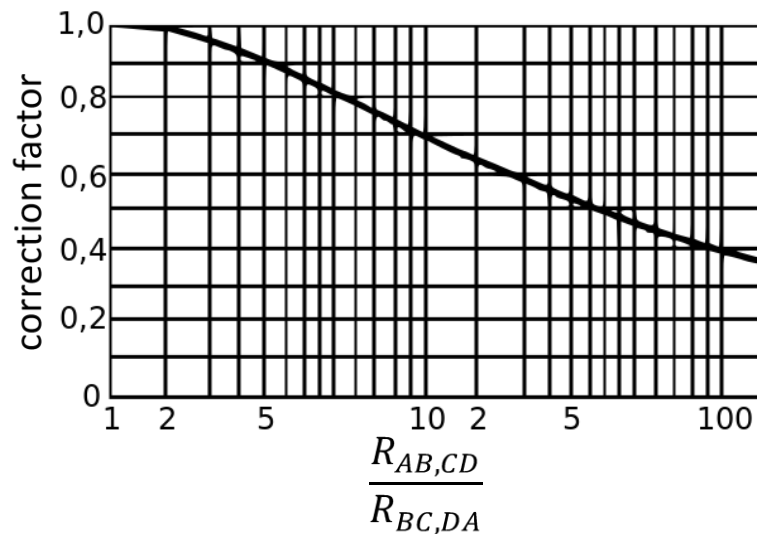


Fig. 29: Correction factor according to [117]

IP resistance is dependent on the sample's thickness and can be calculated by:

$$R_{IP} = \frac{\rho}{d} \quad (3-5)$$

Electrical conductivity through plane (TP) has also been investigated by a four-point probe. Two circuit boards each with a contact area of 20.25 cm² (45 mm x 45 mm) are constructed (Fig. 30). A test sample is placed between these boards which are pressed together at 6 bar. Resistance is determined with the devices mentioned above. Current is increased from 300 mA up to 3 A (300 mA step⁻¹). For resistance calculation mean value of all measurements has been taken. TP resistance is dependent on the samples size and can be calculated from

$$R_{TP} = R_{measured} \cdot A_{sample} \quad (3-6)$$

with A_{sample} means the geometrical size of the sample.

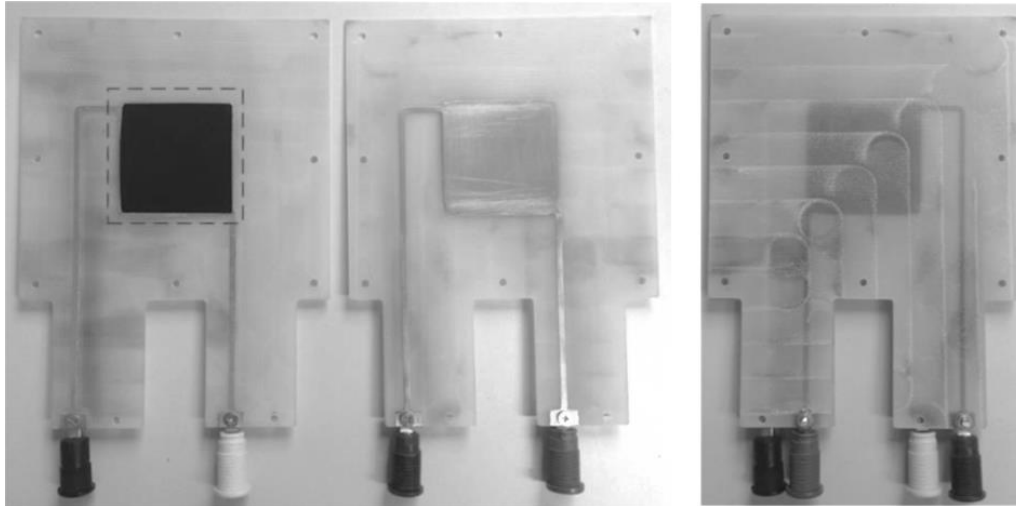


Fig. 30: Photograph of circuit boards for resistivity measurement in z-direction (through plane)

3.2. Carbon Filament Coating and Decoration

Typically, for decoration with metallic particles pre-treatment of CNT as well as CNF raw material is necessary. Surface activation of carbon supports by functional group formation improves the amount and distribution of metal reductions on graphitic structures. In laboratory scale surface activation is often performed for several hours in acids at high temperatures (e.g. HNO_3 or H_2SO_4 at $80\text{ }^\circ\text{C}$). As such pre-treatments are extensive and generally selective formation of functional groups is not possible [120 – 122], CNT and CNF surface activation has been realised by oxygen plasma treatment. Subsequently, carbon filaments are ready for decoration with catalyst particles. For this study electro plating has resulted in useful electrode samples.

3.2.1. Radio Frequency Induced Oxygen Plasma

Plasma is a fundamental aggregation state of matter. It describes a macroscopically neutral substance that contains a fraction of interacting, free electrons as well as ionised atoms. Plasma occurs if e.g. molecules of a gas acquire enough kinetic energy to overcome the binding energy between present particles. As a result of collisions of accelerated particles with electrons of the outer orbitals of a gas molecule, the molecule becomes ionised and the electron is not related to the molecule any more. Formation of atoms (from gas molecules) and radicals is also possible. Naturally, plasma exists at high temperature. Examples for plasma formation can be found at the sun or when lightning emerges at the earth's surface [123].

Technical plasmas are generated by applying an external electrical field to a certain gas in order to increase the particles kinetic energy. Depending on the pressure conditions a plasma occurs at a gas specific temperature. Two main techniques are distinguished. Plasma formation at ambient pressure and about 10^4 K (e.g. electric arc welding) and plasma formation at near vacuum and ambient temperature. Plasma treatment at ambient temperature is a common method for

industrial processing of material. Due to the reactive behaviour of the particles of generated plasma, the surface of material in exposure to this is affected. Depending on the plasma parameters, the treated surface gets etched, functionalised or coated. However all mentioned effects happen at the same time. A dominant effect can be achieved at certain parameters for e.g. process gas, plasma power or frequency of the electric field generator.

Oxygen plasma treatment of graphitic material introduces oxygen containing functional groups (hydroxylic, carboxylic and carbonylic groups) onto the graphite surface and is able to enhance the fibre surface porosity (by etching). Some results from previous research by the working group of Prof. Dr. Waltraut Brandl at the former Fachhochschule Gelsenkirchen in Germany concerning the optimisation of the oxygen plasma parameters for CNT activation have already been reported [120 – 121]. Here, proof has been found for mainly formation of reactive carboxylic groups (-COOH) on the surface of CNTs. Material characterisation of oxygen plasma activated graphitic surfaces was determined by XPS analysis as well as contact angle measurement [120 – 122].

In this study CNTs and CNFs have been pre-treated in radio frequency induced oxygen plasma (RF plasma reactor type Plasma Finish RFG 300 RF). The previously determined parameters have been optimised concerning a subsequent platinum particle deposition. Gas flow through the plasma reactor for oxygen and argon has been set to 0.1 NI min⁻¹ at a gas pressure of 60 Pa. Plasma treatment has been carried out at ambient temperature in order to form mainly COOH⁻ on the carbon filaments' surface. Optimal plasma power and treatment time have been analysed.

3.2.2. Surface Energy

It was observed that the oxygen plasma treatment is feasible to increase the carbon fibre's surface energy. Surface energy is a characteristic value for the wettability of a material and has a polar γ^p and a dispersive γ^d fraction. The polar fraction gives information about presence of polar groups like hydroxylic, carboxylic and carbonylic groups. According to (3-7) the sum of γ^p and γ^d results in γ .

$$\gamma = \gamma^p + \gamma^d \quad (3-7)$$

Surface energy of untreated and oxygen plasma activated CNTs was systematically determined by means of dynamic contact angle measurements in liquids with different surface tensions (water, i-propanol, formamide, diiodomethane). Furthermore, it was analysed if the values of γ^p and γ^d vary as a function of the plasma parameters. For analyses of surface energy a tensiometer type Dataphysics DCAT 11 has been used.

3.2.3. Ink Formulation

Increasing the CNF's surface energy is necessary for the formulation of CNTs and CNFs containing dispersions due to the very hydrophobic character of the raw material. Fig. 31 and Fig. 32 show dispersions of untreated CNTs in water as well as ethanol (C₂H₅OH). It is obvious that the nanotubes tend to agglomerate and sediment to the bottom of the glass due to poor wettability of CNT raw material. In contrast to this Fig. 33 to Fig. 36 show examples of dispersions of plasma treated CNTs in H₂O as well as C₂H₅OH which are stable over a time period of 60 minutes. This is the result

of increasing the surface energy of the fibres by functional group formation on the carbon surface.



Fig. 31: CNT dispersion in H₂O (w/o previous plasma treatment)



Fig. 32: CNT dispersion in C₂H₅OH (w/o previous plasma treatment)



Fig. 33: Plasma treated CNT dispersed in H₂O



Fig. 34: Plasma treated CNT dispersed in H₂O after 60 minutes

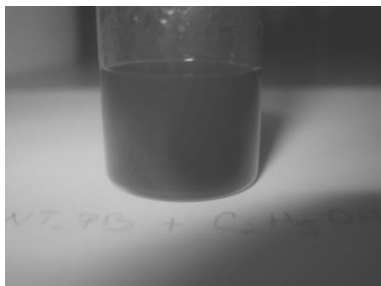


Fig. 35: Plasma treated CNT dispersed in C₂H₅OH

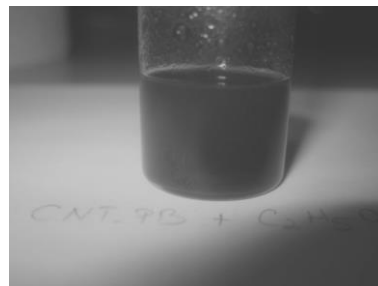


Fig. 36: Plasma treated CNT dispersed in C₂H₅OH after 60 minutes

For investigations on electrodes without noble metal catalyst, inks have been formulated containing 20 mg CNTs (with and without plasma activation). As dispersant for all prepared inks isopropanol (ROTISOLV purity 99.95% from Carl Roth) has been used. Before processing, prepared dispersions have been ultrasonicated for 15 minutes in an ultrasonicator type Palsonic PT-20-H (50 W; 40 kHz) at room temperature.

For anode preparation, ink formulae containing CNTs or CNFs as well as hydrophilic Nafion[®] solution (5 wt.-% in alcohol) as binder and for improving platinum connection to the ions conducting membrane have been developed. CNT as well as CNF loading has been altered. Sets of electrodes with varying CNF to Nafion[®] weight

ratio have been prepared. As platinum particle deposition is performed subsequently, no noble metal is contained within the developed dispersions. Furthermore, for comparison with state of the art Pt/C electro catalysts an ink has been formulated with Pt/C powder (50 wt.-% Pt, 50 wt.-% C) and Nafion® solution.

3.2.4. Preparation of Carbon Filament Layers

Usually, catalyst layers are prepared from Pt/C catalyst particles which are commercially available as a powder. An ink or a paste is formulated containing the catalyst powder as well as hydrophobic (e.g. PTFE) or hydrophilic polymers (e.g. PFSA). The raw materials are dispersed in water or alcohol for further processing. This mixture is coated either onto a polymer electrolyte membrane (preparation of a CCM) or onto a GDL (preparation of a GDE). Different coating techniques are reported in the literature, e.g. rolling, casting or spraying. Subsequently, MEAs are fabricated from two GDLs and a CCM or from two GDEs and an un-coated membrane by hot pressing (or pressing without additional heating) [27 – 28].

In order to manufacture CNT as well as CNF based MEAs for the described preparatory work, CLs have been prepared by spray-coating a dispersion (compare to chapter 3.2.3. Ink Formulation) onto GDL material. Different GDLs for example type Freudenberg H2315 I2C6 or type AvCarb MGL 370 have been used as substrate material. After spray-coating samples need to be dried on an oven at about 80 °C. Platinum catalyst particles are deposited subsequently on prepared carbon filament layers (compare to chapter 3.2.5 Catalyst Particle Deposition). For CV analyses in H₂SO₄ graphite disks with 15 mm diameter (graphite from Schunk Kohlenstofftechnik type FU4413/7) have been coated with carbon filaments.

Due to the poor reproducibility of previous manual attempts worked out before, the development of an automated coating facility emerged. E.g. brushing, dropping or manual air brush painting lead to inhomogeneous coatings on the surface of a GDL sample.

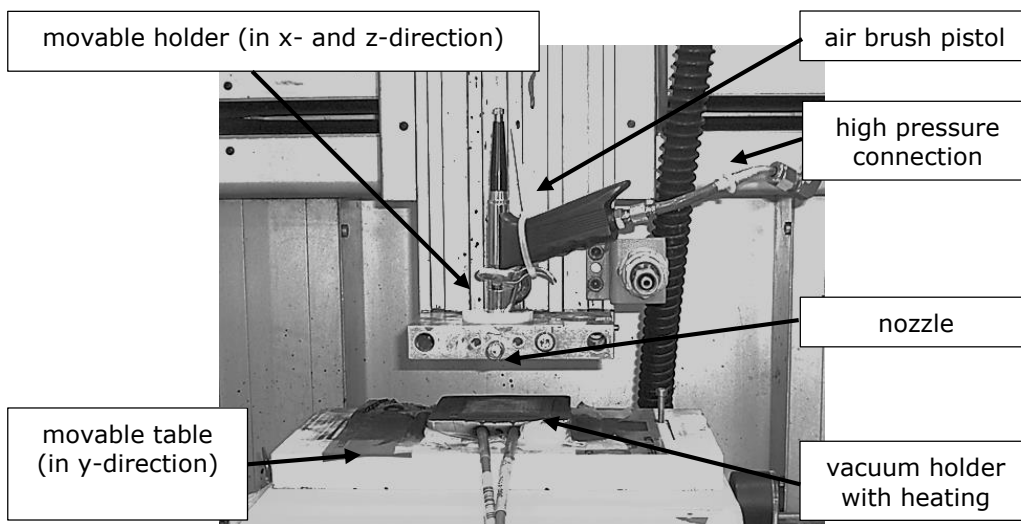


Fig. 37: Automated ink coating facility

For spray-coating, a GDL is inserted into an automated facility which has a holder for an air brush pistol and a holder for the sample to be coated with carbon filaments (Fig. 37). The air brush pistol has a reservoir which is filled with ink. As tubing and channels within the pistol are very narrow (nozzle diameter is 0.2 mm) ink components need to be well dispersed as agglomerates block the ink flux. The pistol is connected to pressurised air (3 bar) so that incoming air can transport ink drops through the nozzle.

The holder for the air brush pistol is movable in x- and in z-direction. The sample holder is made from porous aluminium which is connection to a vacuum pump so that an inserted sample will be sucked into a pocket. Furthermore, the sample holder has an integrated electrical heating ($2 \times 24 \text{ V}/1 \text{ A}$) to heat up a sample to about $80 \text{ }^\circ\text{C}$. The sample holder is mounted on a table which is movable in y-direction. All movements are executed by a programmable logic controller (PLC). The PLC moves the air brush pistol over the sample. Travel path can be seen in Fig. 38. At the same time pressurised air is connected to the pistol to distribute the ink onto the sample homogeneously, whereat any travel path can be programmed with the controller. At a sample temperature of $80 \text{ }^\circ\text{C}$ the sprayed isopropanol evaporates quickly, just leaving the solid material on the GDL.

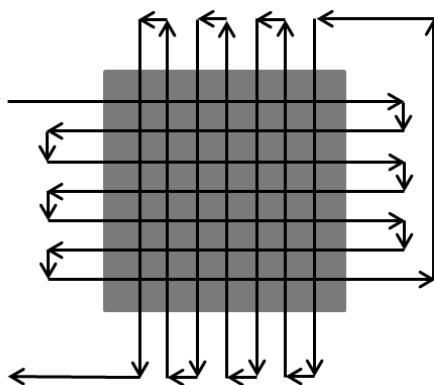


Fig. 38: Travel path of the coating facility

3.2.5. Catalyst Particle Deposition

In order to decorate the spray coated graphitic fibres with noble metal particles an electro plating process has been developed. For this work the advantage is utilised that particle deposition only occurs on surfaces, which are electrically contacted to the rest of an electrode. This is one of the issue for an active particle regarding the formation of a three phases reaction room. Furthermore, an improved localisation (directly at the interface to the polymer membrane) is expected by particle deposition subsequently to a coating of an electrode with fibres. For these reasons, it is likely that a lot of deposited catalyst particles will contribute to a large reaction room. By high porosity of the layer of carbon fibres, the third condition for an active particle (gas transport) is also fulfilled.

Electro plating is an electrochemical method regarding metal deposition from a metal ions containing electrolyte (bath) onto an electrical conductive surface. As metal ions appear as positively charged cations, the cathode (which refers to the WE in a galvanic cell) is negatively charged and the anode (which refers to the CE) is

positively charged. In comparison to chemical deposition (electroless), electro plating is achieved by applying additional electrical energy to a galvanic system. According to Faraday's law (2-11) every z electrons transferred to WE nucleation of Me^{z+} occurs⁸ [124]. A typical electro plating setup with a nickel anode, nickel chloride bath (NiCl_2) and a metallic cathode is shown schematically in Fig. 39. Here the nickel electrode is anodically dissolved and nickel deposition occurs at the cathode. With increasing voltage applied to the electrodes, deposition current increases. In order to determine potential at the WE an additional RE can be applied to the galvanic cell with a three electrodes configuration [125].

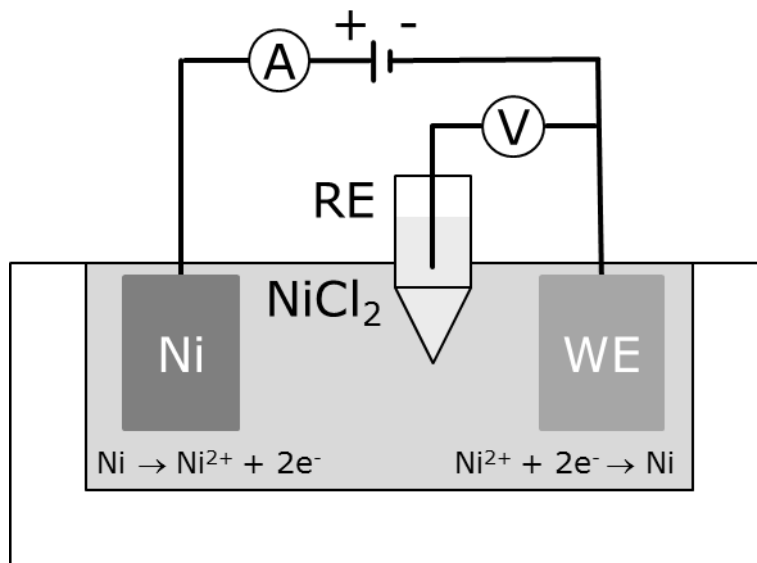


Fig. 39: Schematic drawing of nickel plating

A further electro plating process describes the deposition of a metal without dissolution of the anode material. In this case a CE is necessary which is stable in the used electrolyte environment. Furthermore, it is necessary that no corrosion product evolves. Therefore, often a platinum CE is utilised. An example for this process is the deposition of noble metals from bathes containing noble metal complexes like potassium gold cyanide ($\text{K}[\text{Au}(\text{CN})_2]$) or chloroplatinic acid ($\text{H}_2[\text{PtCl}_6]$). Furthermore, it is possible to deposit alloys from bathes containing two or more metal ion species [126 – 127].

Growth of a deposited coating is either two dimensional (formation of a bunch of monoatomic layers) or three dimensional (formation of coalescence crystallites). Which growth form occurs during the treatment is highly dependent on overpotential at the WE. Technical or decorative coatings on electrical conductive items are achieved by deposition with small current density e.g. below 10 mA cm^{-2} referred to surface of the WE. Due to low cathodic overpotential, nucleation of isolated metal atoms is

⁸ As e.g. also hydrogen evolves at the working electrode, not all transferred electrons refer to metal deposition. For an electro plating process, current efficiency is calculated from determined charge for metal deposition divided by the total charge measured during the treatment.

suppressed and layer formation is stimulated [124]. Depending on bath parameters an even coating with a thickness in sub μm range is achieved after ten to thirty minutes treatment time. Fig. 40 shows cross section of a stainless steel sample with an anticorrosive gold coating (about $0.3 \mu\text{m}$ thickness) achieved by electro plating.

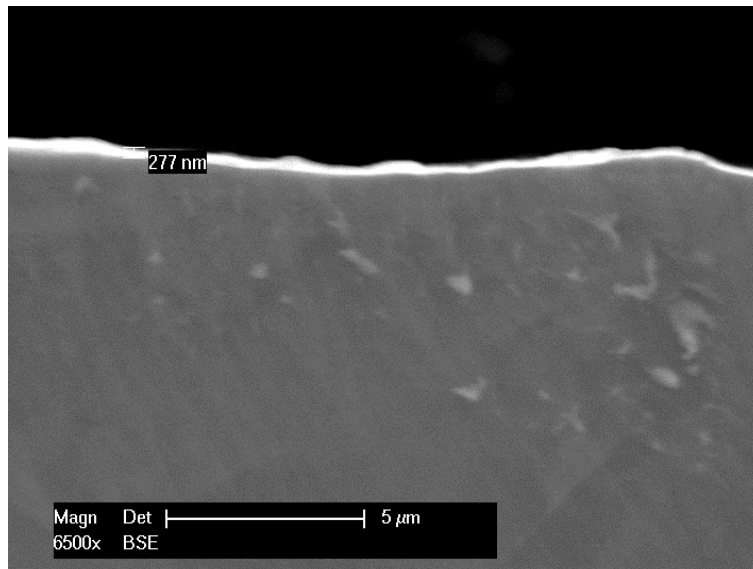


Fig. 40: SEM of a stainless steel pole plate with an anticorrosive gold coating (BSE mode)

In comparison to coatings, crystallite formation is supported by higher current density and higher overpotential, respectively. Furthermore, formation of isolated nuclei is increased by interruption of treatment by means of a pulsed electro plating process. Three typical waveforms for pulsed electro deposition are shown in Fig. 41 (a – c). Here, the pulse length is defined as λ . λ is the sum of t_{on} and t_{off} , where t_{on} means the time when current is switched on and, respectively, t_{off} means the time when current is switched off (a). In some cases it is necessary to change polarity while t_{off} . This results in anodic dissolution of metallic particles back into the electrolyte. Metallic dissolution is then dependent on anodic current density and t_{off} length (b). Furthermore, pulses can be achieved by an alternating current signal (AC) overlain to the applied direct current (DC) resulting in sinusoidal pulse form (c). In this case also polarity change can be achieved by setting the AC amplitudes accordingly.

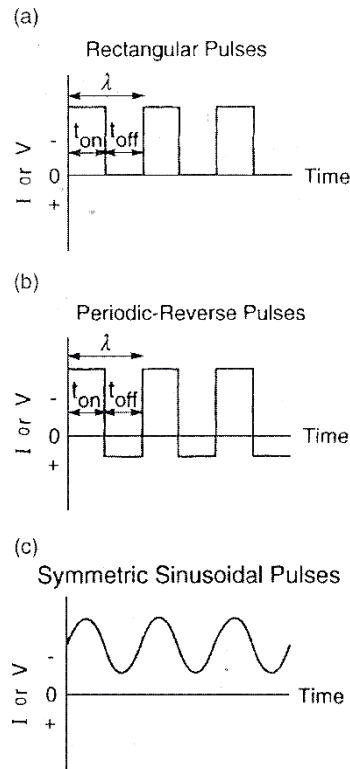


Fig. 41: Typical waveforms for pulsed electro plating processes [124]

Electro plating processes for platinum deposition on carbon supports are described in the literature [127 – 133]. Regarding the decoration of carbon filaments with catalyst particles continuous as well as pulsed electro deposition have been investigated within the scope of this experimental work. After GDL coating with a prepared dispersion platinum is deposited on a carbon filament layer from H_2PtCl_6 (Galvatron Platinbad from Wieland Edelmetalle) in order to prepare the electro catalyst for investigated electrodes. A potentiostat/galvanostat type Materials Mates 510 has been used. Bath parameters for the pulse plating process have been kept constant for all samples. The electrolyte is heated to 60 °C. The pH-value is adjusted to 2 by adding hydrochloric acid to the platinum electrolyte.

For this purpose a plating facility has been designed and constructed which is shown in Fig. 42. The device consists of a glass container for the bath, a platinum CE and a sample holder for carbon filament coated GDLs like presented above. The Plexiglas® sample holder has a pocket for specimen with a size of 50 mm x 50 mm. The inlay of that pocket is from graphite paper type AvCarb MGL 370 in order to lead the electrical contact out of the bath. A frame applied to the GDL presses the sample against the graphite paper for good electrical contact. Frame thickness is 2.5 mm. Therefore, a geometrical surface area which is in touch with the bath has the dimensions of 45 mm x 45 mm. A sample assembled in this way is inserted into a cassette which can easily be applied to the bath.

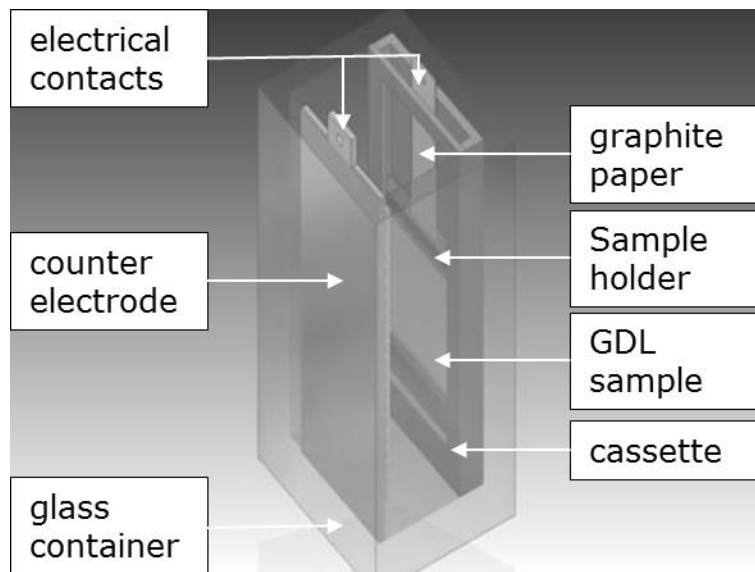


Fig. 42: Schematic drawing of an electro plating facility

3.3. Membrane Electrode Assembly Testing

Electrodes prepared like presented above have been used as anode material for MEA manufacturing. In order to determine polarisation behaviour and operation characteristics of MEAs, a novel PEMFC test environment has been developed within the scope of this described work. This test environment consists of a PEMFC stack based on hydraulic compression like explained in in chapter 2.2.7. The favourable operating conditions (homogeneous cell compressing and temperature distribution) of such a fuel cell stack are utilised for MEA testing. Due to the hydraulic compression it is possible to operate several samples with identical conditions. Therefore, differences in operation characteristics can be explained by differences in electrode configuration. With this device up to three test cells can be operated simultaneously.

3.3.1. Membrane Electrode Assembly

For this experimental work prepared MEAs have been investigated in novel test environment. Regarding the manufacturing of MEAs from GDEs, two electrodes are assembled with an un-coated PEM type Nafion 212. Prepared GDE samples have been used as well as commercially available GDEs.

Prepared and standard GDEs have been cut with the aid of an automated facility. GDE size is 45 mm x 45 mm. A tool has been constructed which helps adjusting the electrodes in order to position them on top of each other, having the membrane in between. Such a MEA is cased into two polyester films type DuPont® Mylar® A 12 – 36 µm with a window in the shape of the assembled GDEs. This polyester film works as an insulator between the two pole plates of a test cell. Such an assembly is inserted into the standard test cells of the novel MEA testing environment.

3.3.2. Test Cell Design

Test cells have been designed with mono-polar pole plates. Each graphitic pole plate has a symmetric flow field with four serpentine channels for gas distribution. Channel width and height is 1 mm. A pocket with a depth of 0.2 mm is shaped for a GDL/GDE positioning. Pole plates have been manufactured by milling. Graphite raw material type Schunk Kohlenstofftechnik FU4413/7 has been used.

Geometry of this flow field is suitable for 20.25 cm² (45 mm x 45 mm) MEAs and the pocket depth is suitable for a lot of commercially available GDL with a thickness of around 250 μm in uncompressed state. Furthermore, a set of pole plates has been manufactured with a GDL pocket depth of 0.3 mm for investigation on GDLs with thickness of 370 μm (un-compressed). The final flow field design for a standard test cell has been developed by variation of the channel arrangement and comparing polarisation behaviour of standard MEAs.

For electrical insulation the graphitic pole plates are separated by a 23 μm thin polyester film. MEAs are tightened against atmosphere with vacuum moulded silicon sealing around the flow field as well as the intake and outlet channels. During operation each pole plate has a clip which connects the half-cell to a feed gas manifold for O₂/air or H₂ respectively. At high temperature operation a special heating for the pole plates' clips is used to keep constant conditions.

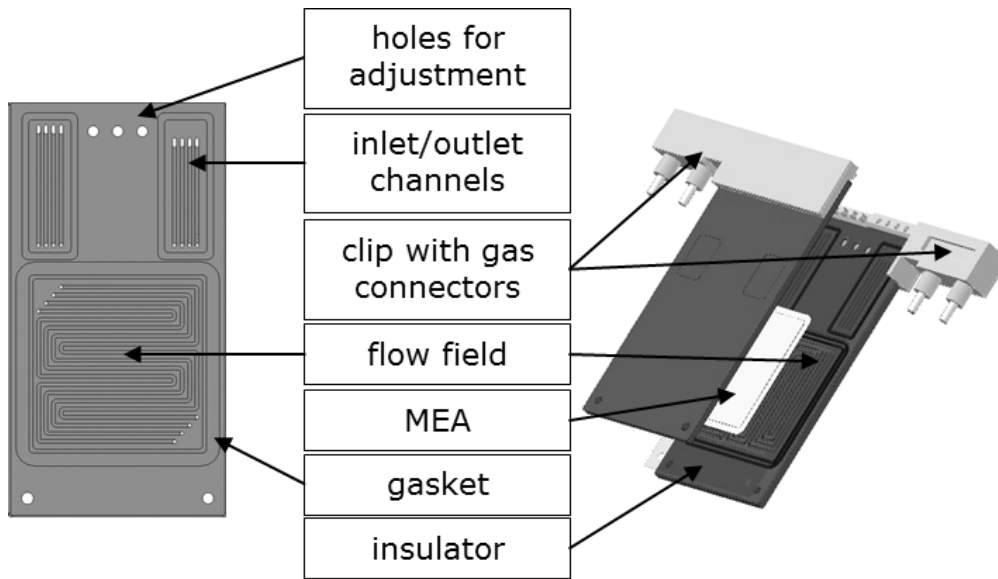


Fig. 43: Schematic drawing of a PEMFC test cell (left: front view of a pole plate; right: explosion drawing of a test cell)

3.3.3. PEMFC Test Stack in Pocket Design with Hydraulic Compression

Typically, MEA tests are performed in short PEMFC stacks with few cells or in test environments with only one sample holder. With these test systems cell compression is realised by tie bolts situated around the cell area, or by forcing heavy pressure plates to compress a sample holder pneumatically. A major problem occurs with state of the art MEA test systems due to the mechanical cell compression. As manufacturing of cell components like pole plates, current collectors and pressure plates is not ideal, compression results in inhomogeneous contact of the MEA's components. Especially, for short stacks changing the MEA samples results in a certain effort to keep constant conditions. The compression scenario may be not the same after mounting the stack with new samples, which can lead to different operation characteristics. Furthermore, for test stacks with just one sample holder, comparison between different MEA samples is difficult due to changing operation conditions – at least opening and closing the mechanical compressed test cell. Therefore, differences in electrode composition of a series of samples may not be considered by a typical test environment.

A novel PEMFC stack design has been suggested, which is described in chapter 2.2.7. Due to hydraulic compression of each cell in the stack compression is even over the active cell area. Cell temperature is the same for all cells due to a completely surrounding hydraulic medium. Upon this design considerations a novel test environment has been developed within the scope of this experimental work. This test system is suitable for those cells presented in the previous sub-section.

The patented modular PEMFC stack concept [101] uses single cells in separate elastic pockets encapsulated by a pressure apparatus filled up with hydraulic medium. These pockets have their openings at bottom and top of the pressure container (Fig. 44). The invented pocket design results in an easy assembling and disassembling of separated PEM fuel cells. Due to the ability to change cells in a short time the concept is user-friendly for MEA testing. Gas supply for inserted fuel cells is realised over an intelligent clip construction on top of each pole plate. Feed gas is supplied in parallel or in series from a central gas manifold. For operation of the fuel cell test stack the hydraulic medium within the pressure apparatus needs to be pressurised for cell compression. Dissipated heat due to losses within the fuel cells is transferred to the pressurised fluid and can be removed from the process via heat exchangers.

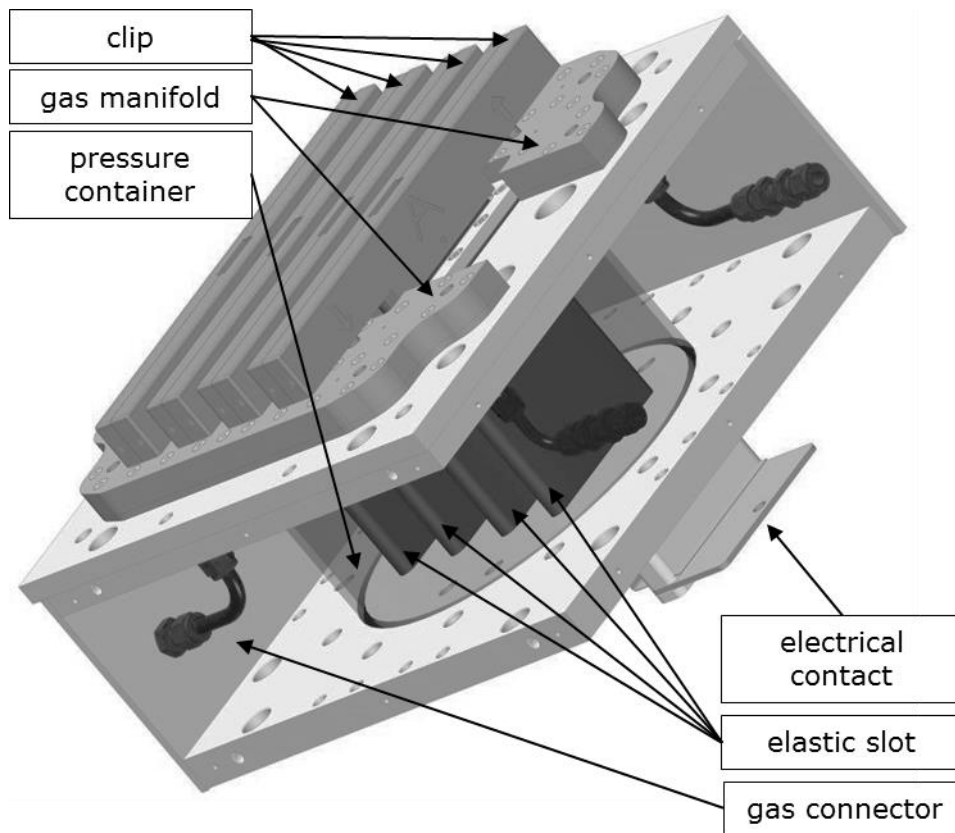


Fig. 44: Schematic drawing of a PEMFC stack in pocket design with hydraulic compression (with four single fuel cells inserted)

The realised test stack (Fig. 45) used for this experimental work has three slots formed by elastic polyurethane (PUR) tubes. Those tubes are fixed up with screws at top and bottom of the pressure container which is filled up with water. Top and bottom plate are pulled together by twelve massive tie bolts. A sealing between pressure container and those plates is compressed in order to prevent the test system from water leakage at operation (hydraulic pressure up to 10 bar). Water can be exchanged over two connectors (water inlet and outlet) which is necessary for stack temperature controls. Furthermore, hydraulic pressure controls are connected to the water system. Water inlet and outlet are situated at the rear side of the stack.

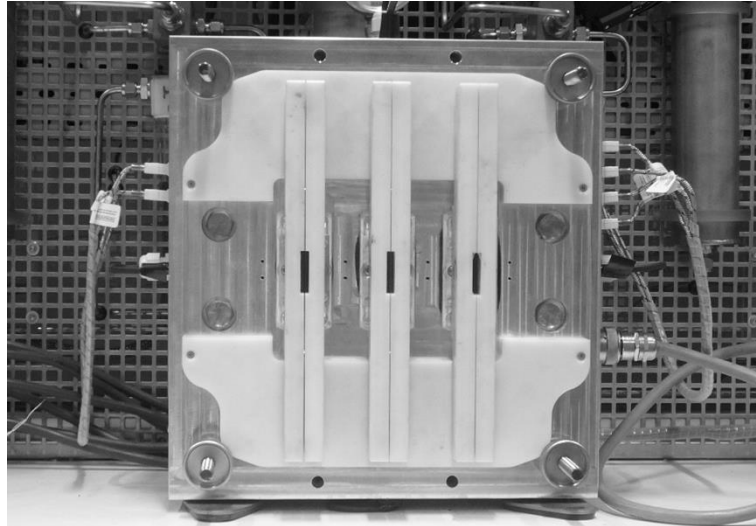


Fig. 45: Photograph of the realised test stack for PEMFC MEAs (already integrated into the test bench)

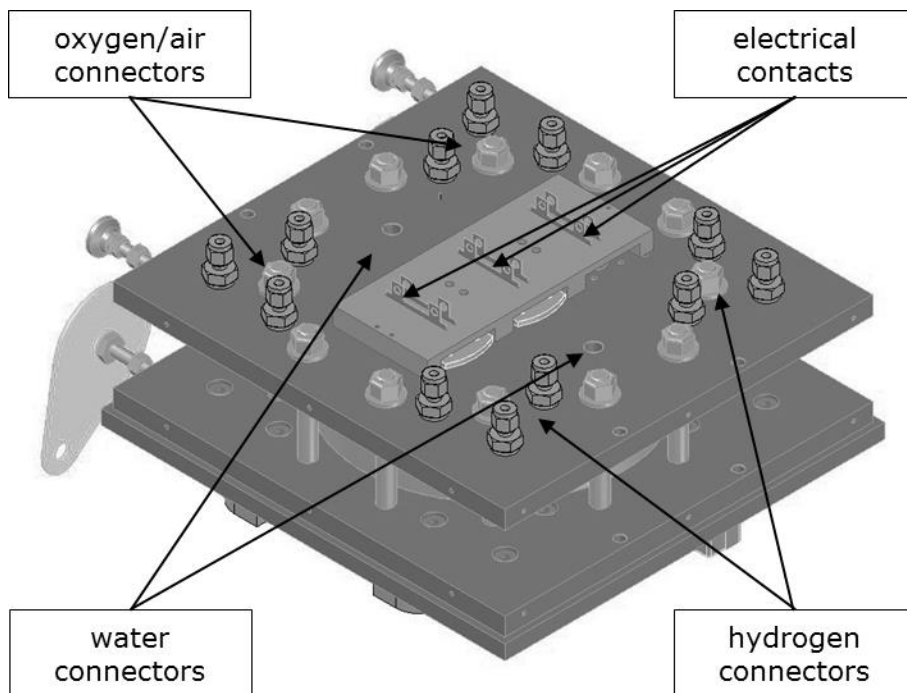


Fig. 46: Rear view of the novel MEA test stack with hydraulic compression

The gas manifold is made from acrylonitrile-butadiene-styrene (ABS). ABS is thermal stable up to 80 °C. Furthermore, the manifold is constructed of two parts which are agglutinated to each other. This is possible by the use of dichloromethane (CH_2Cl_2). Gas channels within the manifold distribute the feed gases to the test cells. Each test cell is supplied separately. The main gas connectors are on the back side of the stack (Fig. 46).

3.3.3.1. Pressure Distribution

Cell compression has major influence on the operation characteristic of a fuel cell. By increasing the compression forces, contact resistance decreases which leads to decreased voltage drop at operation with higher current density. An even pressure distribution is needed to result in even distributed current density. It is necessary to keep the current density distribution homogeneous in order to avoid locally higher temperatures above acceptable limits. These hot spots can occur due to pressure gradients and may lead to punctuation of the membrane which leads to accelerated cell degradation. Therefore, pressure distribution, current density distribution and temperature (chapter 3.3.3.2) distribution is determined for this novel test cell design which are expected to be homogeneous due to the hydraulic compression.

To determine pressure distribution over the geometrical cell area, investigations have been carried out with pressure sensitive film from FUJIFILM®. For qualitative determination Prescale Super Low Pressure (LLW – 6 to 25 bar) has been used. According to show differences in cell compression of the novel MEA test stack in comparison to conventional compressed fuel cells, a fuel cell test stack has been developed with pole plates which have identical flow field, sealing as well as GDL pocket geometry like above. The tie bolts are situated around graphitic pole plates. Compression forces are induced via aluminium pressure plates with a thickness of 20 mm (Fig. 47).

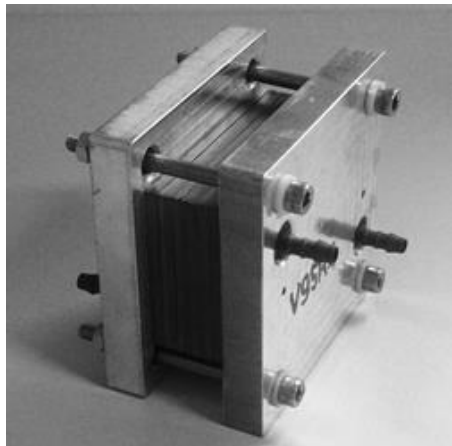


Fig. 47: Photograph of a PEMFC stack with mechanical compression over tie bolts

The experimental setup is prepared by applying a GDL to each pole plate of an investigated test cell. Furthermore, pressure sensitive film is inserted in each test cell in place of a membrane. The novel test stack has been pressurised hydraulically at 6 bar. The conventional stack with three test cells has been compressed mechanically. Compression forces have been increased as far as the silicone sealing tightens the test cells.

3.3.3.2. Current Density and Temperature Distribution

Due to homogeneous compression and cooling by the hydraulic medium uniform current distribution is expected. In order to investigate current distribution a special pole plate is realised which has eight separate segments. Flow field design is identical to the already described test cell. Insulation between the segments is achieved by epoxy resin. The active geometrical cell area is decreased due to epoxy frames around each segment. Segment have a geometrical area of 2 cm^2 resulting in an active cell area of 16 cm^2 . Each segment is connected to a shunt resistance with 0.1 Ohm . Voltage drop at operation is measured simultaneously in order to determine current density distribution. Furthermore a type K thermocouple is integrated into each segment. Temperature and voltage drop are measured simultaneously.

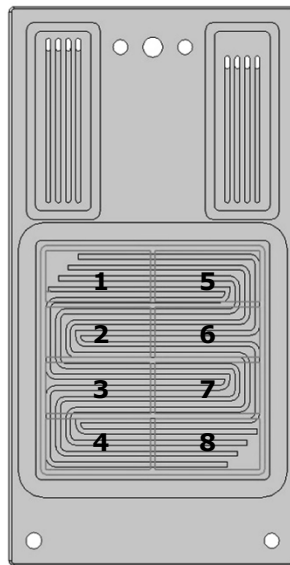


Fig. 48: Schematic drawing of a segmented pole plate

3.3.4. PEMFC Test Bench

The MEA test stack has been integrated into a full automated test bench designed and constructed at the Westphalian University. The three main functions of the developed test bench are: providing feed gases, controlling stack pressure as well as temperature, and fuel cell testing. For safety issues the test bench is connected to the laboratory's emergency shutdown facility. A software has been developed for automation and controls as well as for an operator console. Operating the test bench

is possible over a touch screen. Furthermore, process data is saved into a SQL (structured query language) database. Recent values are visualised at the operator console. Human device interface (HMI) software is programmed with MATLAB from National Instruments. Photograph of the realised test bench is shown in Fig. 49.

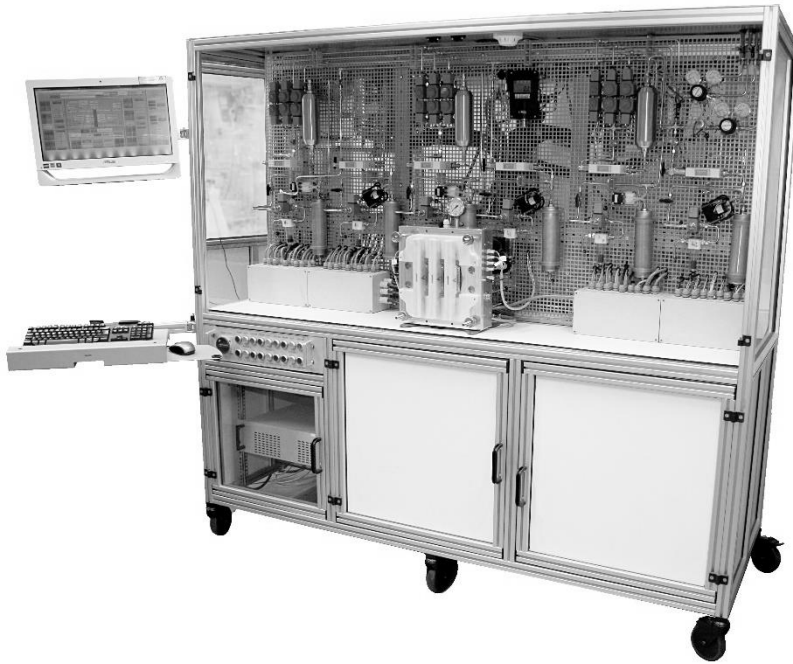


Fig. 49: Photograph of the novel test bench which is optimised for MEA testing (without front doors)

3.3.4.1. Feed Gas Supply

The test bench is connected to the laboratory's central hydrogen storage. Hydrogen with a purity of 5.0 (99.999%) is distributed to the test device at room temperature. For gas distribution within the test bench pressure is reduced from about 6 bar to about 1 bar overpressure. Starting at the pressure regulation valve hydrogen is distributed over stainless steel tubing. Pressure and temperature are monitored. Each test cell (FC1 to FC3) has its own gas supply (Fig. 50).

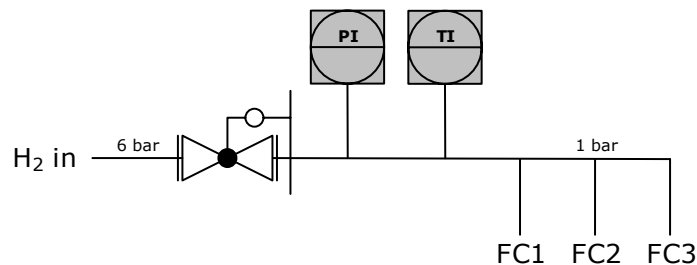


Fig. 50: Main gas distribution within the test bench

For each gas channel hydrogen is conditioned according to pressure level, temperature and humidity. Gas flux into the gas path is monitored by MFM. Pressure is reduced further in order to adjust the gas pressure at the test cell inlet to e.g. 0.2 bar overpressure. A pressure sensor as well as a temperature sensor is situated in front of the gas manifold's inlet. For setting temperature and humidity a novel humidifier based on water evaporation has been developed [134]. Process diagram of the humidifier is presented in (Fig. 51). Tubing from the humidifier to the test cell's inlet is tempered to desired temperature. After hydrogen passed the test cell moisture is decreased by a condensate trap. Hydrogen is pumped in circle through humidifier, test cell and condensate trap by a diaphragm pump. This means test cell outlet is connected to the gas path right behind the MFM. Only the amount of hydrogen which is consumed by the fuel cell is delivered to the gas path. A purge valve is provided for maintenance reasons (e.g. purging with nitrogen). Hydrogen flux through the test cell is controlled by adjusting operation voltage of the pump. In order to avoid pressure peaks buffer volumes are integrated into the gas path (Fig. 52).

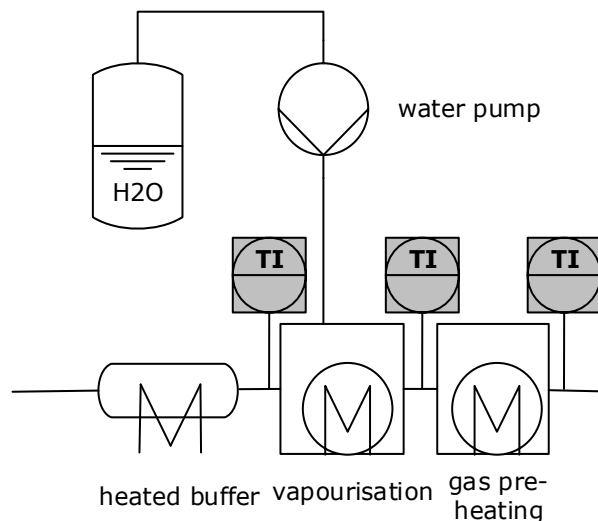


Fig. 51: Process diagram of the humidifier with integrated gas heating

The fuel cell test bench is operated with ambient air from the laboratory. The gas path for air consists of the same components as for hydrogen (MFM, humidifier, temperature and pressure sensor, test cell, moisture trap). However, as air is fed to the cells in open end modus, outlet of the moisture trap is connected to a central suction at the roof of the test bench. This is necessary in order to avoid hydrogen emission to the laboratory. Hydrogen at the cathode can occur by gas crossover or internal leakage (Fig. 53).

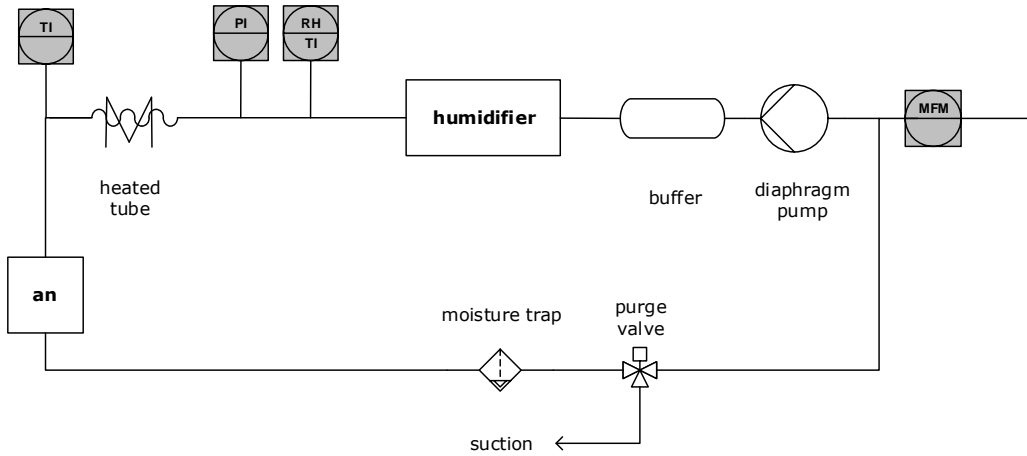


Fig. 52: Anodic gath path

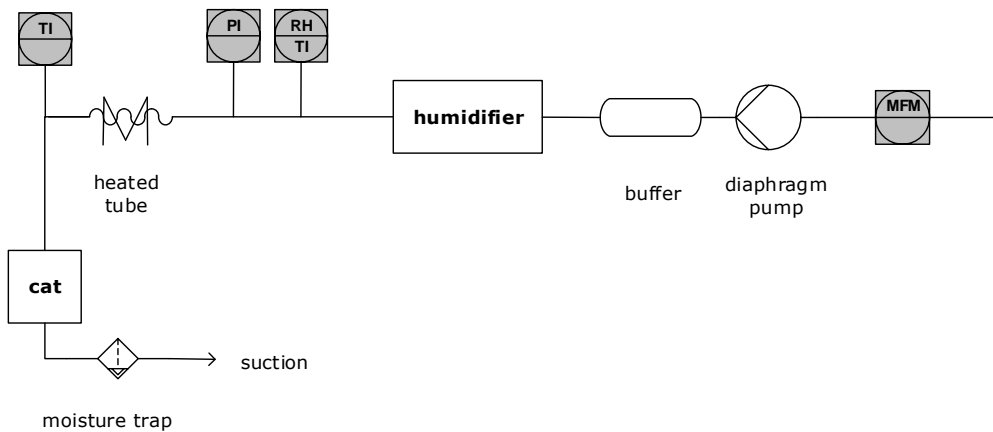


Fig. 53: Cathodic gas path

3.3.4.2. Stack Temperature and Pressure

For MEA testing it is possible to control temperature and pressure level of the test stack. For this reason it is possible to exchange the hydraulic medium by a high pressure diaphragm pump. Temperature is monitored at the water inlet and outlet of the developed stack. For stack tempering water passes a plate heat exchanger. The heat exchanger is connected to the laboratory's water infrastructure. Feed water has a temperature of about 20 °C (may be used for cooling). For stack heating temperature can be increased up to 60 °C.

Hydraulic stack pressure is controlled. Water tubing is connected to a pressure tank which contains a flexible water proofed membrane element. This pressure tank is connected to the laboratory’s pressurised air infrastructure (up to 10 bar). Three solenoid valves are arranged in a way that pressurised air is applied to the membrane element with a desired pressure. Pressure level on each side of the membrane element is identical. A pressure sensor is situated within the stack in order to monitor the pressure level at fuel cell operation.

3.3.4.3. Operator Console

The operator console gives information about recent values of the process variables over a touch screen with a HMI software. All sensors of the test bench are visualised in order to give an operator the necessary information to decide either the fuel cell operation is normal or not. Each test cell is visualised on a separate page (Fig. 54).

Furthermore, the operator is able to control the test bench. While feed gas pressure needs to be adjusted by the pressure regulation valve manually, temperature, humidity and gas flux (diaphragm pump velocity) are set over the HMI. For air flux the operator can choose either λ -controlled or constant flux modus. Stack variables may be controlled over a separate HMI page.

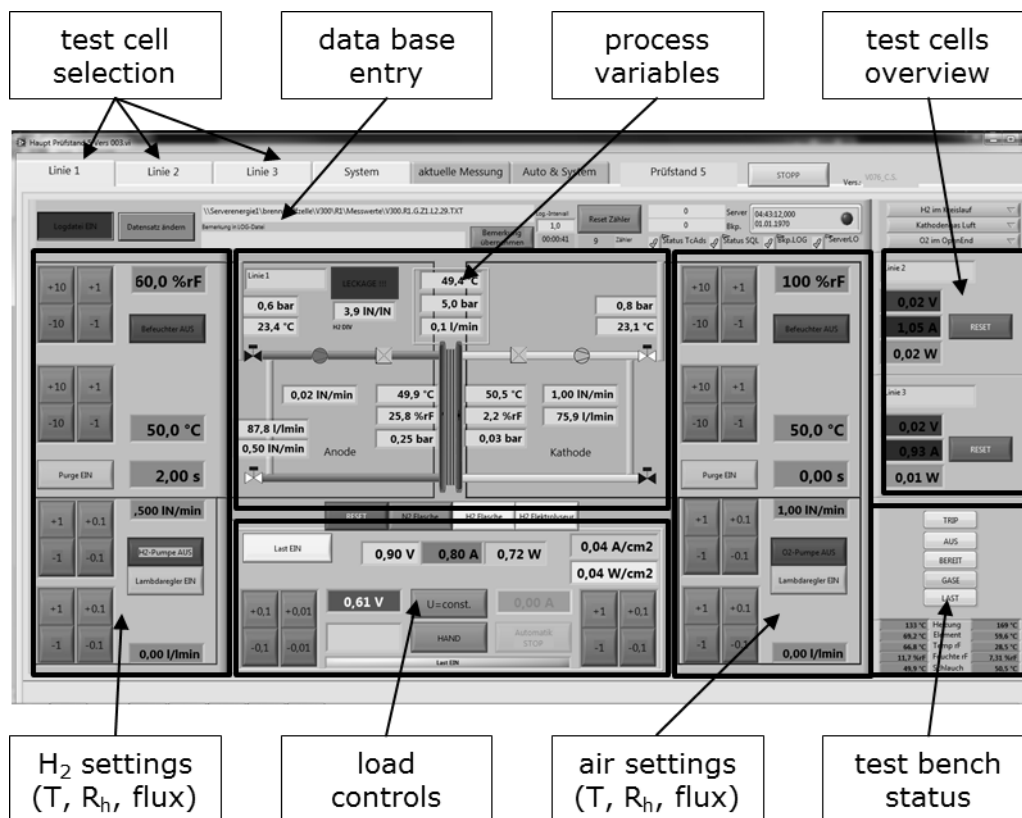


Fig. 54: Human device interface for the novel fuel cell test bench (overview about settings for test cell 1 (feed gas and electronic load controls))

3.3.4.4. Determination of Polarisation Behaviour and Operation Characteristics

Each test cell can be connected to controlled electronic load. From the operator console a desired load point can be achieved by either forcing constant current or constant voltage, respectively. The corresponding value is determined in order to investigate a fuel cell's specific characteristic. Programming a certain load procedure is also possible. E.g. polarisation curves are determined in constant voltage modus. Cell voltage is decreased from open circuit voltage (OCV) to 0 V (short circuit). For long term testing constant current modus is often used as λ -controls refers directly to the applied load current and therefore, operation is more stable over time. Furthermore, current peaks repeated after a certain period may improve operation stability due to short-term increased production of water. This additionally product water humidifies the membrane which prevents the membrane from drying and, therefore, improves membrane resistance. For investigation on MEAs prepared for this Ph.D. thesis an electronic load type Höcherl & Hackl ZS1806NV has been applied.

3.3.4.5. Safety Functions

For safety reasons the test bench is connected to the infrastructure of the fuel cell test laboratory. A concept has been developed which implements the needed safety functions but realises a high availability for the operating researcher. Following described functions are obligatory for fuel cell testing due to the application of explosive hydrogen.

Therefore, the maximum gas leakage into the test bench is limited by a throttle right behind the pressure regulation valve of the 200 bar H₂ gas bottle. This is valid for each test bench in the laboratory. The novel test bench is connected to a central suction which is explosion protected. In case of H₂ leakage the hydrogen concentration within the test bench is reduced below explosion limits by permanent flushing with ambient air. Air flux through the suction inlet is monitored. If air flux drops below the necessary amount for safe operation, the test bench is switched off.

A hydrogen detector is situated central at the roof of the test bench. This sensor monitors hydrogen concentration within the test bench. An alert occurs if a concentration is detected higher than 1% (25% of lower explosion limit) for at least 10 seconds. In this case the test bench is shut down. Exceeding the hydrogen concentration beyond 2% (50% of lower explosion limit) results in immediate test bench shut down.

Furthermore, stack pressure is monitored. As gaskets of the test cells need to be compressed in order to avoid gas leakage, hydrogen feed gas is turned off and electrical load is switched off. The test bench is still running. However, testing is prohibited without sufficient stack pressure.

Further safety issues are related to e.g. to hardware buttons. Emergency switches are provided from each side of the test system. Furthermore, hardware buttons for H₂ are situated at the front to open the valves at the test bench's gas inlet. Even if the control panel's software stopped for any reason, the operator is able to turn off feed-gases. The test bench is integrated into the emergency shutdown chain⁹. For a prospective operation with pure oxygen further safety issues need to be considered.

⁹ Six test benches are operated simultaneously at the fuel cell test laboratory. If one test bench is switched off due to emergency issues, all test benches are switched off immediately.

4. RESULTS AND DISCUSSION

Target of this experimental work is the development of fuel cell electrodes with low platinum loading and improved platinum utilisation in comparison to standard Pt/C electro catalyst based electrodes. Carbon filaments have been investigated as catalyst support material due to favourable properties, especially, high graphitisation degree and high specific surface area. All materials used for GDE preparation have been investigated previously to ensure feasibility for this purpose. Results of material characterisation are presented in section 4.1.

Prepared electrodes have been used for MEA manufacturing. MEAs were tested within the novel test environment with hydraulic compression. In order to ensure functionality of the developed test system, preliminary tests have been carried out with standard MEA components, before testing MEAs based on prepared electrodes. Investigation on the novel test system are described in chapter 4.2. Preliminary tests with standard Pt/C based electrodes have been carried out. Experimental results may be taken from chapter 4.3.

Focus of the preparatory work is on platinum particle deposition by means of an electro plating process. Catalyst deposition subsequently to carbon filament coating results in improved localisation of active particles. Microscopy studies have been performed intensively of prepared catalyst layers in order to determine particle size and distribution. Furthermore, catalyst loading has been determined as well as electrochemical active surface area to get information regarding platinum utilisation. The developed carbon filament based electrodes are discussed in chapters 4.4. and 4.5.

4.1. Materials for MEA Manufacturing

Carbon filaments have some favourable properties for the use in fuel cell electrodes. Major advantages are high specific surface area and high graphitisation degree. Due to high graphitisation degree electrical conductivity is high in comparison to turbostratic graphite like e.g. carbon blacks. Therefore, carbon filaments have been investigated as catalyst support material for this experimental work in order to replace used carbon blacks in state of the art PEMFCs.

For preparation of GDEs, typically used GDL material works as substrate for a carbon filament layer. After catalyst deposition by pulse plating MEAs are manufactured by two GDEs and an uncoated membrane in order to investigate fuel cell characteristics in the novel MEA test system. Prepared GDEs have been used as anodes. For comparison reasons as cathode material standard GDE material with high platinum loading was used. Different types of Nafion[®] membranes have been tested.

4.1.1. Carbon Filaments

For this Ph.D. thesis helical ribbon CNFs type GANF have been investigate as catalyst support for platinum particles. Material properties have been compared with CNTs which were studied previously by the working group. CNT and CNF raw material was produced in industrial scale and supplied by Grupo Antolin, Spain [135] (Appendix A.1).

By XRF spectroscopy catalyst material has been identified. XRF measurements are performed at three different points of a powder sample. It was found that CNF catalyst is only nickel. Catalyst content from fibres production of investigated CNFs has been determined by thermogravimetric analysis (TGA). For TGA three powder samples have been analysed. Catalyst content is varying in the range of $13.2\% \pm 4\%$.

By XRD studies interlayer spacing (d_{002}) of powder samples has been determined in order to calculate graphitisation degree G_p . Here, measured value for d_{002} is compared with d_{002} for ideal graphite (highly oriented pyrolytic graphite – HOPG) which is 0.3554 nm and d_{002} for turbostratic graphite which is 0.344 nm according to the following equation [136]:

$$G_p[\%] = \frac{d_{002\text{tg}} - d_{002}}{d_{002\text{tg}} - d_{002\text{HOPG}}} \cdot 100 = \frac{0.344 - d_{002}}{0.344 - 0.3554} \cdot 100\% \quad (4-1)$$

A mean value for d_{002} of 0.33625 nm has been obtained resulting in a graphitisation degree of $90.0\% \pm 2\%$. Measured XRD spectra for investigated CNTs as well as for CNFs is shown in Fig. 55. Tab. 3 gives an overview about the material properties of investigated carbon fibres.

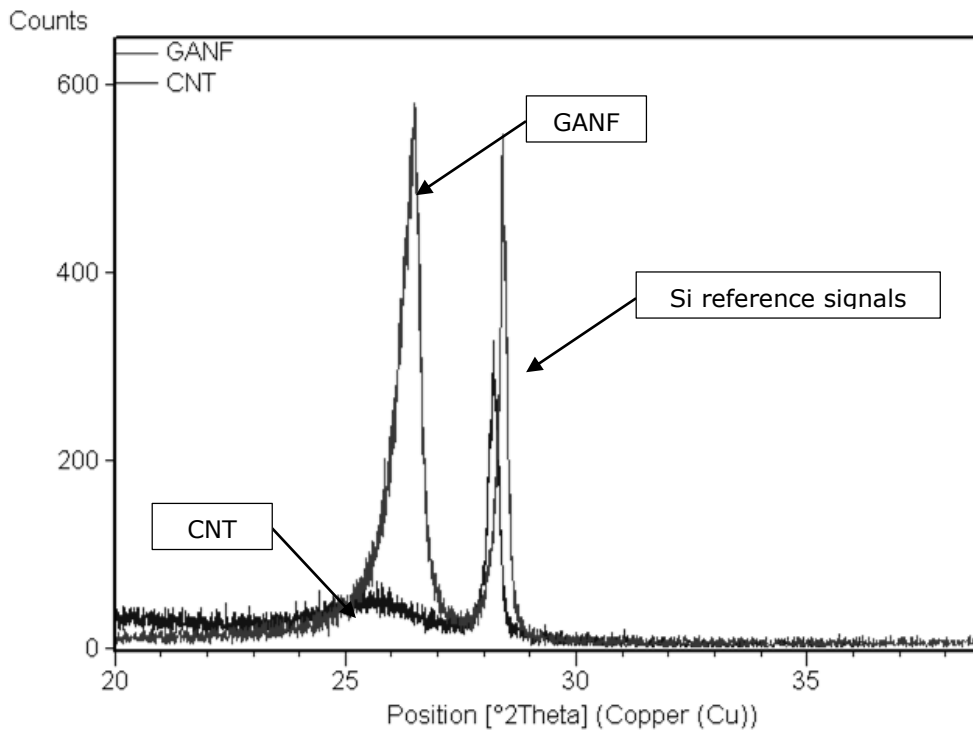


Fig. 55: XRD spectra of CNT and CNF raw material (powder)

Tab. 3: Properties of investigated carbon fibres

Property	GANF (data sheet)	GANF (analysed)	CNT (data taken from [80])
Fibre diameter [nm]	20 - 80	50	
Wall thickness [nm]		10	
Fibre length [μm]	> 30		
BET surface [$\text{m}^2 \text{g}^{-1}$]	150 - 200		45
G_p [%]	70	90.0 ± 2	31.27
Electrical resistivity [Ωm]	1×10^{-3}		8×10^{-5}
Metallic particles content (Ni) [%]	6 - 8	13.2 ± 4	2

From Fig. 56 the diameter of an investigated CNF have been determined to be about 50 nm. This corresponds well to the data sheet which states a 20 nm to 80 nm fibres diameter. Length has not been identified by microscopy. From the data sheet length is known to be > 30 μm . From Fig. 57 one can obtain the wall thickness, where graphene layers of the fibres are clearly visible. Wall thickness of CNFs is in the range of 10 nm. Visible high parallelism of graphene layers is further evidence for high graphitisation degree.

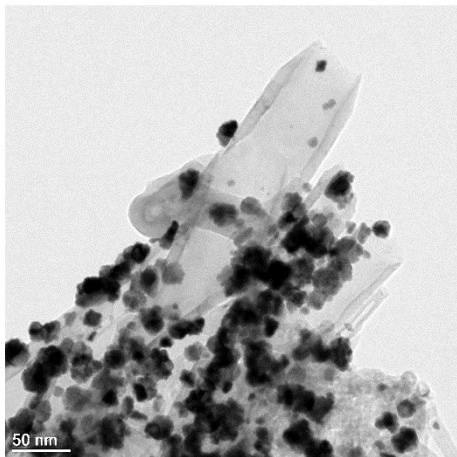


Fig. 56: TEM microscope image of CNFs with Pt decoration

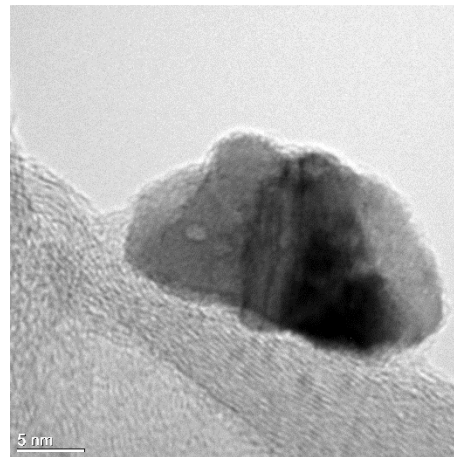


Fig. 57: TEM microscopy of a CNF with adhered Pt cluster

It becomes evident that CNF characteristics change with the production batch. Ni content and graphitisation degree which have been measured for this work, differ from values in the data sheet. A variety of different GANF batches have been analysed. The described results were obtained for GANF presented in this subsection.

4.1.1.1. Oxygen Plasma Functionalisation

The investigated CNF raw material has a hydrophobic character, which is problematic regarding the formulating of a stable dispersion. It is known that the formation of oxygen containing functional groups on the surface of the CNFs occurs due to a treatment in oxygen plasma. These functional groups are able to increase

the wettability of the fibres. A quick method to characterise a functionalisation by oxygen plasma is to measure the contact angle and the surface energy of the carbon fibres before and subsequently to the plasma treatment. Wettability is achieved for low contact angle and high surface energy. For this experimental work suitable plasma parameters (plasma power and treatment time at a constant gas flux of 0.1 l min^{-1} oxygen through the reactor) have been obtained, which result in increasing wettability. The initial point for this investigation has been a study on plasma activated CNTs carried out by the working group previously [80].

Contact angle of the CNF raw material was determined to be 88° . Contact angle after the oxygen plasma treatment with a plasma power of 150 W is shown in Tab. 4 depending on the treatment time. It has been possible to obtain a contact angle below 65° for 5 min duration in the plasma reactor.

Tab. 4: Contact angle in water of oxygen plasma activated CNFs with plasma power of 150 W depending on treatment time

Treatment time [min]	Raw material	1	2	5	7.5	10	15	25
Contact angle [$^\circ$]	88 ± 2	87 ± 2	75 ± 1	64 ± 2	74 ± 1	80 ± 2	71 ± 2	72 ± 2

As can be noticed from the table, the contact angle decreases with increasing treatment time. A minimum contact angle has been found for a treatment time of 5 minutes. Increasing duration in the plasma reactor beyond 5 minutes results in a raise of contact angle. Increasing and decreasing of the contact angle as a function of time is observed for a plasma treatment up to 25 min. This phenomenon can be explained by the etching process, which occurs simultaneously to the formation of functional groups. This etching results in removal of the outer graphene layers of the treated fibres. Also functional groups, which appeared with the oxygen plasma treatment, will be removed by the etching effect. Therefore, a sinusoidal plot is expected for the contact angle depending on the treatment time. In Tab. 5 contact angle and surface energy γ including the two fractions of the surface energy, namely the polar γ^p and the dispersive fraction γ^d , of selected plasma parameters are presented.

Tab. 5: Contact angle in water and surface energy of plasma activated CNFs depending on different plasma parameters

Plasma parameter [W/min]	Raw material	80/30	100/20	120/10	150/5
Contact angle [$^\circ$]	88	59	65	66	64
γ [mN m^{-1}]	22	42	36	38	38
γ^p [mN m^{-1}]	6	33	27	17	16
γ^d [mN m^{-1}]	16	9	9	21	22

Selected parameters result in a similar contact angle as well as surface energy. It becomes obvious, that with increasing plasma power a shorter treatment time is necessary to achieve a sufficient functionalisation. Although fibres surface energy for all parameters is similar, regarding the wettability only the polar fraction has an influence. From the table one can obtain, that for smaller plasma power rates

(80 W and 100 W) a higher polar fraction is achieved. However, for all parameters wettability is improved in comparison to the raw material. As a result of the increase of surface energy, it was possible to maintain stable dispersions.

Furthermore, it has been investigated, if there is catalytic activity achieved by the functional group formation due to the plasma treatment. Especially, the apparent carboxylic groups are believed to be catalytically active according to the hydrogen oxidation reaction. Cyclic voltammetry measurements have been performed in 0.5 sulphuric acid at room temperature. CV diagram of selected samples is shown in Fig. 58.

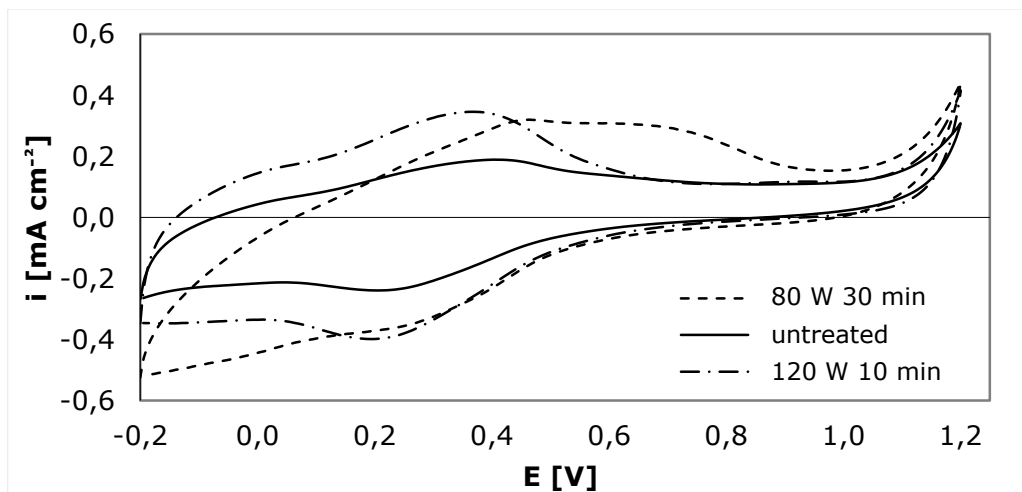


Fig. 58: CV diagram of selected carbon fibres samples depending on the plasma treatment

A significant increase in maximum current for the potential range of 0.2 V to 0.5 V was determined for plasma treated samples. These signals may occur due to redox reactions of the functional groups in this acid environment. A certain catalytic activity for hydrogen adsorption and hydrogen desorption can be assumed. Therefore, MEAs have been prepared with platinum free electrodes based on plasma activated carbon fibres (120 W/10 min) working as anode. As cathode material a standard BC-H225-10F electrode has been used as well as a Nafion® 212 membrane. In Fig. 59 polarisation curve is shown for such a MEA.

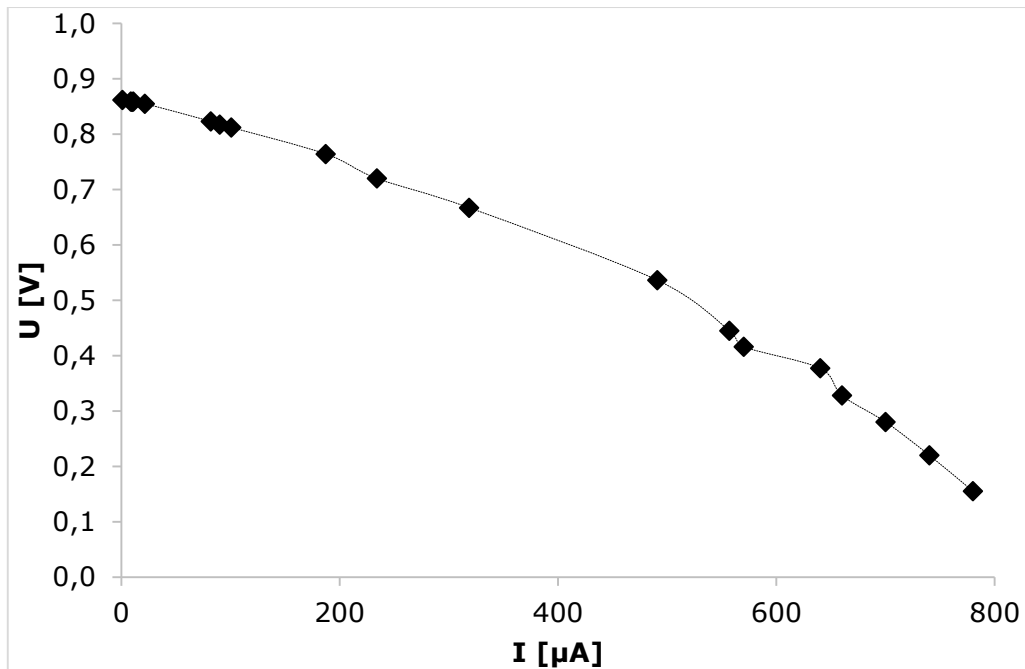


Fig. 59: Polarisation curve of a MEA with platinum free anode

From the diagram it can be seen, that an open circuit potential above 0.85 V was obtained. However, already for small load current, voltage drops immediately to zero. Therefore, the cell has been loaded with standard resistors instead of the electronic controlled load. Current and corresponding voltage have been measured separately. Maximum power output has been determined in the μW range. It was not possible to realise a useful device by this material for this described work. However, prospective solutions e.g. for hydrogen sensors may be achieved by such electrodes, but it is not relevant for this study.

4.1.2. Gas Diffusion Layer

As substrate for a catalyst layer based on carbon nanofibres typically used GDL material was investigated. Two types of GDL material have been chosen for deeper analyses: AvCarb type MGL 370 [137] and Freudenberg type H2315 I2C6 [138] (Appendix A.2 and Appendix A.3). While MGL 370 is a moulded graphite paper without having a further layer, H2315 I2C6 is woven graphite cloth with an additional carbon blacks based MPL. Fig. 60 shows microscope image of a cross section of GDL type Freudenberg H2315 I2C3. The MPL is clearly visible on top of the woven fibres. Thickness of the MPL is about 30 to 40 μm . The woven cloth has a thickness of about 210 μm . Due to different sorts of investigated GDL raw material handling is different for both types. The paper is very stiff and brittle. The cloth is more flexible.

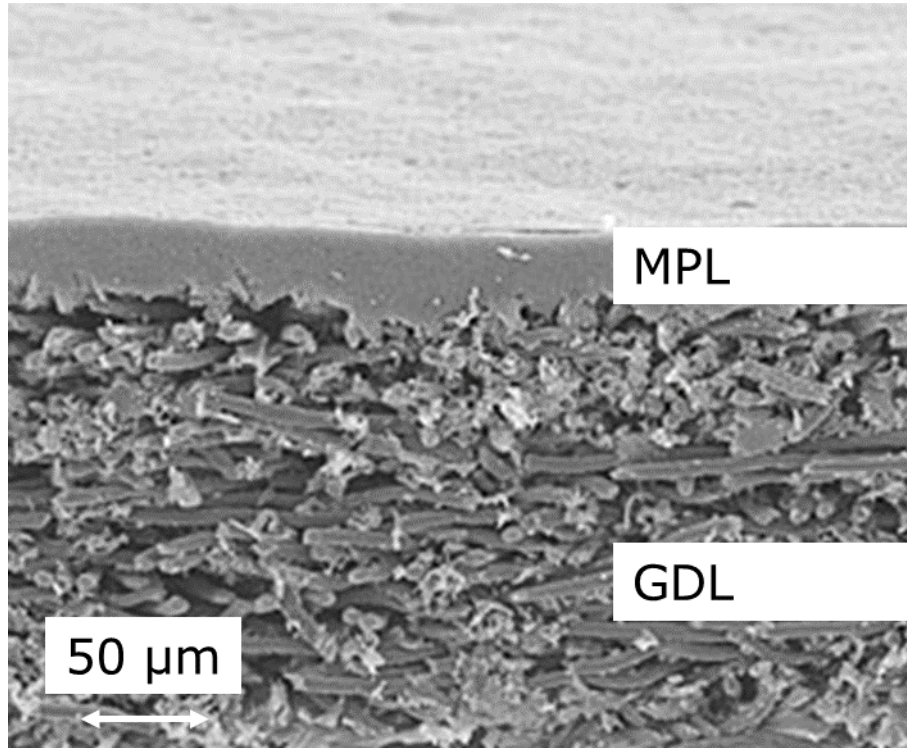


Fig. 60: Cross section of a GDL type Freudenberg H2315 I2C6 with friendly permission of Freudenberg FCCT [137]

High electrical conductivity is essential for a fuel cell electrode. As cell voltage at operation is below 1 V, ohmic resistance needs to be as low as possible (maximum current up to 2 A cm^{-2} is stated by the literature for PEMFC operation). Electrical conductivity (in plane as well as through plane) has been determined with the aid of developed test equipment (compare chapter 3.1.5.). In order to analyse the effect of an additional MPL a GDL type H2315¹⁰ has been compared with GDL type H2315 I2C6. Furthermore, graphitisation degree has been determined as a high value for G_p is an evidence for electrical conductivity of fibres used for GDL production. For each type of GDL three samples have been tested. Results for graphitisation degree are given in Tab. 6. Results for in plane resistance as well as through plane resistance may be taken from Tab. 7 and, respectively, from Tab. 8.

Tab. 6: Graphitisation degree of selected GDL samples

	G_p [%]
H2315 I2C6 woven fibres	turbostratic
H2315 I2C6 MPL	88.5
MGL 370	87.5

¹⁰ H2315 is a woven graphite cloth produced from the same fibres as H2315 I2C6. However, H2315 is delivered without PTFE treatment and without additional MPL.

Tab. 7: In plane resistance of selected GDL samples

	R_{IP} data sheet [Ω]	ρ [Ω mm² m⁻¹]	R_{IP} [Ω]
H2315	0.8	175.8 ± 3.6	0.837 ± 0.017
H2315 I2C6	0.8	189.3 ± 1.3	0.757 ± 0.005
MGL 370	no data	41.33 ± 1.5	0.112 ± 0.004

Tab. 8: Through plane resistance of selected GDL samples

	R_{TP} data sheet [mΩ cm⁻²]	R_{TP} [mΩ cm⁻²]
H2315	7.1	8.699 ± 0.46
H2315 I2C6	11	10.18 ± 0.09
MGL 370	8.8 ¹¹	43.51 ± 1.39

XRD measurements for GDL type AvCarb MGL 370 result in high G_p of 87.5%. It can be concluded, that the investigated carbon paper is heat treated in order to increase graphitisation degree. For GDL type H2315 I2C6 G_p is determined for woven fibres as well as for the additional MPL. While the MPL shows high graphitisation degree of 88.5% the woven fibres are made from turbostratic graphite (G_p about 1%).

In plane conductivity is important as compression forces to a MEA are induced over the "land areas" of a pole plate's flow field. Uncompressed areas (gas channels) will lead to crossing current from channel to land area. Values of in plane resistance determined for GDLs type Freudenberg H2315 and H2315 I2C6 are in good correspondence to the data sheet information. This may be taken as a proof for feasibility of the measurement setup. In plane conductivity for H2315 I2C6 is slightly higher than for a GDL without additional MPL. This is a result of higher thickness by the additional MPL and therefore higher cross sectional area for electrical current. Apparently, GDL type AvCarb MGL 370 has a seven to eight time higher IP conductivity than H2315 and H2315 I2C6. High electrical conductivity in plane for the carbon paper corresponds to the high degree of graphitisation of the fibres used for GDL production of MGL 370.

Through plane resistance is a characteristic value for voltage drop due to perpendicular current through the GDL. Values for H2315 as well as for H2315 I2C6 are in good correspondence to the data sheet. However, data for MGL 370 does not fit to information of the data sheet due to uncertainties about the compression forces used for the manufacturer's study. Data sheet values for H2315 and H2315 I2C6 as well as the measured values show major influence of an additional coating on a GDL. TP resistance is about 1.5 times higher for H2315 I2C6. Measurements of through plane resistance for MGL 370 result in about 5 time lower conductivity. However, product information for MGL 370 state a much lower through plane resistance than determined experimentally. It can be assumed that higher compression pressure is needed in order to result in the data sheet value. However, for this work maximum

¹¹ Compression forces, which are applied for measuring, for this value are not known from the data sheet.

fuel cell test stack pressure is limited to 8 bar. Prospective developments may lead to higher maximum pressure level for the hydraulic medium.

As the development of an electrode (including pole plate with flow field, GDL if necessary with MPL and a CL) is a multidimensional task due to electrical current as well as gas and liquid transports, further analyses are necessary in order to determine which type of GDL is more suitable for GDE preparation. Therefore, operation characteristic of GDLs type H2315 I2C6 and MGL 370 has been investigated in-situ in a fuel cell test bench. MEAs have been assembled by the use of two GDLs and a CCM from Gore®. Gore® CCM is used due to its reproducible fuel cell characteristic. Fuel cell testing has been performed for robust operation conditions (room temperature, un-humidified ambient air, stack pressure 8 bar). Polarisation curve of prepared MEAs is shown in Fig. 61.

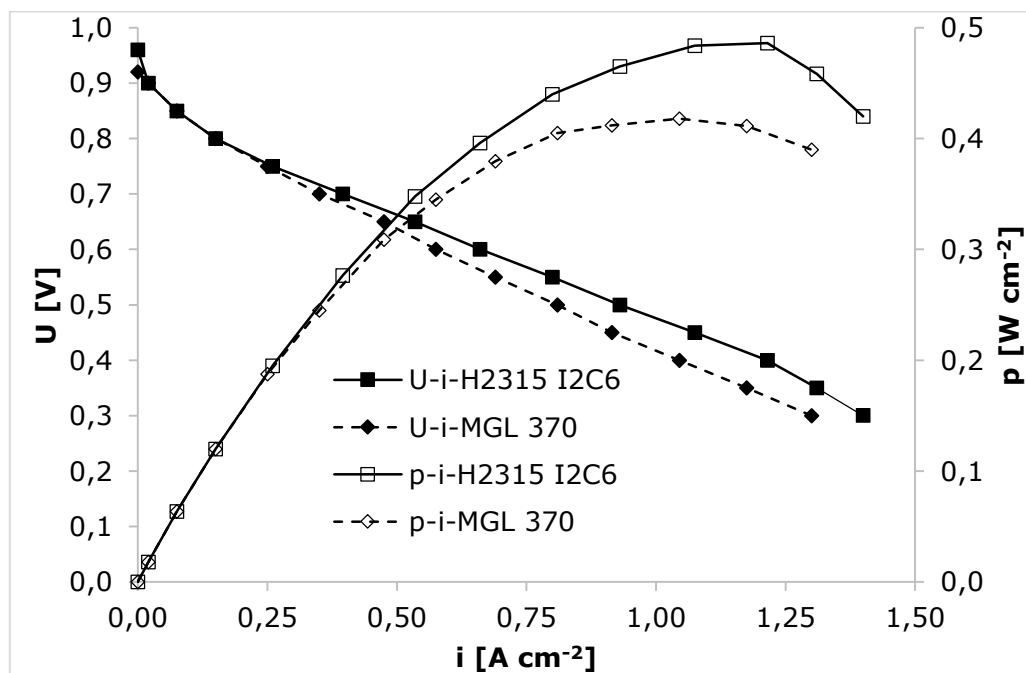


Fig. 61: Polarisation curve of MEA based on Gore® CCM depending on assembled GDL

Polarisation behaviour of a MEA with GDL type H2315 I2C6 shows higher power output than MEA with GDL type MGL 370. Ohmic voltage drop of the H2315 I2C6 based MEA is lower, which is a result of lower electrical resistance. This corresponds to the difference in through plane resistance of H2315 I2C6 and MGL 370 which is presented above.

Measurements performed on GDLs type H2315 I2C6 and MGL 370 result in higher graphitisation degree for graphitic fibres used for production of the graphitic paper. However, electrical conductivity through plane and specific power output at fuel cell operation is slightly increased for H2315 I2C6. Therefore, in this work development of a CNF based GDEs is promoted by the use of GDL type Freudenberg H2315 I2C6 as substrate for an advanced catalytic layer.

4.1.3. Cathode Material

For this study, MEAs are prepared from two GDEs and an uncoated Nafion® membrane. Therefore, suitable electrode material is needed for the cathode as well as for the anode. Prepared GDEs for this experimental work are used only as anodes. Commercially available GDE material type BC-H225-10F with high platinum loading (1 mg cm^{-2}) and additional PTFE treatment was assembled [139]. For a systematic comparison of prepared GDEs, cathode material has never been changed within the scope of the preparatory work.

Electrode material type BC-H225-10F is designed especially for the use as cathodes in PEMFCs as well as in direct methanol fuel cells. Here preparation of a CL is based on a platinum on carbon blacks electro catalysts. GDL type Freudenberg H2315 I2C6 works as substrate which makes it an ideal material for comparison with prepared CNF based GDEs, if it is used also as an anode. Analyses carried out on this material are described in chapter 4.3.

4.1.4. Polymer Electrolyte Membrane

Regarding the MEA manufacturing, two electrodes are assembled with an uncoated PEM type DuPont Nafion®. Three different membranes have been investigated: Nafion 212, Nafion 115 as well as Nafion XL. These differ in number of sulphuric acid side chains per gram membrane material [given in meq g^{-1}] which is a measure for ion conductivity. Furthermore, these membranes are distinct from thickness.

From the data sheet total acid capacity for Nafion 115 as well as Nafion 212 is in the range of 0.95 to 1.01 meq g^{-1} (Appendix A.4 and Appendix A.5). This results in ion conductivity equivalent to electrical conductivity of 0.100 S cm^{-1} for a humidified membrane at very high temperature of $100 \text{ }^\circ\text{C}$ [140, 141]. Acid capacity for Nafion XL is not given from the data sheet (Appendix A.6). However, conductivity is stated to be 0.052 S cm^{-1} [142]. Thickness for these types of membranes are 0.127 mm for Nafion 115, 0.050 mm for Nafion 212 and 0.028 mm for Nafion XL, respectively. Fig. 62 shows polarisation behaviour of MEAs prepared with standard Pt/C based GDE material (BC-H225-10F) for the anode as well as for the cathode depending on membrane material. Fuel cells have been operated with ambient air at room temperature.

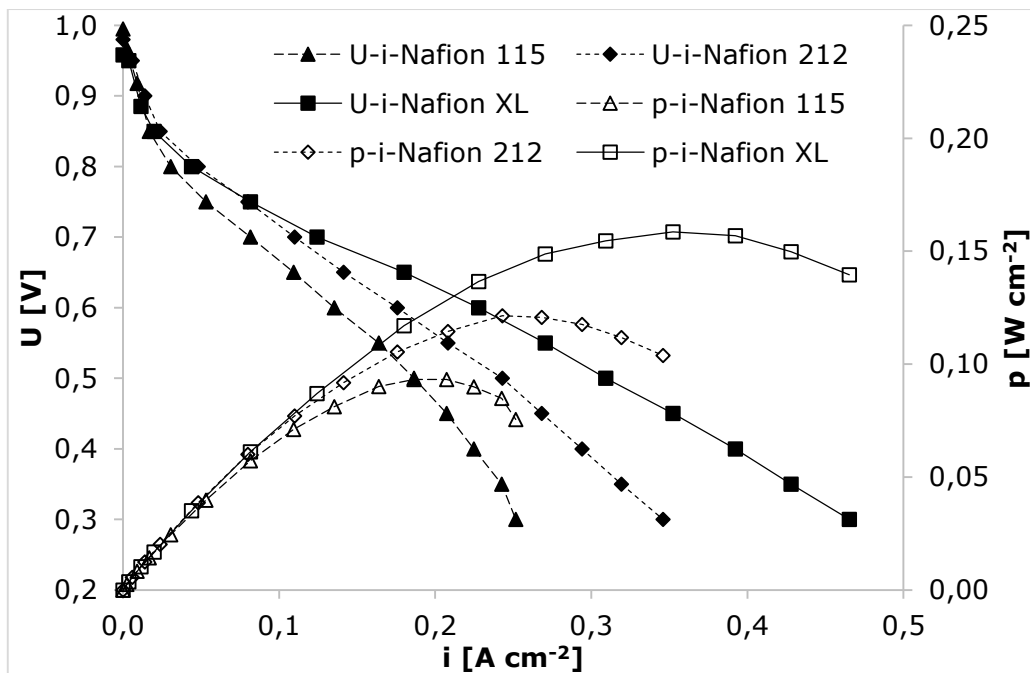


Fig. 62: Polarisation characteristics of MEA depending on membrane material

Due to much higher thickness, membrane resistance for Nafion 115 is higher than for thinner membranes tested. As a result maximum power output from this cell is only in the range of 0.095 W cm^{-2} . Furthermore, from long time tests with ambient air without additional humidification MEAs with Nafion 115 suffered from drying which decreases cell voltage over time (Appendix B.1). Maximum power output from fuel cells with Nafion 212 has been determined to be 0.122 W cm^{-2} , and 0.158 W cm^{-2} for Nafion XL, respectively. Differences can be explained by different thickness. Except of typical degradation both MEAs can be operated at ambient conditions without losing cell voltage (Appendix B.2 and Appendix B.3).

Within the scope of the described study problems emerged by assembling fuel cells with membranes type Nafion XL. Due to very low thickness, puncture is likely by manual MEA preparation. As a result operation is unsafe and lower power output is expected due to gas crossover. Although higher power output has been achieved with a proper Nafion XL membrane, fuel cell experiments for in this work have therefore been carried out with membrane type Nafion 212. This is a compromise between handling and power output.

4.2. A Novel MEA Test Environment

The developed MEA test environment based on a modular PEMFC test stack with hydraulic compression is novel in fuel cell laboratories. Already, two prototypes have been constructed, of which one is operated at Westphalian Energy Institute and the other at a partner company's test laboratory. Therefore, this test system has been investigated in order to ensure functionality as well as to underline advantages due to the patented stack design.

Commercially available MEA components have been tested in the novel PEMFC test environment as reproducible fuel cell characteristic is expected for a series of MEA samples which is necessary for these preliminary investigations. Fuel cell tests have been carried out in order to ensure functionality of the novel PEMFC test environment. The two main advantages of the developed test stack are homogeneous cell compression and tempering (cooling and heating) due to the hydraulic medium which completely surrounds each test cell. Compression homogeneity has been investigated by pressure sensitive film. Furthermore, current density distribution as well as temperature distribution have been analysed.

MEA components from Gore® are standard material for fuel cell development at the Westphalian University. Therefore, CCMs type Gore® Primea FCM have been assembled with two GDLs type Gore® Carbel® GDM CNW20B in order to manufacture MEAs. Furthermore, different GDLs were tested. Variations have been carried out by the use of GDLs type AvCarb MGL 370 (raw as well as PTFE treated), Freudenberg H2315, H2315 I6, H2315 I2C6 as well as H2315 I2C8. Polarisation behaviour of Gore® CCM based MEAs may be taken from Appendix B.4 to Appendix B.8.

4.2.1. Analysis of Pressure Distribution

Compression of all components of a fuel cell is necessary due to electrical contacts as well as catalyst contact to the membrane. Homogeneity of cell compression is an issue as hot spots may occur with uneven pressure distribution. These hot spots can lead to locally exaggerated degradation and accelerated fuel cell malfunction. In order to visualise cell compression by the hydraulic medium, pressure distribution has been analysed by the aid of pressure sensitive film. Pressure distribution for test cells within the novel MEA test stack has been compared with mechanical compression (Fig. 63).

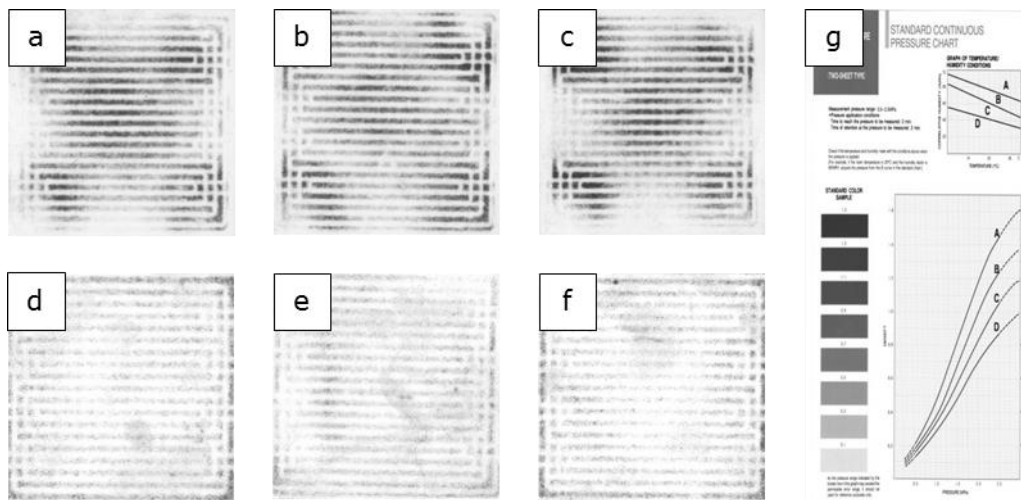


Fig. 63: Analysis of pressure distribution over the active cell area by pressure sensitive film (a to c: mechanical compression; d to f: hydraulic compression; g: measuring scale)

It becomes obvious that the mechanically compressed cells (pictures a to c) show a typical inhomogeneous pressure distribution according to the four tie bolts of the test stack via which compression forces are induced (compare to chapter 3.3.3.1. Pressure Distribution). This result underlines that homogeneous compression is a serious issue even for small test cells. In contrast to the mechanical compression the pressure distribution within the hydraulically compressed test cells is homogeneous (pictures d to f). This nearly ideal compression is explained by the pressure medium which surrounds each cell of the novel test stack completely. As pocket material is flexible, pressure is distributed homogeneously over the geometrical active cell area. Therefore, at any point within the pressurised stack the same pressure forces affect the cell area.

4.2.2. Analysis of Current Density and Temperature Distribution

An even current and temperature distribution is expected due to homogeneous compression and heat transfer by the hydraulic medium. In order to investigate current density and temperature distribution, a special segmented pole plate has been constructed. Three measurements have been performed with Gore components based fuel cells. Investigations have been carried out for a constant current operation with 4, 8, and 16 A. Average current density is 0.25 A cm^{-2} , 0.5 A cm^{-2} , and 1 A cm^{-2} , respectively. Every second, voltage drop over the shunt is measured automatically by the aid of an analogue input module type Beckhoff EL3068 (0 – 10 V; 12 bit resolution). Current density for each segment is determined from Ohm's law. Temperature is measured by a type K thermocouple module Beckhoff EL3318 (eight channels, $0.1 \text{ } ^\circ\text{C}$ resolution). Results of current density and temperature distribution measurements are presented in Fig. 64, Fig. 65 and Fig. 66.

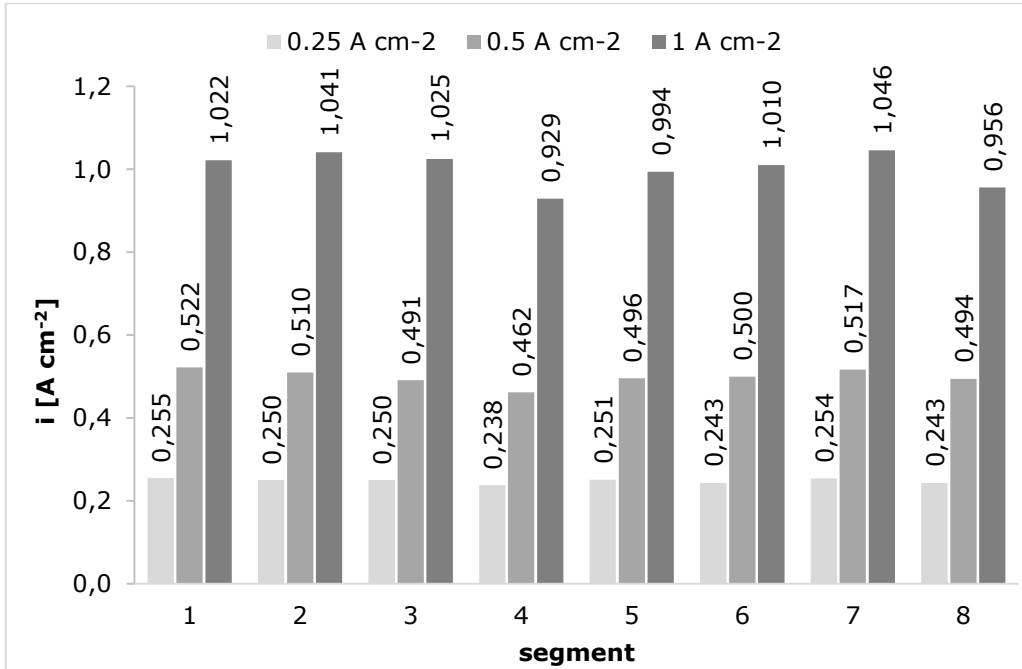


Fig. 64: Current density distribution for 4, 8 and 16 A load current

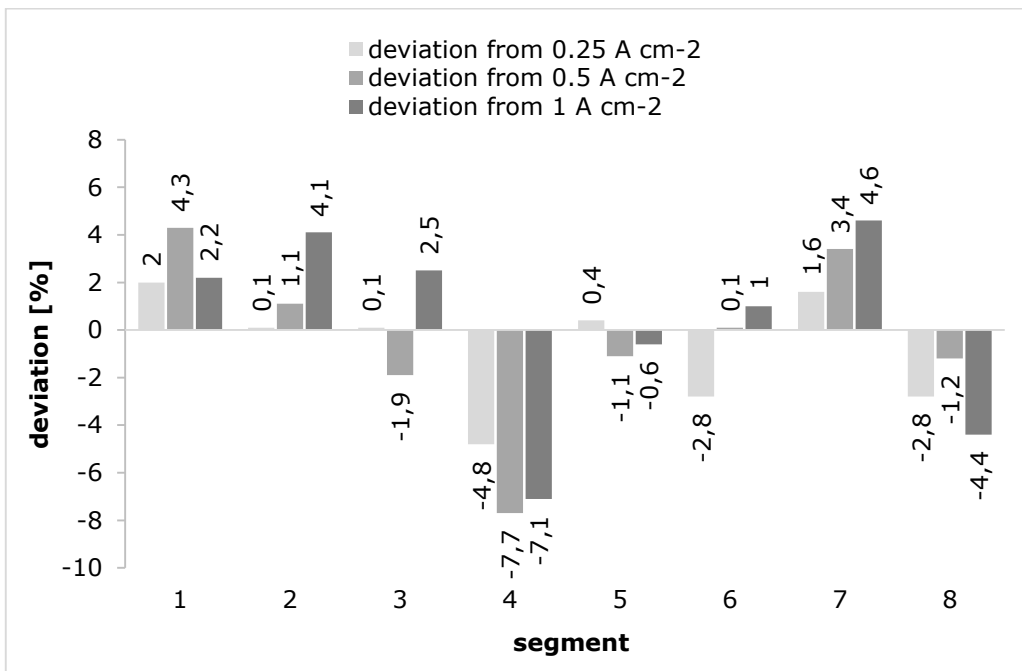


Fig. 65: Deviation of measured current density from arithmetic average current density for 4, 8 and 16 A load current

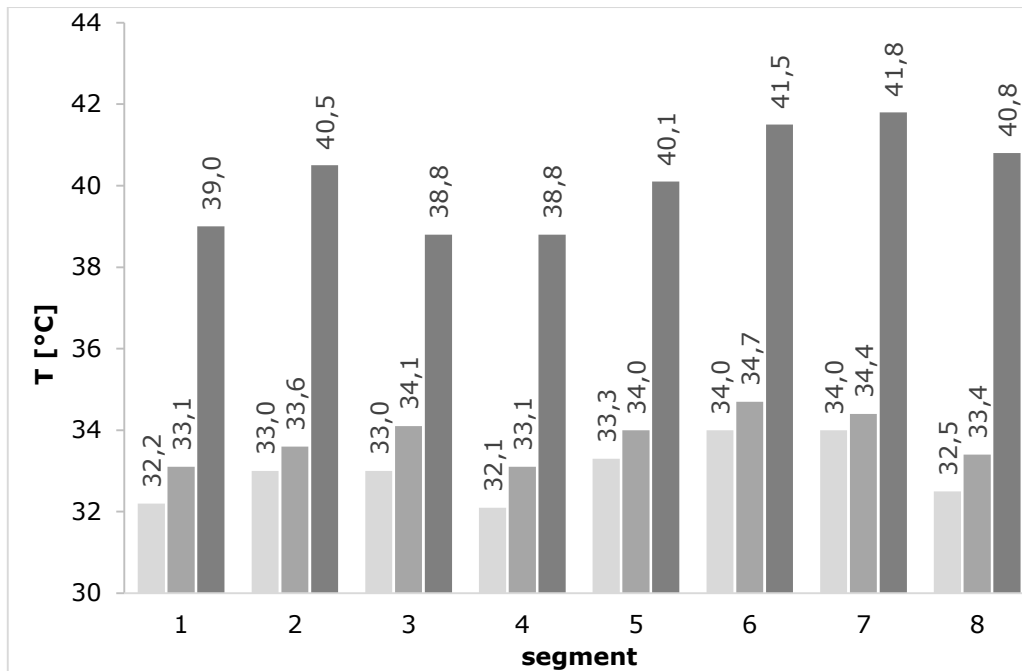


Fig. 66: Temperature distribution for 4, 8 and 16 A load current

Segments No. 4 and No. 8, which are situated near to the gas outlet, show negative deviation from average current density for all three measurements. Especially, current density of segment No. 4 is lowest for all measurements carried out. This may be an evidence for gas flow differences within the flow field at this specific segment, as partial pressure is decreased with the length of the flow field (due to gas consumption).

However, it becomes obvious that current density over the flow field is homogeneously distributed as a result of homogeneous operation conditions. At constant current operation at 4 A, determined current density for each segment differs from -4.8% to +2% from the average value of 0.25 A cm^{-2} . For operation at 8 A (average of 0.5 A cm^{-2}) and 16 A (average of 1 A cm^{-2}) the measured deviation is -7.7% to +4.3% and -7.1% to +4.6%, respectively.

As a result of cooling by the hydraulic medium temperature for each segment is nearly identical. Mean temperature of each segment measured simultaneously to current density distribution is in the range of $33.0 \text{ °C} \pm 0.8 \text{ °C}$ at constant current operation with 4 A. For operation at 8 A as well as 16 A the mean segment temperature is $33.8 \text{ °C} \pm 0.6 \text{ °C}$ and $40.2 \text{ °C} \pm 1.2 \text{ °C}$ respectively. As waste heat increases, cell temperature rises with higher load current.

4.2.3. Effect of Compression Variation

Cell compression is vital for the electrical contact resistance of all components within a MEA. With higher cell compression level, a decreased contact resistance is achieved. This results directly in lower voltage drop at fuel cell operation with higher current and, therefore, higher power output. As already mentioned, porosity of GDL, MPL as well as CL decreases at higher compression forces. This leads to a decreased

gas flux to the catalyst particles within the anodic and cathodic CL. Therefore, an optimum cell pressure is needed. Cell compression may be varied with the novel MEA test system due to pressure controls of the hydraulic medium. Polarisation curves of a sample based on Gore® CCM depending on stack pressure is shown in Fig. 67.

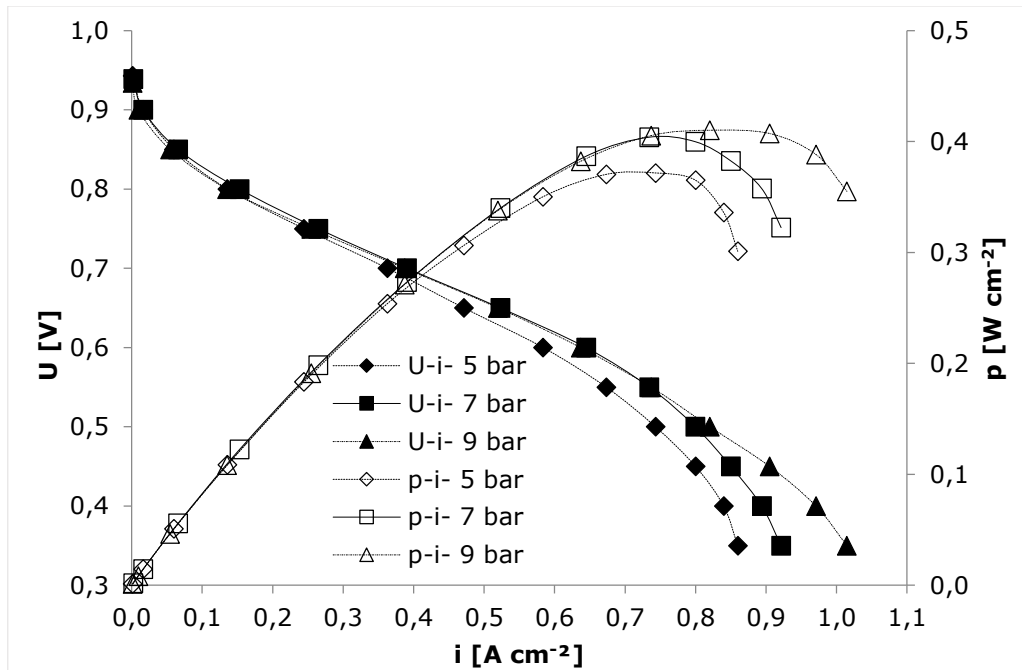


Fig. 67: Polarisation curves depending on stack pressure

It was observed that for 7 bar hydraulic pressure, optimal power output has been achieved. Lower stack pressure results in higher contact resistance and, therefore, leads to lower power output. Further increase in stack pressure does not result in further increase in power output. Polarisation behaviour is similar up to the point of maximum power output. Investigations on MEAs based on GDL type Freudenberg H2315 I2C6 confirmed this result. Therefore, in this experimental study polarisation curves have been obtained for 7 bar stack pressure.

4.2.4. Effect of Temperature Variation

As an effect of higher reaction kinetics, increased power output of PEMFCs is expected if operation is performed at higher temperature level (according to Arrhenius' law a ten degree Celsius increase in temperature, results in two times higher reaction kinetics). Furthermore, humidification is more efficient at higher gas temperature, which leads to higher ions conductivity of the utilised membrane. Due to limited material stability (especially of the polymer membrane), maximum operation temperature is 80 °C for low temperature PEMFCs. With the novel test system, temperature variation has been investigated for Gore® based fuel cells. Polarisation curves depending on the cell temperature is shown in Fig. 68.

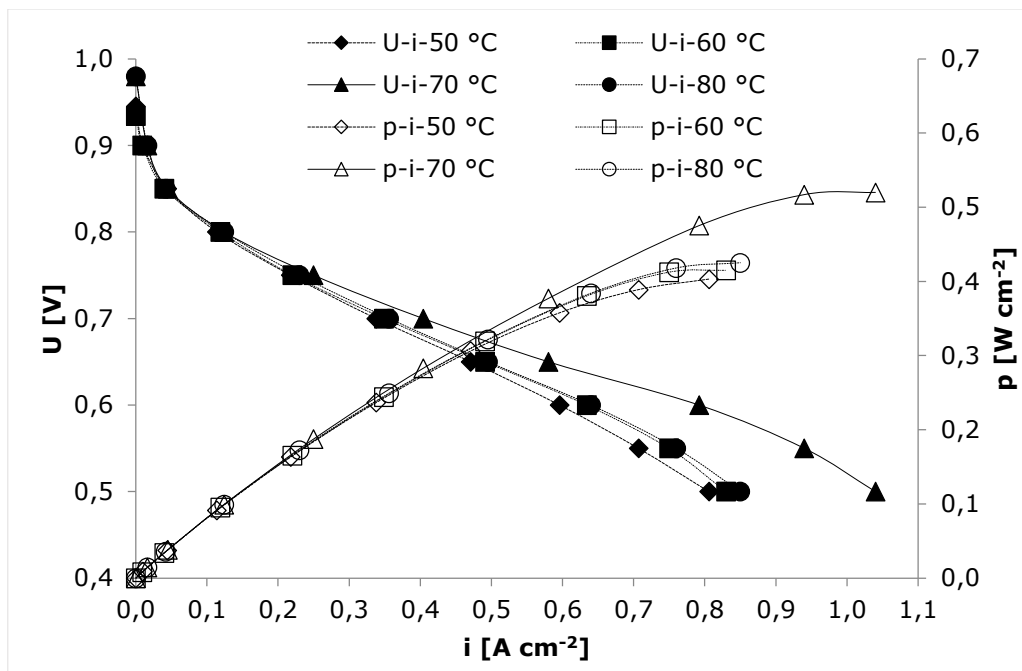


Fig. 68: Polarisation curves depending on cell temperature

Polarisation curves in the literature are often described for higher operating temperatures (test cell and feed gases). In order to compare achieved power density for these test cells, it is necessary to perform PEMFC tests at higher temperature levels. Maximum power output for this MEA sample has been found for a cell temperature of 70 °C. Power density has been found to be 0.55 W cm⁻² at 0.5 V. Values for this certain type of MEA can be confirmed for typically used test cells with mechanical compression [143 – 145]. Prospective improvement for the PEMFC test stack with hydraulic compression is expected by the optimisation of pole plates, especially, the flow field. However, this is not matter of the presented work.

For most fuel cell applications, operation at ambient temperature and with ambient air is more likely as effort is high, especially, for gas conditioning. Therefore, most polarisation curves in this experimental work are measured at about 30 °C with ambient air (without additional humidification). It is necessary to mention, that these robust operation conditions generally lead to decreased power output compared to high temperature operation with additional humidification.

4.2.5. Effect of Changing Air Stoichiometry

From Nernst equation it is known that cell potential rises with increasing concentration of the delivered gases. In order to ensure even distribution of gas molecules to the catalyst particles, MPL and CL have very small pore size (below 1 μ m). For an entire reaction air stoichiometry factor of $\lambda = 1$ is needed. However, PEMFCs are operated over stoichiometrically to prevent the cell from partial oxygen starvation. As an effect of increasing air stoichiometry, gas flux and partial pressure of oxygen changes on the cathode side. Polarisation curves dependent on variation of

air stoichiometry is presented in Fig. 69. Hydrogen flux in this work is realised by circulation of the gases from the cell outlet to the cell intake.

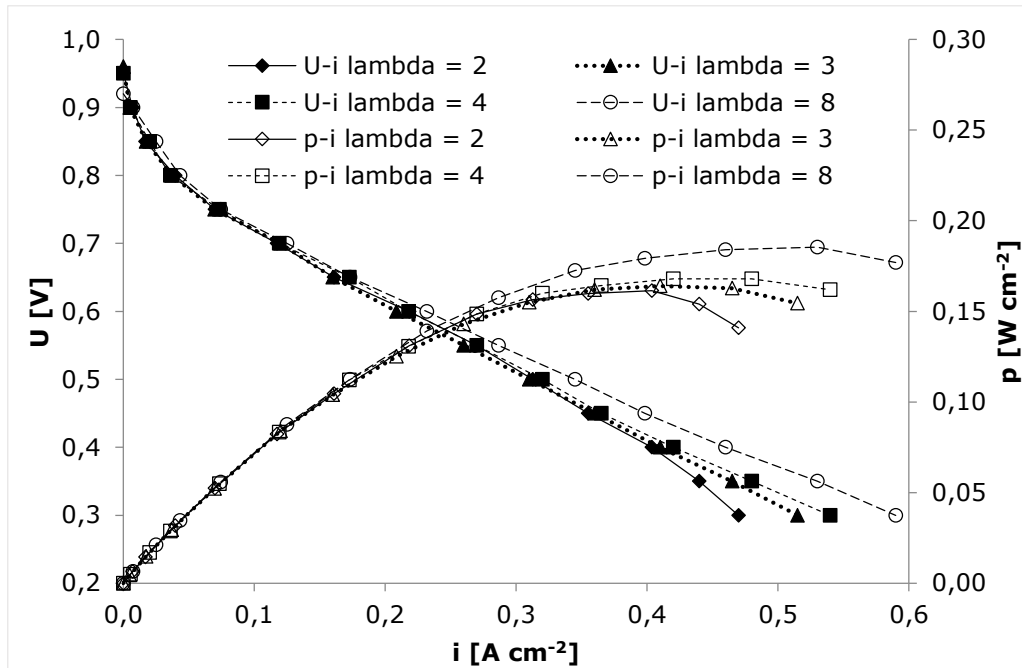


Fig. 69: Polarisation curves dependent on λ variation

It becomes visible that overpotential due to diffusion losses are increased for $\lambda = 2$. This is seen by comparison of polarisation plot for $\lambda = 2$ with $\lambda = 3$. Improved polarisation behaviour was determined for $\lambda = 4$. Although, in Fig. 69 it can be noticed that highest power output has been found for a higher stoichiometry factor of $\lambda = 8$, at normal fuel cell operation λ values above 4 lead to membrane drying and in increased membrane resistance. Therefore, MEA samples in this work have been tested with an air stoichiometry of $\lambda = 4$.

4.3. Standard Pt/C Electro Catalyst Based GDEs

The approach of this experimental work is the development of gas diffusion electrodes for the use as anode material in PEMFCs. Improvements are expected by the use of carbon supports with high graphitisation degree and high specific surface area as well as by the electrochemical catalyst preparation (pulsed electro plating). For comparison also platinum on carbon blacks based electrodes have been investigated.

As cathode material a commercially available electrode BC-H225-10F (supplied by Quintech, Germany) has been investigated. This electrode material is developed especially for the use as fuel cell cathode (for PEMFCs as well as direct methanol fuel cells - DMFC). Electrodes are delivered with the dimensions 150 mm x 150 mm. For analysis in the novel MEA test environment, samples were cut off from the raw material with the dimensions 45 mm x 45 mm.

The supplied electrodes BC-H225-10F are manufactured from a Freudenberg GDL type H2315 I2C6 with catalyst layer prepared by platinum on high surface area advanced carbon blacks and PTFE (necessary for water droplet removal). Platinum loading is in the range of 1 mg cm^{-2} . The thickness of this electrode is $270 \text{ }\mu\text{m}$ [139].

In this section material characterisation of BC-H225-10F is presented. Samples have been studied electrochemically in sulphuric acid (CV and corrosion test). By thermogravimetric analysis loading has been investigated. MEAs have been prepared for in-situ investigation in the fuel cell test environment. The Pt/C based electrodes have been used as cathode as well as anode material.

Furthermore, an experimental catalyst powder (platinum on carbon blacks) has been used for preparation of Pt/C based electrodes as a reference to prepared Pt/CNF based samples (described later in this section). In order to compare both types of electrodes, Freudenberg GDL type H2315 I2C6 has been used as substrate for a spray coated CL based on this Pt/C powder. Characterisation of this set of prepared electrodes is also presented in this subsection.

4.3.1. Platinum Loading

Platinum loading of the investigated electrodes has been analysed by thermogravimetry. Residual mass after TGA is presented in Tab. 9. Measurements have also been carried out for a blank GDL without a CL. Ash content for the Freudenberg GDL is determined to be in the range of 0.03 mg cm^{-2} which needs to be subtracted for further calculations regarding platinum loading.

Tab. 9: Results from TGA for Pt/C based electrodes

Sample	Residual Mass [mg cm^{-2}]	Platinum Loading [mg cm^{-2}]
Blank GDL H2315 I2C6	0.030 ± 0.001	-
BC-H225-10F	1.500 ± 0.201	1.470 ± 0.202
H2315 I2C6 with Pt/C coating	0.162 ± 0.005	0.132 ± 0.006

It was observed that platinum loading for the investigated BC-H225-10F electrode material platinum loading was higher than given by the data sheet. This is taken into account for the determination of specific electrochemical active surface area (see chapter 4.3.3.). Preparation of a CL by the use of Pt/C powder aimed to receive a Pt loading of about 0.1 mg cm^{-2} , which has been confirmed by TGA. Platinum loading of the prepared Pt/C based electrode has been about 11 times less than the commercially available material BC-H225-10F.

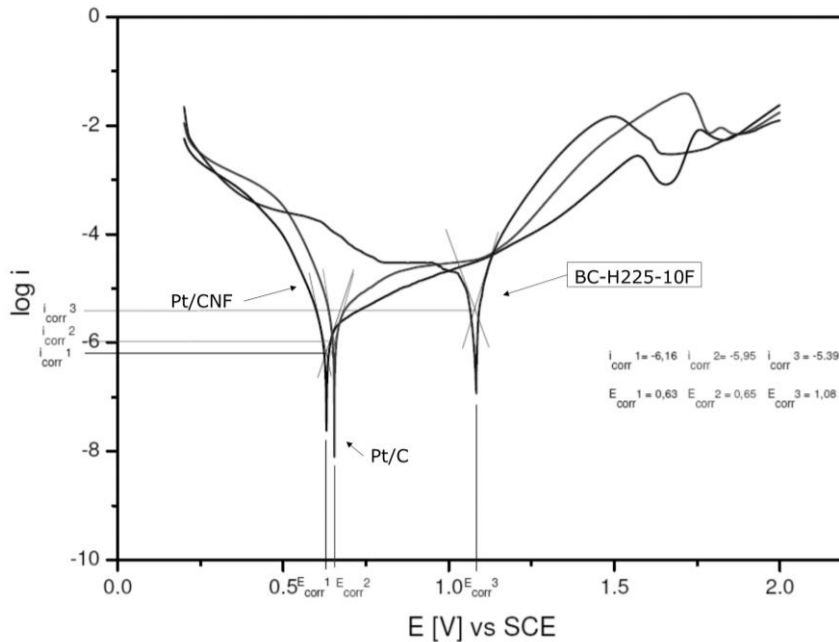
4.3.2. Corrosion Resistance

Carbon corrosion is a serious issue for state of the art PEMFC electrodes. Especially, cathodic CL is affected at fuel cell operation. However, carbon corrosion also occurs on the anode side. One aspect which contributes to the corrosion behaviour of graphitic materials is the graphitisation degree. Therefore, graphitisation degree of both investigated electro catalysts, namely the commercially available BC-H225-10F electrode material and the experimental Pt/C powder, have been analysed by XRD. G_p has been calculated by the determined interlayer spacing. Results may be taken from Tab. 10.

Tab. 10: Graphitisation degree of typical Pt on carbon blacks electro catalysts in comparison to CNFs

Sample	G _p [%]
Pt/CNF	90
BC-H225-10F	turbostratic
Pt/C	73

In order to determine corrosion current of carbon blacks based electrodes, corrosion tests have been performed in acid environment (0.5 M H₂SO₄). For comparison, corrosion current was also determined for a platinum on CNF based electrode. Results of corrosion tests for selected electrodes is shown in Fig. 70.

Fig. 70: Corrosion test of selected PEMFC electrodes in 0.5 M H₂SO₄

Corrosion potential of the BC-H25-10F electrode material is determined at 1.03 V vs. SCE according to the environment of the galvanic cell at room temperature. This is significantly higher than that measured for the experimental Pt/C catalyst as well as for Pt/CNF catalyst. Tafel lines have been plotted by a software (Origin 8), in order to determine corrosion current. Results for the corrosion current can be taken from Tab. 11.

Tab. 11: Corrosion current of investigated PEMFC electrode samples

	Pt/CNF	Pt/C	BC-H225-10F
i_{corr} [mA cm ⁻²]	8.30×10^{-7}	1.17×10^{-6}	4.07×10^{-6}
E_{corr} [V vs. SCE]	0.63	0.65	1.08

For these investigated specimen the CNF based electrode is the most stable in acid environment as a result of lowest corrosion current and lowest corrosion potential. Furthermore, it was observed that the experimental Pt/C catalyst is nearly as corrosion resistance as the CNFs. However, further investigation of that particular catalyst is not attempt of this work. For the commercially available electrode material BC-H225-10F lowest stability in acid environment has been determined.

4.3.3. Electrochemical Active Surface Area

As electrochemical reactions occur on the surface of catalyst material, a high electrochemical active surface area is necessary for PEMFC electrodes to provide high power density. ECSA has been obtained from CV measurements and calculation of the charge exchanged for hydrogen oxidation reaction in acid environment (0.5 M H₂SO₄). HOR occurs in the potential range of -0.2 to 0.1 V vs. SCE. By comparison of the charge for a blank platinum electrode, ECSA can be calculated.

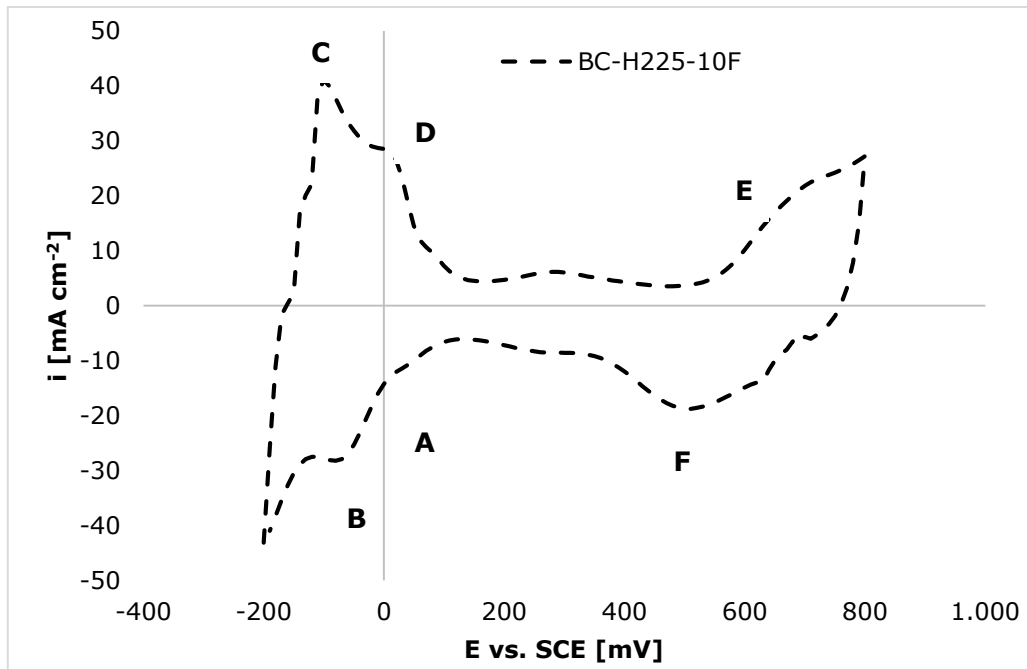
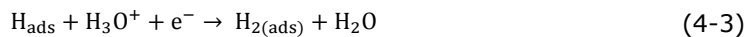


Fig. 71: CV diagrams of BC-H225-10F electrode sample (after 100 cycles)

From the CV diagram it can be obtained, peaks A and B, corresponding to atomic H formation and adsorption, respectively, H₂ formation and adsorption:



Similarly, peaks C and D correspond to H₂ and H oxidation. Also, it can be observed the anodic region E, in which carbon support material is oxidised, and in which Pt-oxide is formed. While carbon oxidation is irreversible (CO₂ formation), cathodic peak F is assigned to Pt-oxide reduction. Taking into account the platinum loading determined from TGA, specific ECSA was calculated. Results can be taken from Tab. 12.

Tab. 12: Electrochemical active surface area for standard Pt/C based electrodes

	BC-H225-10F
ECSA [cm²]	194.39
Spec. ECSA [cm² mg⁻¹]	132.23

4.3.4. Polarisation Behaviour

MEAs have been manufactured for in-situ testing in the fuel cell test environment. The standard BC-H225-10F was used as cathode material. BC-H225-10F as well as the prepared Pt/C based electrode have been investigated as anode material. Nafion[®] 212 is utilized as membrane. Both samples have been tested simultaneously under identical conditions.

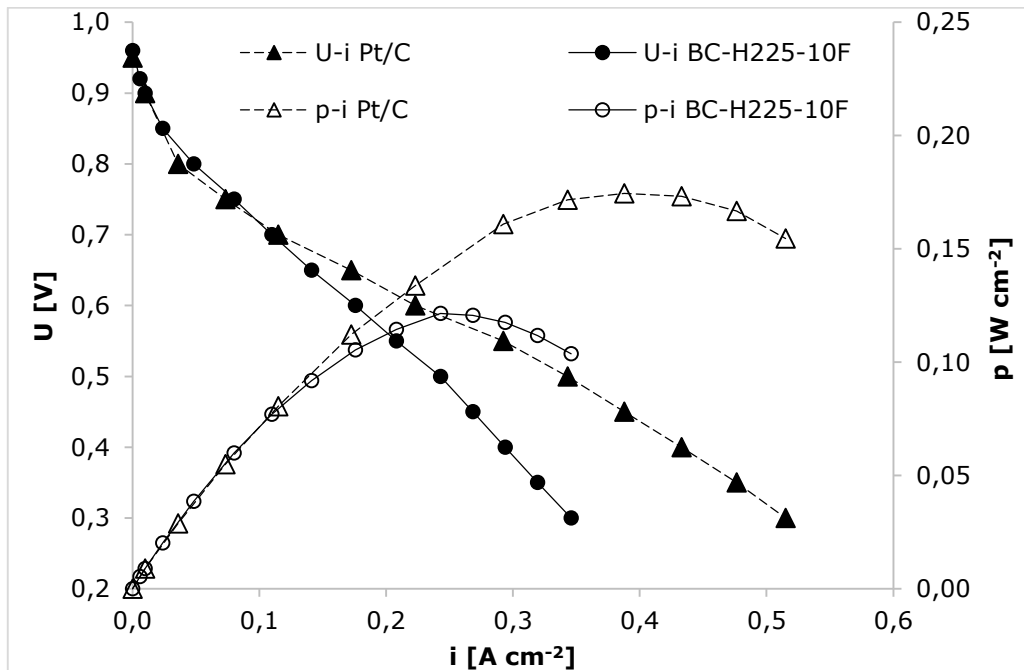


Fig. 72: polarisation curves of Pt/C based MEAs

Maximum power output of MEA samples with electrode material type BC-H225-10F results in maximum specific power density of about 0.121 W cm^{-2} . In comparison to BC-H225-10F, MEAs with anode material, prepared by the experimental Pt/C catalyst powder, result in much higher specific power output (0.174 W cm^{-2}).

One reason for lower power output may be the high ratio of insulation polymer material (mainly PTFE) within the CL which decreases electrical conductivity. However, high hydrophobicity is needed for PEMFC cathodes. Furthermore, high hydrophobicity results in rigorous water removal, which leads to membrane drying and increasing membrane resistance. This indicates that BC-H225-10F is optimised for the use as cathode material. Higher power density is expected for MEAs containing optimised anodes.

Polarisation behaviour was just investigated after start up. Long term testing was performed for both types of MEAs. Results can be taken from Appendix B.2 and Appendix B.9. However, long term testing is not matter of this work and results are not discussed in more details.

4.4. Carbon Filaments Based GDEs

The described experimental work aims on the development of an electrode with low platinum loading and high catalyst utilisation. Improvements in comparison to standard Pt/C based electrodes have been achieved by the use of oxygen plasma activated carbon nano fibres as support material for platinum nano particles. For an optimised localisation of catalyst material a pulsed electro plating process has been investigated.

For the preparatory work, inks have been formulated containing the activated carbon filaments in isopropanol. These dispersions were ultrasonicated for 30 minutes at room temperature. A GDL type Freudenberg H2315 I2C6 has been used as substrate for a CNF coating. Carbon filaments containing inks have been spray coated on porous graphitic substrate. The oxygen plasma activation improves dispersibility in alcohol for processing the investigated carbon filaments. This results from the formation of functional groups on the fibres' surface which increases surface energy. The already coated GDLs were applied to an electro plating facility, in order to deposit catalyst material on the surface of the fibres. It has been noticed that the plasma activation also helps to wet the CNF surface with the platinum containing electrolyte due to the hydrophobic character of the raw material. For investigations in a fuel cell test environment MEAs have been prepared by hot pressing an electrode on each side of a proton conductive membrane type Dupont Nafion® 212 (N212). Prepared CNF based GDEs work as anodes. Standard GDE material type BC-H225-10F has been used as cathode. Design of the prepared MEAs is shown schematically in Fig. 73.

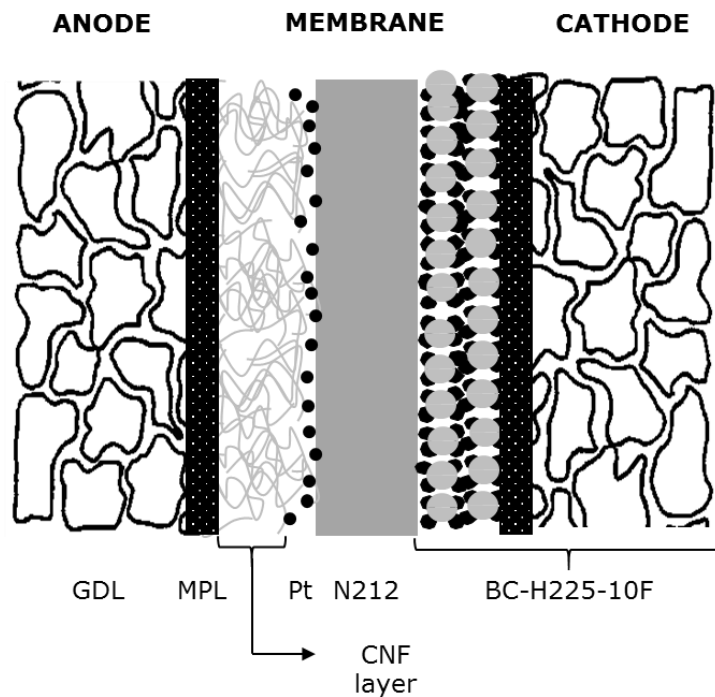


Fig. 73: Schematic cross section of prepared MEAs

4.4.1. Catalyst Preparation

Platinum is used as catalyst material for this experimental work. Catalyst particles are deposited onto a CNF layer by electro plating. The attempt to decorate carbon fibres by electrochemical plating method arises from its two main advantages:

1. Deposition occurs only on fibres, which stay in contact with the rest of the electrode.
2. Catalyst deposition occurs mainly on top of a CNF layer and only a small amount of catalyst material remains inactive within a CNF layer with no direct contact to the polymer membrane.

By using plasma activated carbon material it has been possible to prepare stable carbon filament based dispersions. In addition to this, the fibre surface activation by the oxygen plasma treatment leads to an improved catalyst particle deposition according to the electro plating process. This phenomenon is explained by the formation of oxygen containing functional groups on the surface of graphitic material due to the oxygen plasma. These functional groups act as anchor points for the deposition of metallic platinum from the chloroplatinic acid. A high number of such anchor points leads to a distributed appearance of nuclei instead of layer formation. As a result smaller particles, which are distributed more homogenous over the geometrical electrode surface, are achieved by the plating process. This is necessary in order to obtain a large catalytic active surface. Plasma activation for samples described in this section has been carried out with 120 W for 10 min, which is a compromise between treatment time and sufficient formation of functional groups. In this section the particle morphology and the influence of plasma pre-treatment are discussed.

4.4.1.1. Effect of Plasma Pre-Treatment on the Platinum Particle Deposition Directly on a Gas Diffusion Layer

Improvements in particle morphology due to plasma activation process are clearly observed by microscopy of particles, which are deposited directly on a GDL type Freudenberg H2315 I2C6 (Fig. 74). Samples have been prepared by pulsed electrodeposition of platinum particles (12 pulses, $i = 0.050 \text{ A cm}^{-2}$, 1 sec on-time, 60 sec off-time).

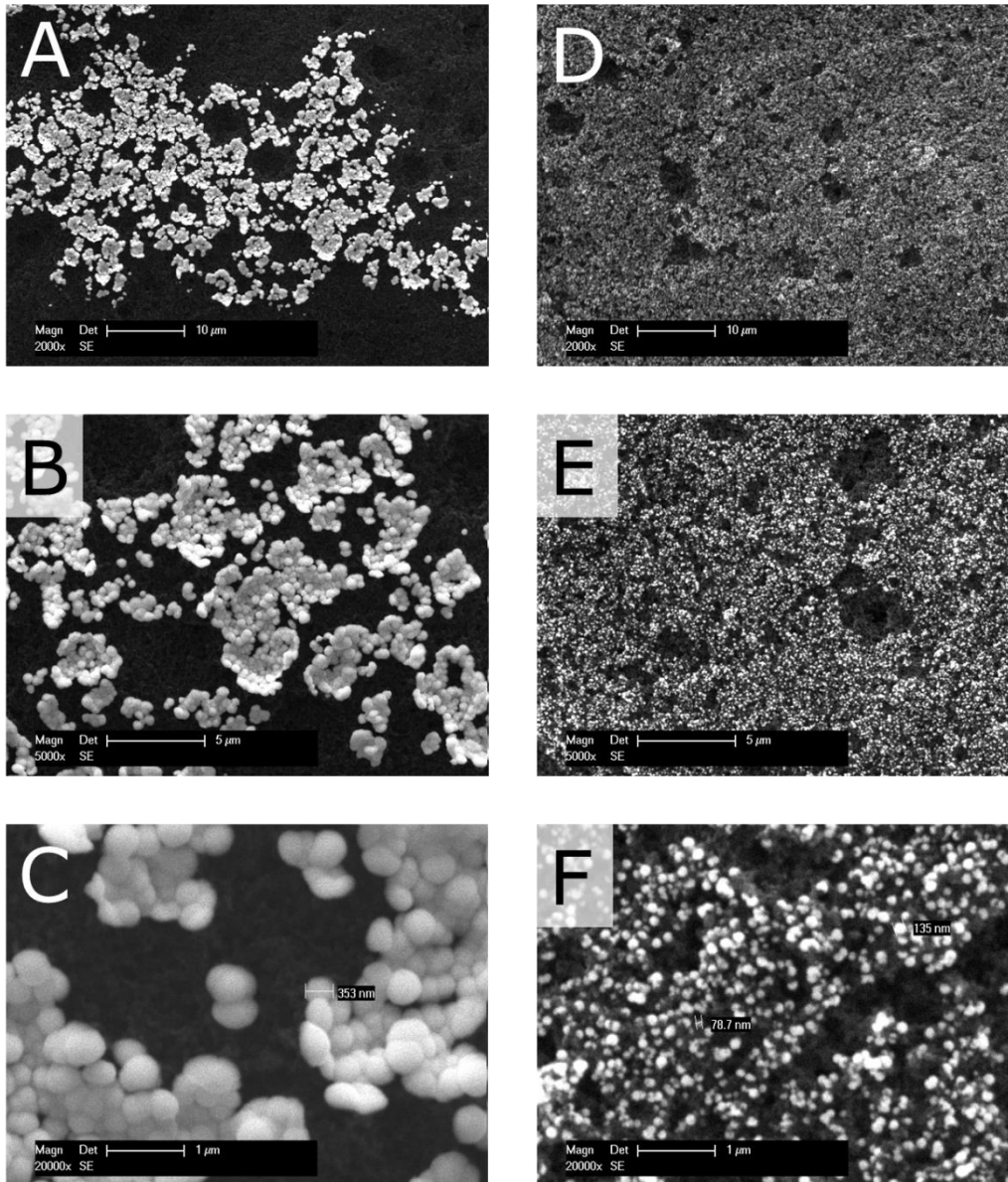


Fig. 74: Micrograph of platinum particles on GDL type Freudenberg H2315 I2C6 without (images A to C) and with previous plasma activation (images D – F)

It can be noticed that platinum particle distribution (light dots) is more homogeneous on the surface of plasma activated graphitic material (Fig. 74 D and E) instead of untreated (Fig. 74 A and B), where metal particles tend to agglomerate. Furthermore, it has been observed that particle size decreases from about 350 nm to about 80nm to 120 nm due to the plasma pre-treatment (Fig. 74 C and F). From TGA it is known, that platinum loading increases with the plasma treatment. 35% higher

loading has been determined (0.088 mg cm^{-2} (w/o pre-treatment); 0.120 mg cm^{-2} (plasma activated)).

MEAs have been prepared by this material working as anode. Polarisation curves show, that power output from investigated fuel cells increases three times due to smaller particles and higher loading (0.03 W cm^{-2} (w/o pre-treatment; 0.09 W cm^{-2} (plasma activation)). Polarisation curves are shown in Appendix B.10.

For this investigation, particles have been deposited onto the MPL of a Freudenberg H2315 I2 C6. This MPL is manufactured of graphitised carbon blacks (compare to chapter 4.1.2.), for which a small specific surface area is assumed. Specific power output is little (0.09 W cm^{-2} @ 0.12 mg cm^{-2}) in comparison to standard MEAs prepared from commercially available components. However, it becomes obvious that performance under robust operation conditions is just 25 percent lower than MEAs based on the standard electrodes type BC-H225-10F (compare to Fig. 72), although platinum loading is over 10 times less. This underlines, that by means of the described deposition method, catalyst is localised directly at the interface between electrode and membrane and a higher percentage of particles are electrochemical active. This results in decreased platinum loading due to less inactive catalyst material within the CL. However, further optimisation of such electrodes is not matter of this work and results are discussed not far in detail.

4.4.1.2. Decoration of Carbon Nanotubes with Platinum Particles

According to their large specific surface area, further optimisation has been expected by the use of carbon filaments as alternative catalyst support instead of carbon blacks. It is assumed that a large surface area of the support contributes to large catalyst surface area. However, certain conditions need to be fulfilled for an optimised PEMFC electrode, in order to achieve sufficient space for electrochemical reactions (three phases reaction room): It is necessary to achieve very small catalyst particles in nanometre scale, as a large electrochemical active surface area results in high power output at fuel cell operation. Particle distribution needs to be distributed homogeneously. Local gradients would lead to inhomogeneous current density distribution, which affects fuel cell performance due to unwanted electrical in-plane currents (in xy-direction of an electrode). This provokes further voltage losses, as in-plane electrical conductivity is lower than through-plane conductivity.

In a first stage of this experimental work, platinum deposition has been performed on a carbon nanotubes layer. The used CNTs are as produced without any further surface cleaning or heat treatment. This makes the investigated material very cheap and therefore interesting regarding the development of PEMFC electrodes.

Electro deposition of platinum particles has been performed with constant current. For deposition currents below 10 mA cm^{-2} , no significant particle formation was observed after 360 sec. Electrical current consumed by the electrode refers to hydrogen formation. This may be explained by the catalytic activity achieved by the oxygen plasma treatment. In Fig. 75 and Fig. 76 platinum particles can be seen on CNTs. Particle deposition has been performed for 360 sec. Deposition current has been set to 200 mA (10 mA cm^{-2}).

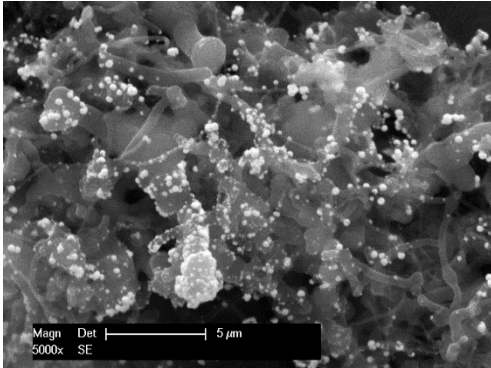


Fig. 75: Micrograph of Pt particles on CNTs (5,000 magnitude)

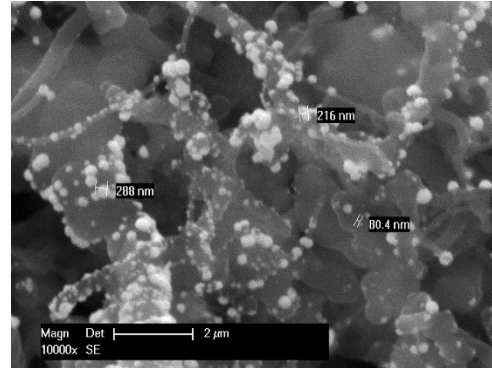


Fig. 76: Micrograph of Pt particles on CNTs (10,000 magnitude)

From microscopy images it becomes obvious, that CNTs could be decorated only with few Pt particles. Diameter of deposited particles have been found from 80 nm to 290 nm. An optimal particle size is found from the literature to be in the range of some¹² nanometres. Furthermore, by TGA it has been found out, that platinum loading is below $1 \times 10^{-3} \text{ mg cm}^{-2}$. In order to increase platinum loading and decrease particle size current has been increased to 20 mA cm^{-2} and deposition has been interrupted by pausing for 10 sec between two sequences. Furthermore, the influence by the CNT loading has been investigated. Visually no clear difference was observed from microscopy images. This means, on the one hand particles size still exceeds the optimum size by far extend. But on the other hand platinum loading could be raised significantly. Results from TGA depending on pulses and CNT loading are presented in Tab. 13.

Tab. 13: Platinum loading depending on pulses and CNT loading

Pulses [sec]	CNT loading [mg cm^{-2}]	Pt loading [mg cm^{-2}]
1 x 360	0.5	0.011
2 x 180	0.5	0.018
3 x 120	0.5	0.024
1 x 360	1.0	0.018
2 x 180	1.0	0.022
3 x 120	1.0	0.025

It was realised that platinum loading increases with a higher CNT loading as well as with increasing pulse number at a constant treatment time. Further settings have been analysed (with different CNT loadings, pulse lengths and pulse numbers). It has been observed, that smaller pulses with higher pulse current can optimise the morphology of deposited platinum. However, the maximum current of the used potentiostat/galvanostat is limited to 1 A. This means for the 20.25 cm^2 samples (geometrical surface area) deposition current density is about 0.050 A cm^{-2} . Smallest pulse length is 1 sec. A selection of microscopy images for this current density is shown in Fig. 77.

¹² Depending on the citation a 5 nm particle sizes is optimal regarding material stability and specific surface area

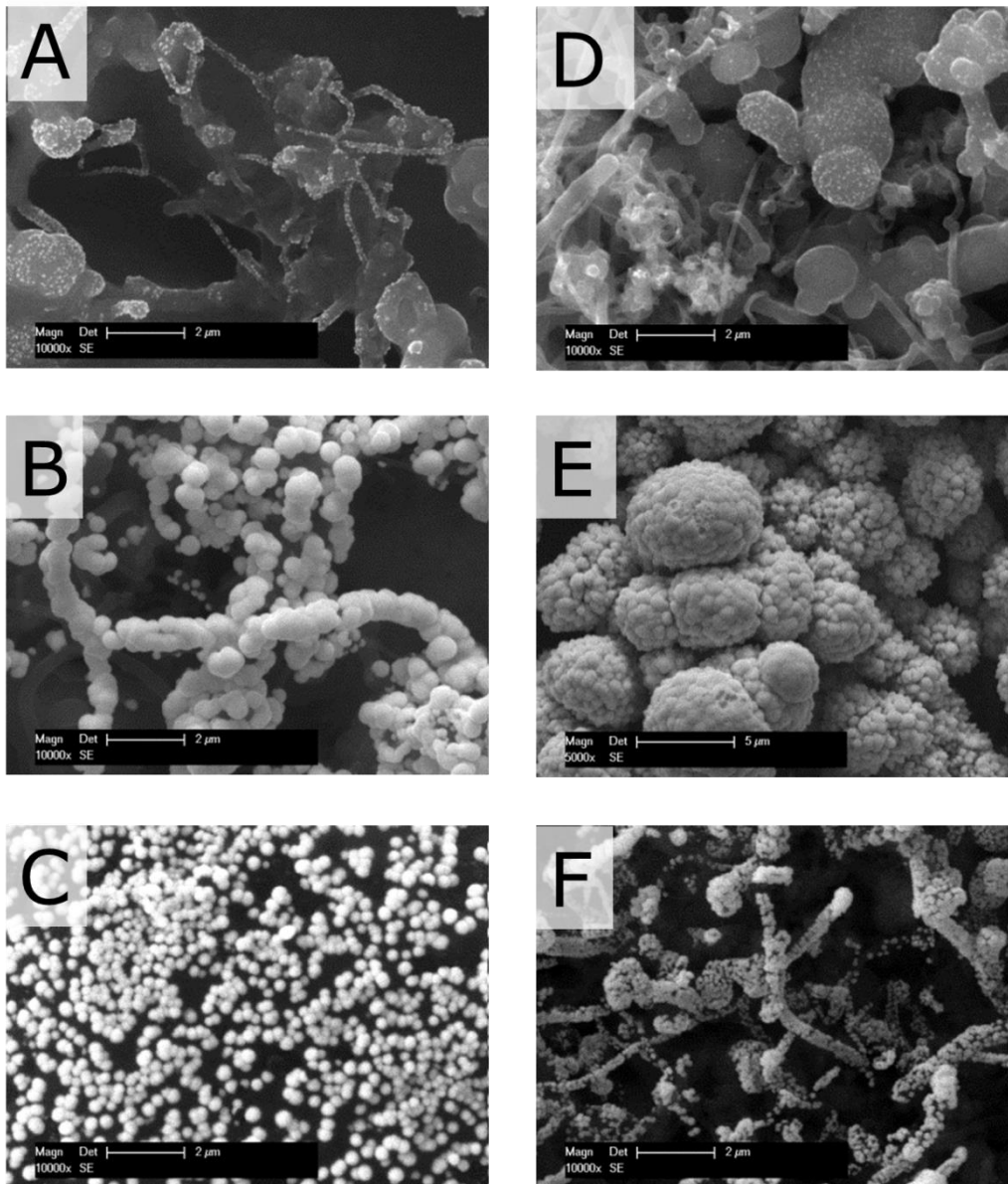


Fig. 77: SEM study on the morphology doped CNTs decorated with Pt particles (10,000 magnitude): A) 10 mA cm^{-2} for 360 sec, B) 12×10 sec, C) 12×5 sec, D) 1×1 sec, E) 120×1 sec, and F) 12×1 sec

Visually, the result presented in Fig. 77; image F was optimal regarding the average diameter of deposited particles as well as coverage of the CNTs surface. Particle deposition has been prepared by twelve pulses. Pause length between each sequence was set to 60 sec. MEAs have been manufactured by the use of these electrodes (working as anodes). Polarisation plots may be taken from appendix B.11.

As can be seen from the fuel cell tests, CNT based electrodes did not result in high power density. Maximum power density was obtained in the range of 0.02 W cm^{-2} . Most likely explanations for the poor performance of these electrodes are the low graphitisation degree, the small specific surface area of the fibres (compare to Tab. 3) leading to large particles and, consequently, only small active platinum loading. Therefore, the development of CNT based electrodes was not further proceeded.

4.4.1.3. Decoration of Carbon Nanofibres with Platinum Nano Particles

According to the optimised settings for platinum deposition on CNTs, CNF decoration has been performed with a deposition current density of 0.05 A cm^{-2} . Pulse length has been kept at 1 sec. Pause length has been set to 60 sec, respectively. The long pause between each pulse sequence is necessary, in order to gain an even platinum ions concentration in front of the working electrode. Prepared samples have been analysed by scanning electron microscopy. An overview of the catalytic layer based on oxygen plasma activated CNFs decorated with platinum particles is shown in Fig. 78, Fig. 79, and Fig. 80.

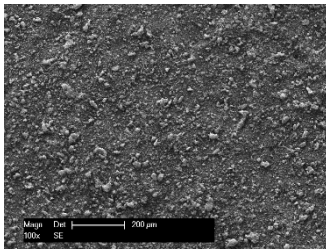


Fig. 78: Catalyst layer of an electrode sample based on platinum decorated CNFs (100 magnitude)

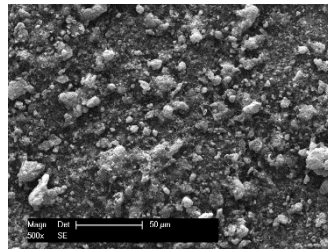


Fig. 79: Catalyst layer of an electrode sample based on platinum decorated CNFs (500 magnitude)

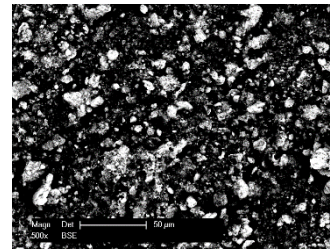


Fig. 80: Catalyst layer of an electrode sample based on platinum decorated CNFs (500 magnitude, BSE mode)

From previous attempts it is known, that an incomplete carbon fibre layer leads to a preferential platinum deposition on the graphitic substrate (appendix C.1). This is explained by the locally higher current density due to the higher specific surface area of the fibres. This is unwanted as platinum deposition tends to form larger particles on the substrate's surface (compare to Fig. 74). SEM images of the CNF based electrode sample show the graphitic substrate (GDL type Freudenberg H2315 I2C6) is completely covered with platinum decorated filaments. It becomes obvious, that the layer exhibit a large number of CNF agglomerates homogeneously distributed over the electrodes surface. This may be explained by an amount of fibres which have not been activated sufficiently, previous to the spray coating. In Fig. 80 the electrode sample is shown in BSE mode. Here it is visualised, that due to the entire CNF coating, platinum has been deposited homogeneously over the whole surface¹³. From EDX spectroscopy the apparent elements have been determined. Mainly platinum and also

¹³ Areas which are not in the focus of the BSE detector do not show illuminated particles (particles with higher electrical conductivity, mainly platinum). The focus is adjusted to the height level of the agglomerates. However, also those fibres lying 'deeper' are decorated with platinum.

some nickel residues from CNF production have been detected (Fig. 81). The carbon peak is not visualised in this diagram.

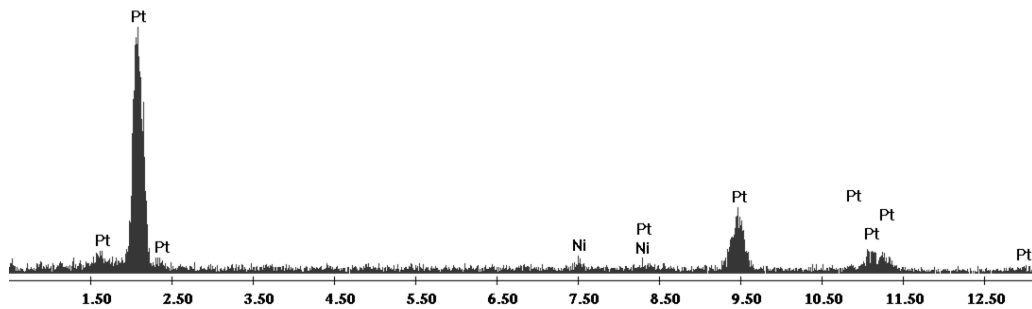


Fig. 81: EDX spectrum of an electrode sample based on Pt/CNF catalyst layer

From SEM images with higher magnitude it is noticed that CNFs are covered all over with platinum nano particles (Fig. 82). In comparison to particle deposition on CNFs without previous plasma treatment, only a small fraction of platinum particles is agglomerated (compare to Appendix C.2). A high specific electrochemical active surface area is assumed by this catalyst material.

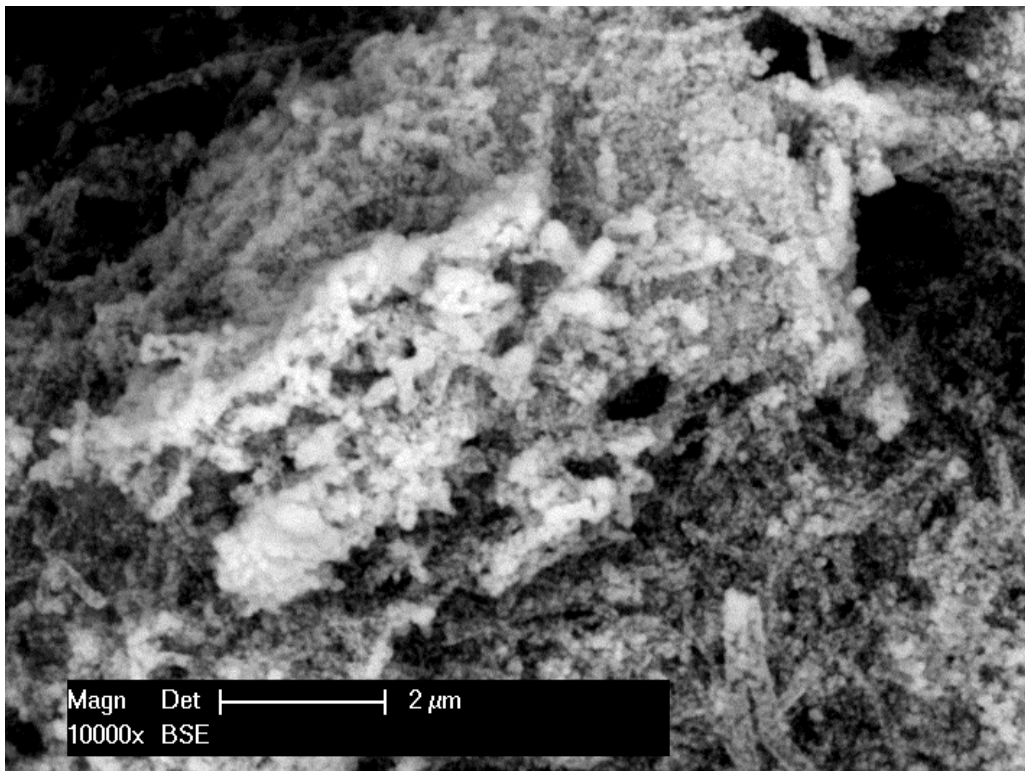


Fig. 82: Micrograph of Pt particles on CNFs (10,000 magnitude)

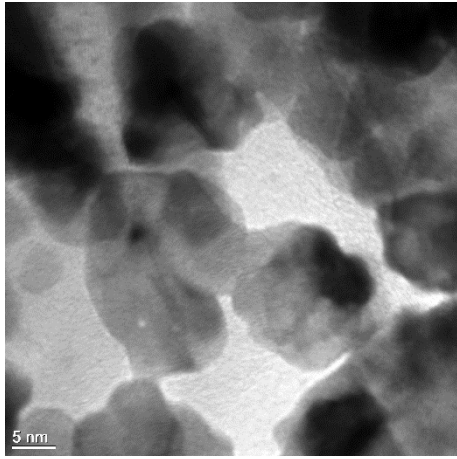


Fig. 83: TEM image of Pt particles

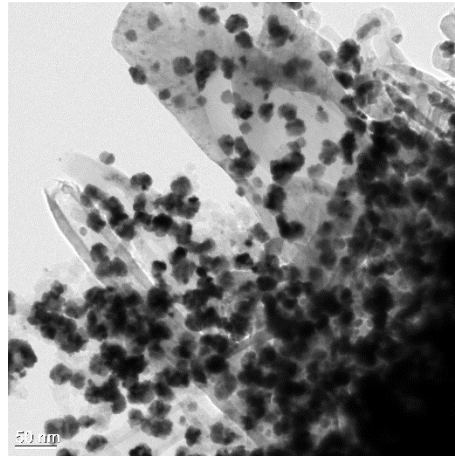


Fig. 84: TEM image of Pt particles on CNFs

In order to determine the particle size of platinum depositions, prepared electrode samples have been analysed in TEM. Particle size has been determined to be in the range of about 5 nm forming platinum clusters with a diameter of about 20 nm to 30 nm (Fig. 56 and Fig. 83). Furthermore, it is observed that dimension of most of the clusters is in the same range (Fig. 57 and Fig. 84). Fractured samples (Fig. 85) and cross sections (Fig. 86) have been prepared, which were analysed in SEM.

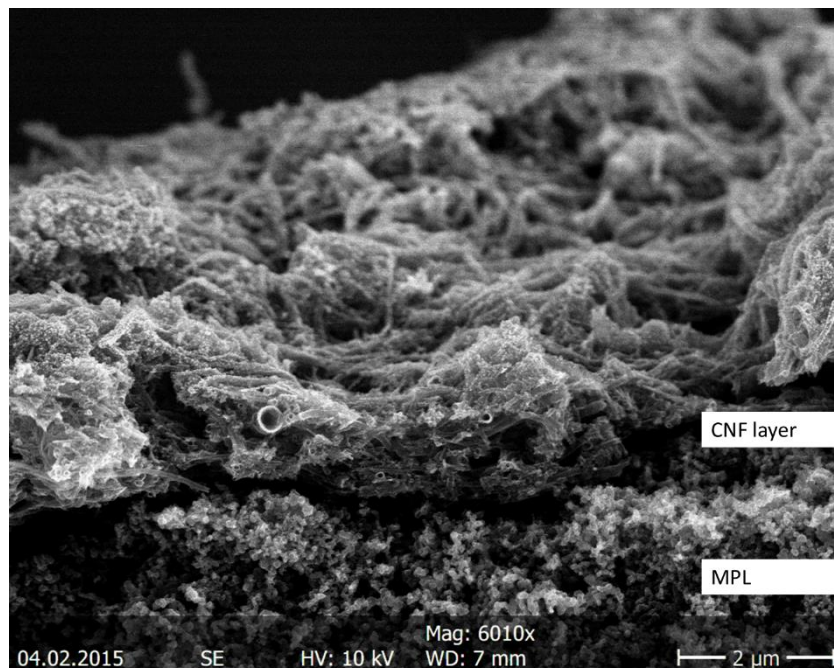


Fig. 85: Micrograph of Pt particles on CNFs - fracture of a sample

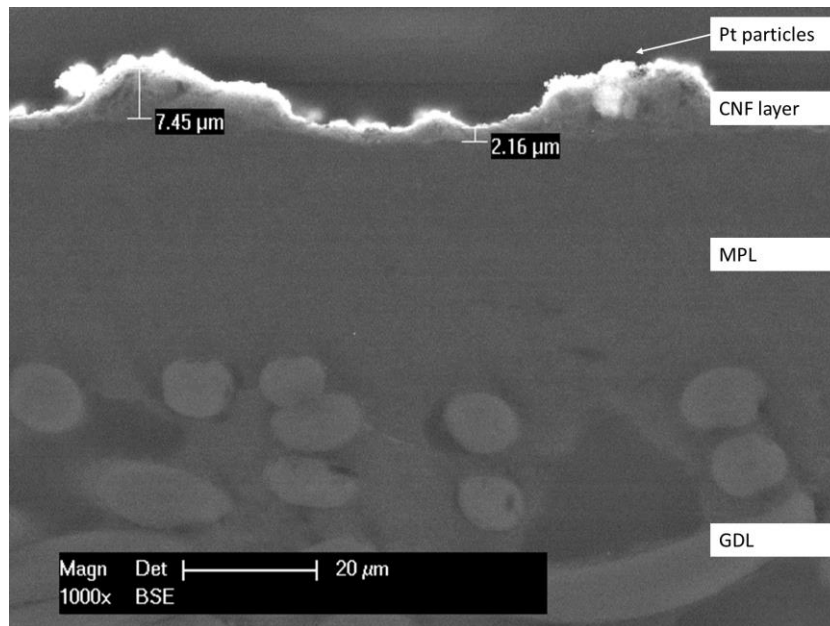


Fig. 86: Cross section of a Pt/CNF based electrode

It was observed that thickness of the CNF layer is not even. In these areas where CNFs have been agglomerated, the height of the layer is up to 7.5 μm. A minimum thickness has been determined to be in the range of 2 μm. The reason for these agglomerates has already been discussed earlier in this section. From SEM images only less particles have been found within the CNF layer. The most of the particles are situated on top. Platinum particles have been found only up to a depth of 300 nm within the CNF layer (Appendix C.3). Platinum location is favourable for PEMFC electrodes. A good platinum utilisation is expected.

Electrochemical determination of the absolute ECSA for prepared electrode samples by CV measurement in a galvanic cell was not successful due to very low surface area below 1 cm². Obtained current densities according to hydrogen adsorption and hydrogen desorption, respectively, have been overlapped by interaction of functional groups on the CNFs surface, which made it impossible to distinguish between both phenomena.

4.4.2. Platinum Loading

Platinum loading of prepared electrodes has been determined by TGA. Three pieces, each having a size of 1.76 cm² (disks with a diameter of 15 mm), have been cut out from a large electrode sample (one from the middle, two from opposite corners). Metallic electrode content has been analysed by XRF, in order to distinguish platinum from CNF catalysts which occur due to the fibres production. XRF measurements are performed at three different points of a sample. Platinum content of prepared electrodes depending on CNF loading is given in Tab. 14.

Tab. 14: Results from XRF and TG analyses of selected electrode samples depending on CNF loading

Sample	CNF loading [mg cm ⁻²]	Pt content [wt.-%]	Residual mass [mg cm ⁻²]	Pt loading [mg cm ⁻²]
Blank GDL H2315 I2C6	-	-	0.030 ± 0.001	-
GDL with CNFs only	0.5	-	0.096 ± 0.020	-
Pt/CNF w/o plasma activation	0.15	30.3 ± 1.4	0.052	0.006
Pt/CNF	0.15	55.5 ± 0.4	0.063	0.013
Pt/CNF	0.3	54.4 ± 1.5	0.091	0.021
Pt/CNF	0.5	52.3 ± 0.7	0.131	0.034

For blank GDL samples ceramic residuals are determined by TGA which belong to ashes content. About 0.03 mg cm⁻² need to be subtracted for the calculation of platinum loading due to GDL residues. Ni content is determined to be in the range of 13.2% ± 3.9% (0.132 ± 0.004 mg_{Ni} mg_{CNF}⁻¹). The platinum fraction from metallic content of prepared samples remains nearly constant with varying CNF (plasma activated) loading (55.5% to 52.3%). This underlines that the platinum loading is highly dependent on the CNF loading of a sample, which was also assumed by analyses of CNT based electrodes. This may be explained by the higher number of available anchor points due to the higher amount of functionalised CNFs. However, a higher CNF loading leads to a higher percentage of particles, which are situated within the CNF layer.

Furthermore, it can be noticed that platinum loading for the sample without previous plasma treatment of the utilised fibres is about only 55% as high as for samples with plasma activated fibres. This phenomenon was also already mentioned for platinum decorated GDL samples. In the following sections prepared electrode samples refer to a CNF loading of about 0.15 mg cm⁻² and a platinum loading in the range of 0.010 to 0.015 mg cm⁻², respectively.

4.4.3. Polarisation Behaviour

In order to investigate performance of prepared Pt/CNF based electrodes, MEAs have been tested in-situ in the novel test system. Tests have been performed at ambient conditions (room temperature) with atmospheric air and pure hydrogen. Hydrogen is circulated through the anode with 0.2 bar overpressure with high excess gas in order to prevent hydrogen starvation over the active cell area. Air is pumped through the cathode. Back pressure measured in front of the cell intake is 0.2 bar at MPP. Stoichiometry factor is controlled to $\lambda = 4$. Previously to the polarisation test, an investigated cell needs to pass a start-up procedure. Here the cell gets cycled at constant cell voltage between 0.65 V, 0.4 V and 0.15 V respectively. Each cell potential is kept constant for 15 sec. The procedure is repeated for 50 times. This start-up procedure results in sufficient hydration of the membrane due to the formation of water at the cathode side at lower cell voltage. Polarisation curve of a selected MEA sample with an anode based on Pt/CNF electro catalyst is shown in Fig. 87.

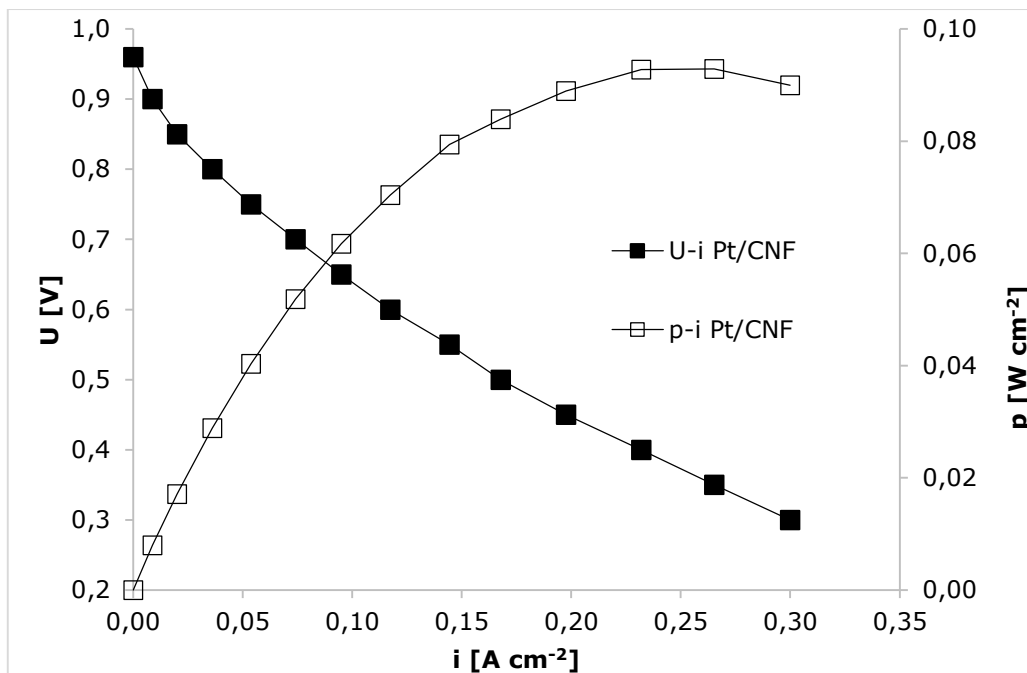


Fig. 87: Polarisation curve of a Pt/CNF based MEA sample

An open circuit voltage for Pt/CNF based samples is determined at 0.96 V. From the diagram one can obtain maximum power output of $0.092\ W\ cm^{-2}$ at a cell voltage of 0.4 V. Short circuit current is in the range of $0.45\ A\ cm^{-2}$. It can be noticed, that with increasing load current, voltage drop is nearly linear. This is a result of high ohmic as well as membrane resistance. As MEA samples have been tested with atmospheric air, membrane hydration is not optimal due to low absolute current. Therefore, a high membrane resistance is likely. Furthermore, polarisation curve gets flattened at higher current. This occurs due to the lambda controls, which results in increasing air flux through the cathode and increasing back pressure, respectively. The higher pressure level improves operation conditions. Increased voltage drop due to decreasing gas concentration (compare to chapter 2.1.) has not been noticed.

In comparison to MEA samples, containing anodes which were prepared without CNF interlayer (presented in Appendix B.10), power output is in the same range. Further improvement has been achieved according to the platinum utilisation. As platinum loading cannot be determined by post mortem analyses¹⁴, values refer to samples manufactured the same way. Supposing an amount of $0.010\ mg\ cm^{-2}$ to $0.015\ mg\ cm^{-2}$, platinum loading could be decreased off a factor of ten in comparison those electrode samples, with platinum particles deposited directly onto the MPL of a

¹⁴ After dismounting a MEA sample carbon fibres and platinum particles will remain on the membrane, which is soft in comparison to the graphitic substrate. From the TG analysis of an entire MEA one obtains the platinum loading of both electrodes. As the variance of Pt loading from BC-H225-10F is higher than the measured loading of prepared Pt/CNF based electrode samples, this method is not feasible. Therefore, for each set of electrodes at least three samples have been prepared only for TGA.

GDL type Freudenberg H2315 I2C6. In comparison to electrodes type BC-H225-10F, platinum content decreases off one hundred times.

From the analysis of the initial voltage drop according to activation polarisation (up to about 0.8 V cell voltage), Tafel equation¹⁵ has been obtained by numerical approximation in order to determine Tafel slope, exchange current density i_0 , and transfer coefficient α . The approximated Tafel line is shown in Fig. 88. Calculated values Tafel slope, i_0 , and α is given in Tab. 15. For comparison reasons calculated values for MEAs based on BC-H225-10F as well as based on the experimental Pt/C catalyst are also given in this table.

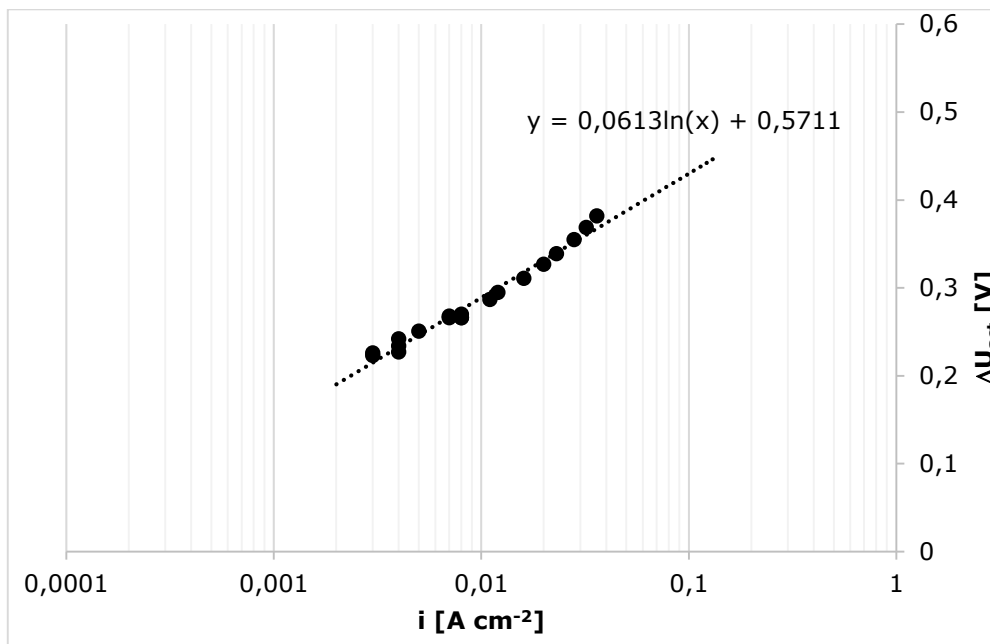


Fig. 88: Tafel approximation for Pt/CNF based MEA

The presented results are an estimation of a full cells characteristic values, as Tafel equation is typically calculated for investigations of only one electrode process (e.g. HOR on an anode). The exchange current density for the presented MEA in Fig. 87 was calculated to be $8.99 \times 10^{-2} \text{ mA cm}^{-2}$. This is the highest measured value for i_0 , which underlines the potential of the prepared Pt/CNF catalyst. However, Tafel slope is high. This may be a result of lower electrical conductivity by the prepared CNF interlayer. The higher resistance may be explained undesirable contact resistance between the various electrode layers. As transfer coefficient is below 0.5 it can be assumed, that power output for the Pt/CNF based anode may be increased by the use of a cathode, which results in higher performance under this robust conditions.

¹⁵ Further information concerning the calculation of Tafel equation may be taken from [27, 30]

Tab. 15: Results from Tafel approximation

	Tafel slope [V dec ⁻¹]	i_0 [mA cm ⁻²]	α
BC-H225-10F	0.100	5.39×10^{-3}	0.585
Pt/C	0.122	4.54×10^{-2}	0.246
Pt/CNF	0.141	8.99×10^{-2}	0.418

4.4.4. Long-Term Operation

The determination of a polarisation curve is a method to obtain power output of a cell (or a stack) dependent on the applied load. However, operation conditions change dynamically while performing the polarisation test and power output in constant fuel cell operation is not necessarily the same due to different membrane conditions. Therefore, a MEA sample has been analysed in a long-term run, which is performed in constant current mode. In order to load a cell without damaging it (e.g. due to overheating at operation in short circuit), the MEA sample has been operated at 6 A. Corresponding voltage is measured. As ambient air is used, every five minutes current pulses (7, 8, and 9 A for five seconds, each) have been performed. These pulses result in an increased water formation in this short period, which leads to hydration of the membrane and maintains a sufficient membrane conductivity. Furthermore, anodic gas path is purged every five minutes, in order to remove condensate droplets and undesirable air, which introduces the anodic half-cell due to gas cross-over. Long-term test is presented in Fig. 89.

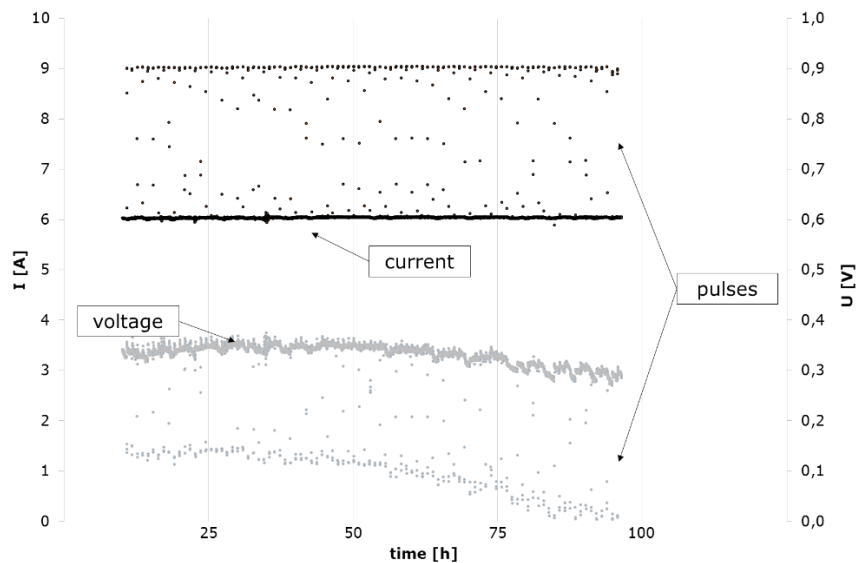


Fig. 89: Long-term test of a Pt/CNF based MEA

Operation of this MEA sample has been established for about 80 h. After a slight increase within the first operating hours, cell voltage decreases over time. The long-term test has been stopped, as the peak current became equal to the short circuit current which is an unwanted operating condition, due to likely hot spot appearance. This voltage drop may be explained by the following reasons:

- Humidity change of the laboratory air
- Consecutive changing water content within the membrane (drying)
- Increasing water content on the anode (flooding the electrode)
- Cell degradation (due to carbon corrosion and Pt losses, consequently)
- Membrane puncture (internal leakage and pressure drop, consequently)

Membrane drying due to the high lambda value seems most likely to lead to the determined voltage drop. However, optimising the parameters for MEA operation is not matter of this experimental work. Further and extended long-term runs have not been performed due to limited test capacity of the institute's laboratory.

4.4.5. Current Density Distribution

Current density distribution has been determined, in order to obtain possible gradients in operation. Current gradients would lead to in-plane currents, which lead to losses due to low in-plane electrode conductivity. It is expected that current distribution is homogenous, if the active catalyst particles are even distributed. Selected electrode samples have been used for MEA manufacturing. In-situ tests have been performed in the novel PEMFC test environment. In order to determine current density distribution, the segmented test cell ($8 \times 2 \text{ cm}^2$ active geometrical cell size) has been utilised. Tests have been performed at 2 A (0.125 A cm^{-2}), 4 A (0.250 A cm^{-2}), and 6 A (0.375 A cm^{-2}). Current density distribution and deviation from average current density are presented in Fig. 90 and Fig. 91.

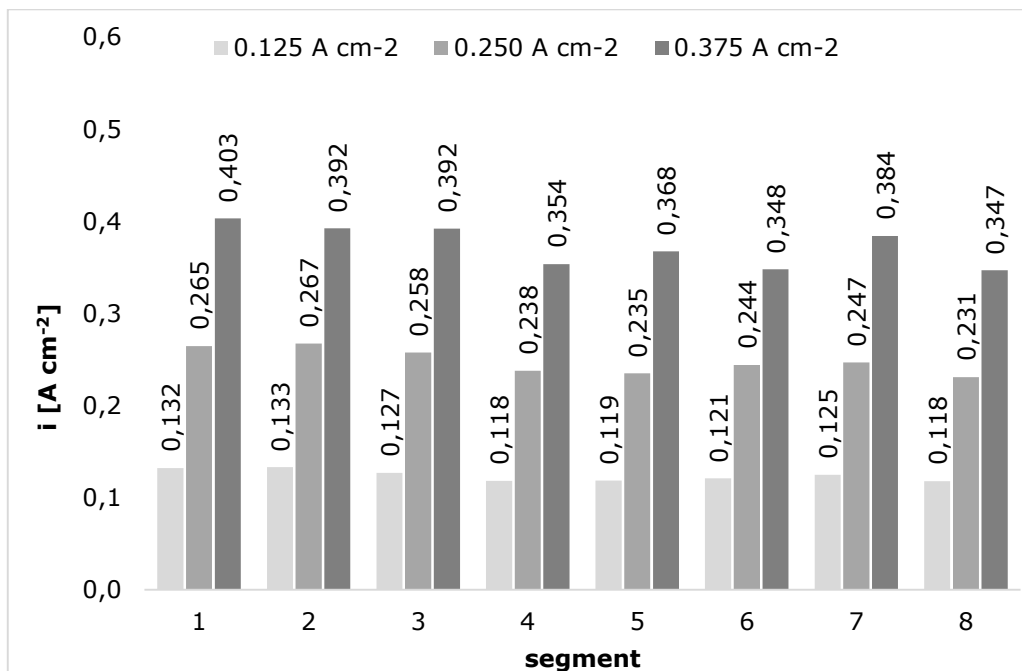


Fig. 90: Current density distribution of Pt/CNF based MEA

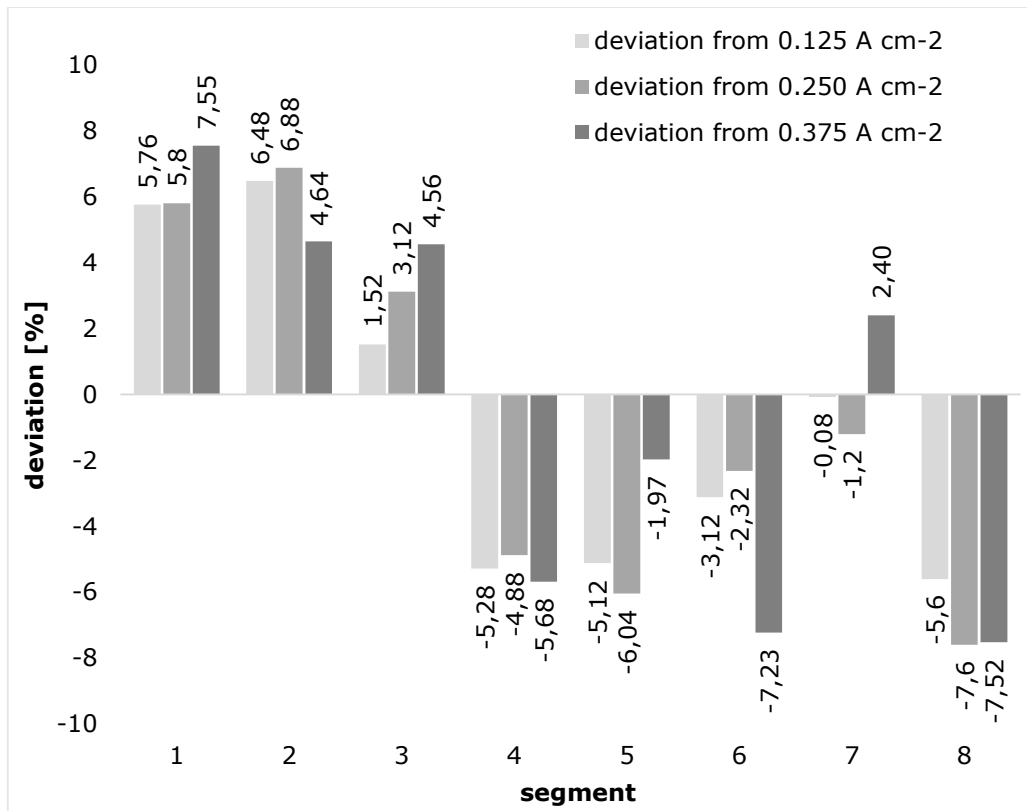


Fig. 91: Deviation of measured current density from arithmetic average current density for 2, 4 and 6 A load current

It becomes obvious, that deviation from arithmetic average current density is in the range - 7.5% to +7.5% depending on the applied load. In comparison to the current density distribution of Gore® based MEAs, which are presented earlier in chapter 4, differences between each segment become slightly larger. However, current is still even distributed. As operation conditions are homogeneous due to the hydraulic compression, the presented result proves even distributed active catalyst particles.

4.5. Optimisation of Pt/CNF Based Electrodes

The prepared Pt/CNF based anodes perform well in combination with BC-H225-10F cathodes. Regarding platinum utilisation, achieved power density is superior over the tested Pt/C based anodes. However, power output is limited due to the little amount of platinum. Although platinum content is low, an economic operation would not be possible¹⁶. Therefore, further optimisation aim on increasing the catalyst utilisation as well as on increasing the platinum loading, in order to obtain higher power density.

Three approaches have been studied regarding an improvement in power output for Pt/CNF based electrodes.

- Addition of polymers (Nafion® solution) within the prepared catalyst layer
- Utilisation of fibres with higher graphitisation degree
- Further optimisation of the pulse plating process

4.5.1. Variation of Polymer Content

Due to the pulsed electrochemical deposition of catalyst particles, localisation of platinum is directly at the interface between membrane and MPL. As already described, the surface of the electrode is not flat but has a varying height level. Due to the cell compression it can be assumed that the electrode gets flattened. However, there may be still catalyst particles, which remain inactive due to poor contact to the membrane.

For this reason membrane material is added to the catalyst layer by addition of Nafion® solution (5 wt.-% in alcohol) to the CNF dispersion. Furthermore, Nafion® solution has been spray coated on top of the prepared Pt/CNF layer, in order to fill gaps of the uneven electrode surface. This impregnation with Nafion® is performed after drying the electrode after Pt deposition. The following formulations have been tested:

- Samples w/o Nafion® (10:0:0) – compare to Fig. 87
- 10 parts CNFs, 2 parts Nafion® (10:2:0)
- 10 parts CNFs, 2 parts Nafion®, impregnation with 1 part Nafion® (10:2:1)
- 10 parts CNFs, 2 parts Nafion®, impregnation with 2 parts Nafion® (10:2:2)
- 10 parts CNFs, 3 parts Nafion®, impregnation with 2 parts Nafion® (10:3:2)
- 10 parts CNFs, 5 parts Nafion®, impregnation with 5 parts Nafion® (10:5:5)
- 10 parts CNFs, impregnation with 2 parts Nafion® (10:0:2)

Prepared electrode samples have been used for MEA testing. Polarisation curves of selected MEA samples are presented in Fig. 92 and Fig. 93.

¹⁶ As more cells would be needed in comparison to the use of other commercially available MEAs, the main cost drivers for a fuel cell containing prepared MEAs like presented above would be the membrane material and the pole plates.

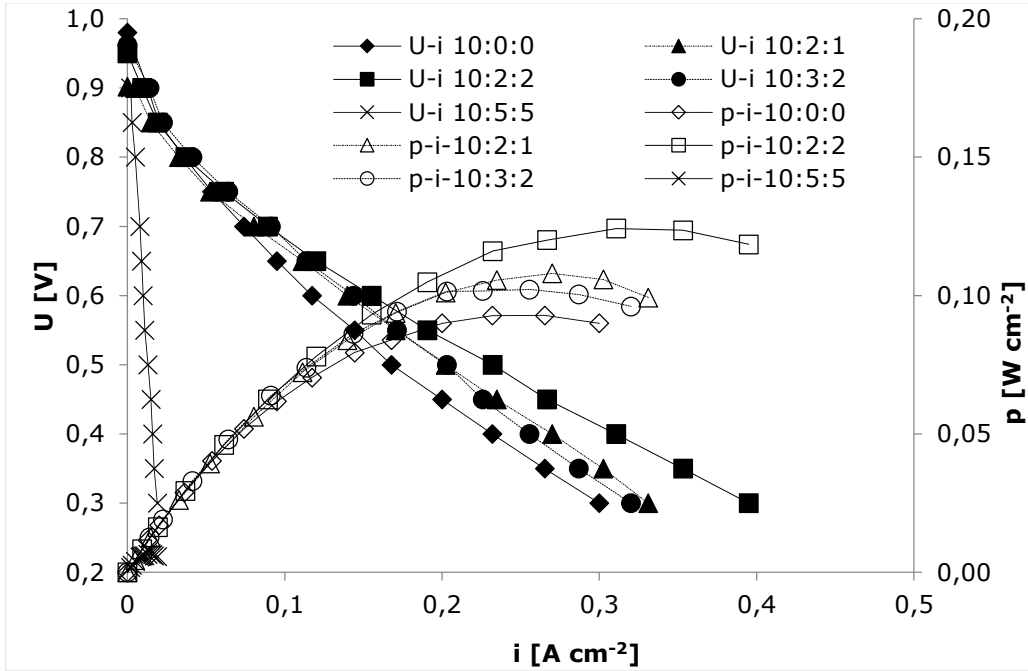


Fig. 92: Polarisation curves of MEAs containing Pt/CNF based anodes with varying Nafion® content

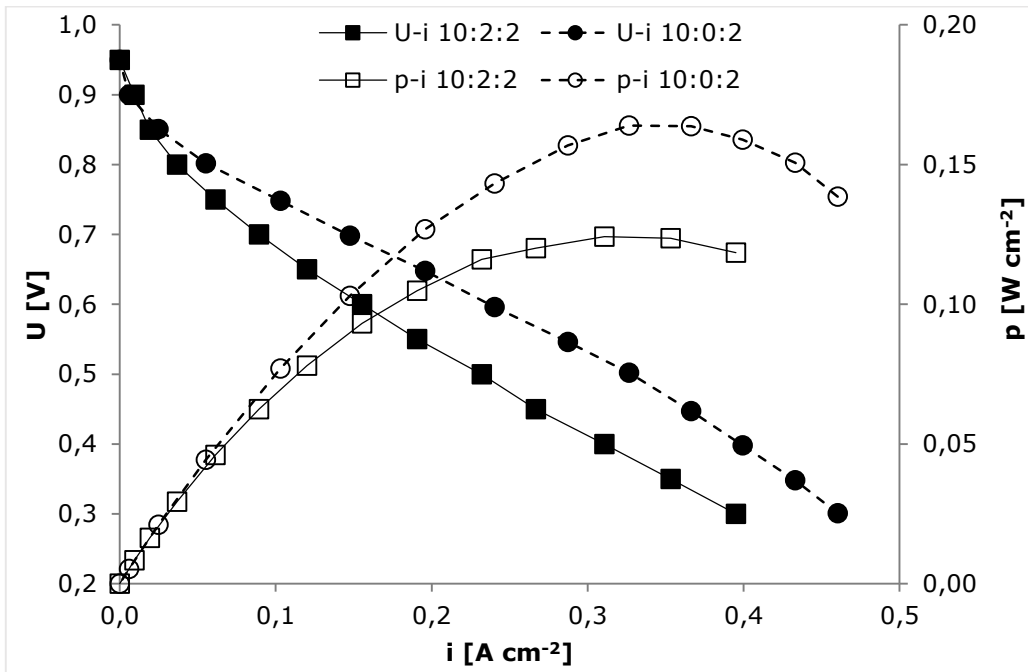


Fig. 93: Polarisation curves of selected MEA samples with and without Nafion® content within the catalyst layer

It was determined that an amount of Nafion® content within the CL can increase specific power output of prepared Pt/CNF based MEA samples. This effect arises from an improved catalyst connection to the membrane. An increased Nafion loading decreases power output again, due to decreased conductivity of the electrode. However, significant optimisation has been achieved by impregnating the electrode with Nafion® solution subsequently to Pt deposition. Different loadings have been tested for the impregnation step. A CNF to Nafion® ratio of 10:2 has been found as optimum for the subsequent spray coating of polymer solution. A higher Nafion loading does not result in further optimisation but in decreasing power output again, due to the electrical insulating character of Nafion®. As expected a sample with very high Nafion® content (10:5:5) showed nearly no power output.

An interesting effect has been observed. As can be seen from Fig. 93 power output of the sample without having Nafion fraction within the CNF layer (10:0:2) is 30% higher than for sample containing a certain share of polymer (10:2:2). This may be explained by the low number of Pt particles in the depth of the CNF layer which should be connected by the membrane material. This means, unnecessary insulating material is localised within the anode which decreases electrical conductivity. Gas flux may be reduced by the addition of Nafion® to the CNF ink. Therefore, power output is decreased.

This result indicates the favourable localisation of the catalyst particles on top of the CNF interlayer, due to the described preparation process. The amount of platinum particles within the CNF layer seems insignificant for the fuel cell performance. As a result, the presented MEA sample utilising an anode prepared by a Pt/CNF electro catalyst with optimised Nafion® impregnation, specific power output is about 75% higher (0.163 W cm^{-2}) than compared to an electrode without addition of any polymer content (0.092 W cm^{-2}).

4.5.2. Utilisation of Heat Treated Carbon Nanofibres

As electrical conductivity of prepared electrodes is decreased by the CNF interlayer, carbon filaments with higher electrical conductivity are favourable for this purpose. Within the scope of the described work CNFs with a higher electrical conductivity have been investigated for GDE preparation.

Two sorts of fibres are compared in this section – CNFs which were heat treated subsequently to their production as well as CNFs without further heat treatment which were also used for GDE preparation described within the last sections. The additional heating process results in an increased graphitisation degree for the treated fibres, which positively affects electrical and thermal conductivity. However, specific surface area is decreased at the same time. From the data sheet BET surface is known to be $105 - 150 \text{ m}^2 \text{ g}^{-1}$ for the heat treated fibres and $150 - 200 \text{ m}^2 \text{ g}^{-1}$ for the fibres as produced. MEA samples have been prepared by the use of developed GDEs based on both types of fibres. The effect of an additional heat treatment of the CNFs on the performance of PEMFCs is investigated in-situ in the novel fuel cell test environment based on hydraulic compression.

Electrodes have been prepared like presented above but with the use of the heat treated fibres. Nafion impregnation has been achieved according to the optimisation described in the last section. By X-ray diffraction (XRD) graphitisation degree has been obtained for these fibres (Tab. 16). As graphitisation degree influences electrical properties of graphitic material, electrical resistivity of GDLs with CNF coating was determined by four probe measurements in z-direction (through

plane) as well in xy-direction (in-plane). Results are presented in Tab. 17. Platinum loading has been obtained by XRF and TGA studies (Tab. 18).

Tab. 16: Graphitisation degree of investigated CNF raw material

	HOPG	H2315 I2C6 (MPL)	H2315 I2C6 (GDL)	CNF	CNF graphitised
G_p [%]	100	75.34	turbostratic	90.0 ± 0.2	99.8 ± 0.0

As thermal treatment of investigated CNFs results in increasing graphitisation degree, a difference between both types of fibres is observed. It becomes obvious that G_p for heat treated CNFs is in the range of 100%. In comparison to this, CNFs (as produced) have a graphitisation of about 90%. It is expected that investigated fibres differ in electrical conductivity. Therefore, electrical in-plane resistance R_{IP} and through-plane resistance R_{TP} have been determined.

Tab. 17: In-plane and through-plane resistivity of electrode samples depending on CNF coating

Sample	R _{IP} [Ω]	R _{TP} [mΩ cm ²]
H2315 I2C6 data sheet [47]	0.7	8
H2315 I2C6 blank	0.75 ± 0.02	8.46 ± 0.78
H2315 I2C6 + CNF layer	0.69 ± 0.01	10.63 ± 0.98
H2315 I2C6 + CNF graphitised	0.65 ± 0.07	9.07 ± 1.21

It was noticed, that referred to a blank GDL, R_{IP} is decreased off 8% by the CNF coating, respectively, off 14% by the coating based on graphitised fibres. This is explained by additional conductive material which decreases the resistance in-plane (larger diameter of the conductor). Values for R_{TP} result in an increase of 6% (CNFs graphitised), respectively, of 25% (CNFs as produced) referred to the reference measurement. Presented results underline the higher conductivity of CNF fibres, which were thermally treated after production.

Tab. 18: Platinum loading for investigated electrode samples

Sample	Pt content [wt.-%]	Residual mass [mg cm ⁻²]	Platinum loading [mg cm ⁻²]
H2315 I2C6 blank	-	0.030 ± 0.001	-
Pt/CNF	28.3 ± 0.3	0.088	0.016
Pt/CNF graphitised	99.9 ± 0.0	0.097	0.067

As can be seen from the table, catalyst content remaining from CNF production for the heat treated fibres is almost zero. Although, parameters for the deposition of platinum on the CNF layer is kept constant, loading for samples with a CNF layer from heat treated fibres is more than four times higher. This effect may be explained amongst others by the hydrogen evolution occurring simultaneously to platinum deposition. Moreover, one should consider that Ni content of the fibres

without additional heat treatment has an additional contribution as catalyst for the hydrogen evolution. Furthermore, specific surface area is different for the two types of fibres. This implies automatically the appearance of different local current densities (referred to the fibres surface) for the pulse plating process. Therefore, result for platinum loading is different. MEAs prepared like presented above have been analysed in the novel PEMFC test environment, in order to determine specific power output for the compared electrode samples. Measurements have been carried out at room temperature with ambient air (air stoichiometry $\lambda = 4$). Polarisation curves of MEA samples based on graphitised CNFs (marked as CNFg) as well as on CNFs without additional heat treatment (marked as CNF) are presented in Fig. 94.

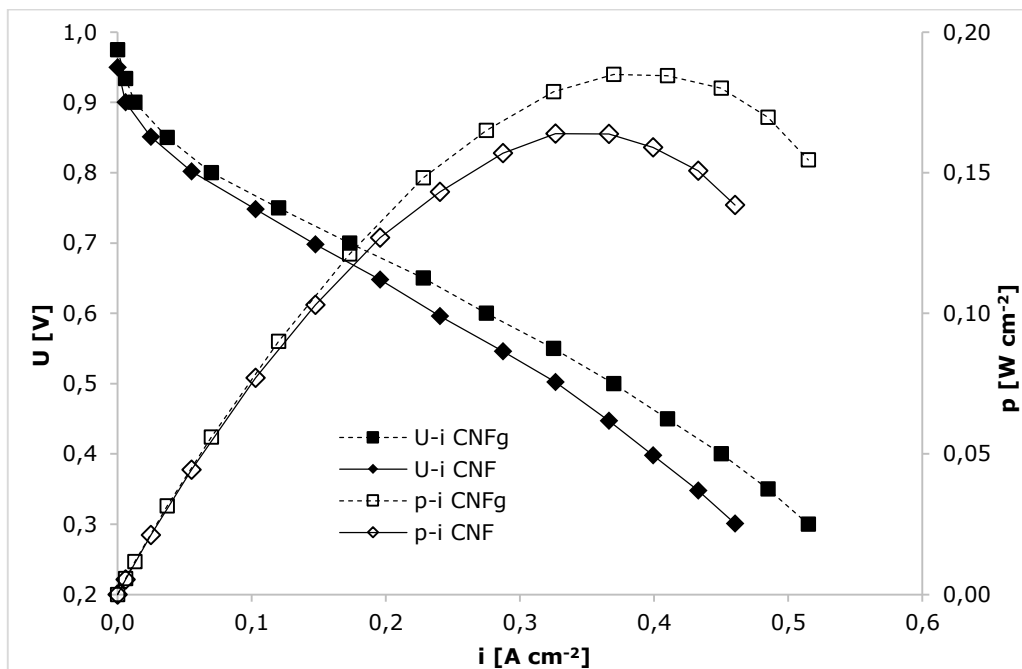


Fig. 94: Comparison of MEAs containing anodes based on CNFs depending on the graphitisation degree

From the diagram one can obtain the open circuit potential for both types is above 0.95 V. For small current densities an initial voltage drop occurs due to activation polarisation. From a cell voltage of 0.8 V on, the voltage drops nearly linear with increasing load current according to membrane and electrode resistance. For the presented MEA sample based on CNFs with high graphitisation degree, voltage drop becomes less than for the sample based on CNFs without additional heat treatment. This can be explained by the higher electrical conductivity of fibres with higher graphitisation degree. As a result of higher electrical conductivity, specific power output at a cell voltage of 0.45 V is about 13.5% higher by the use of heat treated CNFs as catalyst support material (0.185 W cm^{-2}) than by the use of CNFs as produced (0.163 W cm^{-2}).

The higher power output underlines the favourable properties of heat treated CNFs for the use as support material for catalyst nano particles in PEM fuel cells. Due to higher graphitisation degree of heat treated CNFs, electrical properties of

investigated electrode samples are improved compared to samples based on CNFs without additional treatment.

4.5.3. Optimisation of the Catalyst Preparation

For a prospective development of a PEMFC cathodes, increasing platinum loading is necessary. This is an issue due to the lower reaction kinetics for the oxygen reduction reaction which is compensated by a higher amount of platinum. E.g. CCMs from Gore® have four times more catalyst material on the cathode side than on the anode side.

It was observed that increasing the pulse number for the electro plating process higher than 12, leads to a growth of deposited particles above 30 nm. Therefore, it has been investigated, if a further increase of deposition current can increase the loading without changing the particle size significantly. Furthermore, the influence of different plasma parameters for the CNF functionalisation has been studied.

Like presented before, for preparation of electrodes CNF, dispersions are spray coated on porous graphitic substrate (gas diffusion layer type Freudenberg H2315 I2C6). In order to result in functional group formation on the graphitic surface, CNFs are activated by means of radio frequency induced oxygen plasma. Here, the plasma power is varied from 80 to 150 W for an exposure time of 5 to 30 minutes. Plasma parameters (power and duration) have been discussed previously (compare to chapter 4.1.1.1.). For investigation on the material's properties disk samples with 15 mm diameter (1.76 cm²) are prepared.

Subsequently, CNFs are decorated with Pt nano-particles by pulsed electro deposition from hexachloroplatinic acid. Current density for the pulse plating process is investigated from 0.1 A cm⁻² up to 0.5 A cm⁻² in order to result in an optimal particle size and distribution. The electrolyte is heated to 60 °C. The pH-value is adjusted to 2. Pulse length is set to 1 sec and pause length is 60 sec. This procedure is repeated twelve times for each specimen preparation.

Current density for platinum particle deposition regarding pulse plating is investigated by SEM. It is observed that platinum distribution is more homogeneous for particle deposition with higher current density. However, for a deposition current density of 0.5 A cm⁻² particle size increases to about 100 nm and clusters start to agglomerate, leading to a CNF coating. An optimum between platinum particle distribution and cluster size is found for electro deposition current density of 0.2 A cm⁻². Therefore, Pt/CNF based GDEs in this section refer to this parameter. SEM images are presented in Fig. 95.

Platinum loading of prepared electrodes has been determined by TGA. Metallic electrode content is analysed by XRF in order to distinguish platinum from CNF catalysts (Ni). Platinum loading of prepared electrodes depending on CNF loading is given in Tab. 19.

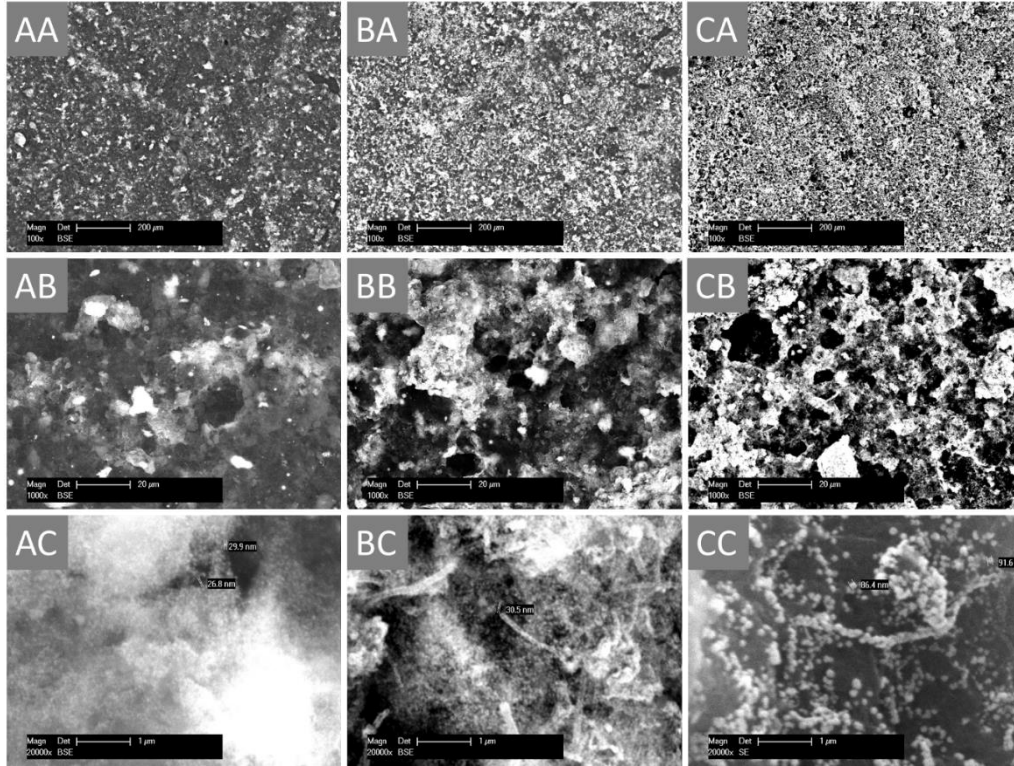


Fig. 95: SEM study of Pt/CNF based electrode depending on current density for Pt particle electro deposition (AA 100 magnitude, $i = 0.1 \text{ A cm}^{-2}$; AB 1,000 magnitude, $i = 0.1 \text{ A cm}^{-2}$; AC 20,000 magnitude, $i = 0.1 \text{ A cm}^{-2}$; BA 100 magnitude, $i = 0.2 \text{ A cm}^{-2}$; BB 1,000 magnitude, $i = 0.2 \text{ A cm}^{-2}$; BC 20,000 magnitude, $i = 0.2 \text{ A cm}^{-2}$; CA 100 magnitude, $i = 0.5 \text{ A cm}^{-2}$ and CB 100 magnitude, $i = 0.5 \text{ A cm}^{-2}$; CC 20,000 magnitude, $i = 0.5 \text{ A cm}^{-2}$)

Tab. 19: Results from XRF and TG analyses of selected samples depending on plasma treatment

Sample	Pt content [wt.-%]	Residual mass [mg cm^{-2}]	Pt loading [mg cm^{-2}]
Pt/CNF no plasma	85.3 ± 6.8	0.189 ± 0.025	0.135 ± 0.026
Pt/CNF 80 W 30 min	93.0 ± 0.5	0.172 ± 0.017	0.132 ± 0.018
Pt/CNF 100 W 20 min	94.1 ± 0.4	0.124 ± 0.025	0.088 ± 0.026
Pt/CNF 120 W 10 min	93.9 ± 0.8	0.145 ± 0.011	0.108 ± 0.012
Pt/CNF 150 W 5 min	81.0 ± 0.2	0.136 ± 0.002	0.086 ± 0.003

Platinum loading of selected electrode samples varies from 0.086 to 0.135 mg cm^{-2} . One can observe that mass fraction of platinum from metallic electrode content changes with the parameters for plasma pre-treatment. Highest mass fraction is found for plasma activation with 100 W and a treatment time of 20 minutes. Electrodes pre-treated with these parameters have platinum mass fraction which is 10.3% higher than for samples without plasma activation. Samples which are plasma activated at 150 W for 5 minutes show slightly lower platinum loading. However, mass fraction for platinum is below samples without previous plasma treatment. This can be explained due to a dominant etching effect by the plasma. Therefore, these samples have not been considered for electrochemical investigation.

CV diagram of selected samples in 0.5 M H_2SO_4 is shown in Fig. 96. One may observe that hydrogen adsorption and hydrogen desorption occurs between -0.2 and 0.1 V vs. SCE. Charge is calculated from the area below the plot for hydrogen adsorption. ECSA is obtained by division of calculated charge with the charge for a plane platinum disk which is taken from the literature ($210 \mu\text{C cm}^{-2}$). CV analyses of prepared GDEs result in different ECSA depending on the plasma process. Calculation for ECSA as well as for specific ECSA can be taken from Tab. 20.

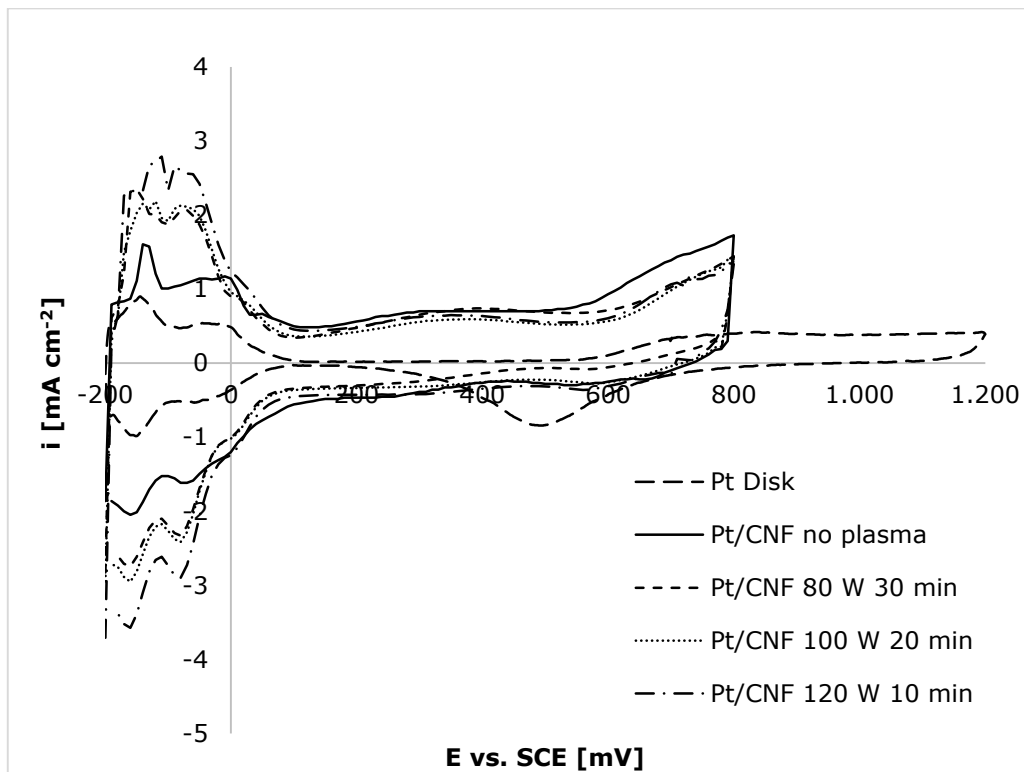


Fig. 96: CV diagram of selected electrode samples (after 100 cycles)

Tab. 20: Electrochemical surface area of selected electrode samples depending on plasma treatment

Sample	ECSA [cm ²]	spec. ECSA [cm ² mg ⁻¹]
Blank Pt disk	1.01	-
BC-H225-10F	194.39	132.23
Pt/CNF no plasma	6.44 ± 0.07	47.7
Pt/CNF 80 W 30 min	13.55 ± 0.06	102.7
Pt/CNF 100 W 20 min	11.97 ± 2.31	136.4
Pt/CNF 120 W 10 min	16.03 ± 0.75	148.6

For the prepared electrodes CNF functionalisation in RF oxygen plasma at 120 W for 10 minutes results in highest specific ECSA of 148.6 cm² mg⁻¹. This is about three times higher than for samples without previous plasma activation (47.7 cm² mg⁻¹). As platinum loading is slightly higher for electrode samples without activation, higher platinum utilisation is achieved by the pre-treatment. This may be explained due to smaller particles which are distributed more homogeneously on the CNF layer as a result of formation of functional groups at the fibres surface.

By the aid of a potentiostat/galvanostat Mmates 560 (up to 100 A), GDEs have been prepared based heat treated CNFs plasma activated with the optimised pre-treatment parameters (120 W for 10 min). Puls current for platinum deposition has been set to 4 A according to the optimised plating parameter of 0.2 A cm⁻². Subsequently, the electrode has been impregnated with Nafion[®] solution, in order to maintain a good contact between catalyst particles an membrane. MEAs have been manufactured, using these electrodes as anode material (BC-H225-10F has been used as cathode material).

MEA testing is performed at ambient conditions (room temperature) with atmospheric air and pure hydrogen. Hydrogen is circulated through the anode with 0.2 bar overpressure with high excess gas in order to prevent hydrogen starvation over the active cell area. Air is pumped through the cathode. The cathode's outlet is open to atmosphere. Polarisation curve of a MEA optimised like presented above is shown in Fig. 97.

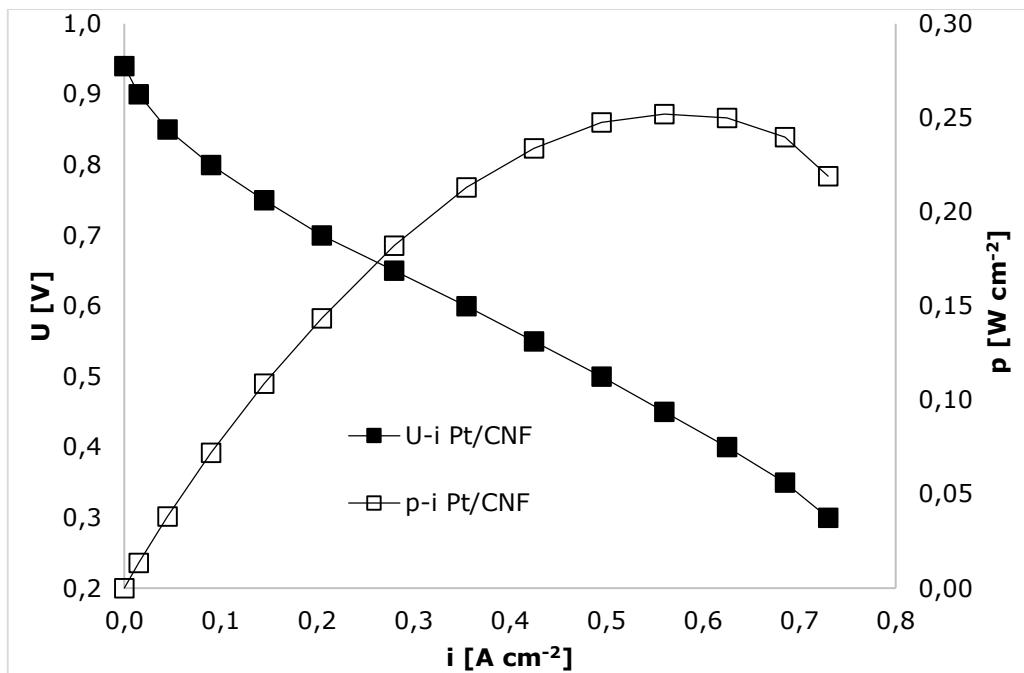


Fig. 97: Polarisation curve of an optimised MEA based on Pt/CNF electro catalyst

For the optimised Pt/CNF based MEA maximum power density of $0.25\ W\ cm^{-2}$ is obtained at a cell voltage of 0.45 V. Due to the higher platinum loading the specific power output has been further improved. However, according to the determined amount of platinum one needs to consider, that loading has been increased to factor of up to ten in comparison to GDEs prepared like presented in chapter 4.5.1. Power output of this sample just increased about 50%. Further optimisation of catalyst particle size is needed, in order to improve platinum utilisation and further increase power output of prepared MEAs.

5. CONCLUSIONS

Aim of this work was the development of a feasible method to reduce noble metal content in PEMFCs. For this purpose different approaches have been analysed to optimise utilisation of catalyst material in fuel cell electrodes. In order to result in significant savings, carbon nano fibres have been investigated as support material for platinum catalyst particles, as these offer high surface area for catalyst decorations as well as high electrical conductivity for low-loss electron transfer. Due to particle deposition subsequently to preparing a CNF interlayer, an optimised localisation of catalyst material has been expected.

Preliminary research on the plasma activation of carbon nano tubes already indicated the possibility to increase surface energy of treated graphitic fibres, in order to disperse these for any purpose (e.g. CNT powder as additive in resins for composite materials with increased mechanical stability). Within the scope of the described experimental work, this phenomenon has also been confirmed for plasma treated CNFs. As a result, dispersibility of CNFs in alcohol and water has been enhanced, which permits processing of the investigated fibres regarding the preparation of PEM fuel cell electrodes. In respect to the formulation of stable CNF dispersions, the main advantages of the plasma process became obvious. As functionalisation in acids, such as HNO_3 , at 80 °C lasts several hours, in comparison to wet chemical activation the physical plasma treatment at room temperature is much quicker and less complicated in respect of handling. Depending on the plasma power, a five minutes treatment time leads to the aspired result. This significantly decreases the duration for the electrode preparation. Furthermore, no acidic wastes remain after the preparation, which reduces the environmental impact as no subsequent water conditioning is necessary.

By obtaining stable CNF dispersions, it has been possible to prepare gas diffusion electrodes based on a CNF interlayer, which has been spray coated on commercially available GDL material. The CNF pre-treatment in oxygen plasma also improves spray coating, as agglomeration of fibres is suppressed by the increased surface energy. This is necessary in order to avoid blocking of tubing and nozzles by CNF agglomerates, otherwise.

Furthermore, it could be shown, that the formation of oxygen-containing functional groups on the surface of treated CNFs result in a certain electrochemical activity. By testing electrode material based on plasma treated CNFs in a galvanic cell as well as in-situ in a PEM fuel cell test environment, electrochemical activity concerning the hydrogen adsorption and desorption has been recognised. However, no sensible fuel cell device could be established by this material as power output was determined to be in the range of 10^{-6} W. However, for prospective electrochemical sensor applications, plasma activated CNFs may be useful electrode material.

For this experimental work catalyst preparation has been performed by pulsed electro plating of platinum nano particles onto a porous CNF interlayer. The favourable material properties of investigated CNFs (high graphitisation, large surface area) lead to the preparation of a large number of active catalyst particles regarding the development of PEM fuel cell electrodes. Electrodes with low platinum loading and improved catalyst utilisation were obtained. Here, the oxygen plasma activation assisted the catalyst preparation regarding the loading and morphology of deposited Pt particles. It can be concluded, that achieved functional groups on the CNFs surface provide preferential anchor points for the nucleation of catalyst particles. This leads to an even distribution of particles. Particle size could be decreased due to the plasma

activation, which results in a favourable increase in electrochemical active surface area. Furthermore, loading could be increased for a higher power output of manufactured PEM fuel cells. Suitable plasma parameters for this purpose have been obtained within the described work.

Further improvements were achieved by the impregnation of prepared electrodes with the membrane material itself. Although the localisation of deposited catalyst particles was improved due to the described preparation route, a small fraction of ionomer, which was spray coated on top of the Pt/CNF based catalyst layer, has optimised catalyst connection to the polymer membrane. It can be concluded that the roughness of prepared electrodes lead to certain gaps, which need to be filled with further membrane material. As a result power output increased significantly. By the use of CNFs with nearly ideal graphitisation degree a further increase in power output was observed. However, it is necessary to mention higher costs for the fibres due to the additional production step (heat treatment). Furthermore, a higher platinum loading was determined according to the performed preparation process. It can be concluded, that contrarily to the improved fuel cell performance, the cost savings specific to power output (due to less catalyst usage) will be decreased by the use of this material.

Fuel cell testing of manufactured MEAs regarding the developed electrode samples working as anodes, was performed in a novel test environment. Unique features, such as improved cell compression and homogeneous temperature conditions, result from the hydraulic compression of single cells. The possibility to obtain nearly identical operation conditions for each cell of a fuel cell was utilised for simultaneous testing of several MEA samples. As operation conditions are equal, differences in operation characteristics can be explained by differences between the tested electrodes. The possibility to compare several tested samples directly is superior to state of the art test systems working with mechanical cell compression. Furthermore, the ease of changing cells due to the modular stack design makes fuel cell testing more comfortable in comparison to typically used test stacks. From the favourable operation conditions it can be further concluded, that prospective (stationary) fuel cell developments will also be superior over systems with mechanical compression.

Fundamental assumptions concerning catalyst material savings by the investigated electrode preparation process have been proofed in this work. It was possible to manufacture PEM fuel cell electrodes with low platinum loading, which showed increased catalyst utilisation for the use as anode material. Significant improvements regarding the prospective development of fuel cell cathodes are also expected by the use of oxygen plasma activated CNFs. It can be assumed that the development of membrane electrode assemblies for PEM fuel cells will result in an overall reduction of necessary noble metals. By the presented optimisations, achieved by means of the oxygen plasma treatment, time savings during the electrode production as well as a decreased effort for cleaning processes are expected. Due to these obvious advantages it can be concluded, that after some process improvements the laboratory scale electrode preparation route is feasible for an industrial production of low cost electrodes in the future. The application of such low cost electrodes developed in this work can, consequently, lead to significant cost savings for the production of fuel cell devices and may help to initiate commercially available systems in the market. This is necessary for prospective stationary or mobile fuel cell applications, which may be possible solutions in order to reduce CO₂ emissions in the future as well as to achieve the transformation of the energy sector into a renewable one, the so-called 'Energiewende' in German.

LIST OF PUBLICATIONS

Ulrich Rost, Michael Brodmann, Viorel-Aurel Șerban, Cristian Mutascu, Jeffrey Roth, Bruno Zekorn, STATE OF THE ART OF PEM FUEL CELLS WITH A FOCUS ON A MODULAR FUEL CELL STACK WITH HYDRAULIC COMPRESSION, BULETINUL ȘTIINȚIFIC AL UNIVERSITĂȚII „POLITEHNICA” DIN TIMIȘOARA, ROMÂNIA SERIA MECANICĂ, Vol. 57 (71), Iss. 2, 2012, ISSN 1224 – 6077

Ulrich Rost, Gabriela Marginean, Waltraut Brandl, Michael Brodmann, Oxygen Plasma Activated Carbon Nanotubes as Electrode Material for Proton Exchange Membrane Fuel Cells, 2nd International Conference on Materials for Energy - EnMat II, Karlsruhe, 2013

Michael Brodmann, Martin Greda, Cristian Mutascu, Jörg Neumann, Ulrich Rost, Jeffrey Roth, Andre Wildometz, METHOD AND SYSTEM FOR OPERATING AN ELECTROLYSER, International patent, 2014, WO002014040746A1

Michael Brodmann, Martin Greda, Cristian Mutascu, Jörg Neumann, Ulrich Rost, Jeffrey Roth, Andre Wildometz, ENERGY CONVERSION DEVICE HAVING REVERSIBLE ENERGY STORAGE, International patent, 2014, WO002013107619A1

Michael Brodmann, Ulrich Rost, A Modular Stack Technology for Electrochemical Cells Based on Hydraulic Compression, OZ-14 7th German-Japanese Symposium on Nanostructures, Wenden, 2014

Ulrich Rost, Michael Brodmann, Neuartige Messvorrichtung basierend auf hydraulischer Verpressung zur Untersuchung von Brennstoffzellen und Elektrolyseurkomponenten, IEEE WORKSHOP Industrielle Messtechnik & Kraftfahrzeugsensorik, Mülheim a.d.R., 2014, p. 11 – 13, ISBN 978-3-9814801-5-3

Ulrich Rost, PEM-Hochdruckelektrolyseur in Taschenbauweise, 7. Workshop AiF - Brennstoffzellen-Allianz elektrochemische Energiewandlung und Speicherung, Duisburg, 2014, <http://www.zbt-duisburg.de/aktuell/veranstaltungen/tagungen/aif-bz-allianz-2014/>

Ulrich Rost, Michael Brodmann, Development of Membrane Electrode Assemblies Based on Oxygen Plasma Activated Carbon Nanotubes and their Application in a Novel Modular Test System with Hydraulic Compression, 14th Ulm ElectroChemical Talks, Ulm, 2014

Ulrich Rost, Gabriela Marginean, Veronica Rigou, Waltraut Brandl, Michael Brodmann, Oxygen Plasma Activated Carbon Nanotubes as Electrode Material for Proton Exchange Membrane Fuel Cells, Junior Euromat 2014, Lausanne, 2014

Ulrich Rost, Jeffrey Roth, Michael Brodmann, Modular Polymer Electrolyte Membrane Fuel Cell and Electrolyser Stack Design with Hydraulic Compression, Power and Energy Student Summit 2015, Dortmund, 2015, DOI: 10.17877/DE290R-7265

Roxana Muntean, Ulrich Rost, Gabriela Marginean, Nicolae Vaszilcsin, Determination of the electrochemical surface area for CNTs-PT electro catalyst using cyclic voltammetry, 9th International Conference on Materials Science and Engineering BRAMAT 2015, Braşov, 2015

Ulrich Rost, Roxana Muntean, Gabriela Marginean, Nicolae Vaszilcsin, Michael Brodmann, Effect of the Process Parameters for Oxygen Plasma Activation of Carbon Nanofibres on the Characteristics of Deposited Platinum Catalyst Nanoparticles, Carbon 2015, Dresden, 2015

Roxana Muntean, Ulrich Rost, Gabriela Marginean, Nicolae Vaszilcsin, Studies on electrodeposition of platinum nanoparticles as a function of differently activated carbon nanofibers, Carbon 2015, Dresden, 2015

Ulrich Rost, Cristian Mutascu, Jeffrey Roth, Christoph Sagewka, Michael Brodmann, Proof of Concept of a Novel PEM Fuel Cell Stack Design with Hydraulic Compression, Journal of Energy and Power Engineering, 9 (2015) 775 – 783, DOI: 10.17265/1934-8975/2015.09.003

Ulrich Rost, Roxana Muntean, Pit Podleschny, Gabriela Marginean, Michael Brodmann, Viorel-Aurel Şerban, Influence of Graphitisation Degree of Carbon Nano Fibres Serving as Catalyst Support Material for Noble Metal Electro Catalysts on the Performance of PEM Fuel Cells, Advanced Materials and Structures - AMS 2015, Timişoara, 2015 (accepted contribution)

Ulrich Rost, Jeffrey Roth, Michael Brodmann, A Novel Concept for Modular High Pressure Water Electrolyser Systems for Generation of Hydrogen from Excess Energy by Renewables, Smart Energy 2015, Dortmund, 2015 (accepted contribution)

REFERENCES

- [1] K. Zwingmann, *Ökonomische Analyse der EU- Emissionshandelsrichtlinie*. Deutscher Universitätsverlag, Hamburg, 2007.
- [2] A. Born et al., *Biologie*, Cornelsen, Berlin, 2009.
- [3] K. Munk, *Grundstudium Biologie – Biochemie, Zellbiologie, Ökologie, Evolution*. Spektrum, Akademischer Verlag, Berlin, Heidelberg, 2000.
- [4] IPCC, *Climate Change 2007: The Physical Science Basis. Contribution of Working Group I to the Fourth Assessment Report of the Intergovernmental Panel on Climate Change* [S. Solomon et al.], Cambridge University Press, Cambridge, New York, 2007.
- [5] IPCC, *Climate Change 2001: The Scientific Basis. Contribution of Working Group I to the Third Assessment Report of the Intergovernmental Panel on Climate Change* [J.T. Houghton et al.], Cambridge University Press, Cambridge, New York, 2001.
- [6] Information on <http://www.ipcc.ch>, Accessed: 2015-09-01
- [7] SEC, *REPORT FROM THE COMMISSION TO THE EUROPEAN PARLIAMENT AND THE COUNCIL – PROGRESS TOWARDS ACHIEVING THE KYOTO OBJECTIVES*, published by the European Union, 2010.
- [8] European Parliament, *Klimawandel: Parlament debattierte Fahrplan für Klimakonferenz in Paris*, 2015, http://www.europarl.europa.eu/pdfs/news/expert/infopress/20150126IPR15004/20150126IPR15004_de.pdf, Accessed: 2015-09-01
- [9] IEA, *CO2 CAPTURE AND STORAGE – A key carbon abatement option*, IEA Publications, Paris, 2008.
- [10] IEA, *Key World Energy STATISTICS*, IEA Publications, Paris, 2010.
- [11] Bundesministerium für Wirtschaft und Technologie und Bundesministerium für Umwelt, Naturschutz und Reaktorsicherheit, *Energiekonzept*, 2010, http://www.bundesregierung.de/ContentArchiv/DE/Archiv17/_Anlagen/2012/02/energiekonzept-final.pdf?__blob=publicationFile&v=5, Accessed: 2014-11-11
- [12] Umweltbundesamt, *Entwicklung der spezifischen Kohlendioxid-Emissionen des deutschen Strommix in den Jahren 1990 bis 2012*, ISSN 1862-4359, 2013

- [13] Information on <https://www.destatis.de/DE/ZahlenFakten/Wirtschaftsbereiche/Energie/Erzeugung/Tabellen/Bruttostromerzeugung.html;jsessionid=6DFACE955C0FAFA1DDF6AC4358415EDD.cae1>, Accessed: 2015-09-01
- [14] Information on https://www.bdew.de/internet.nsf/id/DE_Energiedaten, Accessed on 2015-09-01
- [15] Information on <http://www.eex.com/en/>, Accessed on 2015-09-01
- [16] J. Meyer, Electricity Spot-Prices and Production Data in Germany 2013, http://www.ise.fraunhofer.de/en/renewable-energy-data/electricity-production-data?set_language=en, Accessed: 2015-09-01
- [17] S. Köhler, What Price is a Fair Price?, Energy Risk 04/2014
- [18] F. Kaiser, Steady State Analyse of existing Compressed Air Energy Storage Plants, Power and Energy Student Summit 2015, Dortmund, 2015, DOI: <http://hdl.handle.net/2003/33983>
- [19] D. Stolten (Ed.): Hydrogen and Fuel Cells. Wiley-VCH, Weinheim, 2010, pp. 207-226.
- [20] D. Stolten (Ed.): Hydrogen and Fuel Cells. Wiley-VCH, Weinheim, 2010, pp. 121-148.
- [21] Ballard, press release (2010): Ballard Tests 1 MW PEM Power Plant. Available at: <http://www.h2euro.org/2010/ballard-tests-1-mw-pem-power-plant>. Accessed: 2014-11-11
- [22] D. Stolten (Ed): Hydrogen and Fuel Cells. Wiley-VCH, Weinheim, 2010, pp. 755-786.
- [23] K. Klug (2013): Wasserstoff als Energiespeicher. Available at: http://www.brennstoffzelle-nrw.de/fileadmin/daten/jahrestreffen/2013/11_Klug_WF-HS-GE_Windstrom-Herten_NBW20131114.pdf. Accessed: 2014-11-11
- [24] E.ON, press release (2013): E.ON nimmt „Power to Gas“-Pilotanlage im brandenburgischen Falkenhagen in Betrieb. Available at: <http://www.eon.com/de/presse/pressemitteilungen/pressemitteilungen/2013/8/28/eon-nimmt-power-to-gas-pilotanlage-im-brandenburgischen-falkenhagen-in-betrieb.html>. Accessed: 2014-11-11
- [25] T. Smolinka, M. Günther, J. Garche (2011): Stand und Entwicklungspotenzial der Wasserelektrolyse zur Herstellung von Wasserstoff aus regenerativen Energien. Available at: http://www.now-gmbh.de/fileadmin/user_upload/RE_

- Publikationen_NEU_2013/Publikationen_NIP/NOW-Studie-Wasserelektrolyse-2011.pdf, Accessed: 2014-11-11
- [26] J. Larminie, A. Dicks, *Fuel Cell Systems Explained Second Edition*, Wiley, Chichester, 2003.
- [27] F. Barbir: *PEM Fuel Cells Theory and Practice 2nd Edition*, Academic Press, Waltham, 2013.
- [28] J. Zhang (Ed.): *PEM Fuel Cell Electrocatalysts and Catalyst Layers – Fundamentals and Applications*, Springer, London, 2008.
- [29] A. Heinzl, F. Mahlendorf, *Brennstoffzellen: Entwicklung, Technologie, Anwendung*, C. S. Müller, 2006.
- [30] C. H. Hamann, W. Vielstich: *Elektrochemie 3rd ed.*, Wiley-VCH, Weinheim, 1998.
- [31] J. Zhang, H. Zhang, J. Wu, J. Zhang, *PEM Fuel Cell Testing and Diagnosis*, Elsevier, Amsterdam, 2013.
- [32] Roland Reich, *Thermodynamik – Grundlagen und Anwendungen in der allgemeinen Chemie, sec. ed.*, VCH Verlagsgesellschaft, Weinheim, 1993.
- [33] Information on <http://www.ceramicfuelcells.de/de/technologie/gennex-modul/>, Accessed: 2015-09-01
- [34] F. Büchi, M. Inaba, T. Schmidt (Eds.): *Polymer Electrolyte Fuel Cells Durability*, Springer, New York, 2009.
- [35] S. Karimi et al., *A Review of Metallic Bipolar Plates for Proton Exchange Membrane Fuel Cells: Materials and Fabrication Methods*, *Advances in Materials Science and Engineering*, Volume 2012 (2012), DOI: 10.1155/2012/828070.
- [36] F. Büchi, M. Inaba, T. Schmidt (Eds.): *Polymer Electrolyte Fuel Cells Durability*, Springer, New York, 2009, pp. 243 – 268.
- [37] Zentrum für Brennstoffzellentechnik, <http://www.zbt-duisburg.de/de/portfolio/bz-komponenten/spritzgiess-bpp/>
- [38] X. Li, I. Sabir: *Review of bipolar plates in PEM fuel cells: Flow-field designs*, *International Journal of Hydrogen Energy*. Vol. 30, Iss. 4 (2005) 359–371.
- [39] J. Kleemann, F. Finsterwalder, W. Tillmetz: *Characterisation of mechanical behavior and coupled electrical properties of polymer electrolyte membrane fuel cell gas diffusion layers*, *Journal of Power Sources* 190 (2009) 92 – 102.

- [40] S. Park, J.-W. Lee, B. N. Popov: A review of gas diffusion layer in PEM fuel cells: Materials and design, *International Journal of Hydrogen Energy* 37 (2012) 5850 – 5865
- [41] M. S. Ismail et al.: Effect of polytetrafluoroethylene-treatment and microporous layer-coating on the electrical conductivity of gas diffusion layers in proton exchange membrane fuel cells, *Journal of Power Sources* 195 (2010) 2700 – 2708.
- [42] T. Smolinka, S. Rau, C. Helbig, *Polymer Electrolyte Membrane (PEM) Water Electrolysis*, World Hydrogen Energy Conference 2010, Essen, 2010, DOI: <http://hdl.handle.net/2128/3989>
- [43] K.-V. Peinemann, S. Pereira Nunes (Eds.): *Membranes for Energy Conversion*, Volume 2, Wiley-VCH, Weinheim, 2008, pp. 47 – 60.
- [44] G. Merle, M. Wessling, K. Nijmeijer: Anion exchange membranes for alkaline fuel cells: A review, *Journal of Membrane Science* 377 (2011) 1 – 35.
- [45] K.-V. Peinemann, S. Pereira Nunes (Eds.): *Membranes for Energy Conversion*, Volume 2, Wiley-VCH, Weinheim, 2008, pp. 1 – 46.
- [46] J. Zhang (Ed.): *PEM Fuel Cell Electrocatalysts and Catalyst Layers – Fundamentals and Applications*, Springer, London, 2008, pp. 89 – 134.
- [47] J. Zhang (Ed.): *PEM Fuel Cell Electrocatalysts and Catalyst Layers – Fundamentals and Applications*, Springer, London, 2008, pp. 135 – 164.
- [48] J. Zhang (Ed.): *PEM Fuel Cell Electrocatalysts and Catalyst Layers – Fundamentals and Applications*, Springer, London, 2008, pp. 1 – 88.
- [49] T. R. Ralph, M. P. Hogarth: Catalysis for Low Temperature Fuel Cells, Part I: The Cathode Challenges, *Platinum Metals Review*, Vol. 46, Iss. 1 (2002) 3 – 11.
- [50] A. Therdthianwong, P. Saenwisetb, S. Therdthianwongb: Cathode catalyst layer design for proton exchange membrane fuel cells, *Fuel* 91 (2012) 192 – 199.
- [51] G. Sasikumara, J.W. Ihma, H. Ryu, Optimum Nafion content in PEM fuel cell electrode, *Electrochimica Acta* 50 (2004) 601 – 605.
- [52] S. Litster, G. McLean: PEM fuel cell electrodes, *Journal of Power Sources* 130 (2004) 61 – 76.
- [53] C. Sung, C. Liua, C. C. J. Cheng: Performance improvement by a glue-functioned Nafion layer coating on gas diffusion electrodes in PEM fuel cells, *International Journal of Hydrogen Energy* 39 (2014) 11700 – 11705.

- [54] D. Stolten (Ed.): Hydrogen and Fuel Cells. Wiley-VCH, Weinheim, 2010, pp. 1 – 16.
- [55] C. Kulp: Synthese und Charakterisierung von Kern-Schale-Katalysatoren für die Sauerstoffreduktion, Ph.D. thesis, Bochum, 2012, online available at <http://www-brs.ub.ruhr-uni-bochum.de/netahtml/HSS/Diss/KulpChristian/diss.pdf>
- [56] A. Holewinski, S. Linic: Kinetic Analysis of Electrochemical Oxygen Reduction and Development of Ag-alloy Catalysts for Low Temperature Fuel Cells, Materials for Energy II – EnMatII, Karlsruhe, 2013.
- [57] W. Vielstich, A. Lamm, H. A. Gasteiger, H. Yokokawa (Eds.): Handbook of Fuel Cells – Fundamentals, Technology and Applications, John Wiley & Sons, Chichester, 2009, Vol. 5, p. 18.
- [58] H. A. Gasteiger, S. S. Kocha, B. Sompalli, F. T. Wagner: Activity benchmarks and requirements for Pt, Pt-alloy, and non-Pt oxygen reduction catalysts for PEMFCs, Applied Catalysis B: Environmental, Vol. 56, Iss. 1–2 (2005) 9 – 35.
- [59] A. Bonnefont et al.: Advanced catalytic layer architectures for polymer electrolyte membrane fuel cells, WIREs Energy Environ, 2014, DOI: 10.1002/wene.110
- [60] M. Debe et al. Advanced Cathode Catalysts and Supports for PEM Fuel Cells, DOE Hydrogen and Fuel Cells Program. FY2011 Annual Progress Report (2011) pp. 699 – 707.
- [61] L. Calvillo et al.: Synthesis and performance of platinum supported on ordered mesoporous carbons as catalyst for PEM fuel cells: Effect of the surface chemistry of the support, International Journal of Hydrogen Energy 36 (2011) 9805 – 9814.
- [62] F. J. Nores-Pondal et al.: Catalytic activity vs. size correlation in platinum catalysts of PEM fuel cells prepared on carbon black by different methods, International Journal of Hydrogen Energy 34 (2009) 8193 – 8203.
- [63] Y. Lin et al.: The corrosion of PEM fuel cell catalyst supports and its implications for developing durable catalysts, Electrochimica Acta 54 (2009) 3109 – 3114.
- [64] A. N. Golikand, M. Asgari, E. Lohrasbi: Study of oxygen reduction reaction kinetics on multi-walled carbon nano-tubes supported Pt-Pd catalysts under

- various conditions, *International Journal of Hydrogen Energy* 36 (2011) 13317 – 13324.
- [65] X. Zhang et al.: Deposition of platinum–ruthenium nano-particles on multi-walled carbon nano-tubes studied by gamma-irradiation, *Radiation Physics and Chemistry* 79 (2010) 1058 – 1062.
- [66] Yu Chen et al.: Electro-oxidation of methanol at the different carbon materials supported Pt nano-particles, *International Journal of Hydrogen Energy* 35 (2010) 10109 – 10117.
- [67] A. A. Fedotov et al.: Plasma-assisted Pt and Pt–Pd nano-particles deposition on carbon carriers for application in PEM electrochemical cells, *International Journal of Hydrogen Energy* 38 (2013) 8568 – 8574.
- [68] M. J. Larsen, E. M. Skou: ESR, XPS, and thin-film RRDE characterization of nano structured carbon materials for catalyst support in PEM fuel cells, *Journal of Power Sources* 202 (2012) 35 – 46.
- [69] A. Marinkas et al.: Graphene as catalyst support: The influences of carbon additives and catalyst preparation methods on the performance of PEM fuel cells, *Carbon* 58 (2013) 139 – 150.
- [70] H. Wu, D. Wexler, H. Liu, Durability investigation of graphene-supported Pt nanocatalysts for PEM fuel cells, *Journal of Solid State Electrochemistry* (2011) 15:1057 – 1062.
- [71] P. Morgan: *Carbon Fibers and their Composites*, Taylor & Francis, Boca Raton, 2005.
- [72] F. Büchi, M. Inaba, T. Schmidt (Eds.): *Polymer Electrolyte Fuel Cells Durability*, Springer, New York, 2009, pp. 29 – 53.
- [73] G. Srinivas et al.: Synthesis of graphene-like nanosheets and their hydrogen adsorption capacity, *Vol. 48, Iss. 3* (2010) 630 – 635.
- [74] H. Kim et al.: All-graphene-battery: bridging the gap between supercapacitors and lithium ion batteries, *Scientific Reports* 4, Article number 5278, DOI: 10.1038/srep05278.
- [75] B. Bhushan (Ed.): *Springer Handbook of Nano-technology*, Springer, Berlin, 2004, pp. 39 – 98.
- [76] H. Raghubanshi, M. Sterlin Leo Hudson, O. N. Srivastava: Synthesis of helical carbon nanofibres and its application in hydrogen desorption, *International Journal of Hydrogen Energy*, Vol. 36, Iss. 7 (2011) 4482 – 4490.

- [77] V. Barranco et al.: Amorphous carbon nanofibres inducing high specific capacitance of deposited hydrous ruthenium oxide, *Electrochimica Acta*, Vol. 54, Iss. 28 (2009) 7452 – 7457.
- [78] J.L. Gonzales Moral, J. Vera Agullo, C. Merino Sanchez, M. Gullon, EU Patent EP 1 990 449 B1 (2007).
- [79] M. Weisenberger et al.: The effect of graphitization temperature on the structure of helical-ribbon carbon nanofibers, *Carbon* Vol. 47 (2009) 2211 – 2218.
- [80] G. Marginean: Vapour Grown Carbon Fibres: Morphologie und plasmachemische Funktionalisierung, Ph.D. thesis, Bochum, 2004.
- [81] W. Zhang et al.: Carbon nanotube architectures as catalyst supports for proton exchange membrane fuel cells. *Energy and Environmental Science*, Vol. 3, Iss. 9 (2010) 1286 – 1293.
- [82] F. Büchi, M. Inaba, T. Schmidt (Eds.): *Polymer Electrolyte Fuel Cells Durability*, Springer, New York, 2009, pp. 159 – 195.
- [83] F. Büchi, M. Inaba, T. Schmidt (Eds.): *Polymer Electrolyte Fuel Cells Durability*, Springer, New York, 2009, pp. 257 – 268.
- [84] F. Büchi, M. Inaba, T. Schmidt (Eds.): *Polymer Electrolyte Fuel Cells Durability*, Springer, New York, 2009, pp. 243 – 255.
- [85] F. Büchi, M. Inaba, T. Schmidt (Eds.): *Polymer Electrolyte Fuel Cells Durability*, Springer, New York, 2009, pp. 7 – 53.
- [86] H. Lv et al.: Heat-treated multi-walled carbon nanotubes as durable supports for PEM fuel cell catalysts, *Electrochimica Acta* 58 (2011) 736 – 742.
- [87] N. Cheng et al.: Enhanced life of proton exchange membrane fuel cell catalysts using perfluorosulfonic acid stabilized carbon support, *Electrochimica Acta* 56 (2011) 2154 – 2159.
- [88] O. Reid, F.S. Saleh, E. B. Easton: Determining electrochemically active surface area in PEM fuel cell electrodes with electrochemical impedance spectroscopy and its application to catalyst durability, *Electrochimica Acta* 114 (2013) 278 – 284.
- [89] P. Zhou, P. Lin, C.W. Wu, Z. Li: Effect of nonuniformity of the contact pressure distribution on the electrical contact resistance in proton exchange membrane fuel cells, *International Journal of Hydrogen Energy* 36 (2011) 6039 – 6044.

- [90] S. Asghari, M.H. Shahsamandi, M.R. Ashraf Khorasani: Design and manufacturing of end plates of a 5 kW PEM fuel cell, *International Journal of Hydrogen Energy* 35 (2010) 9291 – 9297.
- [91] S. Asghari, A. Mokmeli, M. Samavati: Study of PEM fuel cell performance by electrochemical impedance spectroscopy, *International Journal of Hydrogen Energy* 35 (2010) 9238-9290.
- [92] P.A. Garcia-Salaberri, M. Vera, R. Zaera: Nonlinear orthotropic model of the inhomogeneous assembly compression of PEM fuel cell gas diffusion layers, *International Journal of Hydrogen Energy* 36 (2011) 11856 – 11870.
- [93] S. Park et al.: Simulation and experimental analysis of the clamping pressure distribution in a PEM fuel cell stack, *International Journal of Hydrogen Energy* 38 (2013) 6481 – 6493.
- [94] D. Qiu, P. Yi, L. Peng, X. Lai: Study on shape error effect of metallic bipolar plate on the GDL contact pressure distribution in proton exchange membrane fuel cell, *International Journal of Hydrogen Energy* 38 (2013) 6762 – 6772.
- [95] X. Wang, Y. Song, B. Zhang: Experimental study on clamping pressure distribution in PEM fuel cells, *Journal of Power Sources* 179 (2008) 305 – 309.
- [96] X.Q. Xing, K.W. Lum, H.J. Poh, Y.L. Wu: Optimization of assembly clamping pressure on performance of proton-exchange membrane fuel cells, *Journal of Power Sources* 195 (2010) 62 – 68.
- [97] J. G. Pharoah, O. S. Burheim: On the temperature distribution in polymer electrolyte fuel cells, *Journal of Power Sources* 195 (2010) 5235 – 5245.
- [98] H. Sun et al.: A novel technique for measuring current distributions in PEM fuel cells, *Journal of Power Sources* 158 (2006) 326 – 332.
- [99] A. Hakenjos et al.: A PEM fuel cell for combined measurement of current and temperature distribution, and flow field flooding, *Journal of Power Sources* 131 (2004) 213-216.
- [100] M. D. Runge, *Entwicklung eines flüssigkeitsgekühlten Polymer-Elektrolyt-Membran-Brennstoffzellenstapels mit einer Leistung von 6,5 kW*, VDI-Verlag, Düsseldorf, 2013, DOI: <http://dx.doi.org/10.3929/ethz-a-004511373>
- [101] M. Brodmann et al.: German patent, DE102009057494 A1 (2011).
- [102] M. Brodmann, M. Greda: Taschenkonzept schafft neue Freiheitsgrade Modulare Stacks mit austauschbaren Verschleißteilen, *Hzwei* 04/12 (2012) 14 – 15.

- [103] J. Zhang (Ed): PEM Fuel Cell Electrocatalysts and Catalyst Layers Fundamentals and Applications. Springer Verlag, London, 2008, pp. 965 – 1002.
- [104] Product information: qCf – quickCONNECT fixture, www.balticfuelcells.de/qcf.html, Accessed 2014-07-07.
- [105] R. Glises et al.: New design of a PEM fuel cell air automatic climate control unit, *Journal of Power Sources* 150 (2005) 78 – 85.
- [106] Sylvie Bégot et al.: Fuel cell climatic tests designed for new configured aircraft application, *Energy Conversion and Management* 51 (2010) 1522 – 1535.
- [107] Félix Barreras et al.: Design and development of a multipurpose utility AWD electric vehicle with a hybrid powertrain based on PEM fuel cells and batteries, *International Journal of Hydrogen Energy* 37 (2011) 15367 – 15379.
- [108] A. Basile, A. Iulianelli (Eds.): *Advances in Hydrogen Production, Storage and Distribution*, Elsevier, Woodhead Publishing, Cambridge, Waltham, Kidlington, 2014, pp. 499 – 524.
- [109] S. Barrett (Ed.): *Fuel Cells Bulletin*, Vol. 2013, Iss. 2, p. 2.
- [110] R. M. Dell, P. T. Moseley, D. A. J. Rand: *Towards Sustainable Road Transport*, Elsevier, Academic Press, Kidlington, Waltham, 2014, pp. 260 - 295.
- [111] D. Stolten (Ed): *Hydrogen and Fuel Cells*. Wiley-VCH, Weinheim, 2010, pp. 681 – 710.
- [112] Press release from European Hydrogen Association: <http://www.h2euro.org/2010/ballard-tests-1-mw-pem-power-plant>. Accessed 2015-31-01.
- [113] D. Stolten (Ed.): *Hydrogen and Fuel Cells*. Wiley-VCH, Weinheim, 2010, pp. 755 – 786.
- [114] J. Goldstein et al.: *Scanning Electron Microscopy and X-Ray Microanalysis*. Kluwer Academic/Plenum Publishers, New York, 2003.
- [115] R. F. Egerton: *Physical Principles of Electron Microscopy An Introduction to TEM, SEM, and AEM*. Springer, New York, 2005.
- [116] E. Lifshin (Ed.): *X-ray Characterization of Materials*. Wiley-VCH, Weinheim, 1999.
- [117] L. van der Pauw: *Philipps Technical Review*, Vol. 20, No. 8 (1958) pp. 220-224.

- [118] W. Runyan: *Semiconductor Measurements and Instrumentation*. McGraw-Hill Book Company, New York, 1975.
- [119] H. Czichos, T. Saito, L. Smith (Eds.): *Springer Handbook of Materials Measurement Methods*. Springer, Heidelberg, 2006, pp. 432-484.
- [120] W. Brandl, G. Marginean: Functionalisation of the carbon nanofibres by plasma treatment, *Thin Solid Films* 447-448 (2004) 181-186.
- [121] V. Chirila, G. Marginean, W. Brandl: Effect of the oxygen plasma treatment on the carbon nanotubes surface properties, *Surface & Coatings Technology* 200 (2005) 548-551.
- [122] H. Bubert et al.: Analytical investigation of plasma-treated carbon fibres, *Anal Bioanal Chem* (2002) 374:1237-1241.
- [123] J. A. Bittencourt: *Fundamentals of Plasma Physics*, Springer, New York, 2004.
- [124] M. Schlesinger, M. Paunovic (Eds.): *Modern Electroplating*, 5th ed., Wiley, Hoboken, 2010, pp. 1 - 32.
- [125] M. Schlesinger, M. Paunovic (Eds.): *Modern Electroplating*, 5th ed., Wiley, Hoboken, 2010, pp. 79 - 114.
- [126] M. Schlesinger, M. Paunovic (Eds.): *Modern Electroplating*, 5th ed., Wiley, Hoboken, 2010, pp. 115 - 130.
- [127] S. Woo et al.: Preparation of cost-effective Pt-Co electrodes by pulse electrodeposition for PEMFC electrocatalysts, *Electrochimica Acta* 56 (2011) 3036 - 3041.
- [128] N. Rajalkshmi, K.S. Dhathathreyan: Nanostructured platinum catalyst layer prepared by pulsed electrodeposition for use in PEM fuel cells, *International Journal of Hydrogen Energy* 33 (2008) 5672 - 5677.
- [129] S. Lertviriyapaisan, N. Tantavichet: Sublayers for Pt catalyst electrodeposition electrodes in PEMFC, *International Journal of Hydrogen Energy* 35 (2010) 10464 - 10471.
- [130] M. Tsai, T. Yeh, C. Tsai, Methanol oxidation efficiencies on carbon-nanotube-supported platinum and platinum-ruthenium nanoparticles prepared by pulsed electrodeposition, *International Journal of Hydrogen Energy* 36 (2011) 8261 - 8266.
- [131] J. Zhang (Ed): *PEM Fuel Cell Electrocatalysts and Catalyst Layers Fundamentals and Applications*. Springer, London, 2008, pp. 447 - 486.

- [132] H. Kim, N.P. Subramanian, B. Popov, Preparation of PEM fuel cell electrodes using pulse electrodeposition, *Journal of Power Sources* 138 (2004) 14 – 24.
- [133] G. Lu, G. Zangari, Electrodeposition of platinum nanoparticles on highly oriented pyrolytic graphite: Part II: Morphological characterization by atomic force microscopy, *Electrochimica Acta* 51 (2006) 2531 – 2538.
- [134] C. Sagewka, Aufbau und Inbetriebnahme eines Prüfstands für Brennstoffzellenmembranen, Master thesis, Westfälische Hochschule Gelsenkirchen, 2013.
- [135] Technical datasheet Grupo Antolin Carbon Nanofibers: GANF. Grupo Antolin Ingenieria, S.A., Burgos, Spain, <http://www.grupoantolin.com>.
- [136] J. Maire, J. Mering, Proc. First Conference of the Society of Chemical Ind. Conf. on Carbon and Graphite (London), 204, 1958.
- [137] Specification Sheet AvCarb MGL, Ballard Power Systems, Lowell, USA, 2010, www.ballard.com, Accessed: 2015-09-01
- [138] Technical Data Freudenberg Gas Diffusion Layers, Freudenberg FCCT SE & Co. KG, 2014, www.freudenbergfct.com, Accessed: 2015-09-01
- [139] Specification of GDE material supplied by Quintech. http://quintech.de/deutsch/produkte/forschung_entwicklung/Elektroden.php, Accessed: 2014-11-11
- [140] Specification sheet DuPont Nafion PFSA Membrane NR-211 and NR-212, www.fuelcellstore.com, Accessed: 2015-09-01
- [141] Properties of Nafion PFSA Membrane. www.fuelcellstore.com, Accessed: 2015-09-01
- [142] DuPont Fuel Cells, DuPont Nafion PFSA Membranes, Dupont, 2010, www.fuelcells.dupont.com, Accessed: 2015-09-01
- [143] W. M. Yan, X. D. Wang, D. J. Lee, X. X. Zhang, Y. F. Guo, A. Su, Experimental study of commercial size proton exchange membrane fuel cell performance, *Applied Energy* 88 (2011) 392–396.
- [144] X. D. Wang et al., Effects of operating temperatures on performance and pressure drops for a 256cm² proton exchange membrane fuel cell: An experimental study, *Journal of Power Sources* 185 (2008) 1040–1048.

- [145] J. Roth, Optimization of PEMFCs by applying hot pressed MEAs using different GDL and favourable driving scenarios for operation without humidification, Master thesis, Westfälische Hochschule Gelsenkirchen, 2011.

APPENDICES

APPENDICES	132
Appendices.....	132
Appendix A: Data Sheets	133
Appendix A.1 GANF	133
Appendix A.2 AvCarb MGL.....	134
Appendix A.3 Freudenberg GDL	135
Appendix A.4 Nafion N115.....	136
Appendix A.5 Nafion N212.....	137
Appendix A.6 Nafion XL.....	138
Appendix B: Fuel Cell Testing	139
Appendix B.1 (Long-Term Run with N115)	139
Appendix B.2 (Long-Term Run with N212)	140
Appendix B.3 (Long-Term Run with XL)	140
Appendix B.4 (U-I GDM)	141
Appendix B.5 (U-I H2315 I2C6)	141
Appendix B.6 (U-I H2315).....	142
Appendix B.7 (U-I H2315 I2C8)	142
Appendix B.8 (U-I H2315 I6).....	143
Appendix B.9 (Long-Term Run Pt/CB).....	143
Appendix B.10 (U-I no CNF)	144
Appendix B.11 (U-I CNT)	144
Appendix C: Microscopy Analyses	145
Appendix C.1 (Pt/CNT).....	145
Appendix C.2 (Pt/CNF Without Plasma)	146
Appendix C.3 (Pt/CNF Cross Section).....	146
Appendix C.4 (Metallic Residues)	147
Appendix C.5 (Pt/CNF with Polymers)	148
Appendix C.6 (Pt/CNF (TEM))	149

Appendix A: Data Sheets

Appendix A.1 GANF

Grupo Antolin Carbon Nanofibres (GANF)
www.grupoantolin.com

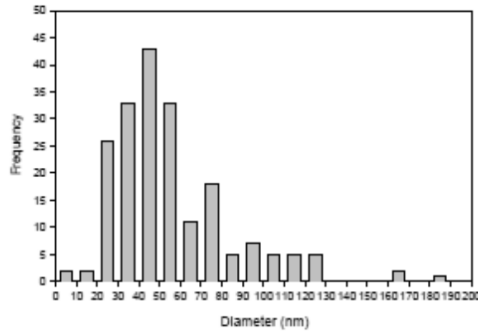


GANF TECHNICAL DATA SHEET

GRUPO ANTOLIN CARBON NANOFIBRES PROPERTIES:

MEASURED PROPERTY	UNIT	GANF	GANF graphitized
FIBRE DIAMETER (TEM)	nm	20 - 80	20-80
FIBRE LENGTH (SEM)	µm	>30	>30
BULK DENSITY	g/cc	>1.97	~2.1
APPARENT DENSITY	g/cc	0.060	0.085
SURFACE ENERGY	mJ/m ²	~100	-
SPECIFIC SURFACE AREA BET (N ₂)	m ² /g	150-200	105-115
GRAPHITIZATION DEGREE	%	~70	~100
ELECTRICAL RESISTIVITY	Ohm-m	1·10 ⁻³	1·10 ⁻⁴
METALLIC PARTICLES CONTENT	%	6-8	0.1 - 0.2

DIAMETER DISTRIBUTION GANF NANOFIBRES TEM (Transmisión Electron Microscopy)



Appendix A.2 AvCarb MGL

GDL type AvCarb MGL



AvCarb® Carbon Fiber Papers (e.g. EP40), Carbon Fabrics (e.g. 1071HCB) and Molded Graphite Laminates (e.g. MGL400) are classified as gas diffusion substrates, used as electrode backings for fuel cell applications. 'T' grade products (e.g. EP40T) are water repellent, PTFE treated versions of AvCarb Carbon Fiber Papers.

The table below lists nominal properties of commercially available AvCarb Substates for fuel cells. Please contact us for assistance in selecting the right product for your application or for more information.

SUBSTRATE GRADE	UNITS										
		AvCarb EP40	AvCarb P50	AvCarb P75	AvCarb EP40T	AvCarb P50T	AvCarb P75T	AvCarb MGL 200	AvCarb MGL 400	AvCarb 1071 HCB	
Nominal Thickness (@ 1 psi / 0.7 N/cm ²)	microns	200	170	245	200	180	255			356	
	(@ 7.3 psi / 5.1 N/cm ²)	microns	190	150	205	190	160	240	200	400	319
Nominal Basis Weight	g/m ²	36	50	75	43	62	85	100	190	123	
Break Strength	machine direction	MPa	5.0	5.0	6.5	6.5	15.2	20.0	15.0	51.0	<17.73 lbf MD
	cross machine direction	MPa	3.5	3.0	3.9	4.0	7.6	12.6			
Stiffness	machine direction	Taber	9.5	7.5	20.0	22.0	8.5	21.0		155.0	<1
	cross machine direction	Taber	3.5	3.0	3.5	4.5	3.1	14.6		115.0	<1
Bulk Density (@ 0.69 N/cm ² / 1psi)	g/cm ³	0.20	0.31	0.29	0.22	0.34	0.33	0.45-0.55	0.45-0.55	0.35	
Air Permeability (Gurley)	through-pane permeability	sec/100cc	4.5	35	15	7.5	50	25	2.5	7.7	1.3
	in-plane permeability	sec/100cc	50.9	295	83	75	596	26	11	6.6	8.7
Compressibility (22N - 113N)/22 x 100%	%	14.0	11.5	10.7	10.50	12.5	11.0	12.0	4.9	weave count 49/inch warp, 47/inch fill	
Through-Plane Resistivity	mOhm*cm ²	8.0	6.7	7.8	13.0	11.7	13.4	11.2	8.8	<8.0	
Typical Roll Width	mm	400/800	400/800	400/800	400/800	400/800	400/800	550 x 550	550 x 550	500/1170	

Specifications and descriptions in this document were in effect at the time of publication. Ballard Material Products, Inc. reserves the right to change specifications, product appearance or to discontinue products at any time (10/2010).

BALLARD AvCarb®, Ballard®, Powered by Ballard®, FCgen® and FCvelocity™ are trademarks of Ballard Power Systems Inc.

Ballard Material Products, Inc. TEL: (+1) 978.934.7500
Two Industrial Avenue FAX: (+1) 978.934.7590
Lowell, MA 01851-5199 USA
materialproducts@ballard.com www.ballard.com

Appendix A.3 Freudenberg GDL

GDL type Freudenberg

http://www.freudenbergfuelcellproducts.com/sites/default/files/2014-12-15_technical_data_sheet_gdl.pdf



FREUDENBERG FCCT SE&CO.KG

FREUDENBERG GAS DIFFUSION LAYERS FOR PEMFC AND DMFC

TECHNICAL DATA

PRODUCT NAME	H23		H14	H15	H2316	H23C2 H24C2		H23C4 H24C4		H23C6 H23C7		H23C8 H23C9		H23C3 H24C3		H23CE H24CE		H15C9		
	H2313 H253	H2314	H111	H2315	H2318	H2312 H2532	H2310	H2311	H2313 H2531	H2315 H2535	H2317 H2537	H2319 H2539	H2321 H2541	H2323 H2543	H2325 H2545	H2327 H2547	H2329 H2549	H2331 H2551	H111C9	
HYDROPHOBIC TREATMENT	■	■	■	■	■	■	■	■	■	■	■	■	■	■	■	■	■	■	■	■
MICROPOROUS LAYER	■	■	■	■	■	■	■	■	■	■	■	■	■	■	■	■	■	■	■	■
Thickness @ 0.025 MPa (Intral [®]) in µm	210	160	155	155	210	255	255	255	255	250	250	250	250	200	270	270	270	175	180	185
Thickness @ 1 MPa (Intral [®]) in µm	270	215	210	210	270	315	315	315	315	310	310	310	310	260	330	330	330	235	240	245
Area weight (IN EN ISO 29013) in g/cm ²	95	65	65	65	95	135	135	135	135	135	135	135	135	100	150	150	150	100	100	100
Compression Set @ 1 MPa (Intral [®]) in µm	2	1.5	4	4	2	3	3	3	3	3	3	3	3	3	3	3	3	1.5	1.5	1.5
TP electrical resistance @ 1 MPa (Intral [®]) in mΩ·cm ²	4.5	4	5.5	5.5	7	10	8	8	8	8	8	8	8	8	8	8	8	6	6	6
TP electrical resistance (Intral [®]) in Ω	0.8	1.1	1.2	1.2	0.8	0.8	0.8	0.8	0.8	0.7	0.7	0.7	0.7	0.6	0.7	0.7	0.7	1.0	1.0	1.1
TP air permeability* (DM EN ISO 9237) in l/m ² ·s	400	570	600	600	180	-	-	-	-	-	-	-	-	-	-	-	-	-	-	-
TP air permeability acc. to CEN ISO 5606-5 in s	-	-	-	-	70	50	50	50	50	70	50	50	50	50	40	50	50	40	50	40
TP air permeability @ 1 MPa (Intral [®]) in µm ² /s	4.2	4.0	7.0	7.0	1.7	2.5	2.5	2.5	2.5	1.8	1.8	1.8	1.8	1.5	2.5	2.5	2.5	1.0	1.0	1.0
Tensile strength FAN EN ISO 20073-3 in N/50 mm	25	20	20	20	80	80	80	80	80	70	70	70	70	70	50	70	70	70	70	70

* Freudenberg/Intral measurement standard
 at 200% pressure drop
 TP = thickness of the membrane
 (Rev. 15 - 12/2014)

All values represent averages which are subject to usual production tolerances. The values do not represent specifications.
 Any warranty and liability is subject to Freudenberg FCCT SE & CO. KG's General Terms of Delivery and Payment applicable at the date of delivery.

CONTACT

FREUDENBERG FCCT SE & CO. KG Hochweg 2-4, 69165 Weidheim, Germany, www.freudenbergfcct.com
 FAX: +49 6202 85 4459 E-MAIL: hschl@freudenbergfcct.com

Appendix A.4 Nafion N115

Nafion® 115



www.fuelcellstore.com
sales@fuelcellstore.com
(979) 735-1925

Properties of Nafion® PFSA Membrane

A. Thickness and Basis Weight Properties¹

Membrane Type	Typical Thickness (microns)	Basis Weight (g/m ²)
N-115	127	250
N-117	183	360
N-1110	254	500

B. Physical and Other Properties²

Property	Typical Value	Test Method
Physical Properties		
Tensile Modulus, MPa (kpsi)		
50% RH, 23 °C	249 (36)	ASTM D 882
water soaked, 23 °C	114 (16)	ASTM D 882
water soaked, 100 °C	64 (9.4)	ASTM D 882
Tensile Strength, maximum, MPa (kpsi)		
50% RH, 23 °C	43 (6.2) in MD, 32 (4.6) in TD	ASTM D 882
water soaked, 23 °C	34 (4.9) in MD, 28 (3.8) in TD	ASTM D 882
water soaked, 100 °C	25 (3.6) in MD, 24 (3.5) in TD	ASTM D 882
Elongation at Break, %		
50% RH, 23 °C	225 in MD, 310 in TD	ASTM D 882
water soaked, 23 °C	200 in MD, 275 in TD	ASTM D 882
water soaked, 100 °C	180 in MD, 240 in TD	ASTM D 882
Tear Resistance - Initial, g/mm		
50% RH, 23 °C	6000 in MD, TD	ASTM D 1004
water soaked, 23 °C	3500 in MD, TD	ASTM D 1004
water soaked, 100 °C	3000 in MD, TD	ASTM D 1004
Tear Resistance³ - Propagating, g/mm		
50% RH, 23 °C	>100 in MD, >150 in TD	ASTM D 1922
water soaked, 23 °C	92 in MD, 104 in TD	ASTM D 1922
water soaked, 100 °C	74 in MD, 85 in TD	ASTM D 1922
Specific Gravity	1.98	—
Other Properties		
Conductivity, S/cm	0.10 min	see footnote ⁴
Available Acid Capacity, meq/g	0.90 min	see footnote ⁵
Total Acid Capacity, meq/g	0.95 to 1.01	see footnote ⁵

¹ Measurements taken with membrane conditioned to 23 °C, 50% relative humidity (RH).

² Physical Properties measured for N-115. Where specified, MD - machine direction, TD - transverse direction. Conditioning state of membrane given. Measurements taken at 23 °C, 50% RH.

³ Tear resistance (g/mm) of dry membrane increases with thickness. Values given measured using 50 micron membrane.

⁴ Conductivity measurement as described by Zawodzinski, et al, *J. Phys. Chem.*, 95 (15), 6040 (1991). Membrane conditioned in 100 °C water for 1 hour. Measurement cell submerged in 25 °C D.I. water during experiment. Membrane Impedance (real) taken at zero Imaginary Impedance.

⁵ A base titration procedure measures the equivalents of sulfonic acid in the polymer, and uses the measurement to calculate the acid capacity or equivalent weight of the membrane.

Appendix A.5 Nafion N212

Nafion® 212

Properties of Nafion® PFSA Membrane

A. Thickness and Basis Weight Properties¹

Membrane Type	Typical Thickness (micrometer)	Basis Weight (g/m ²)
NR-211	25.4	50
NR-212	50.8	100

B. Physical Properties

Property ²	Typical Values				Test Method
	NR-211		NR-212		
	MD	TD	MD	TD	
Physical Properties					
- measured at 50% RH, 23 °C					
Tensile Strength, max., MPa	23	28	32	32	ASTM D 882
Non-Std Modulus, MPa	288	281	286	251	ASTM D 882
Elongation to Break, %	252	311	343	352	ASTM D 882

C. Other Properties

Property	NR-211	NR-212	Test Method
Specific Gravity ¹	1.97	1.97	DuPont
Available Acid Capacity ³ meq/g	0.92 min.	0.92 min.	DuPont NAE305
Total Acid Capacity ⁴ meq/g	0.95 to 1.01	0.95 to 1.01	DuPont NAE305
Hydrogen Crossover ⁵ , (ml/min-cm ²)	< 0.020	< 0.010	DuPont

D. Hydrolytic Properties

Property	Typical Value	Test Method
Hydrolytic Properties		
Water content, % water ⁶	5.0 ± 3.0%	ASTM D 570
Water uptake, % water ⁷	50.0 ± 5.0%	ASTM D 570
Linear expansion, % increase ⁸		
from 50% RH, 23 °C to water soaked, 23 °C	10	ASTM D 756
from 50% RH, 23 °C to water soaked, 100 °C	15	ASTM D 756

¹ Measurements taken with membrane conditioned to 23 °C, 50% RH.

² Where specified, MD - machine direction, TD - transverse direction. Condition state of membrane given.

³ A base titration procedure measures the equivalents of sulfonic acid in the polymer, and used the measurements to calculate the available acid capacity of the membrane (acid form).

⁴ A base titration procedure measures the equivalents of sulfonic acid in the polymer, and used the measurements to calculate the total acid capacity or equivalent weight of the membrane (acid form).

⁵ Hydrogen crossover measured at 22 °C, 100% RH and 50-psi delta pressure. This is not a routine test.

⁶ Water content of membrane conditioned to 23 °C and 50% RH (dry weight basis).

⁷ Water uptake from dry membrane to conditioned in water at 100 °C for 1 hour (dry weight basis).

⁸ Average of MD and TD. MD expansion is similar to TD expansion for NR membranes.

Appendix A.6 Nafion XL

Nafion® XL

Page 2 of 5

Properties of Nafion® PFSA Membrane

A. Thickness and Basis Weight Properties¹

Membrane Type	Typical Thickness (micrometer)	Basis Weight (g/m ²)
XL	27.5	55

B. Physical Properties

Property ²	Typical Values		Test Method
	MD	TD	
Physical Properties			
- measured at 50% RH, 23 °C			
Tensile Strength, max., MPa	45	40	ASTM D 882
Non-Std Modulus, MPa	613	400	ASTM D 882
Elongation to Break, %	200	185	ASTM D 882

C. Other Properties

Property	Typical Values	Test Method
Conductivity ³ , mS/cm		DuPont
- In-Plane	> 72.0	
- Through-Plane	> 50.5	
Hydrogen Crossover ⁴ , (ml/min-cm ²)	< 0.015	DuPont

D. Hydrolytic Properties

Property	Typical Values	Test Method
Hydrolytic Properties		
Water content, % water ⁵	5.0 ± 3.0%	ASTM D 570
Water uptake, % water ⁶	50.0 ± 5.0%	ASTM D 570
Linear expansion, % increase		
from 50% RH, 23 °C to water soaked, 23 °C	1% (MD), 5% (TD)	DuPont
from 50% RH, 23 °C to water soaked, 100 °C	3% (MD), 11% (TD)	DuPont

¹ Measurements taken with membrane conditioned to 23 °C, 50% RH.

² Where specified, MD - machine direction, TD - transverse direction. Condition state of membrane given.

³ Conductivity measurements at 23 °C, 100% RH.

⁴ Hydrogen crossover measured at 65 °C, 100% RH. This is not a routine test.

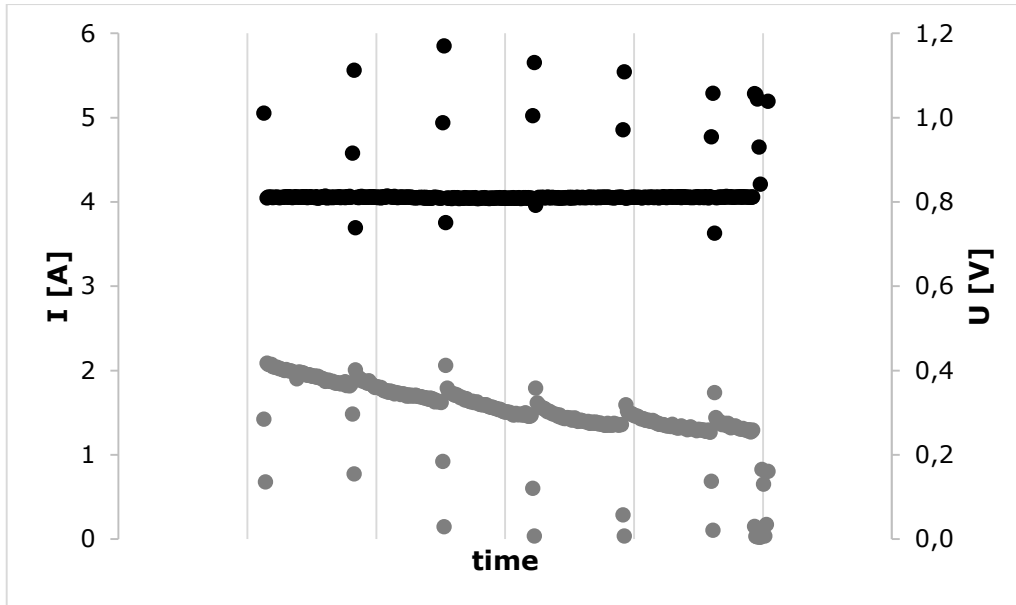
⁵ Water content of membrane conditioned to 23 °C and 50% RH (dry weight basis).

⁶ Water uptake from dry membrane to conditioned in water at 100 °C for 1 hour (dry weight basis).

Appendix B: Fuel Cell Testing

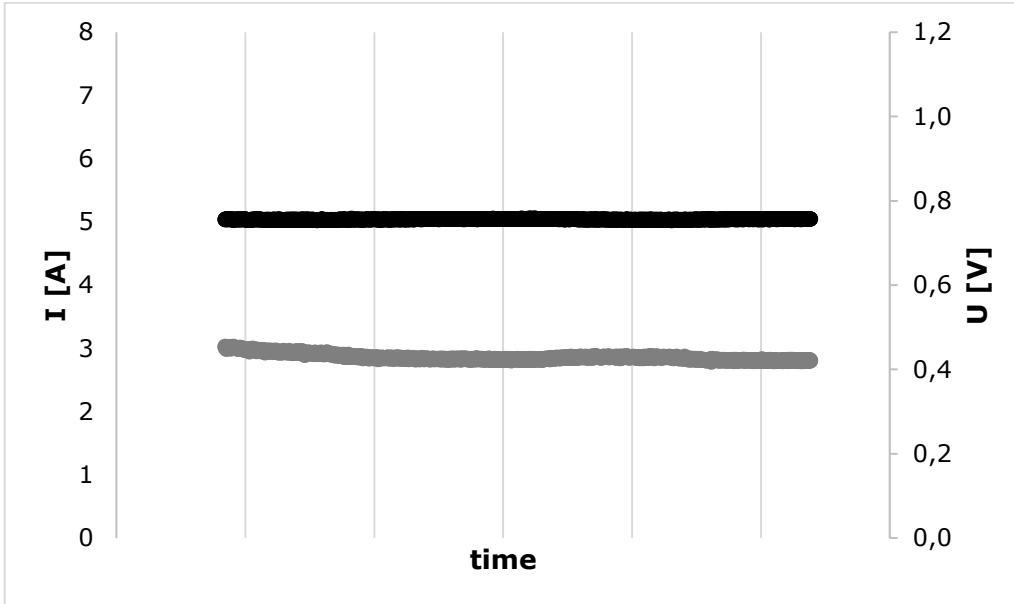
Appendix B.1 (Long-Term Run with N115)

Long-term run BC-H225-10F with Nafion[®] 115 ($I = 4$ A, pulses every 5 minutes, $t = 0.5$ h)



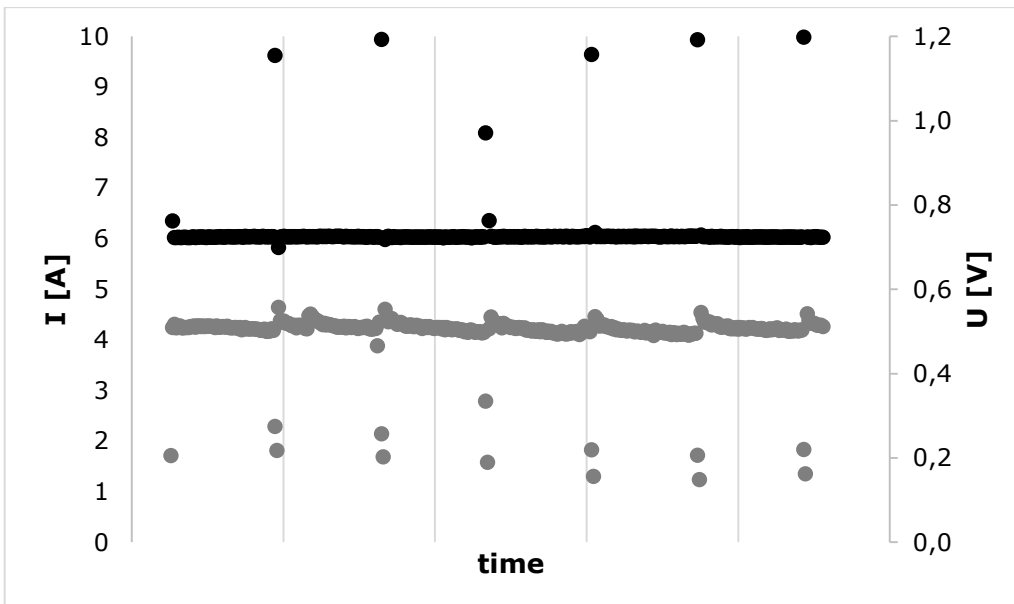
Appendix B.2 (Long-Term Run with N212)

Long-term run BC-H225-10F with Nafion® 212 (I = 5 A, no pulses, t = 0.5 h)



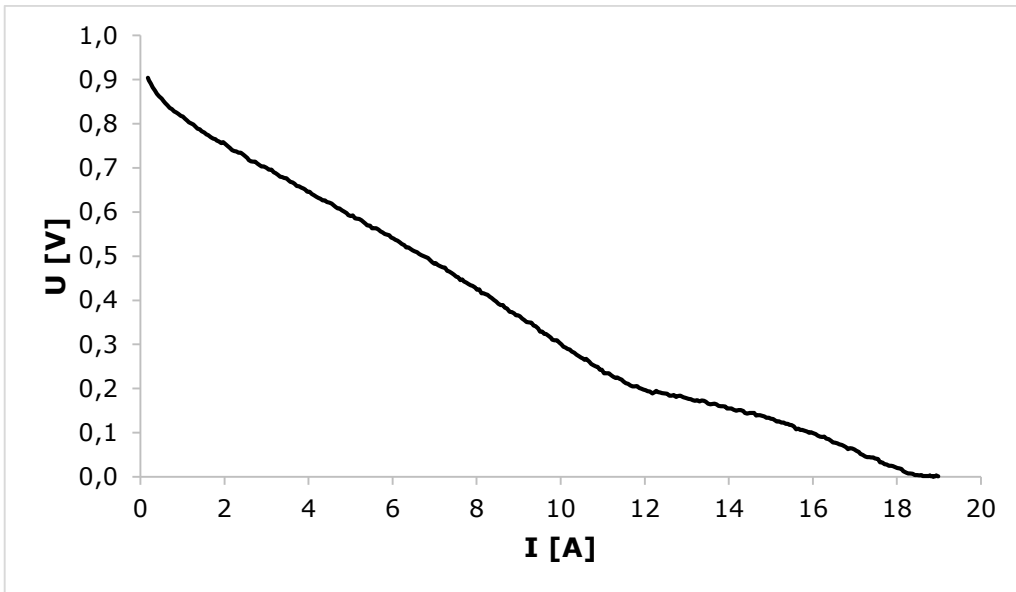
Appendix B.3 (Long-Term Run with XL)

Long-term run BC-H225-10F with Nafion® XL (I = 6 A, pulses every 5 minutes, t = 0.5 h)



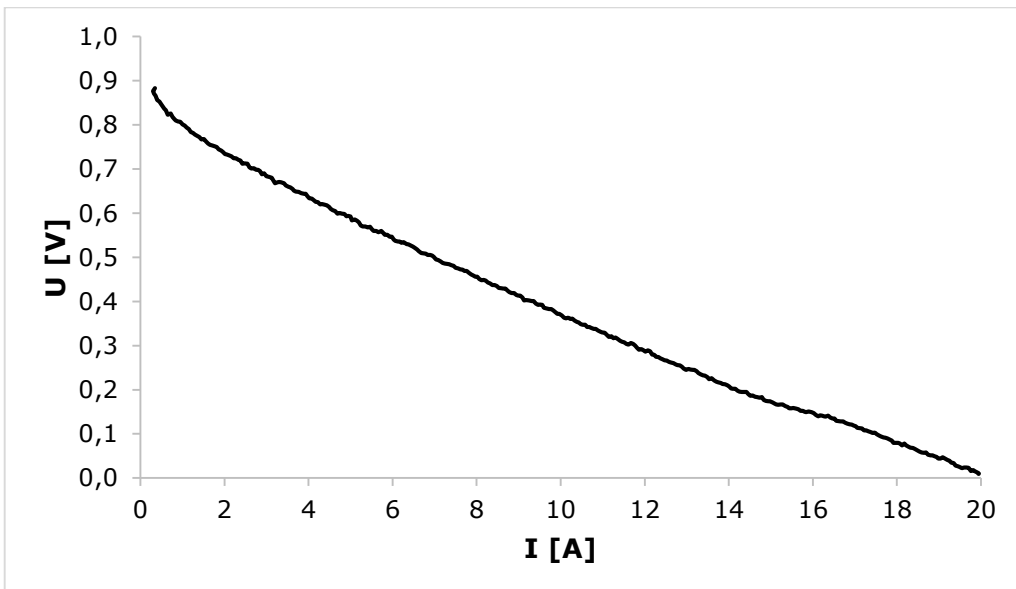
Appendix B.4 (U-I GDM)

Polarisation curve, CCM type Gore® Primea, GDL type Gore® GDM, measurement performed within the segmented pole plate ($A = 16 \text{ cm}^2$)



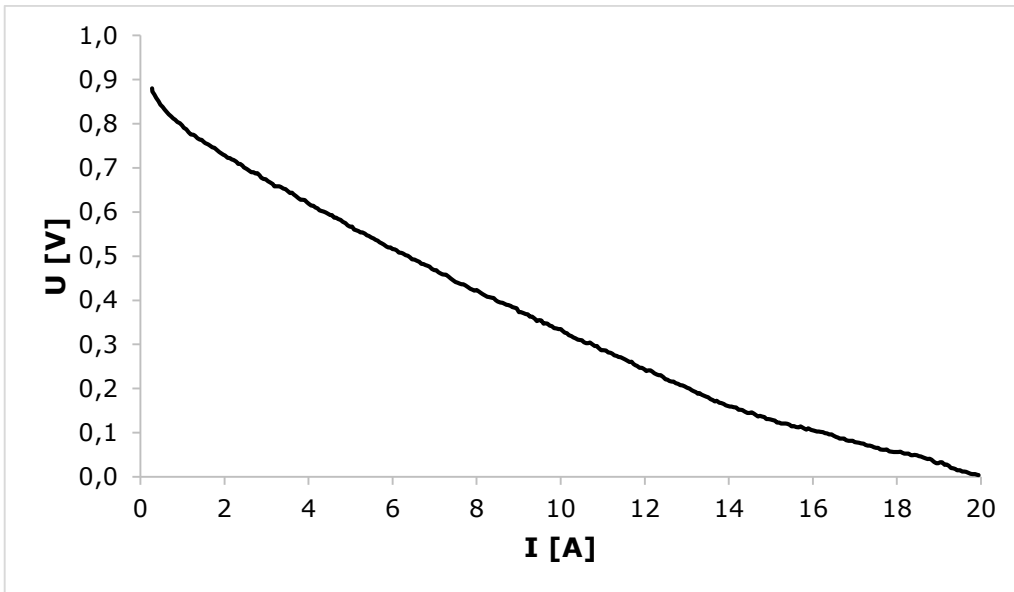
Appendix B.5 (U-I H2315 I2C6)

Polarisation curve, CCM type Gore® Primea, GDL type Freudenberg H2315 I2C6, measurement performed within the segmented pole plate ($A = 16 \text{ cm}^2$)



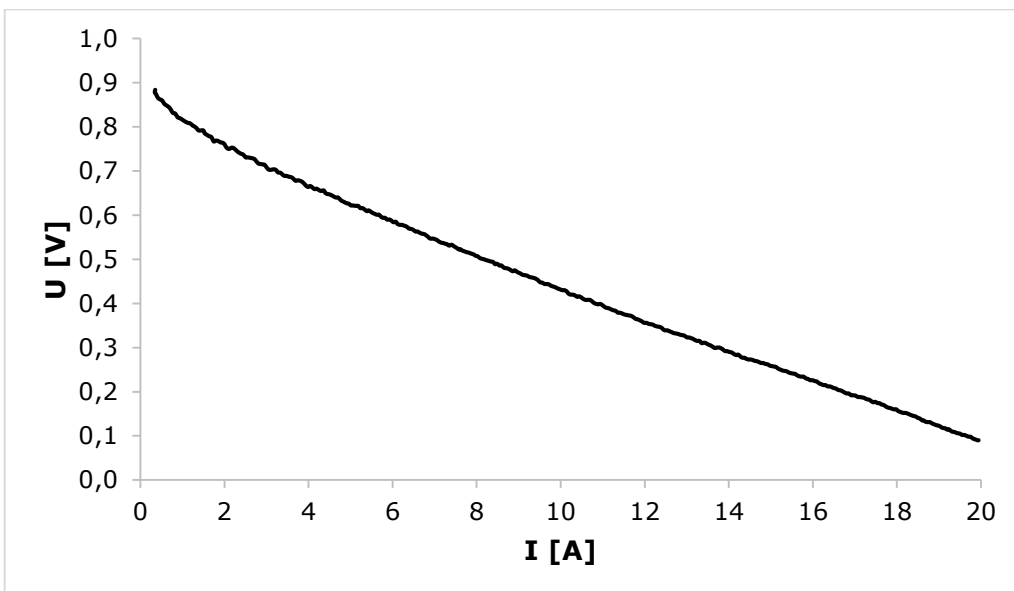
Appendix B.6 (U-I H2315)

Polarisation curve, CCM type Gore® Primea, GDL type Freudenberg H2315, measurement performed within the segmented pole plate ($A = 16 \text{ cm}^2$)



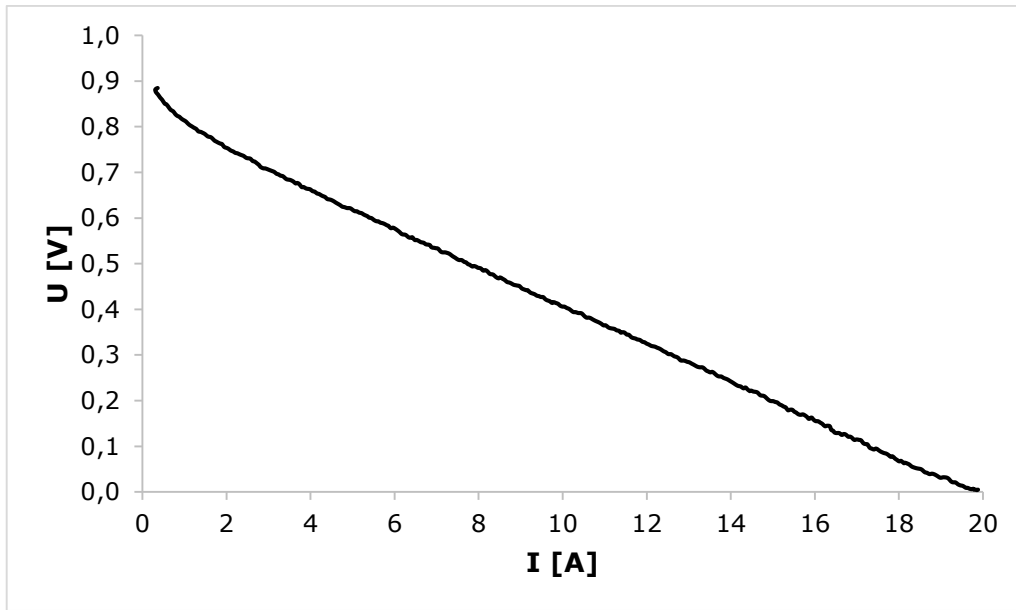
Appendix B.7 (U-I H2315 I2C8)

Polarisation curve, CCM type Gore® Primea, GDL type Freudenberg H2315 I2C8, measurement performed within the segmented pole plate ($A = 16 \text{ cm}^2$)



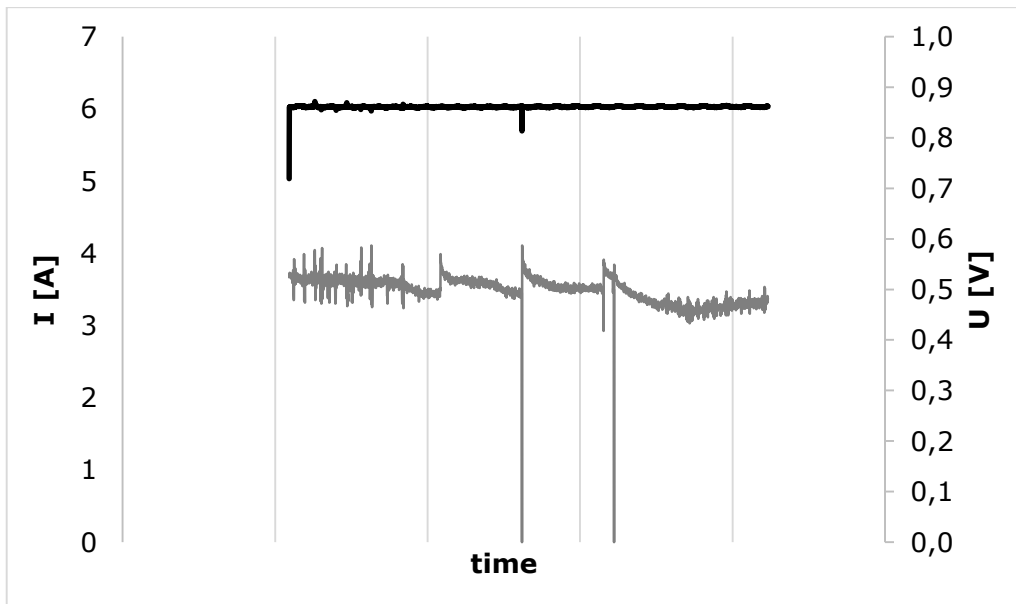
Appendix B.8 (U-I H2315 I6)

Polarisation curve, CCM type Gore® Primea, GDL type Freudenberg H2315 I6, measurement performed within the segmented pole plate ($A = 16 \text{ cm}^2$)



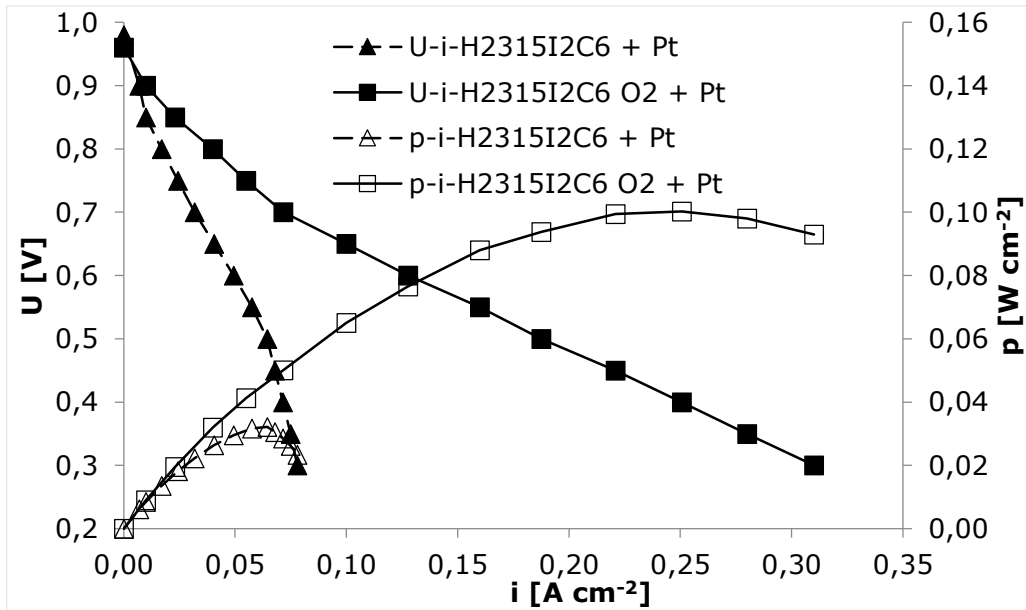
Appendix B.9 (Long-Term Run Pt/CB)

Long-term run Pt/CB based anode with Nafion® 212 ($I = 6 \text{ A}$, no pulses, $t = 9 \text{ h}$)



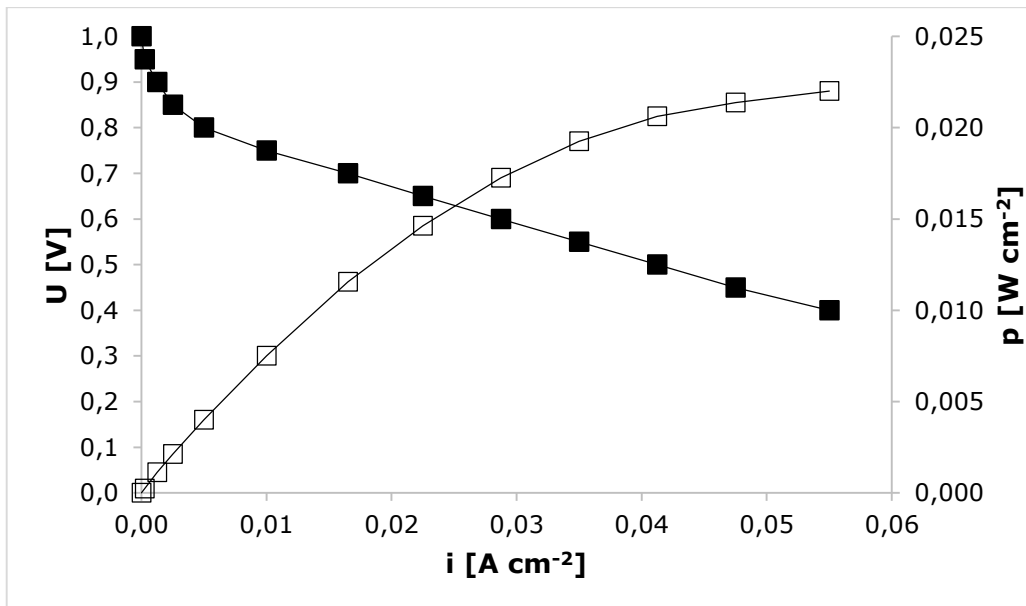
Appendix B.10 (U-I no CNF)

Polarisation curves, GDL + Pt (no CNF interlayer) with Nafion 212, depending on oxygen plasma activation



Appendix B.11 (U-I CNT)

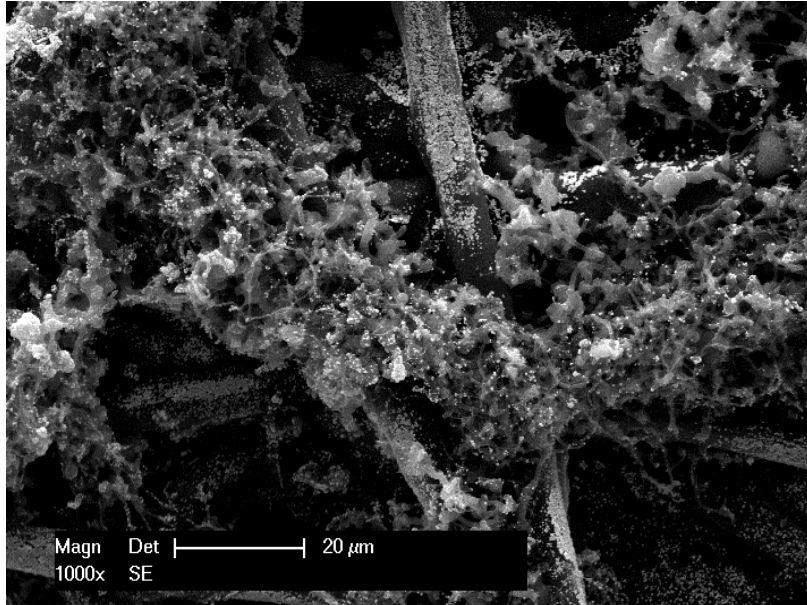
Polarisation curve, Pt/CNT with Nafion 212



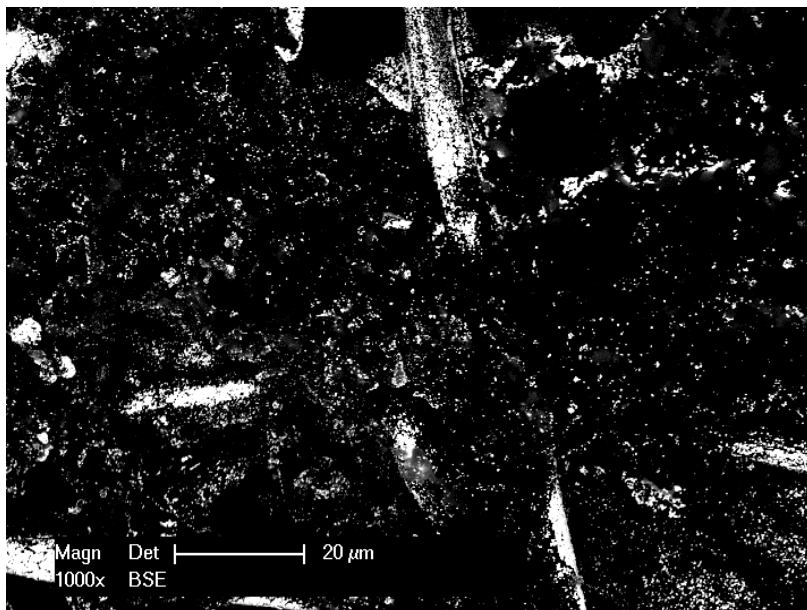
Appendix C: Microscopy Analyses

Appendix C.1 (Pt/CNT)

Pt/CNT on AvCarb MGL 370, 1,000 magnitude, SE mode

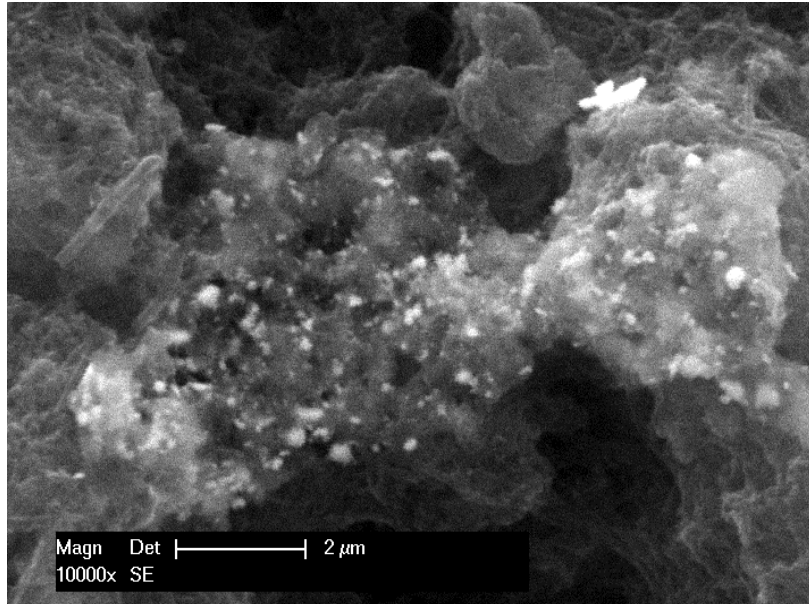


Pt/CNT on AvCarb MGL 370, 1,000 magnitude, BSE mode



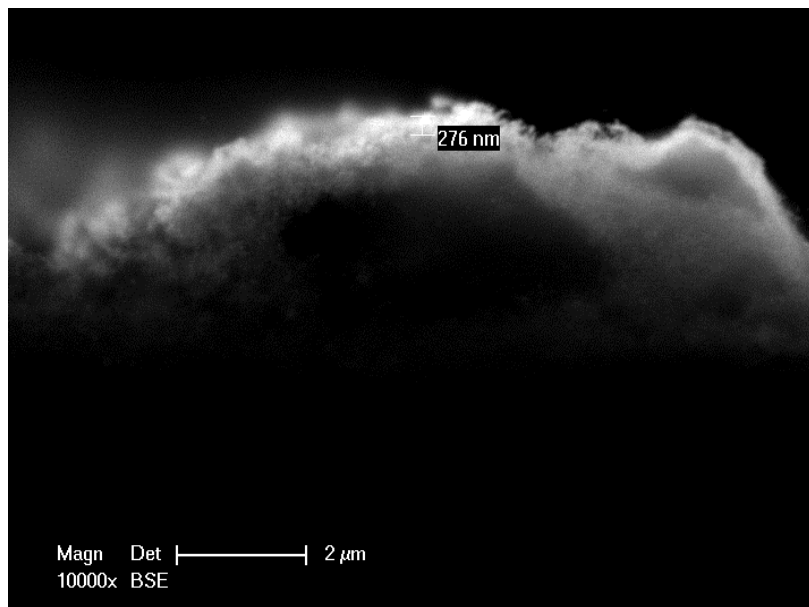
Appendix C.2 (Pt/CNF Without Plasma)

Pt/CNF without previous plasma activation, 10,000 magnitude, SE mode



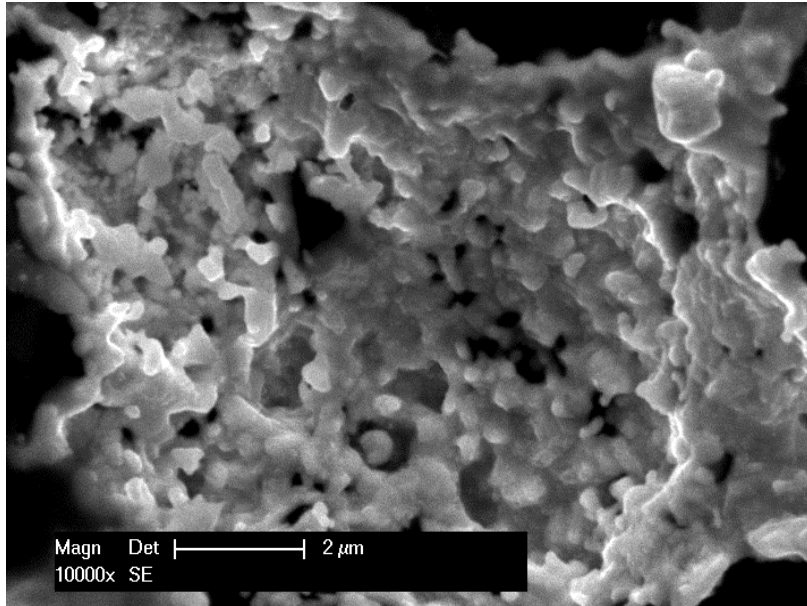
Appendix C.3 (Pt/CNF Cross Section)

Pt/CNF cross section, 10,000 magnitude, BSE mode

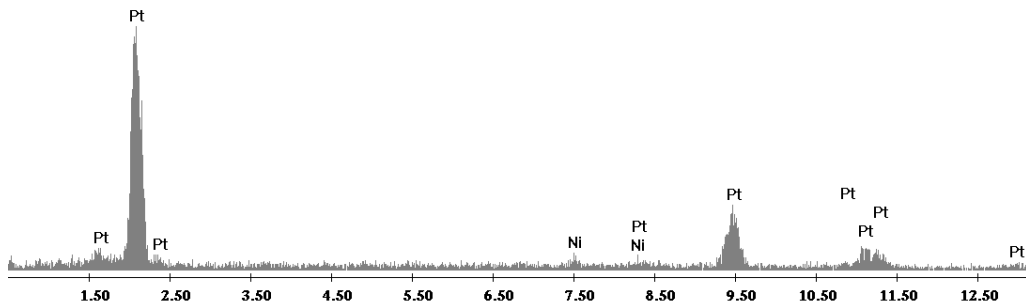


Appendix C.4 (Metallic Residues)

Metallic residues after TGA, 10,000 magnitude, SE mode

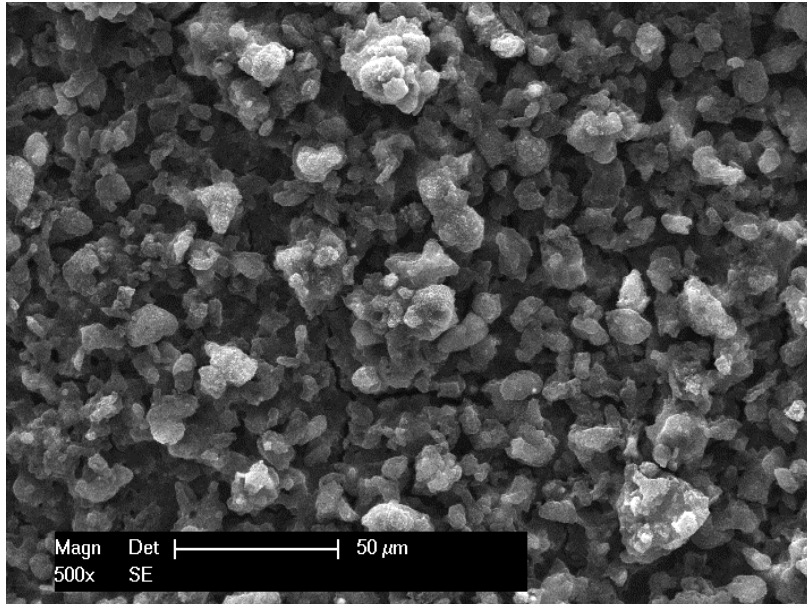


EDX analysis of metallic residues after TGA

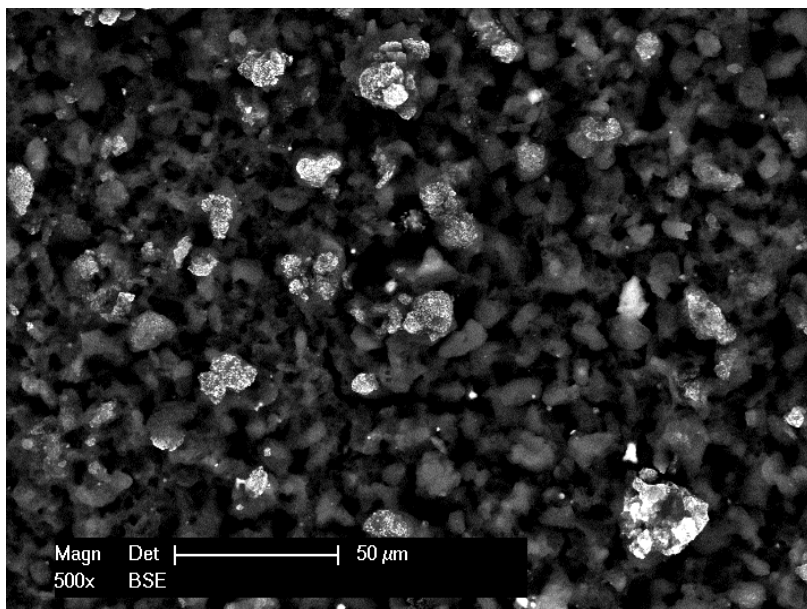


Appendix C.5 (Pt/CNF with Polymers)

Pt/CNF with high Nafion[®] loading, 500 magnitude, SE mode

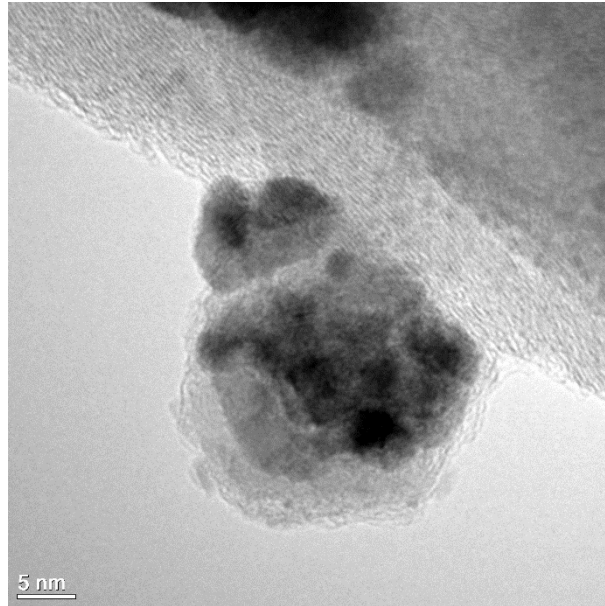


Pt/CNF with high Nafion[®] loading, 500 magnitude, BSE mode

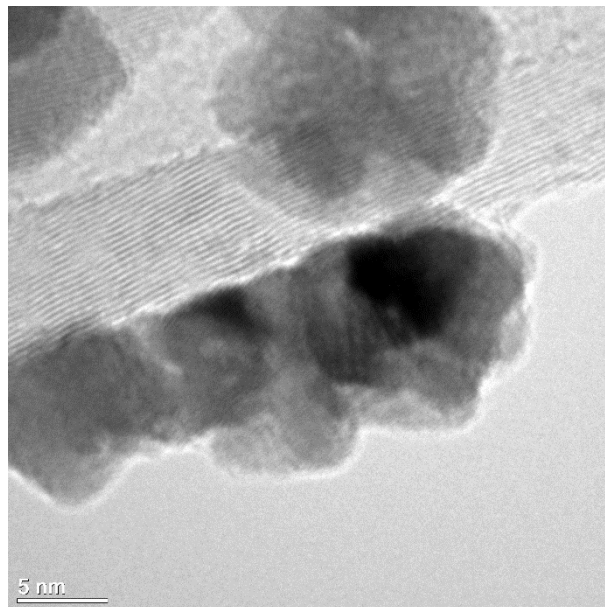


Appendix C.6 (Pt/CNF (TEM))

Pt/CNF, TEM image



Pt/CNF, TEM image



CURRICULUM VITAE

Personal Details

Name Ulrich Wilhelm Rost
Adress Bockholtweg 2, D-44149, Dortmund, Germany
Date of Birth 12.12.1983
Place of Birth Mülheim an der Ruhr
Nationality German
E-Mail ulrich_rost@web.de
Marital Status Married, 1 child

Education and Work Experience

2011 – today Westphalian University Gelsenkirchen, Department of Electrical Engineering and Applied Natural Science, division Westphalian Energy Institute, scientific assistant in the fields of fuel cells, electrolysers, and batteries

Activities:

- Electro plating
- Catalyst preparation
- Cell development
- System design
- Project management

2015 Doctoral degree (Ph.D.)

2011 – 2015 Politehnica University Timisoara in cooperation with the Westphalian University Gelsenkirchen, Ph.D. candidate, domain: material science

2011 Master of Engineering (M.Eng.)

2010 RWE nPower, Swindon (UK), internship at the research and development department, survey on carbon capture and storage for coal and gas fired power plants

2008 – 2011 Westphalian University Gelsenkirchen, Department of Mechanical Engineering and Facility Management, master course: Energy Systems Engineering, domain: low emission energy generation

2008 Bachelor of Engineering (B.Eng.)

2005 – 2008 University of Applied Sciences and Arts Dortmund, Department of Electrical Engineering, bachelor course: Electrical Engineering, domain: energy and environmental engineering